

Linköping Studies in Science and Technology  
Dissertations, No. 1661

# Optimal Control of Electrified Powertrains

*Martin Sivertsson*



**Linköpings universitet**  
**INSTITUTE OF TECHNOLOGY**

Department of Electrical Engineering  
Linköping University  
SE-581 83 Linköping, Sweden

Linköping 2015

Linköping studies in science and technology. Dissertations, No. 1661

# Optimal Control of Electrified Powertrains

Martin Sivertsson

ISBN 978-91-7519-092-1

ISSN 0345-7524

© 2015 Martin Sivertsson, unless otherwise noted. All rights reserved.

Martin Sivertsson

*marsi@isy.liu.se*

*www.vehicular.isy.liu.se*

*Division of Vehicular Systems*

*Department of Electrical Engineering*

*Linköping University*

*SE-581 83 Linköping*

*Sweden*

**The cover:** Front: Formulation and solution of an optimal control problem, coincidentally the benchmark problem in Paper 6. Back: Positive and not so positive exit messages from the solvers used in the dissertation.

Typeset with L<sup>A</sup>T<sub>E</sub>X 2<sub>ε</sub>

Printed by LiU-Tryck, Linköping, Sweden 2015

## Abstract

Vehicle powertrain electrification, i.e. combining the internal combustion engine (ICE) with an electric motor (EM), is a potential way of meeting the increased demands for efficient and low emission transportation, at a price of increased powertrain complexity since more degrees of freedom (DoF) have been introduced. Optimal control is used in a series of studies of how to best exploit the additional DoFs.

In a diesel-electric powertrain the absence of a secondary energy storage and mechanical connection between the ICE and the wheels means that all electricity used by the EMs needs to be produced simultaneously by the ICE, whose rotational speed is a DoF. This in combination with the relatively slow dynamics of the turbocharger in the ICE puts high requirements on good transient control. In optimal control studies, accurate models with good extrapolation properties are needed. For this aim two nonlinear physics based models are developed and made available that fulfill these requirements, these are also smooth in the region of interest, to enable gradient based optimization techniques. Using optimal control and one of the developed models, the turbocharger dynamics are shown to have a strong impact on how to control the powertrain and neglecting these can lead to erroneous estimates both in the response of the powertrain as well as how the powertrain should be controlled. Also the objective, whether time or fuel is to be minimized, influences the engine speed-torque path to be used, even though it is shown that the time optimal solution is almost fuel optimal. To increase the freedom of the powertrain control, a small energy storage can be added to assist in the transients. This is shown to be especially useful to decrease the response time of the powertrain, but the manner it is used, depends on the time horizon of the optimal control problem.

The resulting optimal control solutions are for certain cases oscillatory when stationary controls would have been expected. This is shown to be neither an artifact of the discretization used nor a result of the modeling assumptions used. Instead it is for the formulated problems actually optimal to use periodic control in certain stationary operating points. Measurements show that the pumping torque is different depending on whether the controls are periodic or constant despite the same average value. Whether this is beneficial or not depends on the operating point and control frequency, but can be predicted using optimal periodic control theory.

In hybrid electric vehicles (HEV) the size of the energy storage reduces the impact of poor transient control, since the battery can compensate for the slower dynamics of the ICE. For HEVs the problem instead is how and when to use the battery to ensure good fuel economy. An adaptive map-based equivalent consumption minimization strategy controller using battery state of charge for feedback control is designed and tested in a real vehicle with good results, even when the controller is started with poor initial values. In a plug-in HEV (PHEV) the battery is even larger, enabling all-electric drive, making it desirable to use the energy in the battery during the driving mission. A controller is designed and implemented for a PHEV Benchmark and is shown to perform well even for unknown driving cycles, requiring a minimum of future knowledge.



## Populärvetenskaplig sammanfattning

Elektrifiering av drivlinan i fordon är ett sätt att möta kraven på transporter med hög effektivitet och låga utsläpp. Att byta ut förbränningsmotorn mot en elmotor kan ge vinningar avseende effektivitet, prestanda och utsläpp, men till en kostnad av lägre mobilitet på grund av elektriska energilagars relativt låga energitäthet i jämförelse med fossila bränslen. Att istället komplettera förbränningsmotorn med en elmotor erbjuder möjligheten att kombinera de två systemens fördelar och samtidigt undvika nackdelarna.

Att använda mer än en motor i drivlinan ökar komplexiteten eftersom fler frihetsgrader har introducerats. Detta ställer ökade krav på utformningen av reglersystemet för att få ut det mesta av potentialen i drivlinan. I optimal styrning använder man matematiska modeller och optimeringsalgoritmer för att beräkna hur man bäst styr det modellerade systemet. Storleken på det elektriska energilagret påverkar dock valet av optimal styrningsmetod samt vilken detaljnivå på modellerna som behövs. I avhandlingen används optimal styrning i en serie studier av hur man bäst utnyttjar de extra frihetsgraderna som elektrifieringen har introducerat.

I en diesel-elektrisk drivlina finns det ingen mekanisk koppling mellan motorn och hjulen, likt en växellåda i ett vanligt fordon, vilket gör att dieselmotorns varvtal är en frihetsgrad som måste styras. Avsaknaden av elektriskt energilagrar leder också till att all elektrisk energi till elmotorn måste produceras av förbränningsmotorn exakt då den behövs. Dessa två egenskaper, i kombination med den långsamma dynamiken hos turboaggregatet, ställer höga krav på god transientreglering. För att studera optimal styrning krävs bra modeller med goda extrapoleringsegenskaper. Med avseende på detta utvecklas två fysik-baserade modeller som uppfyller dessa krav och dessutom är tillräckligt glatta i det relevanta arbetsområdet för att möjliggöra gradient-baserade optimeringstekniker. Med optimal styrning och en av de utvecklade modellerna visas turbons dynamik ha stor påverkan på hur drivlinan bör styras. Att försumma turbodynamiken kan leda till felaktiga uppskattningar, både av drivlinans responstid, men även hur den bör styras. Kriteriet, det vill säga om bränsle eller tidsåtgången minimeras, påverkar också vilken motorvarvtal-motormoment-väg som är optimal, även om det visas att den tidsoptimala lösningen är nästan bränsleoptimal. För att ytterligare öka frihetsgraden i drivlinan kan ett elektriskt energilagrar användas för att assistera i transienterna. Detta visar sig vara särskilt användbart för att minska responstiden hos drivlinan, men hur det ska användas beror på tidshorisonten på optimeringsproblemet

De resulterande optimala styrsignalerna är i vissa fall oscillerande där konstanta styrsignaler förväntas. Detta visar vara vare sig en effekt av den använda diskretiseringen eller modelleringsvalen som är gjorda. Istället är det för de lösta problemen faktiskt optimalt att använda periodiska styrsignaler för vissa stationära arbetspunkter. I experiment visas att pumparbetet skiljer sig beroende på om periodiska eller konstanta styrsignaler används, även om medelvärdet är detsamma. Huruvida detta ökar effektiviteten eller inte beror på arbetspunkt och periodtid.

För hybridelektriska fordon (HEV) så minskar batteriets storlek effekten

av dålig transientreglering då batteriet kan användas för att kompensera för den långsamma förbränningsmotordynamiken. Istället blir problemet i huvudsak hur mycket och när batteriet ska användas för att få god bränsleekonomi. En adaptiv mapp-baserad ekvivalentförbruknings-minimerande styrlag (ECMS) med återkopplad reglering baserad på batteriets laddningsnivå, utvecklas och testas i riktigt fordon med gott resultat, även vid dålig initialisering av regulatorn.

För plug-in hybrider (PHEV) är batteriet större och kan dessutom laddas från elnätet, vilket medför möjlighet till rent elektrisk drift och att det är önskvärt att använda energin i batteriet under köruppdraget. För att minska energiåtgången är det däremot ofta lönsamt att blanda energin från bränsle och batteriet kontinuerligt under köruppdraget och se till att batteriet töms lagom till slutet av köruppdraget. För att åstadkomma detta måste då även urladdningstakten bestämmas. En regulator utvecklas för att minimera energiåtgången för en PHEV, det vill säga som försöker använda lagom av batteriet så det ska räcka hela vägen, men inte längre. Denna regulator implementeras för ett referensproblem, med gott resultat även för okända körcykler, trots ett minimum av framtidskunskap.

## Acknowledgment

What seemed like a daunting task almost five years ago, to produce a PhD dissertation, is now finished. It turns out that time really flies when you are solving NLPs, and all of a sudden it is time to concentrate the five years into one readable dissertation. Being a *more is more* type of person, the result is what you know hold in your hand. During these years several people have contributed in different ways making the journey more pleasant and the result possible.

First I would like to thank Lars Nielsen for giving me the chance to start my PhD at Vehicular Systems, but also for raising my awareness about the dangers of stretching, Lars Eriksson for supervising me through my PhD and being constantly interested in every little detail of optimal control of powertrains, pushing me to pursue every idea. I would also like to thank everyone at FS for never accepting *facts*, turning everything into discussions. Special thanks goes to Vaheed “it’s shameful” Nezhadali for showing me Iran, Kristoffer “gunz” Lundahl for being my constant traveling companion, Erik Frisk for all the discussions both concerning AIK and otherwise, and Tomas Nilsson and Christofer Sundström for proofreading parts of this manuscript.

The support and funding from Swedish Energy Agency FFI, BAE Systems in Örnköldsvik, SCANIA CV AB, and the Swedish Hybrid Vehicle Centre (SHC) is gratefully acknowledged.

Thanks to Mats Nordlöf for the valuable input during the first years of my PhD, but especially for setting up and helping me conduct the measurements used in the thesis, and also for being good company during countless hours in the test cell.

I would like to thank my family and friends for enriching the time between optimal control problems; my father for telling me to do something I was good at, my sister for leading the way and showing me it is possible to be this old and **not** have a *real* job, my mother for telling me I know it all (like I didn’t already know that), my brother for taking an opposing stance most of the time, and all of my friends, the ones starting with P and everyone else, you make me laugh!

Finally I want to thank Rebecca for pretending to be interested in all the fun stuff I did at work, even though material like periodic wastegate control sells itself, but mostly for just being there and making my life better.

*Martin Sivertsson*  
Linköping, April 2015



---

# Contents

<b>1</b>	<b>Introduction</b>	<b>3</b>
1.1	Outline . . . . .	5
1.2	Summary and Main Contributions of the Papers Included in the Dissertation . . . . .	6
1.3	Other publications by the author . . . . .	8
<b>2</b>	<b>Background</b>	<b>11</b>
2.1	Modeling and Optimal Control of Hybrid Electric Vehicles . . . . .	11
2.2	Modeling of Diesel-Electric Powertrains . . . . .	13
2.3	Optimal Control of Diesel Engines . . . . .	13
2.4	Selecting the Appropriate Solver . . . . .	14
<b>3</b>	<b>Experimental setups</b>	<b>17</b>
3.1	Pressures . . . . .	18
3.2	Turbocharger Speed . . . . .	18
3.3	Generator power . . . . .	18
3.4	Wastegate Position . . . . .	18
3.5	Massflow . . . . .	18
3.6	Fuel Flow . . . . .	19
3.7	Temperature . . . . .	19
3.8	Air/fuel equivalence ratio . . . . .	19

<b>References</b>	<b>21</b>
<b>Papers</b>	<b>31</b>
<b>1 Optimal Transient Control Trajectories in Diesel-Electric Systems- Part 1: Modeling, Problem Formulation and Engine Properties</b>	<b>33</b>
1 Contributions . . . . .	36
2 Outline . . . . .	37
3 Model . . . . .	37
4 Optimal control scenarios . . . . .	42
5 Power transients . . . . .	46
6 Extending the Transients to Driving Missions . . . . .	49
7 More complex output profiles . . . . .	58
8 Discussion . . . . .	62
9 Conclusions . . . . .	63
References . . . . .	63
<b>2 Optimal Transient Control Trajectories in Diesel-Electric Systems- Part 2: Generator and Energy Storage Effects</b>	<b>69</b>
1 Model . . . . .	72
2 Problem Formulation . . . . .	74
3 Effect of generator losses . . . . .	79
4 Effects of generator limits . . . . .	81
5 Effects of energy storage . . . . .	83
6 Discussion . . . . .	85
7 Impact of energy storage properties . . . . .	87
8 Trade-off between $\min T$ and $\min m_f$ . . . . .	90
9 Concluding discussion . . . . .	91
10 Conclusion . . . . .	92
References . . . . .	92
<b>3 Turbocharger dynamics influence on optimal control of diesel engine powered systems</b>	<b>95</b>
1 Model . . . . .	99
2 Problem Formulation . . . . .	102
3 Results . . . . .	104
4 Conclusions . . . . .	109
References . . . . .	110
<b>4 Optimal and real-time control potential of a diesel-electric power- train</b>	<b>113</b>
1 Model . . . . .	116
2 Problem Formulation . . . . .	117
3 Optimal control trajectories . . . . .	118
4 Optimal Line . . . . .	120
5 Control using SAE J1939 . . . . .	121
6 Optimal control using SAE J1939 . . . . .	123
7 Conclusion . . . . .	125
References . . . . .	127
A Nomenclature . . . . .	129

<b>5</b>	<b>Modeling for Optimal Control: A Validated Diesel-Electric Powertrain Model</b>	<b>131</b>
1	Contributions . . . . .	135
2	Model structure . . . . .	136
3	Modeling . . . . .	136
4	Results . . . . .	148
5	Conclusion . . . . .	148
	References . . . . .	149
A	Data used . . . . .	151
<b>6</b>	<b>An Optimal Control Benchmark: Transient Optimization of a Diesel-Electric Powertrain</b>	<b>153</b>
1	Contributions . . . . .	156
2	Model . . . . .	156
3	Problem Formulation . . . . .	157
4	Solution accuracy . . . . .	158
5	With time varying constraints . . . . .	158
6	Without time varying constraints . . . . .	161
7	Conclusion . . . . .	163
	References . . . . .	163
<b>7</b>	<b>Model and discretization impact on oscillatory optimal control for a diesel-electric powertrain</b>	<b>165</b>
1	Contributions . . . . .	168
2	Model . . . . .	168
3	Problem Formulation . . . . .	170
4	Numerical Solution . . . . .	171
5	Oscillating controls . . . . .	172
6	Model extensions . . . . .	172
7	Results . . . . .	178
8	Conclusions . . . . .	180
	References . . . . .	180
A	Excerpts from original model . . . . .	182
<b>8</b>	<b>Optimal stationary control of diesel engines using periodic control</b>	<b>183</b>
1	Contributions . . . . .	187
2	Measurements . . . . .	187
3	Simulation and Optimization . . . . .	196
4	Results and discussion . . . . .	204
5	Conclusions . . . . .	206
	References . . . . .	206
A	Nomenclature . . . . .	208
B	Measured signals and sensors . . . . .	209
<b>9</b>	<b>Adaptive Control of a Hybrid Powertrain with Map-based ECMS</b>	<b>211</b>
1	Vehicle Model . . . . .	214
2	Reference Consumptions . . . . .	214
3	The ECMS . . . . .	215
4	Real-time Implementation Details . . . . .	217
5	Equivalence Factor Considerations . . . . .	218
6	Tests . . . . .	221
7	Conclusion . . . . .	224

References . . . . .	225
<b>10 A control benchmark on the energy management of a plug-in hybrid electric vehicle</b>	<b>227</b>
1 Simulator . . . . .	230
2 Benchmarking . . . . .	236
3 Proposed Solutions . . . . .	239
4 Results . . . . .	246
5 Conclusions . . . . .	249
References . . . . .	253
<b>11 Design and evaluation of energy management using map-based ECMS for the PHEV benchmark</b>	<b>257</b>
1 IFPEN PHEV Benchmark . . . . .	260
2 Problem Formulation . . . . .	262
3 Offline Optimization . . . . .	263
4 Controller . . . . .	264
5 Energy Management . . . . .	266
6 Benchmark evaluation . . . . .	272
7 Discussion . . . . .	276
8 Controller Extensions . . . . .	277
9 Conclusions . . . . .	278
References . . . . .	280
A Notation used . . . . .	282
B Benchmark Data . . . . .	284

# Introduction

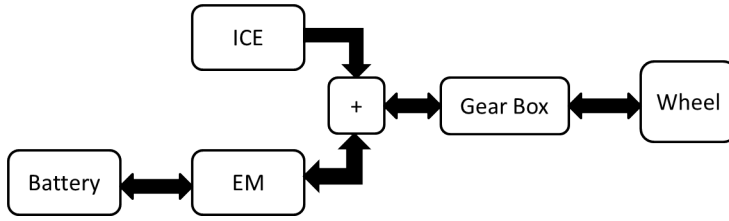


# Introduction

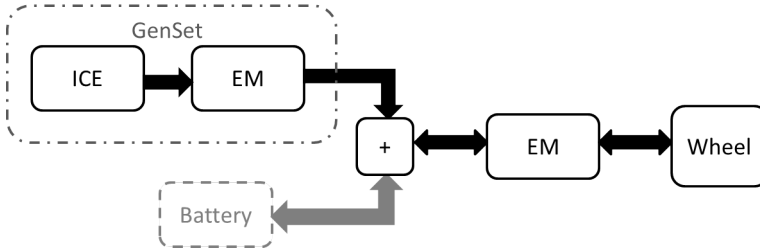
The most common source of power in vehicles is the internal combustion engine (ICE), converting chemical energy from fossil fuels to mechanical force. Since its invention it has undergone continuous development, leading to a quadrupling of the power output without a significant increase in engine size in the last 70 years [69]. Key aspects of realizing the seen performance and efficiency increase are supercharging concepts and downsizing [24, 99]. Using turbochargers to supercharge the engine is a way of exploiting the energy in the exhaust to increase the amount of air flowing into the engine. This increases the power that can be produced by a certain engine displacement, but also introduces a difference between the power that can be produced in transients versus steady-state, since it takes time to spin up the turbocharger, a phenomenon normally called *turbocharger lag* [69]. Further, the mature nature of the ICE means that additional efficiency increases are getting harder to accomplish, while the efficiency of the combustion engine at part load is still relatively low [35, 36].

Electric motors (EM) on the other hand have significantly higher efficiency [28], and also the potential to recuperate kinetic energy when braking, making them a promising technology for efficient and low emission transportation. The energy density of the electric energy storages, e.g. batteries and supercapacitors, is however substantially lower than that of fossil fuels [36], decreasing the range of the vehicle.

Combining an ICE and an EM seems to be a good compromise both ensuring range and increasing efficiency at the price of increased cost of the vehicle. There are several ways, both with and without electrical energy storage, the two can be combined. If the vehicle has more than one source of energy, e.g. battery and fuel, it is denoted a hybrid. Several different hybrid architectures exist but the main delimitation is if the ICE is mechanically connected to the wheels, together with an EM this is called parallel hybrid, see Fig. 1.1-a, or if it is only used together with a generator to produce electrical power, i.e. series hybrid,



(a) Architecture of a parallel hybrid electric vehicle



(b) Architecture of a diesel-electric powertrain, or in the presence of battery, a series hybrid electric vehicle.

Figure 1.1: Main architectures of a electrified powertrain.

Fig. 1.1-b. There also exist combinations of the two denoted series-parallel or power split hybrids.

In a diesel-electric powertrain the architecture is that of a series hybrid, but without an energy storage, see Fig. 1.1-b. This means that a generator is mounted on the output shaft of the diesel engine and that the ICE-generator combination (GenSet) produces electrical power to the motors that propel the vehicle. These complex powertrains all have in common that they have at least one extra Degree of Freedom (DoF) compared to the conventional powertrain, EM torque in a parallel hybrid, generator power and engine speed for series hybrid and engine speed for the diesel-electric powertrain. In order to realize the full potential of the powertrain this DoF needs to be exploited, which requires a sophisticated control system optimizing the energy flow [70].

The size of the battery has a strong impact on the energy management of a vehicle. For a hybrid electric vehicle (HEV) a typical goal is to minimize the amount of fuel used while maintaining the battery state of charge (SOC), which is a measure on how much energy is left in the battery, around a prescribed level, see for instance [20, 50, 64, 71]. In a plug-in HEV (PHEV) the battery is larger and rechargeable from the power grid meaning that the vehicle can be driven as an electric vehicle for parts of, or entire, driving missions. Then, due to the higher efficiency and lower emissions of the EM, it is desirable to make use of the energy stored in the battery and deplete it during the driving mission, see for instance [45, 68, 93, 97]. In a diesel-electric powertrain the energy driving the vehicle needs to be produced simultaneously by the GenSet, any delay in power production, for instance due to turbocharger lag, will be a delay experienced by

the operator. The difference in energy paths also impacts the complexity of the ICE. In an HEV the ICE can be made quite small since the EM and battery can assist when high power is demanded. In order to decrease cost, the ICE can also be of simpler type, and is therefore seldom turbocharged. In a diesel-electric powertrain on the other hand, the ICE has to be dimensioned for the maximum power of the powertrain.

The complexities of the discussed systems lead to that it is not obvious how they should be controlled in order to best exploit the benefits and avoid the drawbacks of the powertrains. Optimal control is an interesting tool that can be used to gain insights into how to best control the powertrain, and which effects are important, but also to implement in the powertrain controller. Even though the common goal for the control of all the discussed powertrains is to increase efficiency and/or decrease emissions, the difference in architectures and components lead to different types of models and optimal control techniques being suitable.

## 1.1 Outline

The first three introductory chapters aim at introducing the topics covered in the dissertation, relating the contributions to the research field and finally describing the experimental setups used.

In Chapter 2 the contributions in the dissertation are related to the research field. In Section 2.1 energy management of HEVs is discussed and related to what is done in Paper 9-11. Section 2.2 discusses modeling of diesel engines, the topic of Paper 5. Section 2.3 summarizes the related field of optimal control of diesel engines and relates it to Paper 1-4 and Paper 7-8. Section 2.4 discusses the different optimal control strategies and solvers used in the dissertation, which is the motivation for Paper 6. Chapter 3 discusses the experimental setups used in dissertation. The appended papers then cover the contributions in the dissertation regarding modeling and optimal control of electrified powertrains.

## 1.2 Summary and Main Contributions of the Papers Included in the Dissertation

This section summarizes the eleven papers included in the dissertation and highlights the main contributions. Unless specifically noted the author performed the study and wrote the majority of the paper.

In Paper 1 [89] optimal control of a diesel-electric powertrain in transient operation is studied. The main contributions are the presented model, how to formulate the optimal control problem to receive relevant solutions, and also the nature of the optimal control when only engine properties are considered. The paper demonstrates both the influence of the turbocharger dynamics as well as how the criteria and constraints affect the solution, both for simple steps in requested power, but also for a more complex sequence of steps.

Paper 2 [90] continues on Paper 1 and contributes with a study of how a non-ideal generator model as well as adding an energy storage to assist in the transients changes the results from Paper 1. Further contributions are a detailed study of how the energy storage efficiency influences the optimal solution and insights into optimal sizing of the energy storage, and also what the limiting factors are. Finally the trade-off between the minimum time and minimum fuel solutions, and how it changes with the presence of an energy storage, is studied.

The contribution in Paper 3 [52] is a quantitative and qualitative study of the impact of turbocharger dynamics on the optimal control of diesel powered powertrains. Two different applications, wheel loader and diesel-electric, are studied where the author contributed with the diesel-electric study. It is shown that the turbocharger impact is dependent on the architecture of the powertrain, but for a diesel-electric powertrain the optimal trajectories differ substantially, and that neglecting the turbocharger dynamics can underestimate the optimal transient duration and consumption.

In Paper 4 [83] the potential performance of different control strategies using the control principles used in industry is studied and evaluated, i.e. the SAE J1939-standard for engine control. Two main approaches are discussed and implemented with the control parameters tuned for minimum fuel or minimum time. This is then performed for several cases and the results are related to the previously presented optimal results, investigating the potential for optimal control. As a further contribution the controllers are extended and it is shown that it is possible to control the diesel-electric powertrain in an optimal manner using the SAE J1939-standard.

Paper 5 [85] contributes with a model of a diesel-electric powertrain. The developed model is a four state, three control physically based mean value engine model that is smooth in the region of interest and provided fully parametrized to the research community. This provides researchers without engine models or data with a relevant and validated open source model on which control design or optimization can be performed. A further contribution is the methodology how to model and parametrize a model of a diesel-electric powertrain, using measurements that are conducted without a dynamometer, the only requirements are a diesel-electric powertrain and sensors.

The contribution of Paper 6 [86] is the formulation and solution of an optimal

control problem to serve as a benchmark on which to evaluate optimal control tools. The considered problem is the optimal control of the power response of a diesel-electric powertrain. The intent of the benchmark is to provide the research community with a relevant problem of reasonable complexity on which to benchmark optimal control tools. The benchmark is provided together with a simultaneously developed model, both available for download. To ensure that the benchmark is relevant for tools at different stages of development the problem is provided both with and without path constraints as well as with and without time as a parameter.

The resulting optimal control trajectories for diesel-electric powertrains are in certain operating conditions oscillatory, when stationary controls would have been expected. In Paper 7 [88] the model and discretization impact on the oscillating optimal control of a diesel-electric powertrains is presented. More specifically it studies whether the seen oscillations are an artifact of the discretization or if the oscillations can be explained by the models used and whether or not extending the model impacts the oscillating solutions. The paper also contributes with a computationally fast and accurate residual gas model suitable for use in an optimal control context.

Paper 8 [87] continues on Paper 7 and studies whether or not gains can be made by controlling the wastegate in a periodic manner in an otherwise stationary operation of a diesel engine. Experiments are conducted on an actual powertrain for several wastegate controls, both periodic and fixed, showing how the wastegate control strategy affects the efficiency and pumping torque of the engine. Further the model from Paper 5, built using measurements on the same powertrain, is used in an simulation and optimal control study, showing the operating point dependence of the seen phenomenon as well as that the oscillating controls under certain circumstances can be predicted by optimal periodic control theory. Further, the effect of the time constant of the wastegate actuator on the optimal controls is shown.

In Paper 9 [91] an adaptive Equivalent Consumption Minimization Strategy (ECMS) for the energy management problem of a HEV, is developed, implemented and experimentally tested in a real HEV. The optimal torque distribution is calculated offline and stored in tables and the effects of discretization on the fuel consumption is shown. Two ways of adapting the control to maintain the SOC within the desired limits are investigated and due to it's robustness to unknown driving missions one is suggested and implemented in a real vehicle.

Paper 10 [72] presents a benchmark PHEV energy management problem, on which to evaluate different control strategies, and analyzes a set of solutions. The benchmark was developed for a special session of the IFAC Workshop on Engine and Powertrain Control, Simulation and Modeling (E-COSM '12), held in Rueil-Malmaison, France, in October 2012. The author participated in the writing of the paper and also designed and implemented the best performing controller for the benchmark, analyzed at length in the paper.

Paper 11 [84] presents the design, implementation, and analysis of the best performing controller for the benchmark in Paper 10. The contribution of the method proposed in the paper is an efficient way of solving and implementing the ECMS control strategy for a PHEV that is also self-contained, using driving

distance and average speed to estimate the initial equivalence factor and then adapting it continuously throughout the driving mission to ensure that it is robust to unknown driving missions and that the desired discharge profile is followed. Further the performance in the benchmark is evaluated, the influence of some of the design choices is discussed, and finally, the controller is extended to incorporate topology information from GPS to improve the performance in the presence of altitude variations in the driving missions.

### 1.3 Other publications by the author

This section summarizes research publications that the author has been involved in, but that is not included in the dissertation.

- A** Lars Eriksson and Martin Sivertsson, *Computing optimal heat release rates in combustion engines*, 2015, SAE International Journal of Engines. [26]
- B** Lars Eriksson and Martin Sivertsson, *Computing optimal heat release rates in combustion engines*, Technical paper 2015-01-0882, 2015, SAE World Congress & Exhibition, Detroit, Michigan, United States [25]
- C** Vaheed Nezhadali, Martin Sivertsson and Lars Eriksson, *Turbocharger Dynamics Influence on Optimal Control of Diesel Engine Powered Systems*, Technical paper 2014-01-0290, 2014, SAE World Congress & Exhibition, Detroit, Michigan, United States [51]
- D** Martin Sivertsson and Lars Eriksson, *Generator Effects on the Optimal Control of a Power Assisted Diesel-Electric Powertrain*, 2013, IEEE Vehicle Power and Propulsion Conference, Beijing, China [82]
- E** Martin Sivertsson and Lars Eriksson, *Optimal Transient Control and Effects of a Small Energy Storage for a Diesel-Electric Powertrain*, 2013, Advances in Automotive Control, Tokyo, Japan [81]
- F** Bernhard Bachmann, Lennart Ochel, Vitalij Ruge, Mahder Gebremedhin, Peter Fritzson, Vaheed Nezhadali, Lars Eriksson, and Martin Sivertsson, *Parallel Multiple-Shooting and Collocation Optimization with OpenModelica*, 2012, International Modelica Conference, Munich, Germany [7]
- G** Martin Sivertsson and Lars Eriksson, *Optimal Short Driving Mission Control for a Diesel-Electric Powertrain*, 2012, IEEE Vehicle Power and Propulsion Conference, Seoul, Korea [80]
- H** Martin Sivertsson and Lars Eriksson, *Time and Fuel Optimal Power Response of a Diesel-Electric Powertrain*, 2012, IFAC Workshop on Engine and Powertrain Control, Simulation and Modeling, Paris, France [78]
- I** Martin Sivertsson, *Adaptive Control Using Map-Based ECMS for a PHEV*, 2012, IFAC Workshop on Engine and Powertrain Control, Simulation and Modeling, Paris, France [77]

**J** Martin Sivertsson and Lars Eriksson, *Optimal Step Responses in Diesel-Electric Systems*, 2012, The 13th Mechatronics Forum International Conference, Linz, Austria [79]

**K** Martin Sivertsson *Optimization of Fuel Consumption in a Hybrid Powertrain*, 2010, Masters Thesis, LiTH-ISY-EX-10/4376-SE, Linköping University [76]

The author's contributions to these publications are indicated by the author list, where the first author is the main contributor to a publication.

In the optimal heat release in combustion engines studies in **A** and **B**, the author contributed to the modeling and also performed the free combustion study and wrote that part of the paper. In **C** the author performed the diesel-electric study, a publication preliminary to Paper 3 in the dissertation [52]. Publications **D** and **E** are preliminary to Paper 2 in the dissertation [90]. In publication **F** the author contributed with the modeling and problem formulation and also assisted in the solution of the optimal control problems. Publications **G**, **H**, and **J** are preliminary to Paper 1 in the dissertation [89]. In publication **I**, describing the controller for the PHEV benchmark in Paper 10 [72], the author did all the work, a publication preliminary to Paper 11 in the dissertation [84]. Publication **K** is the author's masters thesis that contains work preliminary to Paper 9 in the dissertation [91].



# Background

This chapter gives an introduction to modeling and optimal control of electrified vehicles. The aim is to give a short overview of the models and optimization methods commonly used and the previously published research and its relation to the dissertation.

## 2.1 Modeling and Optimal Control of Hybrid Electric Vehicles

In HEVs and PHEVs the main energy management control problem is how and when to use the battery in order to minimize energy consumption and emissions. The models of the energy converters, ICE and EM, are normally simplified either to polynomials, [49, 59], or the efficiency/fuel consumption map [45, 71, 73]. Thus, only stationary operating points are assumed, leading to a quasistatic approach. The underlying assumption is that the dynamic effects of the components are faster than that of the energy flows to be optimized, [70]. Following this assumption, the state-space can be kept small and if the driving profile is known before-hand the optimal solution can be found using for instance Dynamic Programming (DP), [12], as in [1, 65, 66, 71], Pontryagin's Maximum Principle (PMP), [67], as in [19, 73], Convex Optimization, [14], as in [49], or a combination of dynamic programming and convex optimization as in [59].

For real-time energy management of hybrid powertrains there exist several solutions, for an overview see, [70] and [66]. A common choice for HEVs is the equivalent consumption minimization strategy (ECMS), going back to [63], used by for instance [20, 50]. ECMS is a convenient realization of PMP [73] and is normally expressed as that an equivalent consumption of both electrochemical power in the battery,  $P_{ech}$ , and fuel power,  $P_f$ , is minimized, and that the

applied controls is the argument that minimizes this sum according to (2.1).

$$u^* = \arg \min (P_f + \lambda P_{ech}) \quad (2.1)$$

$\lambda$  in (2.1) is called equivalence factor, or sometimes costate, relating the two costs. Other costs can also be included, like emissions and battery ageing, however each additional state introduced requires an additional equivalence factor [74]. If  $\lambda$  is known, the optimal controls can be found [19]. Thus, estimating  $\lambda$  is the key aspect of the controller [18, 20, 50], which is complicated by the driving mission dependency of the optimal  $\lambda$ . Paper 9-11 contribute to this field. Paper 9 and Paper 11 are focused on the efficient solution and implementation of the energy management problem for power split hybrids, using no, or a minimum of, information about the future driving conditions. Paper 10 instead presents a benchmark energy management problem for PHEVs on which to evaluate different control strategies, something also performed in the paper.

In the real-time control the motors are normally modeled using either simple polynomials or efficiency maps, as in the offline case. For parallel HEVs using naturally aspirated spark ignited ICEs, the engine speed is a fixed function of the wheel speed, the torque response of the ICE is fast, and the emissions are handled by the three-way catalyst. For compression ignited ICE parallel hybrids, especially if turbocharged, both the emissions and response time of the engine needs to be considered and there are publications where effects of transient fuel consumption as well as emissions are included in the optimal control problem (OCP) [58, 98, 100].

For series hybrids the engine speed of the GenSet is a DoF that needs to be controlled. Normally the same approach is used, i.e. using the stationary efficiency maps when solving the OCP. This means that the stationary map is used to generate setpoints for the GenSet, see [8, 37, 75, 101]. This approach does not account for the transient cost of switching operating point and how to actually control the GenSet to the setpoints in an optimal manner is rarely studied. In [16, 101] the assumption is that the GenSet should not deviate too far from the optimal operating line, both stationary and during the transients. In [101] this is achieved by limiting the power after the setpoint generation, whereas in [16] the possible setpoint candidates are restricted, but both solutions mean that the battery is used to compensate for the GenSet dynamics. In [37], where a model for a turbocharged diesel GenSet is used, this leads to the engine not being able to produce the requested power, due to the time constant of the diesel engine. This power therefore has to be produced by the supercapacitor, an effect not accounted for in the optimization. The only paper known to the author studying optimal engine speed control for the GenSet of a series-hybrid is [56]. The considered problem is that a certain energy is required in a fixed amount of time. The engine of the GenSet is naturally aspirated and in the optimization the systems stationary efficiency maps are used. For a turbocharged diesel-electric powertrain, lacking energy storage to compensate for any power deficits, but incorporating turbolag, the question how to control the GenSet is highly relevant. Paper 1-4 contribute to this field by studying optimal transient control of turbocharged GenSets.

## 2.2 Modeling of Diesel-Electric Powertrains

To study optimal control of GenSets, control oriented models describing the dynamics are necessary. Since the model is evaluated a large number of times the model evaluation needs to be fast, but still capture the qualitative phenomena, be quantitatively accurate as well as have good extrapolation properties [3]. Further in order for gradient based optimization techniques to work well the model needs to be smooth in the region of interest. This leads to models of the Mean Value Engine Model (MVEM) type [38, 42]. MVEMs, 0-D, or *lumped* parameter models, ignore in-cycle events that occur on a crank angle basis, and instead average these effects over one or several cycles [24]. The MVEMs can be divided into two groups: data driven black-box models and physics based grey-box models [15, 33, 34]. For more information on modeling of combustion engines the reader is referred to [24, 35, 39].

Black-box models rely on auto-regression techniques to identify the model from data, [27, 62]. The advantages of this approach is its relative simplicity, both in that no prior knowledge of the system is required and also that the resulting models are often very fast, [21, 33]. The resulting states often have no physical meaning, making analysis difficult [15, 62]. Further, the model is only valid around the operating conditions for which it was tuned, leading to questionable extrapolation properties and putting high requirements on training data [21].

Grey-box models are models based on physical properties, using tuning parameters to increase their fit to data. Due to the physical motivation the analysis and extrapolation properties are good, but the parametrization and derivation requires high effort and prior knowledge about the system [21, 62]. Further, the resulting model might be too complex for direct implementation in a control framework [15, 34, 62]. Discussions on grey-box MVEMs can be found in [23, 95]. Paper 1 and Paper 5 contribute with two grey-box MVEMs of two different engines that are smooth in the region of interest. Further, Paper 7 studies modeling extensions to the model presented in Paper 5, investigating whether the seen characteristics of the optimal control solutions depend on the modeling assumptions used.

## 2.3 Optimal Control of Diesel Engines

How to optimally control the GenSet in transients has received very little attention, especially for turbocharged GenSets. The related field of optimal control of diesel engines has gotten more attention, especially in diesel engines with variable geometry turbines (VGT) and exhaust gas recirculation (EGR). Unless specifically noted, a grey-box MVEM is used in the discussed study. In [6] optimal control of a VGT-EGR diesel is studied for fixed output power and engine speed. The fuel consumption is minimized subject to limits on emissions. A lot of attention is given to formulating and solving the problem, a topic also studied in [5], investigating effects of different discretization techniques as well as different nonlinear program (NLP) solvers. The optimal solutions are also validated on a real engine. In [10] sequential quadratic programming (SQP)

together with single shooting is used to minimize pollutants during different load steps at constant speed. [60, 61] uses a quasi-Newton algorithm to minimize a trade-off between smoke and produced power for a VGT diesel engine over a specified torque and speed trajectory. In [44, 46] the torque and speed responses of VGT-EGR diesel engines are studied. In [46] fuel and time optimal trajectories from low to high output torque are studied and in [44] the final speed of vehicle is maximized.

None of the discussed studies above study optimal control, using the engine speed as a DoF. To the author, the only known publications where the freedom to select engine speed is considered, are [53, 54, 56] where very simplified models, one to two states, are used. Papers 1-7 contribute to this field, studying how to control the engine speed of a diesel powered powertrain in transients.

In [6] it is mentioned that the optimal results seen exhibit oscillations in the control signals. There exists some theory concerning optimal periodic control [11, 13, 17, 31] where it is actually better to oscillate the control than to use constant controls [30, 48]. Papers 7-8 contribute to this field by studying if it is optimal to use periodic control in an otherwise stationary operation of diesel engines.

For real-time implementation of optimal control a couple of different methods have been suggested. One method is implementing the optimal controls as transient compensation maps together with the normal stationary calibration. This approach is advocated in [4, 32, 47]. Another approach along the same lines, i.e. using a fixed mapping, is [61] where the optimal results are used to train an artificial neural network that is then used to control the engine. More flexible approaches are [27, 96], implementing model predictive control (MPC) where an optimization problem is solved online in real-time, or [55] where stochastic DP is used, and the optimal feedback laws are extracted and implemented in a real vehicle. Paper 4 studies how to use the framework common in industry to approximate the optimal trajectories extracted from the optimal control studies in Papers 1-2.

## 2.4 Selecting the Appropriate Solver

This section provides a short summary of the optimal control techniques used in in the dissertation and related research. For an overview on numerical optimal control and numerical optimization the reader is referred to [22, 57].

The model complexity is strongly related to which optimal control technique algorithm is most suitable. For instance in the HEV case a common choice for offline studies is DP, since the state-space is small and the curse of dimensionality [9] is not as severe. However even for PHEVs DP becomes impractical. This is since the battery is large to allow for all-electric drive and the SOC dynamics are slow, resulting in a very fine SOC grid and long computation times [65]. In Paper 9 only one state is used, making the offline problem very suitable for DP and the PMP related control strategy ECMS for the real-time control. This real-time control strategy is also used in Paper 11.

When studying optimal control of diesel engines and the number of states is

larger, the common choice is instead to use a direct method. There exists several software packages implementing different direct methods. In this dissertation three of them are used. In Paper 1 and Paper 6 ACADO Toolkit [40] is used, which is an open source software implementing shooting algorithms and SQP. Papers 1-4 and Paper 6 uses PROPT [92] a commercial software implementing pseudospectral collocation and SQP. In Papers 7-8 CasADi [2] a symbolic framework for algorithmic differentiation is used together with direct collocation and IPOPT, a large-scale interior point algorithm for nonlinear optimization [94], with the MA57 linear solver from the HSL package, [41], for solving the resulting NLPs.

The evolution during the thesis is that larger OCPs with more complex constraints are solved, therefore the method and solver suitable has changed. Both ACADO and PROPT are packages that simplify defining the problem to be solved, however this also introduces a drawback, since the problem definition has to follow a certain format. With CasADi the user has to define the problem more on his own which is both a benefit and drawback. The coding requirements increase but it gives the user full control over defining the problem, which increases the complexity of problems that can be solved.

Evaluating the performance of the solver is not straight forward and often one has to rely on the provided solved examples to get an estimate on how good the solver is. These problems generally have in common that the solution is well known, typically meaning that they are simple and can be solved by most solvers, as for instance the Bryson-Denham problem, see [43]. However during the work on this thesis, problems have been encountered that were not indicated by looking at the solved example list of the used solver. Paper 6 contributes to this field, suggesting a benchmark problem on which to evaluate OCP solvers, as well as presenting the solutions using two different solvers. The intent of this benchmark is to provide developers of optimal control tools with a more challenging problem that can not be analytically solved, but where the solution is still available for comparison.



## Experimental setups

This chapter describes the measurement setups used in Papers 1, 2, 5, 7, and 8 in the dissertation. In Paper 9 the vehicle speed, SOC and equivalence ratio,  $\lambda$ , are measured, however they are signals reported by the powertrain control system and not discussed further. For the diesel-electric studies measurements on two different powertrains are conducted. The first powertrain is the one modeled and used in Papers 1-2 where the measurements were conducted to validate the developed model. Measurements from a different powertrain is used in Papers 5, 7 and 8. In Papers 5 and 7 the measurements are used to build and validate a model over the powertrain. In Paper 8 the measurements are used to study optimal wastegate control. In this chapter the sensors used to measure the relevant quantities are briefly described, for a more thorough text on sensors and their characteristics the reader is referred to [29]. In Table 3.1 all signals measured in the different papers are shown. The quantities of interest in the measurements are:

- Engine Speed
- Pressures
- Turbocharger speed
- Generator power
- Wastegate position
- Massflow through compressor
- Fuel flow
- Temperatures
- Air/fuel equivalence ratio

The engine speed is measured with the internally mounted OEM sensor and accessed via the engine CAN bus and not discussed further. The signals measured with external sensors are discussed below.

### 3.1 Pressures

All pressures in Paper 1, 2, 5, 7 and 8 are measured using Dynisco PT130-50 Pressure Transducers. They have a range of 0-345 kPa and an accuracy of  $\pm 1.72$  kPa including linearity, hysteresis and repeatability.

### 3.2 Turbocharger Speed

In Paper 1, 2, 5, 7 and 8 the turbocharger speed is measured with Acam PicoTurn PT2G Turbocharger Speed Sensor. The Digital-Out option is used, giving one pulse per revolution. The speed range is 390-400000 rpm and the precision is 390 rpm. The time constant is small, allowing for sampling rates in the range of 1-3 MHz.

### 3.3 Generator power

In Paper 1, 2, 5, 7 and 8 the generator and power electronics are lumped together so what is actually measured is the output voltage and current from the DC-converter and from these measurements the output power can be computed. The voltage is measured using a Tektronix P5200 High-voltage Differential Probe, having a bandwidth of up to 50 MHz and the current is measured using a LEM IT 1000-S High Performance Current Transducer with a linearity error less than 3ppm and a response time to 90% of full scale of less than 1  $\mu$ s.

### 3.4 Wastegate Position

In Paper 1, 2, 5, 7 and 8 the wastegate position is measured with Firstmark Controls Series 170 Subminiature Position Transducer with a maximum independent linearity error  $\pm 0.5\%$  per VRCI-P-100A, output smoothness 0.1% max, Resolution infinite signal, and an operating temperature of  $-65^{\circ}\text{C}$  to  $+125^{\circ}\text{C}$ .

### 3.5 Massflow

In Paper 5 and 7 the massflow through the compressor is measured with a ABB FMT500 Thermal Massflow Meter. The measuring error is less than  $0.009 \cdot \dot{m}_{meas} + 2.78 \cdot 10^{-4}$  kg/s. Reproducibility error less than 0.2% and time constant 0.5 s. The time constant is relatively long therefore this measurement is only used for stationary operating points in the submodel tuning and validation.

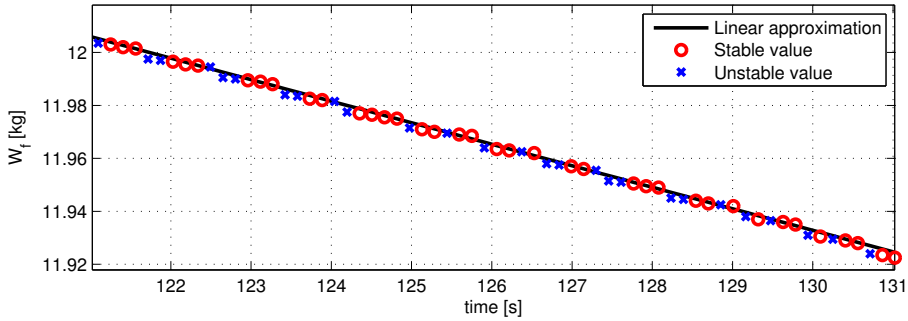


Figure 3.1: Measured fuel weight and the linear approximation.

### 3.6 Fuel Flow

In Paper 5 and Paper 8 the fuel weight is measured using a Kern IFS60K0,5DL Counting scale with a linearity of 2 g, reproducibility of 500 mg and a specified stabilisation time of 3 s. The stabilisation time in the specification is rather long, however the scale also reports when the measurement is stable which is a lot faster. To get an accurate approximation of the fuel flow a first order polynomial is fitted to the weight over time series, that minimizes the error in a least squares sense, using only the stable measurements, see Fig. 3.1. The slope of this polynomial is the fuel flow in kg/s. Due to the recirculating fuel flow of the diesel engine as well as response time of the scale and system itself, this technique only suitable for stationary points and therefore only used in stationary operating conditions.

### 3.7 Temperature

The temperatures in Paper 5, 7 and 8 are measured with TC 1.5mm mineral insulated type K thermocouples. The sensor has a measurement tolerance of  $\pm 0.0075|T|$  and response time of 0.3 s when plunged into boiling water from air at  $20^\circ\text{C}$ . The time constant in air or exhaust gas can be expected to be substantially longer and therefore the temperature measurements are only used in the tuning and validation of stationary models.

### 3.8 Air/fuel equivalence ratio

In Paper 8 the equivalence ratio,  $\lambda$  is measured with ETAS 636 Lambda module using Bosch LSU4.9 Wide Band Lambda Sensor mounted after the turbine. The measurement is only used as a reference since the instantaneous fuel flow into the cylinder is not measured.

Table 3.1: Quantities measured and used in Paper 1, 2, 5, 7 and 8

Name	Description
Measurements used in Paper 1, 2, 5, 7 and 8	
$p_{amb}$	Ambient pressure
$p_{im}$	Intake manifold pressure
$p_{em,f}$	Exhaust manifold pressure, front
$p_{em,r}$	Exhaust manifold pressure, rear
$n_{tc}$	Turbine rotational speed
$u_{wg}$	Wastegate position
$I_{DC}$	DC current
$U_{DC}$	DC voltage
$n_e$	Engine rotational speed
Extra measurements used in Paper 5 and 7	
$p_{es}$	Pressure after turbine
$p_{c,b}$	Pressure before compressor
$p_{c,a}$	Pressure after compressor
$T_{amb}$	Ambient temperature
$T_{im}$	Intake manifold temperature
$T_{em,f}$	Exhaust manifold temperature, front
$T_{em,r}$	Exhaust manifold temperature, rear
$T_{c,b}$	Temperature before compressor
$T_{c,a}$	Temperature after compressor
$\dot{m}_c$	Massflow through compressor
$M_F$	Fuel weight
Extra measurements used in Paper 8	
$\lambda$	Air-fuel equivalence ratio
$M_F$	Fuel weight

---

## References

- [1] D. Ambühl, A. Sciarretta, C. Onder, L. Guzzella, S. Sterzing, K. Mann, D. Kraft, and M. Küsell. A causal operation strategy for hybrid electric vehicles based on optimal control theory. In *Proceedings of the 4th Braunschweig Symposium on Hybrid Vehicles and Energy*, Braunschweig, Germany, February 2007.
- [2] J. Andersson. *A General-Purpose Software Framework for Dynamic Optimization*. PhD thesis, Arenberg Doctoral School, KU Leuven, Department of Electrical Engineering (ESAT/SCD) and Optimization in Engineering Center, Kasteelpark Arenberg 10, 3001-Heverlee, Belgium, October 2013.
- [3] J. Asprion, O. Chinellato, and L. Guzzella. Optimisation-oriented modelling of the {NOx} emissions of a diesel engine. *Energy Conversion and Management*, 75:61 – 73, 2013.
- [4] J. Asprion, O. Chinellato, C. Onder, and L. Guzzella. From static to dynamic optimisation of diesel-engine control. In *52nd IEEE Conference on Decision and Control*, Florence, Italy, 2013.
- [5] J. Asprion, O. Chinellato, and L. Guzzella. Efficient solution of the diesel-engine optimal control problem by time-domain decomposition. *Control Engineering Practice*, 30:34–44, 2014.
- [6] J. Asprion, O. Chinellato, and L. Guzzella. Optimal control of diesel engines: Numerical methods, applications, and experimental validation. *Mathematical Problems in Engineering*, 2014.
- [7] B. Bachmann, L. Ochel, V. Ruge, M. Gebremedhin, P. Fritzson, V. Nezhadali, L. Eriksson, and M. Sivertsson. Parallel multiple-shooting

- and collocation optimization with openmodelica. In *Modelica 2012 – 9th International Modelica Conference*, Munich, Germany, September 2012.
- [8] S. Barsali, C. Miulli, and A. Possenti. A control strategy to minimize fuel consumption of series hybrid electric vehicles. *Energy Conversion, IEEE Transactions on*, 19(1):187–195, March 2004.
- [9] R. Bellman. *Dynamic Programming*. Dover Publications Inc., 2nd edition, 2003.
- [10] M. Benz, M. Hehn, C. H. Onder, and L. Guzzella. Model-based actuator trajectories optimization for a diesel engine using a direct method. *J Eng Gas Turb Power*, 133(3):298–312, 2011.
- [11] D. S. Bernstein and E. G. Gilbert. Optimal periodic control: The  $\pi$  test revisited. *IEEE Transactions on Automatic Control*, AC-25(4):673–684, 1980.
- [12] D. P. Bertsekas. *Dynamic Programming and Optimal Control*. Athena Scientific, 2nd edition, 2000.
- [13] S. Bittanti, G. Fronza, and G. Guardabassi. Periodic control: A frequency domain approach. *IEEE Transactions on Automatic Control*, AC-18(1):33–38, 1973.
- [14] S. Boyd and L. Vandenberghe. *Convex Optimization*. Cambridge University Press, 1st edition, 2004.
- [15] T. Broomhead, C. Manzie, M. Brear, and P. Hield. Model reduction of diesel mean value engine models. In *SAE Technical Paper 2015-01-1248*. SAE International, 2015.
- [16] S. D. Cairano, W. Liang, I. V. Kolmanovsky, M. L. Kuang, and A. M. Phillips. Power smoothing energy management and its application to a series hybrid powertrain. *IEEE Transactions on Control Systems Technology*, 21(6):2091–2103, 2013.
- [17] W. Chan and S. Ng. Normality and proper performance improvement in periodic control. *Journal of Optimization Theory and Applications*, 29(2):215–229, 1979.
- [18] A. Chasse, G. Hafidi, P. Pognant-Gros, and A. Sciarretta. Supervisory control of hybrid powertrains: an experimental benchmark of offline optimization and online energy management. In *IFAC Workshop on Engine and Powertrain Control, Simulation and Modeling*, pages 109–117, 2009.
- [19] A. Chasse, P. Pognant-Gros, and A. Sciarretta. Online implementation of an optimal supervisory control for a parallel hybrid powertrain. *SAE International Journal of Engines*, 2(1):1630–1638, 2009.

- [20] A. Chasse, A. Sciarretta, and J. Chauvin. Online optimal control of a parallel hybrid with costate adaption rule. In *IFAC Symposium on Advances in Automotive Control*, 2010.
- [21] L. del Re, P. Ortner, and D. Alberer. Chances and challenges in automotive predictive control. In L. del Re, F. Allgöwer, L. Glielmo, C. Guardiola, and I. Kolmanovsky, editors, *Automotive Model Predictive Control*, volume 402 of *Lecture Notes in Control and Information Sciences*, pages 1–22. Springer London, 2010.
- [22] M. Diehl. Numerical optimal control, 2011.
- [23] L. Eriksson. Modeling and control of turbocharged SI and DI engines. *Oil & Gas Science and Technology - Rev. IFP*, 62(4):523–538, 2007.
- [24] L. Eriksson and L. Nielsen. *Modeling and Control of Engines and Drivelines*. John Wiley & Sons, 2014.
- [25] L. Eriksson and M. Sivertsson. Computing optimal heat release rates in combustion engines. In *SAE 2015 World Congress & Exhibition*, number SAE Technical Paper 2015-01-0882, Detroit, Michigan, United States, April 2014.
- [26] L. Eriksson and M. Sivertsson. Computing optimal heat release rates in combustion engines. *SAE International Journal of Engines*, 8(2), June 2015.
- [27] H. J. Ferreau, P. Ortner, P. Langthaler, L. del Re, and M. Diehl. Predictive control of a real-world diesel engine using an extended online active set strategy. *Annual Reviews in Control*, 31(2):293 – 301, 2007.
- [28] A. Fitzgerald, C. K. Jr., and S. D. Umans. *Electric Machinery*. McGraw-Hill Book Co., 6th edition, 2003.
- [29] J. Fraden. *Handbook of Modern Sensors - Physics, Designs, and Applications*. Springer, 4th edition, 2010.
- [30] E. G. Gilbert. Vehicle cruise: Improved fuel economy by periodic control. *Automatica*, 12:159–166, 1976.
- [31] E. G. Gilbert. Optimal periodic control: A general theory of necessary conditions. *SIAM Journal of Control and Optimization*, 15(5):717–746, 1977.
- [32] M. Grahn, K. Johansson, and T. McKelvey. Model-based diesel engine management system optimization for transient engine operation. *Control Engineering Practice*, 29(0):103 – 114, 2014.
- [33] C. Guardiola, A. Gil, B. Pla, and P. Piqueras. Representation limits of mean value engine models. In D. Alberer, H. Hjalmarsson, and L. del Re, editors, *Identification for Automotive Systems*, volume 418 of *Lecture Notes in Control and Information Sciences*, pages 185–206. Springer London, 2012.

- [34] L. Guzzella and A. Amstutz. Control of diesel engines. *Control Systems, IEEE*, 18(5):53–71, Oct 1998.
- [35] L. Guzzella and C. Onder. *Introduction to Modeling and Control of Internal Combustion Engine Systems*. Springer, 1st edition, 2004.
- [36] L. Guzzella and A. Sciarretta. *Vehicle Propulsion Systems - Introduction to Modeling and Optimization*. Springer, 3rd edition, 2013.
- [37] J. Halme and J. Suomela. Optimal efficiency based gen-set control for series hybrid work machine. In *IEEE VPPC 2012 – The 8th IEEE Vehicle Power and Propulsion Conference*, Seoul, Korea, October 2012.
- [38] E. Hendricks. The analysis of mean value engine models. In *SAE Technical Paper 890563*. SAE International, 1989.
- [39] J. B. Heywood. *Internal Combustion Engine Fundamentals*. McGraw-Hill Book Co., 1988.
- [40] B. Houska, H. J. Ferreau, and M. Diehl. ACADO toolkit - an open source framework for automatic control and dynamic optimization. *Optimal Control Applications & Methods*, 32(3):298–312, 2011.
- [41] HSL. A collection of fortran codes for large scale scientific computation. <http://www.hsl.rl.ac.uk>, 2013.
- [42] J. Jensen, A. Kristensen, S. Sorenson, N. Houbak, and E. Hendricks. Mean value modeling of a small turbocharged diesel engine. In *SAE Technical Paper 910070*. SAE International, 1991.
- [43] A. E. B. Jr. and Y.-C. Ho. *Applied Optimal Control-Optimization, Estimation and Control*. Taylor & Francis, 1975.
- [44] I. Kolmanovsky, M. van Nieuwstadt, and P. Moraal. Optimal control of variable geometry turbocharged diesel engines with exhaust gas recirculation. In *ASME International Mechanical Engineering Congress and Exposition*, volume 67, pages 265–273, November 1999.
- [45] V. Larsson, L. Johannesson, and B. Egardt. Impact of trip length uncertainty on optimal discharging strategies for phev. In *IFAC Symposium on Advances in Automotive Control*, Munich, Germany, 2010.
- [46] X. Llamas and L. Eriksson. Optimal transient control of a heavy duty diesel engine with EGR and VGT. In *IFAC World Congress*, Cape Town, South Africa, 2014.
- [47] G. Mancini, J. Aspiron, N. Cavina, C. Onder, and L. Guzzella. Dynamic feedforward control of a diesel engine based on optimal transient compensation map. *Energies*, 7(8), 2014.

- [48] K. McDonough, I. Kolmanovsky, D. Filev, D. Yanakiev, S. Szwabowski, and J. Micheline. Stochastic dynamic programming control policies for fuel efficient vehicle following. In *American Control Conference*, Washington DC, 2013.
- [49] N. Murgovski, L. Johannesson, J. Hellgren, B. Egardt, and J. Sjöberg. Convex optimization of charging infrastructure design and component sizing of a plug-in series hev powertrain. In *IFAC World Congress, Milano*, pages 13052–13057, 2011.
- [50] C. Musardo and G. Rizzoni. A-ECMS: An adaptive algorithm for hybrid electric vehicle energy management. In *IEEE Conference on Decision and Control and the European Control Conference*, number 44, pages 1816–1823, 2005.
- [51] V. Nezhadali, M. Sivertsson, and L. Eriksson. Turbocharger dynamics influence on optimal control of diesel engine powered systems. In *SAE 2014 World Congress & Exhibition*, number SAE Technical Paper 2014-01-0290, Detroit, Michigan, United States, April 2014.
- [52] V. Nezhadali, M. Sivertsson, and L. Eriksson. Turbocharger dynamics influence on optimal control of diesel engine powered systems. *SAE International Journal of Engines*, 7(1):6–13, May 2014.
- [53] T. Nilsson, A. Fröberg, and J. Åslund. Optimal operation of a turbocharged diesel engine during transients. In *SAE Technical Paper 2012-01-0711*, Detroit, Michigan, USA, 2012.
- [54] T. Nilsson, A. Fröberg, and J. Åslund. Using stochastic dynamic programming for look-ahead control of a wheel loader diesel electric transmission. In *IFAC World Congress*, Cape Town, South Africa, 2014.
- [55] T. Nilsson, A. Fröberg, and J. Åslund. Predictive control of a diesel electric wheel loader powertrain. *Control Engineering Practice*, submitted.
- [56] C. E. Nino-Baron, A. R. Tariq, G. Zhu, and E. G. Strangas. Trajectory optimization for the engine-generator operation of a series hybrid electric vehicle. *IEEE Transactions on Vehicular Technology*, 60(6):2438–2447, 2011.
- [57] J. Nocedal and S. J. Wright. *Numerical Optimization*. Springer, 2nd edition, 2006.
- [58] T. Nüesch, M. Wang, C. Voser, and L. Guzzella. Optimal energy management and sizing for hybrid electric vehicles considering transient emissions. In *E-COSM'12 – IFAC Workshop on Engine and Powertrain Control, Simulation and Modeling*, Paris, France, October 2012.
- [59] T. Nüesch, P. Elbert, M. Flankl, C. Onder, and L. Guzzella. Convex optimization for the energy management of hybrid electric vehicles considering engine start and gearshift costs. *Energies*, 7(2):834–856, 2014.

- [60] R. Omran, R. Younes, and J.-C. Champoussin. Optimal control of diesel engines: Methods and applications. In *IMSM07 – International Modeling and Simulation Multiconference*, Bueno Aires, Argentina, 2007.
- [61] R. Omran, R. Younes, and J.-C. Champoussin. Optimal control of a variable geometry turbocharged diesel engine using neural networks: Applications on the etc test cycle. *Control Systems Technology, IEEE Transactions on*, 17(2):380–393, March 2009.
- [62] P. Ortner and L. del Re. Predictive control of a diesel engine air path. *Control Systems Technology, IEEE Transactions on*, 15(3):449–456, May 2007.
- [63] G. Paganelli, T. Guerra, S. Delprat, J.-J. Santin, M. Delhom, and E. Combes. Simulation and assessment of power control strategies for a parallel hybrid car. *Proceedings of the Institution of Mechanical Engineers, Part D, Journal of Automobile Engineering*, 214:705 – 717, 2000.
- [64] G. Paganelli, S. Delprat, T. Guerra, J. Rimaux, and J. Santin. Equivalent consumption minimization strategy for parallel hybrid powertrains. In *IEEE Conference on Vehicular Technology*, number 55, pages 2076–2081, 2002.
- [65] R. Patil, Z. Filipi, and H. Fathy. Comparison of supervisory control strategies for series plug-in hybrid electric vehicle powertrains through dynamic programming. *Control Systems Technology, IEEE Transactions on*, 22(2):502–509, March 2014.
- [66] P. Pisu and G. Rizzoni. A comparative study of supervisory control strategies for hybrid electric vehicles. *IEEE Transactions on Control Systems Technology*, 15(3):506–518, May 2007.
- [67] L. Pontryagin, V. Boltyanskii, R. Gamkrelidze, and E. Mishchenko. *The Mathematical Theory of Optimal Processes*. Interscience Publishers, 1962.
- [68] M. Pourabdollah, V. Larsson, L. Johannesson, and B. Egardt. Phev energy management: A comparison of two levels of trip information. In *SAE Technical Paper 2012-01-0745*. SAE International, 2012.
- [69] C. D. Rakopoulos and E. G. Giakoumis. *Diesel engine transient operation - Principles of operation and simulation analysis*. Springer, 2009.
- [70] A. Sciarretta and L. Guzzella. Control of hybrid electric vehicles. *IEEE Control Systems Magazine*, pages 60–70, April 2007.
- [71] A. Sciarretta, M. Back, and L. Guzzella. Optimal control of parallel hybrid electric vehicles. *IEEE Transactions on Control Systems Technology*, 12(3):352–363, 2004.
- [72] A. Sciarretta, L. Serrao, P. C. Dewangan, P. Tona, E. N. D. Bergshoeff, C. Bordons, L. Charmpa, P. Elbert, L. Eriksson, T. Hofman, M. Hubacher,

- P. Isenegger, F. Lacandia, A. Laveau, H. Li, D. Marcos, T. Nüesch, S. Onori, P. Pisu, J. Rios, E. Silvas, M. Sivertsson, L. Tribioli, A.-J. van der Hoeven, and M. Wu. A control benchmark on the energy management of a plug-in hybrid electric vehicle. *Control Engineering Practice*, 29:287–298, August 2014.
- [73] L. Serrao, S. Onori, and G. Rizzoni. Ecms as a realization of pontryagin’s minimum principle for hev control. In *American Control Conference*, pages 3964–3969, June 2009.
- [74] Serrao, L., Sciarretta, A., Grondin, O., Chasse, A., Creff, Y., Di Domenico, D., Pognant-Gros, P., Querel, C., and Thibault, L. Open issues in supervisory control of hybrid electric vehicles: A unified approach using optimal control methods. *Oil & Gas Science and Technology - Rev. IFP*, 68(1): 23–33, 2013.
- [75] V. Sezer, M. Gokasan, and S. Bogosyan. A novel ecms and combined cost map approach for high-efficiency series hybrid electric vehicles. *IEEE Transactions on Vehicular Technology*, 60(8):3557–3570, 2011.
- [76] M. Sivertsson. Optimization of fuel consumption in a hybrid powertrain. Master’s thesis, Linköping University, SE-581 83 Linköping, 2010.
- [77] M. Sivertsson. Adaptive control using map-based ecms for a phev. In *E-COSM’12 – IFAC Workshop on Engine and Powertrain Control, Simulation and Modeling*, Paris, France, October 2012.
- [78] M. Sivertsson and L. Eriksson. Time and fuel optimal power response of a diesel-electric powertrain. In *E-COSM’12 – IFAC Workshop on Engine and Powertrain Control, Simulation and Modeling*, Paris, France, October 2012.
- [79] M. Sivertsson and L. Eriksson. Optimal step responses in diesel-electric systems. In *Mechatronics’12 – The 13th Mechatronics Forum International Conference*, Linz, Austria, September 2012.
- [80] M. Sivertsson and L. Eriksson. Optimal short driving mission control for a diesel-electric powertrain. In *IEEE VPPC 2012 – The 8th IEEE Vehicle Power and Propulsion Conference*, Seoul, Korea, October 2012.
- [81] M. Sivertsson and L. Eriksson. Optimal transient control and effects of a small energy storage for a diesel-electric powertrain. In *AAC’13 – 7th IFAC Symposium on Advances in Automotive Control*, Tokyo, Japan, 2013.
- [82] M. Sivertsson and L. Eriksson. Generator effects on the optimal control of a power assisted diesel-electric powertrain. In *IEEE VPPC 2013 – The 9th IEEE Vehicle Power and Propulsion Conference*, Beijing, China, 2013.
- [83] M. Sivertsson and L. Eriksson. Optimal and real-time control potential of a diesel-electric powertrain. In *IFAC World Congress*, Cape Town, South Africa, 2014.

- [84] M. Sivertsson and L. Eriksson. Design and evaluation of energy management using map-based ECMS for the PHEV benchmark. *Oil & Gas Science and Technology - Rev. IFP*, 70(1):195–211, January-February 2014.
- [85] M. Sivertsson and L. Eriksson. Modeling for optimal control: A validated diesel-electric powertrain model. In *SIMS 2014 - 55th International Conference on Simulation and Modelling*, Aalborg, Denmark, 2014.
- [86] M. Sivertsson and L. Eriksson. An optimal control benchmark: Transient optimization of a diesel-electric powertrain. In *SIMS 2014 - 55th International Conference on Simulation and Modelling*, Aalborg, Denmark, 2014.
- [87] M. Sivertsson and L. Eriksson. Optimal stationary control of diesel engines using periodic control. *Submitted to Control Engineering Practice*, 2015.
- [88] M. Sivertsson and L. Eriksson. Model and discretization impact on oscillatory optimal control for a diesel-electric powertrain. In *Submitted to E-COSM'15 - IFAC Workshop on Engine and Powertrain Control, Simulation and Modeling*, Columbus, Ohio, August 2015.
- [89] M. Sivertsson and L. Eriksson. Optimal transient control trajectories in diesel-electric systems-part 1: Modeling, problem formulation and engine properties. *Journal of Engineering for Gas Turbines and Power*, 137(2), February 2015.
- [90] M. Sivertsson and L. Eriksson. Optimal transient control trajectories in diesel-electric systems-part 2: Generator and energy storage effects. *Journal of Engineering for Gas Turbines and Power*, 137(2), February 2015.
- [91] M. Sivertsson, C. Sundström, and L. Eriksson. Adaptive control of a hybrid powertrain with map-based ECMS. In *IFAC World Congress*, Milano, Italy, 2011.
- [92] TOMLAB. PROPT - Matlab Optimal Control Software, "<http://www.tomdyn.com/>", 2012.
- [93] P. Tulpule, V. Marano, and G. Rizzoni. Effects of different PHEV control strategies on vehicle performance. In *American Control Conference*, St. Louis, USA, 2009.
- [94] A. Wächter and L. T. Biegler. On the implementation of an interior-point filter line-search algorithm for large-scale nonlinear programming. *Mathematical Programming*, 106:25–57, 2006.
- [95] J. Wahlström and L. Eriksson. Modelling diesel engines with a variable-geometry turbocharger and exhaust gas recirculation by optimization of model parameters for capturing non-linear system dynamics. *Proceedings of the Institution of Mechanical Engineers, Part D, Journal of Automobile Engineering*, 225(7):960–986, 2011.

- [96] J. Wahlstrom and L. Eriksson. Output selection and its implications for mpc of egr and vgt in diesel engines. *Control Systems Technology, IEEE Transactions on*, 21(3):932–940, May 2013.
- [97] X. Wang, H. He, F. Sun, X. Sun, and H. Tang. Comparative study on different energy management strategies for plug-in hybrid electric vehicles. *Energies*, 6(11):5656–5675, 2013.
- [98] Y. Wang, H. Zhang, and Z. Sun. Optimal control of the transient emissions and the fuel efficiency of a diesel hybrid electric vehicle. *Proceedings of the Institution of Mechanical Engineers, Part D: Journal of Automobile Engineering*, 227(11):1546–1561, 2013.
- [99] N. Watson and M. Janota. *Turbocharging the internal combustion engine*. The Macmillan Press Ltd., 1982.
- [100] F. Yan, J. Wang, and K. Huang. Hybrid electric vehicle model predictive control torque-split strategy incorporating engine transient characteristics. *IEEE Transactions on Vehicular Technology*, 61(6):2458–2467, 2012.
- [101] H. Yoo, B.-G. Cho, S.-K. Sul, S.-M. Kim, and Y. Park. A power flow control strategy for optimal fuel efficiency of a variable speed engine-generator based series hybrid electric vehicle. In *IEEE ECCE'09 Energy Conversion Congress and Exposition*, pages 443–450, 2009.



# Papers



# Optimal Transient Control Trajectories in Diesel-Electric Systems-Part 1: Modeling, Problem Formulation and Engine Properties<sup>†</sup>

Martin Sivertsson<sup>a</sup> and Lars Eriksson<sup>a</sup>

<sup>a</sup>*Vehicular Systems, Department of Electrical Engineering,  
Linköping University, SE-581 83 Linköping, Sweden.*

---

<sup>†</sup>This is a formatted version of “Optimal Transient Control Trajectories in Diesel-Electric Systems-Part 1: Modeling, Problem Formulation and Engine Properties” by Martin Sivertsson and Lars Eriksson, *Journal of Engineering for Gas Turbines and Power*, Volume 137, Number 2. ©ASME 2015. Reproduced with the permission of ASME. The original paper can be found at [asmedigitalcollection.asme.org](http://asmedigitalcollection.asme.org) <http://asmedigitalcollection.asme.org/>, and can be found using the Digital Object Identifier (DOI): 10.1115/1.4028359. The formatting is restricted to changing the article into a single-column format, adjusting sizes of figures and tables, and adjusting the referencing style.

## **Abstract**

A non-linear four state-three input mean value engine model, incorporating the important turbocharger dynamics, is used to study optimal control of a diesel-electric powertrain during transients. The optimization is conducted for the two criteria, minimum time and fuel, where both engine speed and engine power are considered free variables in the optimization. First, steps from idle to a target power are studied and for steps to higher powers the controls for both criteria follow a similar structure, dictated by the maximum torque line and the smoke-limiter. The end operating point, and how it is approached, is however different. Then the power transients are extended to driving missions, defined as, that a certain power has to be met as well as a certain energy has to be produced. This is done with both fixed output profiles and with the output power being a free variable. The time optimal control follows the fixed output profile even when the output power is free. These solutions are found to be almost fuel optimal despite being substantially faster than the minimum fuel solution with variable output power. The discussed control strategies are also seen to hold for sequences of power and energy steps.

## Introduction

In a diesel-electric powertrain, such as the BAE Systems TorqE<sup>TM</sup> shown in Fig. 1, there is only an electric link between the diesel engine and the electric load. The absence of a mechanical link between the engine and the load introduces an extra degree of freedom, since the engine speed can be chosen freely. This extra degree of freedom offers potential for increasing the performance of the powertrain, due to the torque characteristic of the electric machine, as well as a potential reduction in consumption, due to the freedom of choosing the operating point of the diesel engine. During stationary operation the desired operating point can be found from the combined efficiency map of the engine-generator combination (GenSet). An open question is how to optimally control the GenSet between two power levels, especially when the diesel engine is turbocharged. In transient operation the turbocharger dynamics limits the changes in load and speed that can be achieved, often referred to as turbocharger lag, see [15]. The absence of an energy storage also makes the system more restricted and difficult to manage, compared to a series hybrid, that can use the energy storage to compensate for the dynamics of the engine.

Since the generator is mounted on the output shaft of the engine, a change in generator power has to be coupled with a change in engine torque and engine speed. Otherwise increasing the generator load might lead to the engine stalling. This is since the generator power has to be sustainable by the engine, which is limited by its maximum torque, but most of all, by the smoke-limiter. This raises the question of how to, in an optimal way, control the powertrain to be able to meet the requested power, either as fast as possible or as fuel efficient as possible. This paper, which is part one of a two part study, investigates optimal control of a turbocharged diesel-electric powertrain during transients, using the extra freedom of selecting engine speed and incorporating the transient effects and the turbocharger dynamics of the diesel engine.

Several applications use a diesel-electric powertrain, for example cranes [10], vehicles [3], ships [8], excavators [11], and trains [5]. Little has however been done to study how to control the GenSet in transients. The GenSet is often augmented with an energy storage, making it a series hybrid. This hybridization does not answer the question of how to control the GenSet between power levels.

A common approach is to use the stationary map to generate setpoints for the GenSet, see [23, 2, 6, 16]. How to actually control the powertrain to the setpoints is rarely studied. In [23] and [2] the assumption is that the GenSet should not deviate too far from the optimal operating line, both stationary and during the transients, and therefore the energy storage is used to limit the change in power requested from the GenSet. In [6] on the other hand the energy storage is used to support the output power due to the time constant of the turbocharged diesel engine.

Three examples where transient effects of the diesel engine are included in the optimization are [22, 14, 7]. In [22] the torque split of a parallel hybrid is optimized over a known output torque trajectory and the torque response of the diesel engine is modeled as a first order system together with a smoke-limiter limiting the maximum fuel flow into the engine. In [14] the optimal control

trajectories for the GenSet of a series-hybrid are studied. The considered problem is that a certain energy is required in a fixed amount of time. Only the engine speed dynamics of the naturally aspirated GenSet are considered and in the optimization the systems stationary efficiency maps are used. In [7] a model for the fuel consumption increase from the stationary map, due to the transients, is used in the optimization to account for transient losses.

In related articles, concerning optimal transient control of diesel engines, different optimization methods are used to minimize pollutants during transient operation for known engine speeds, see [1, 12] or, as in [13] the optimal engine operating point trajectory for a known engine power output trajectory is derived. The diesel engine is modeled as an inertia with a Willans-line efficiency model with a first order delay torque reduction representing the turbocharger dynamics. The optimal solution is found using dynamic programming and Pontryagins maximum principle.

Of the discussed papers only two papers study fuel or time optimal control of the diesel engine in transient operation, with the freedom to select engine speed. [14] studies the control of a naturally aspirated diesel engine and use the stationary maps to model the efficiency. While [13] studies fuel optimal control of a turbocharged engine using a simple model and with the output trajectory fixed. In this paper time and fuel optimal control is studied with both engine speed and output power free variables in the optimization, using a model that incorporates both engine and turbocharger dynamics as well as emptying and filling of the manifolds.

## 1 Contributions

The contributions of this paper are the study of optimal control of a diesel-electric powertrain in transient operation and also how to formulate such problems to receive relevant solutions. First the selection of criteria are discussed, then the findings in [18] are summarized. There optimal control to a target power for two different criteria with the engine output power and engine speed considered free variables during the transient is studied.

Then the problem formulation is extended to driving missions. Augmenting the previously studied problem formulation, going from idle to a terminal power, with that a required terminal power as well as required energy has to be produced. This is studied both with output power as a free variable as well as with a fixed output power for both criteria for different required powers and energies. It also studies the optimal control for a sequence of requested output powers and energies, which emulates the drivers request in a driving cycle.

For these studies a nonlinear, four state, three input mean value engine model (MVEM) is used in the study and provided, fully parametrized in the paper. This MVEM incorporates the important turbocharger dynamics as well as the nonlinear multiple input-multiple output nature of the diesel engine. The model also has continuous derivatives in the operating region which enables the solvers to calculate gradients and Hessians in the non-linear program solvers used.

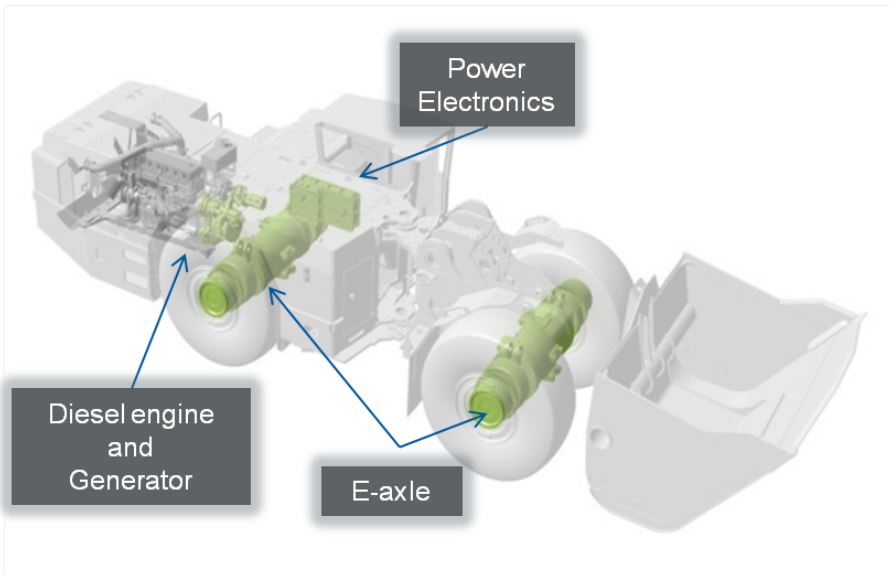


Figure 1: BAE Systems TorqE™ diesel-electric powertrain

## 2 Outline

In Section 3 the model used in the study is presented. The model is the same as in [17] but provided here for completeness. In Section 4.1-5 the power transient study from [18] is summarized, with Section 4.1 formulating the problem and Section 5 presenting the solution method and the results. In Section 6 the problem is extended to driving missions. First the addition to the problem formulation is presented and then the numerical solution path is presented in Section 6.2. Then time and fuel optimal energy transients are studied in Sections 6.3 and 6.4, before the quantitative results as well as the differences due to the criteria are studied in Section 6.5. In Section 7 a sequence of requested powers and energies are studied, emulating a driving cycle, before the concluding remarks in Section 8-9.

## 3 Model

This paper studies optimal control of diesel-electric transients. However the focus is on how the control depends on the diesel engine and turbocharger dynamics, using the extra freedom introduced by the powertrain architecture. Therefore the generator model is simplified, i.e. the generator efficiency is assumed constant and equal to unity, i.e.  $P_{mech} = P_{gen}$ . The generator time constant is also assumed to be much faster than the time constant of the engine. Furthermore the generator is assumed to only be limited by the maximum power of the power electronics, implemented as a constant. The modeled powertrain consists of a 6-cylinder 12.7-liter SCANIA diesel engine with a fixed-geometry turbine and a

wastegate for boost control, equipped with a generator and energy storage. The model is a nonlinear, four state, three input mean value engine model (MVEM). The diesel engine model is a modified implementation of the well validated model found in [21], with minor modifications, ensuring that the model is continuously differentiable and further, only uses a subset of the modeling language so that the software can symbolically differentiate the expressions. In particular this means removal of potentially discontinuous operators as *abs*, *max*, *min*, and *sign*. The motivation for this is that these modifications enable the software to efficiently solve the formulated problems using higher order search methods.

The states of the MVEM are engine speed,  $\omega_{ice}$ , inlet manifold pressure,  $p_{im}$ , exhaust manifold pressure,  $p_{em}$ , turbocharger speed,  $\omega_{tc}$ . The controls are injected fuel mass,  $u_f$ , wastegate position,  $u_{wg}$ , and generator power,  $P_{gen}$ . The engine model consists of two control volumes, intake and exhaust manifold, and four restrictions, compressor, engine, turbine, and wastegate. The control volumes are modeled with the standard isothermal model, using the ideal gas law and mass conservation. The engine and turbocharger speeds are modeled using Newton's second law. The governing differential equations of the MVEM are:

$$\frac{d\omega_{ice}}{dt} = \frac{1}{J_{GenSet}} (T_{ice} - \frac{P_{mech}}{\omega_{ice}}) \quad (1)$$

$$\frac{dp_{im}}{dt} = \frac{R_a T_{im}}{V_{im}} (\dot{m}_c - \dot{m}_{ac}) \quad (2)$$

$$\frac{dp_{em}}{dt} = \frac{R_e T_{em}}{V_{em}} (\dot{m}_{ac} + \dot{m}_f - \dot{m}_t - \dot{m}_{wg}) \quad (3)$$

$$\frac{d\omega_{tc}}{dt} = \frac{P_t - P_c}{\omega_{tc} J_{tc}} - w_{fric} \omega_{tc}^2 \quad (4)$$

Where  $\dot{m}_{c/ac/f/t/wg}$  denotes massflow,  $T_{im/em}$  manifold temperatures,  $J_{GenSet/tc}$  inertias,  $V_{im/em}$  manifold volumes,  $R_{a/e}$  gas constants,  $P_{t/c}$  turbine/compressor powers,  $T_{ice}$  engine torque, and  $P_{mech}$  mechanical generator power, with connections between the components as in Fig 2. For values of the parameters used and a complete nomenclature see Appendix.

For more in-depth information on the structure and details of the diesel engine model see [4, 21], from where the equations are collected. The diesel engine model is tuned to correspond to the validated model in [21] with the EGR-valve closed and the VGT locked in a fixed position.

### 3.1 Component Models

The model consists of nine submodels, connected as seen in Fig. 2. The submodels are models for compressor massflow and power, intake manifold pressure, engine torque and exhaust temperature, exhaust manifold pressure, wastegate massflow, turbine massflow and power, and generator and energy storage losses, all described in the following subsections.

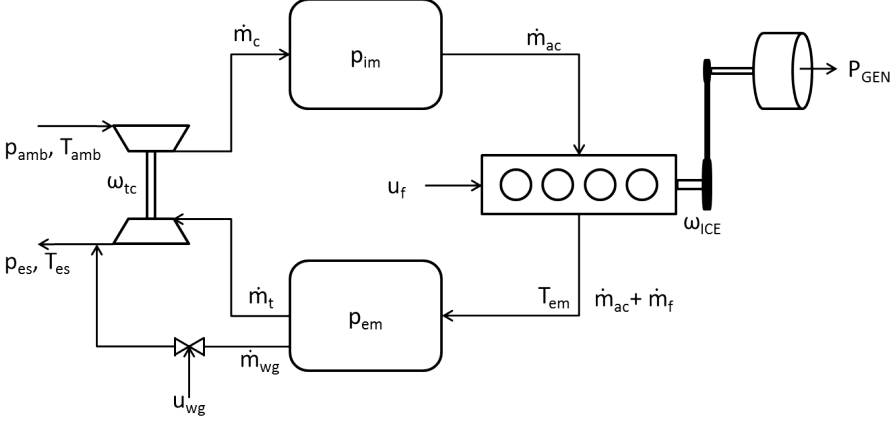


Figure 2: Structure of the MVEM. The modeled components as well as the connection between them.

### Compressor

The compressor model consists of two sub-models, one for the massflow and one for the power consumption. In order to avoid problems for low turbocharger speeds and transients with pressure ratios  $\Pi_c < 1$  a variation of the physically motivated  $\Psi \Phi$  model in [4] is used.

$$\Pi_{c,max} = \left( \frac{\omega_{tc}^2 R_c^2 \Psi_{max}}{2c_p T_{amb}} + 1 \right)^{\frac{\gamma_a}{\gamma_a - 1}} \quad (5)$$

$$\dot{m}_{c,corr} = \dot{m}_{c,corr,max} \sqrt{1 - \left( \frac{\Pi_c}{\Pi_{c,max}} \right)^2} \quad (6)$$

$$\dot{m}_c = \frac{\dot{m}_{c,corr} p_{amb} / p_{ref}}{\sqrt{T_{amb} / T_{ref}}} \quad (7)$$

$$P_c = \frac{\dot{m}_c c_{pa} T_{amb} \left( \Pi_c^{\frac{\gamma_a - 1}{\gamma_a}} - 1 \right)}{\eta_c} \quad (8)$$

The full compressor model has three tuning parameters  $\Psi_{max}$ ,  $\dot{m}_{c,corr,max}$ , and  $\eta_c$ .

## Engine Gas Flow

The engine gas flow model consist of two sub-models, one for air flow and one for fuel flow.

$$\dot{m}_{ac} = \frac{\eta_{vol} p_{im} \omega_{ice} V_D}{4\pi R_a T_{im}} \quad (9)$$

$$\dot{m}_f = \frac{10^{-6}}{4\pi} u_f \omega_{ice} n_{cyl} \quad (10)$$

$$\lambda = \frac{\dot{m}_{ac}}{\dot{m}_f} \frac{1}{(A/F)_s} \quad (11)$$

To avoid problems for  $\dot{m}_f = 0$  a new variable is defined

$$\phi_\lambda = \dot{m}_{ac} - \lambda_{min} \dot{m}_f (A/F)_s \quad (12)$$

where  $\lambda_{min}$  is the lower limit set by the smoke-limiter. The gas flow model has one tuning parameter,  $\eta_{vol}$ .

## Engine Torque

The net torque of the engine,  $T_{ice}$ , is modeled using three torque components, and one efficiency model.

$$T_{ice} = T_{ig} - T_{fric} - T_{pump} \quad (13)$$

$$\eta_{ig} = \eta_{ig,ch} \left( 1 - \frac{1}{r_c^{\gamma_{cyl}-1}} \right) \quad (14)$$

$$T_{ig} = \frac{u_f 10^{-6} n_{cyl} Q_{HV} \eta_{ig}}{4\pi} \quad (15)$$

$$T_{fric} = \frac{V_D}{4\pi} 10^5 (c_{fr1} \omega_{ice}^2 + c_{fr2} \omega_{ice} + c_{fr3}) \quad (16)$$

$$T_{pump} = \frac{V_D}{4\pi} (p_{em} - p_{im}) \quad (17)$$

The net torque,  $T_{ice}$  is limited by the maximum torque of the engine,  $T_{ice,max}(\omega_{ice})$ , shown in Fig. 10. The torque model has five tuning parameters,  $\eta_{vol}$ ,  $c_{fr,i}$ ,  $i \in [1, 2, 3]$ , and  $\eta_{ig,ch}$ .

## Exhaust Temperature

The engine out temperature model is based on ideal gas Seiliger cycle. The engine out temperature and exhaust manifold temperature are assumed to be equal.

$$q_{in} = \frac{\dot{m}_f Q_{HV}}{\dot{m}_f + \dot{m}_{ac}} \quad (18)$$

$$x_p = 1 + \frac{q_{in} x_{cv}}{c_{va} T_{im} r_c^{\gamma_a - 1}} \quad (19)$$

$$T_{em} = \eta_{sc} \Pi_e^{1-1/\gamma_a} r_c^{1-\gamma_a} x_p^{1/\gamma_a - 1} \left( q_{in} \left( \frac{1 - x_{cv}}{c_{pa}} + \frac{x_{cv}}{c_{va}} \right) + T_{im} r_c^{\gamma_a - 1} \right) \quad (20)$$

The engine out temperature model has two tuning parameters  $\eta_{sc}$ , and  $x_{cv}$ .

### Turbine

The turbine model consists of submodels for the turbine massflow and turbine power production. The turbine massflow model is modeled with the standard restriction model and using that half the expansion occurs in the rotor and the other half in the stator, see [4]:

$$\Pi_t^* = \max \left( \sqrt{\Pi_t}, \left( \frac{2}{\gamma_e + 1} \right)^{\frac{\gamma_e}{\gamma_e - 1}} \right) \quad (21)$$

The optimization tools rely heavily on derivatives, therefore functions such as *abs* and *max* are not desirable. Therefore  $\Pi_t^* = \sqrt{\Pi_t}$  is used which is valid down to  $\Pi_t = 0.30$  corresponding to an exhaust manifold pressure of  $p_{em} \approx 3.3p_{amb}$ , which is sufficient for the transients studied. The massflow model is now given by:

$$\Pi_t^* = \sqrt{\Pi_t} \quad (22)$$

$$\Psi_t(\Pi_t^*) = \sqrt{\frac{2\gamma_e}{\gamma_e - 1} \left( (\Pi_t^*)^{\frac{2}{\gamma_e}} - (\Pi_t^*)^{\frac{\gamma_e + 1}{\gamma_e}} \right)} \quad (23)$$

$$\dot{m}_t = \frac{p_{em}}{\sqrt{R_e T_{em}}} \Psi_t A_{t,eff} \quad (24)$$

$$P_t = \dot{m}_t c_{pe} T_{em} \eta_t \left( 1 - \Pi_t^{\frac{\gamma_e - 1}{\gamma_e}} \right) \quad (25)$$

The tuning parameters of the complete turbine model are  $A_{t,eff}$ , and  $\eta_t$ .

### Wastegate

If the standard restriction model is applied to the wastegate, see for instance [4], choking would occur for exhaust manifold pressures of  $p_{em} \approx 1.8p_{amb}$  which is well within the normal operating region. This would require a *max* expression in the model, which has a discontinuity in the derivative, so instead the following non-physical model is used:

$$\Psi_{wg} = c_{wg,1} \sqrt{1 - \Pi_{wg}^{c_{wg,2}}} \quad (26)$$

$$\dot{m}_{wg} = \frac{p_{em}}{\sqrt{R_e T_{em}}} \Psi_{wg} u_{wg} A_{wg,eff} \quad (27)$$

The tuning parameters of the wastegate model are  $c_{wg,1-2}$  and  $A_{wg,eff}$ .

## 3.2 Model validation

The parameters of the engine model are tuned to correspond to the validated model in [21] with the EGR-valve closed and the VGT locked in a fixed position. The modeled engine is basically the same, with the difference that it has a

Table 1: Relative error of the model vs. measurements

State	Mean	800 rpm	1000 rpm	1250 rpm	1500 rpm	1800 rpm
$p_{im}$	6.8	2.2	3.3	5.6	7.5	10.7
$p_{em}$	8.7	2.2	3.7	7.4	11.3	11.6
$\omega_{tc}$	4.6	5.6	5.8	4.5	3.1	6.8

wastegate equipped fixed geometry turbine and no EGR. To ensure that the model is a valid description of the modeled powertrain, the model is validated against five different datasets of measured data, measurements conducted on the modeled powertrain. Each dataset is 100-270 s long and consists of 9-10 steps in generator power of different magnitudes as well as stationary phases in between for different constant engine speeds. Since engine output torque is not measured the torque model is inverted in the validation, resulting in almost no errors in the engine speed tracking. The relative model error vs. measurements for each dataset as well as the mean error over all datasets is shown in Table 1.

There it is seen that the mean relative error of the important intake manifold pressure dynamics are 7 % for all datasets, however the model fit increase with decreasing engine speed, being as low as 2 %, i.e. en par with the original model.

## 4 Optimal control scenarios

In Fig. 3 a performance test for one of the considered applications of the BAE Systems TorqE™ is shown. This test is a step from idle to constant output power, an output power that is then held. This test is conducted on a conventional powertrain, gear shifts can be seen around 4s and 8s. Due to the coupling of the vehicle and engine speed the change from idle to requested power takes up to 3-4s. Based on this, several scenarios are studied to gain knowledge about how one can characterize an optimal trajectory in the engine map.

The basic scenario is the same as in Fig. 3, i.e. the engine is at idle when the operator applies a step in requested output power. In order to study how to fully exploit the freedom in the powertrain the output power of the conventional vehicle is not tracked, instead the output power is a variable to be optimized and the operators request should be met as fast or as fuel efficient as possible. Another scenario is that the powertrain should provide an amount of energy and power, for example to lift a container, without any restrictions on time and energy trajectory. This is the most free driving mission possible. These scenarios allow extreme solutions and is used to give insight into how the freedom built into the powertrain can be utilized. In the final scenario the drivers input is interpreted as a power request, a power that has to be followed. This is also done for a sequence of steps, mimicking a real-world driving mission, where a sequence of tasks are performed.

The performed scenarios are:

1. Section 5: Optimal steps to requested power.

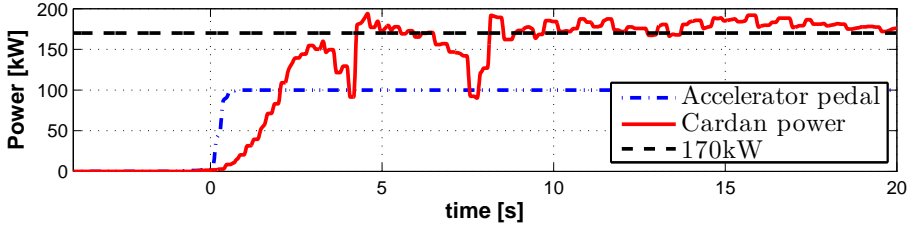


Figure 3: Cardan power for a step from idle measured on one of the considered applications.

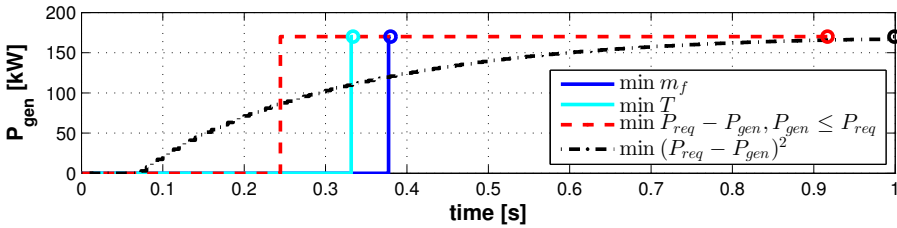


Figure 4: Generator actuation for different criteria. Circles mark the end points.

- (a) Steps from idle to high output power.
  - (b) Transient to the fuel optimal operating point.
2. Section 6: Optimal steps to requested power and energy.
    - (a) With output power a free variable.
    - (b) With fixed output power.
  3. Section 7: Optimal control for a sequence of power and energy steps.

#### 4.1 Mathematical Problem Formulation

The aim is to use optimal control in order to gain insight into how to control the powertrain, and also to get bounds on the performance, for the scenario in Fig. 3. That is, how to control the engine speed, engine torque, and generator power, using the actuators on the powertrain, when the operator requests a step in output power. In the optimization problem, in order to retrieve relevant solutions, the power has to be met in the final time step, it also has to be a power the engine can sustain. A straight forward approach is to minimize the deviation from the requested power, i.e. either  $\int_0^T (P_{req} - P_{gen})^2$  or  $\int_0^T (P_{req} - P_{gen})$ , s.t  $P_{gen} \leq P_{req}$ . However, using such a formulation hides the potential of the powertrain. Looking at Fig. 4 it is seen that minimizing fuel or time, with the added constraints that the final operating point has to be stationary, results in that the requested power is met and sustainable 73 % more fuel efficient, in the case of  $\min m_f$ , or 64% faster in the case of  $\min T$ .

In order to study how to control the powertrain, two optimal control problems are formulated, minimum time and minimum fuel, as follows:

$$\begin{aligned} \min_{u(t)} \quad & \int_0^T \dot{m}_f(x(t), u(t)) dt \quad \text{or} \quad \min_{u(t)} T \\ \text{s.t.} \quad & \dot{x}(t) = f(x(t), u(t)) \\ & (x(t), u(t)) \in \Omega(t) \end{aligned} \quad (28)$$

where  $x$  is the state vector of the MVEM,  $\dot{x}$  is defined by Eqs. (1)-(4), and  $u = [u_f, u_{wg}, P_{gen}]$ . The studied transients are steps from idle to a target power subject to time varying constraints imposed by the components, such as maximum torque and minimum speed, as well as environmental constraints, i.e. a limit on  $\phi_\lambda$  set by the smoke-limiter. The time varying constraints  $(x(t), u(t)) \in \Omega(t)$  are:

$$\begin{aligned} x(0) &= x_0, & \dot{x}(T) &= 0 \\ 0 &\leq u(t) \leq u_{max}, & x_{min} &\leq x(t) \leq x_{max} \\ P_{gen}(T) &= P_{req}, & \phi_\lambda(x(t), u(t)) &\geq 0 \\ T_{ice}(x(t), u(t)) &\leq T_{ice,max}(\omega_{ice}(t)) \end{aligned} \quad (29)$$

In most vehicles the accelerator position can be interpreted as a power request. The problem defined by Eqs. (28)-(29) is thus how to control the GenSet in order to be able to satisfy the operators power request, either as fast as possible, or as fuel efficiently as possible. The initial state,  $x_0$ , corresponds to idle, that is an engine speed of 525 rpm and  $P_{gen} = 0$  W with the wastegate open, i.e.  $u_{wg} = 1$ . The end constraint on the state derivatives is to avoid solutions where the optimal control ends in an operating point that cannot be maintained. This is to avoid under- or overshoots in the control strategies. For example specifying  $\dot{\omega}_{ice}(T) \geq 0$  requires that the engine can deliver the torque necessary for the generator, see Eq. (1). Removing this requirement will lead to the engine stalling since the optimal solution will be to apply  $P_{gen} = P_{req}$  at  $t = 0$ , a power the engine can not sustain. For a more detailed discussion on the end constraints impact on the optimal solution, see [17].

## 4.2 Solution methods and tools

Due to the detailed and complex non-linear model used in this paper methods as dynamic programming aren't feasible. In Section 5 the problem is solved using the ACADO Toolkit, an open-source framework for automatic control and dynamic optimization, that uses multiple shooting together with sequential quadratic programming, see [9], and in Section 6-7 the problem is solved using Tomlab/PROPT, see [20], which uses pseudospectral collocation methods to solve optimal control problems. Such methods only guarantee a local minimum. Care has therefore been taken to ensure that the resulting solutions are at least good local minima.

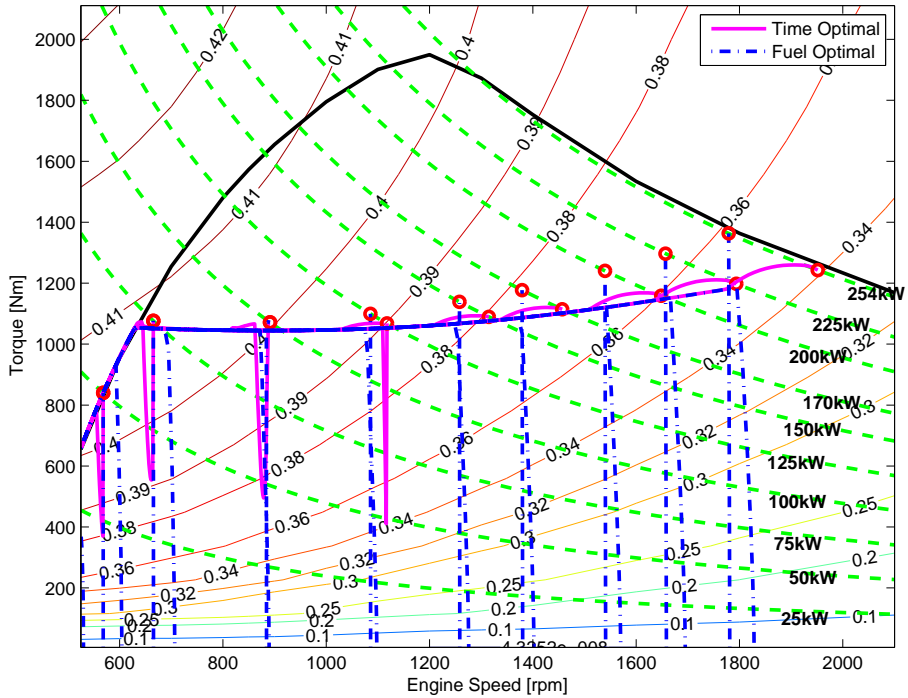


Figure 5: Time and fuel optimal solutions to different load transients. The time and fuel optimal transients have similar structures but differ in how they meet the end constraints. Since several trajectories are plotted the smoke-limit for unloaded engine acceleration is clearly visible.

## 5 Power transients

The optimal torque and speed trajectories to problem Eqs. (28) are shown in Fig. 5. In Fig. 5 the maximum torque line of the engine is also shown as well as, for convenience, the constant power lines for the different requested powers. The solutions are very similar despite the criteria being different, both solutions following the smoke-limiter. The main difference is the end operating point, marked with circles, and how it is approached. It can be seen that the optimal solutions can be divided into two cases. One where the time optimal and fuel optimal paths end in the same operating point ( $P_{req} \leq 100$  kW), and another where they don't ( $P_{req} \geq 125$  kW). For details on the case where they coincide, see [18]. The time and fuel optimal control trajectories for  $P_{req} \geq 125$  kW all follow the same pattern as the transients in Fig. 6 where  $P_{req} = 170$  kW. The time optimal and fuel optimal control strategies are rather similar for the first phase of the transient. The optimal solution for both criteria is to put as much energy as possible into the system in order to build intake manifold pressure and turbo speed, the difference lies in the fine tuning to meet the end constraints. This becomes even more apparent when looking at Fig. 5, where both fuel and time optimal torque-engine speed paths for different required powers are shown.

### 5.1 Time optimal high power transients

The time optimal solution approaches the stationary point from a higher torque, whereas the fuel optimal solution approaches the stationary point from a lower torque. In the first phase the optimal solution follows the maximum torque line and the smoke-limiter of the engine. The time optimal solution follows the smoke-limiter until the end and actuates the wastegate to get stationarity. When the wastegate is actuated to control the turbocharger speed to its target speed the pumping work decreases and the net torque of the engine increases and the path thus approaches the end point from a higher torque.

### 5.2 Fuel optimal high power transients

The fuel optimal solution approaches a different stationary point, one that has a higher  $p_{im}$ ,  $p_{em}$ , and  $\omega_{tc}$  but lower  $\omega_{ice}$ , and consequently higher efficiency. This stationary point is near the operating point with maximum obtainable efficiency without using the generator to restrain the engine speed from increasing as it builds turbocharger speed. In Fig. 7 it is shown how much energy is stored as kinetic energy in the turbocharger and engine at the end of the transient. The fuel optimal control builds less kinetic energy in the engine, but more kinetic energy in the turbocharger than the time optimal control. This reduces the total amount of kinetic energy necessary to be able to meet  $P_{req}$ .

This energy difference scaled with the average efficiency of the engine is roughly of the same size as the difference in consumption between the criteria. Seeing that the kinetic energy in the engine is roughly 20 times larger than that in the turbocharger a lot can be gained by instead increasing the kinetic energy in the turbocharger and thus decrease the kinetic energy in the engine.

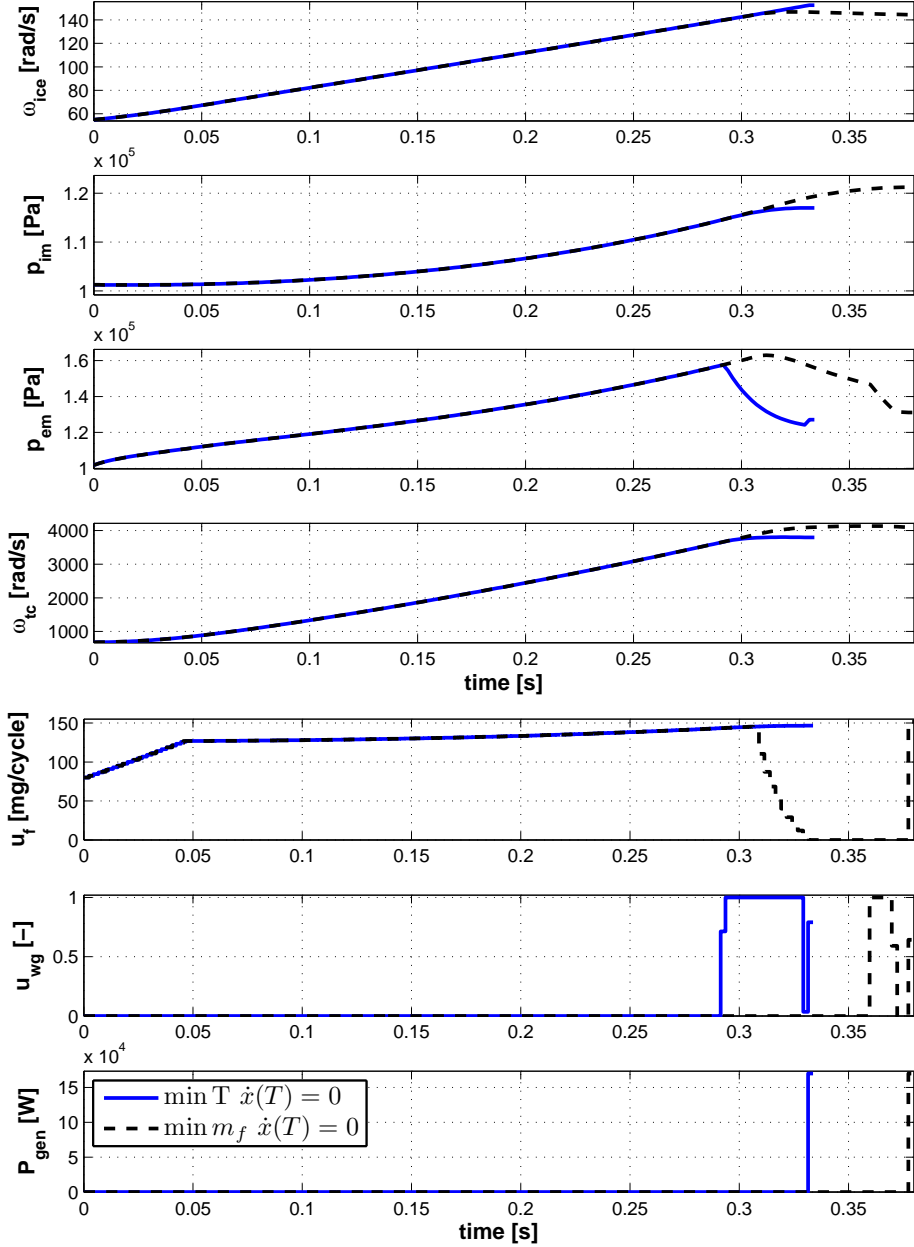


Figure 6: Time and fuel optimal solutions to a load transient from idle to 170 kW.

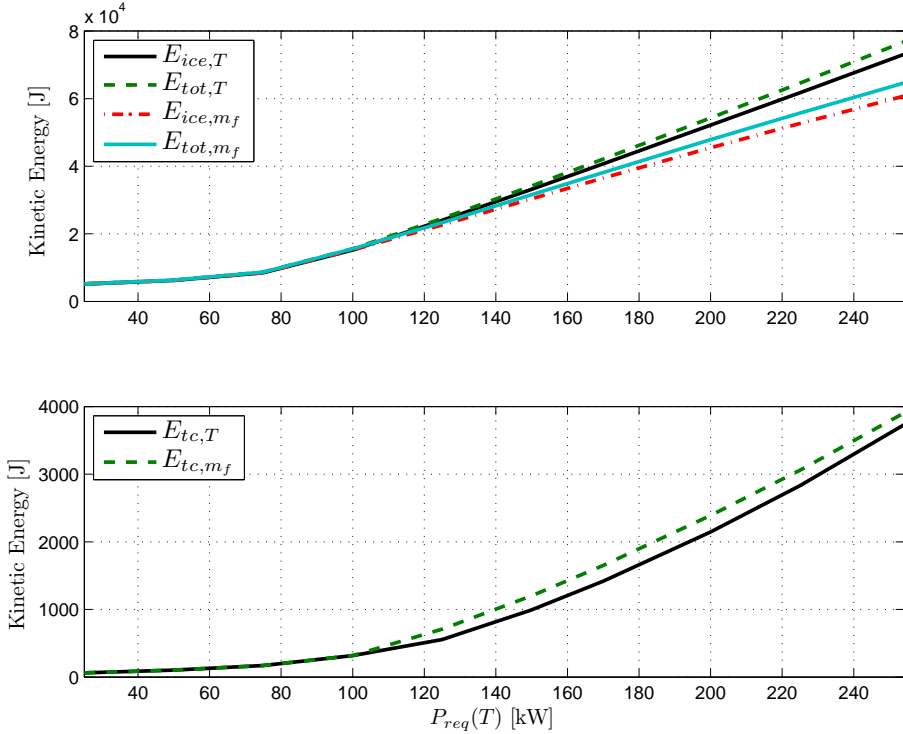


Figure 7: Top: Kinetic energy in the engine as well as the total kinetic energy in the system at time  $T$ . Bottom: Kinetic energy in the turbocharger at time  $T$ .

The time constant of the turbocharger is however larger than that of the engine. When limited by the smoke-limiter, the kinetic energy in the turbocharger increases with roughly 10kJ/s, whereas the kinetic energy of the engine increases with 100kJ/s, causing the two criteria to approach different stationary points. The difference in control of the turbocharger dynamics can be seen in Fig.6 ,  $t \in [0.28, 0.4]$ .

Where the time optimal control follows the smoke-limiter until the end and fully opens the wastegate to release the excess exhaust pressure as it approaches its stationary point, the fuel optimal control decreases and stops the fuel injection with the wastegate closed in order to build/maintain backpressure to convert to turbocharger speed and consequently intake manifold pressure. The transient ends with the wastegate being actuated to control the exhaust manifold pressure to ensure stationarity in  $p_{em}$ ,  $\omega_{tc}$  and  $p_{im}$  together with the final value of  $u_f$ .

In Fig. 8 the change in end time and fuel consumption as a function of  $P_{req}$  for the fuel optimal versus the time optimal transients is shown. In the studied interval the fuel economy of the fuel optimal solution, compared to the time optimal solution, improves with  $P_{req}$  and is between 3 % and 12 %. The corresponding time penalty however decreases with  $P_{req}$  and is between 21% and 9%.

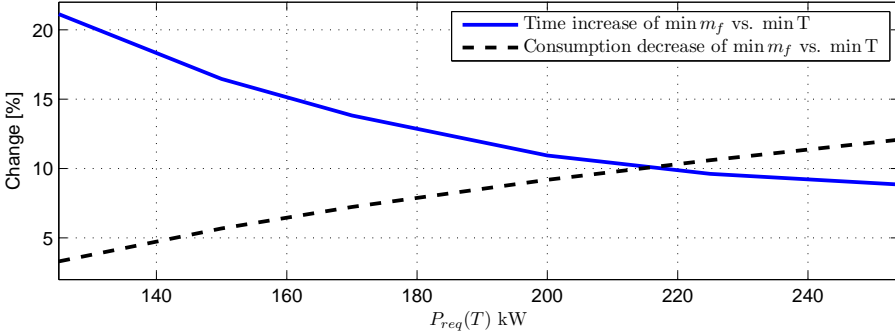


Figure 8: Change in time and consumption as a function of  $P_{req}$ .

### 5.3 Transients to the fuel optimal operating point

As seen in Fig. 5 none of the fuel optimal transients end in the fuel optimal operating point for that power. To reach the more efficient region of the engine map, more kinetic energy has to be stored in the turbocharger without increasing the kinetic energy in the engine. To accomplish this the engine needs to be braked by the generator, that is, energy has to be removed from the system. This is clearly not optimal if the aim is just to go from idle to a target power. However it does raise the question of how to, in a fuel optimal way, go to the fuel optimal operating point, and also how much it costs. In Fig. 9 fuel optimal transients are compared to fuel optimal transients to the fuel optimal operating point. These transients take roughly twice as long as the fuel optimal transients, and consume roughly three times the fuel. This comparison is however not entirely valid since the generated energy is also roughly 200 times larger. Whether this is optimal or not depends on what happens after the transient. To assess the optimality of such transients the requirements should be target energy and not target power, which is studied in Section 6.

## 6 Extending the Transients to Driving Missions

In Section 5 the optimal trajectories for steps in requested power is presented. A driving mission doesn't normally end when the requested power has been met, output power is usually requested for a period of time. Instead a driving mission for off-highway vehicles is often to move something between two locations. The most general definition of a driving mission is that a certain amount of energy has to be produced, as well as meeting the requested power. This is achieved by extending the problem defined in Eqs. (28)-(29) with Eq. (30).

$$\int_0^T P_{gen} dt = E_{req} , P_{gen} \leq P_{req} \quad (30)$$

The output power is allowed to vary, as long as it does not exceed the power requested. The end controls have to fulfill the requested power.  $E_{req}$  can thus

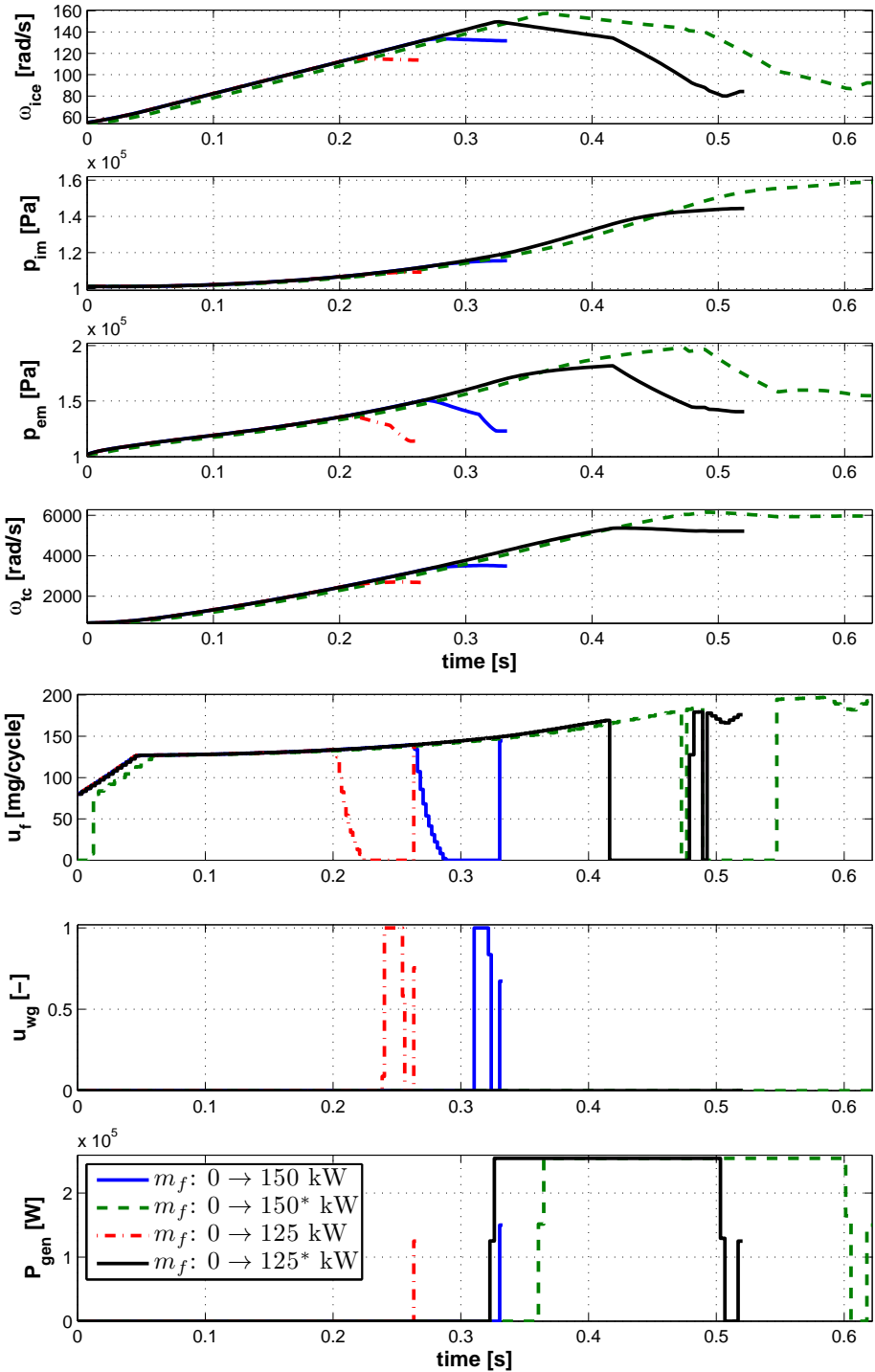


Figure 9: Comparison between fuel optimal transients and transients to the fuel optimal operating point. \* denotes the fuel optimal operating point.

be viewed as a measure of how large portions of the transients can be optimized when the operator applies a step in requested power before this power has to be met. In this study the results for three different requested powers,  $P_{req}$ , and five different requested energies,  $E_{req}$ , are discussed.

## 6.1 Fixed output transients

Allowing the output power to deviate from the requested may not always be desirable and therefore to study fixed power optimal control the problem is also solved as a two-phase problem. Where in the first phase  $P_{gen} = 0$  and in the second phase  $P_{gen} = P_{req}$  according to:

$$\text{Phase 1: } E_{gen}(T) = 0, P_{gen} = 0$$

$$\text{Phase 2: } E_{gen}(T) = E_{req}, P_{gen} = P_{req}$$

Since  $P_{gen}$ ,  $E_{req}$  are fixed in the second phase, the duration of this phase is fixed, however the switching time between the two phases is optimized.

An interesting property of the problem, is that the fixed output power solution, i.e. 2-phase solution, is qualitatively the same for both minimum time and minimum fuel. It is however also the same as the minimum time free output power solution, and thus follows the discussion for minimum time in Section 6.3.

## 6.2 Energy transients: Solution path

When solving minimum fuel required energy problems with PROPT the solution is often very oscillatory. Therefore the sum of the squared state derivatives with the weight  $w$  is added to the cost function, see Eq. (31). The problem is first solved with  $w = 0$  to benchmark the later solutions. Then the problem is solved iteratively first with a large  $w$  which is then decreased, with the solution for the last  $w$  hot-starting the next. In the ideal case  $w$  is decreased all the way to zero, and a smooth solution is obtained. This does not always work, and when not, a smooth solution with the lowest fuel consumption is selected.

$$\min m_f + w \int_0^T \dot{x}^T \dot{x} dt \quad (31)$$

An interesting property of the minimum time formulation is that above a certain  $E_{req}$  the solution is not unique. For lower  $E_{req}$  the solution is limited by the available engine power, but when the pressures and speeds have reached a level where it can produce more than the requested power the solution is no longer unique. This is because the output power is limited below the maximum power of the engine, resulting in several solutions where the excess energy is stored as kinetic energy in the engine itself, and thus resulting in an oscillatory solution, see Fig. 10. To handle this the same method as in [19] is used. First time is minimized and then a second problem is solved where fuel is minimized, with  $T \leq \min T + \epsilon$ , where  $\epsilon$  is selected so that the minimum time is rounded up to the nearest 100 microsecond. The obtained solution is both smooth and with lower fuel consumption and only negligible effects on the duration.

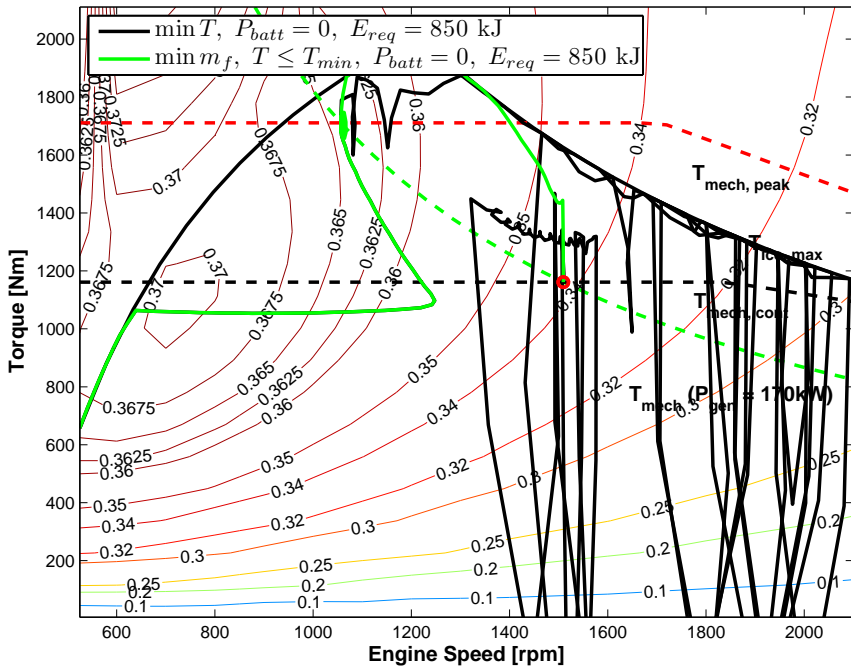


Figure 10: Two trajectories that are both time optimal, but the fuel consumptions differ by 10.6%. For higher  $E_{req}$  the minimum time solution is not unique.

### 6.3 Time Optimal Energy Transients

In Fig. 11 the time optimal solution for the different  $P_{req}$  and  $E_{req}$  are shown, and in Fig. 12 the state and control trajectories for  $P_{req} = 170$  kJ and three different  $E_{req}$  are shown. For the investigated output powers the characteristics are seen to be independent of  $P_{req}$  as well as of  $E_{req}$ , the solution for different  $E_{req}$  landing on top of each other.

The time optimal solution is to accelerate, following the smoke-limiter, to a higher engine speed than that of the target end operating point and then apply a step in generator power  $P_{gen} = 0 \rightarrow P_{req}$  and apply this power until  $E_{req}$  is reached. The main dependence on  $E_{req}$  is the length, which controls if the solution reaches the peak efficiency of the powertrain for  $P_{gen} = P_{req}$ , denoted  $\eta_{gs,max}(P_{req})$ , before  $E_{req}$  is produced.  $P_{req}$  controls at which engine speed the step is applied.

The engine accelerates with an overshoot in engine speed, kinetic energy which is used to produce power. The states then wander towards  $\eta_{gs,max}(P_{req})$  and, if  $E_{req}$  is large enough, stays there almost until the end. This stationary point is not smoke-limited. However, towards the end the wastegate opens, releasing some of the energy stored in the exhaust manifold, resulting in a slight decrease in turbocharger speed as it approaches the final operating point, a point that is on the smoke-limit. The efficiency of this point is lower than during the stationary phase, e.g.  $E_{req} = 850$  kJ,  $1.5 \leq t \leq 4.5$ , however the efficiency increase during the transient going there is higher than the efficiency loss of being there for one sample. This is related to the pumping torque of the engine, see Eq. (17). The time constant from  $u_{wg}$  to  $p_{em}$  is much shorter than to  $p_{im}$  due to the inertia of the turbo. The decrease in  $T_{pump}$  during the transient is therefore larger than the increase of being in a suboptimal point in the last time step.

### 6.4 Fuel Optimal Energy Transients

The fuel optimal solutions for the different powers,  $P_{req}$ , and energies,  $E_{req}$ , are shown in Fig. 13, and in Fig. 14 the state and control trajectories for  $P_{req} = 170$  kW and three different  $E_{req}$  are shown. The characteristics of the solutions are found to be dependent on both  $P_{req}$  and  $E_{req}$ . The solutions follow the maximum torque line with an end acceleration deviating from the maximum torque line towards the point that fulfills the end constraints. If  $E_{req}$  is large enough, or  $P_{req}$  small enough, the solution does not deviate from the maximum torque line. In both cases  $P_{gen} < P_{req}$  for the largest part of the transient.

The control accelerates with  $P_{gen} > 0$  along the maximum torque line and smoke-limiter and if the required energy is large enough the control has a stationary phase at the peak efficiency of the GenSet, denoted  $\eta_{gs,max}$ , before a final acceleration towards  $\eta_{gs,max}(P_{req})$ . For lower energies the control departs from the maximum torque-line during the final acceleration.

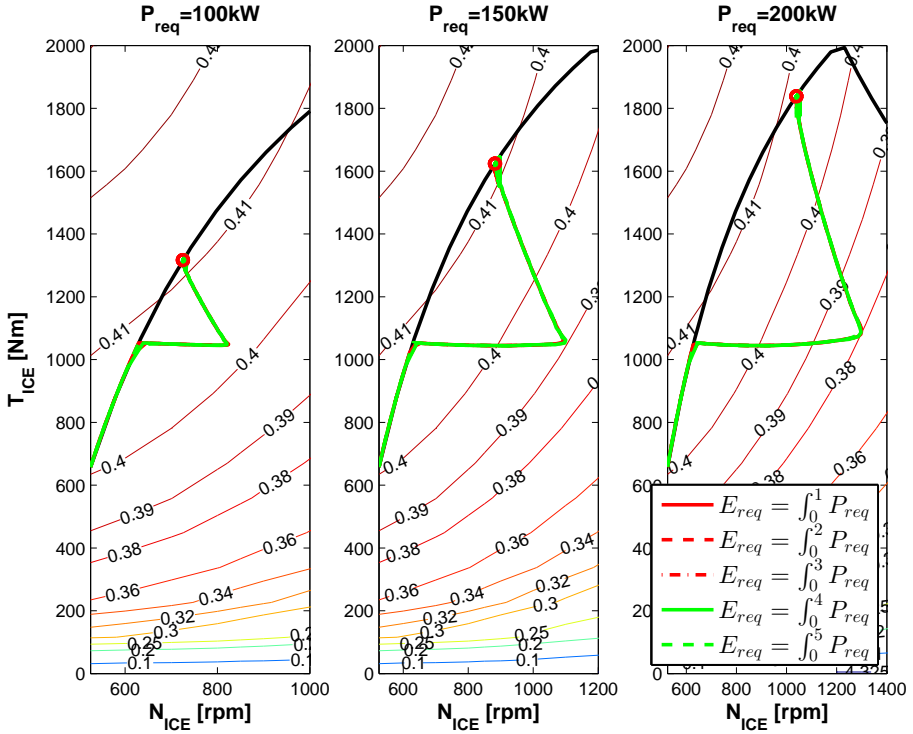


Figure 11: Minimum time transients from idle to  $P_{req} = [100 \ 150 \ 200]$  kW for different  $E_{req}$ . The characteristics of the solution are independent of both  $E_{req}$  and  $P_{req}$ .

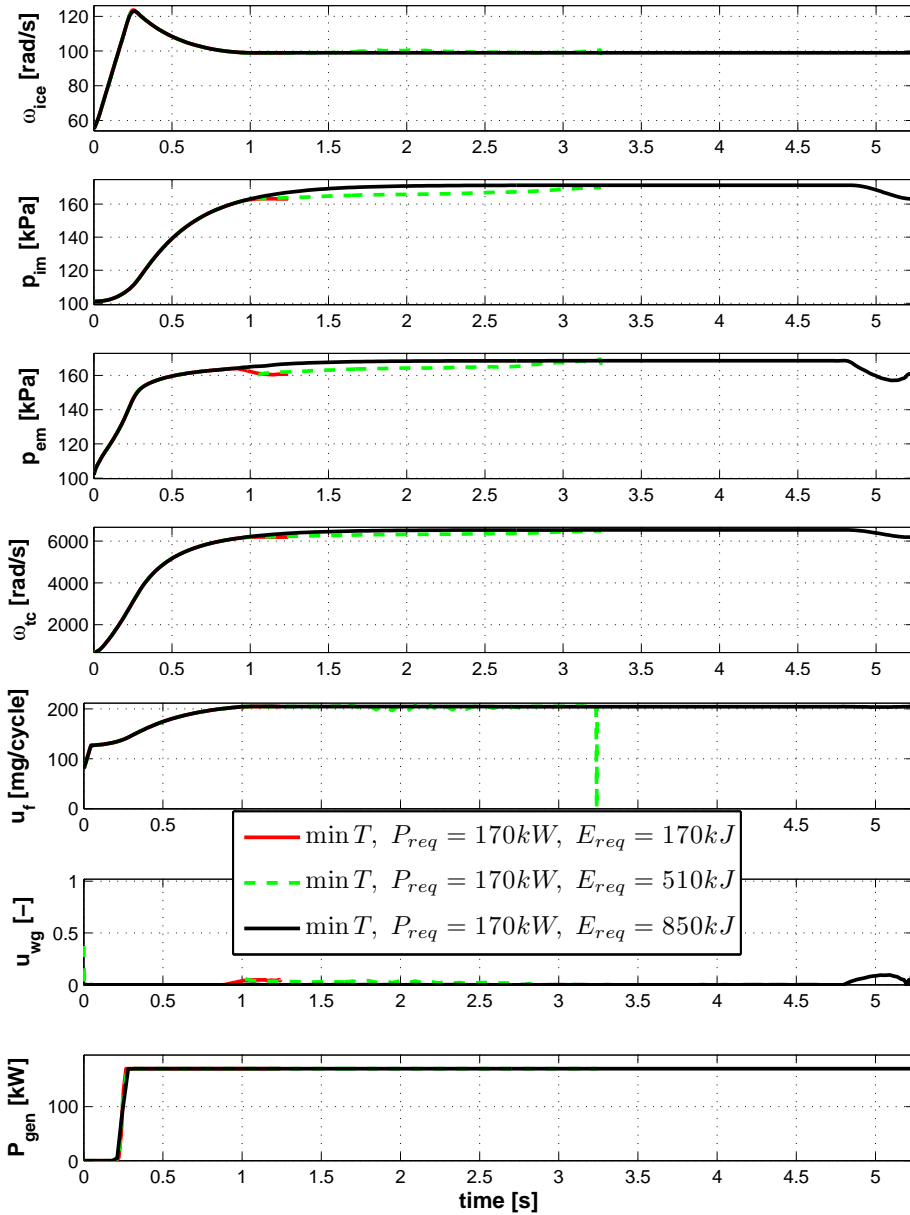


Figure 12: State and control trajectories for  $\min T$ ,  $P_{req} = 170 \text{ kW}$  for different  $E_{req}$ .

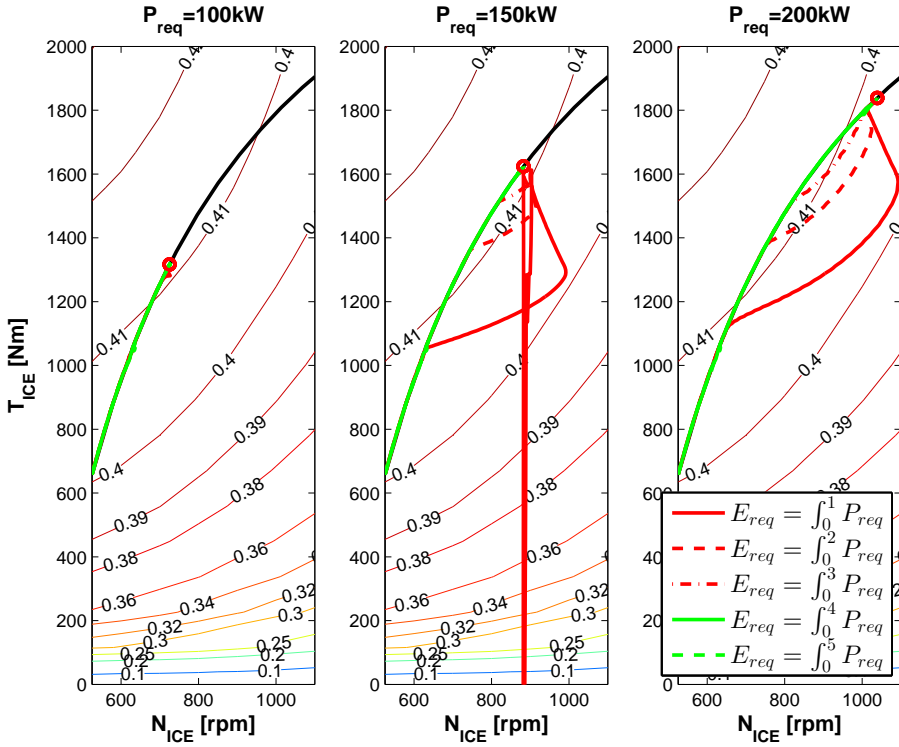


Figure 13: Minimum fuel transients from idle to  $P_{req} = [100 \ 150 \ 200]$  kW for different  $E_{req}$ .

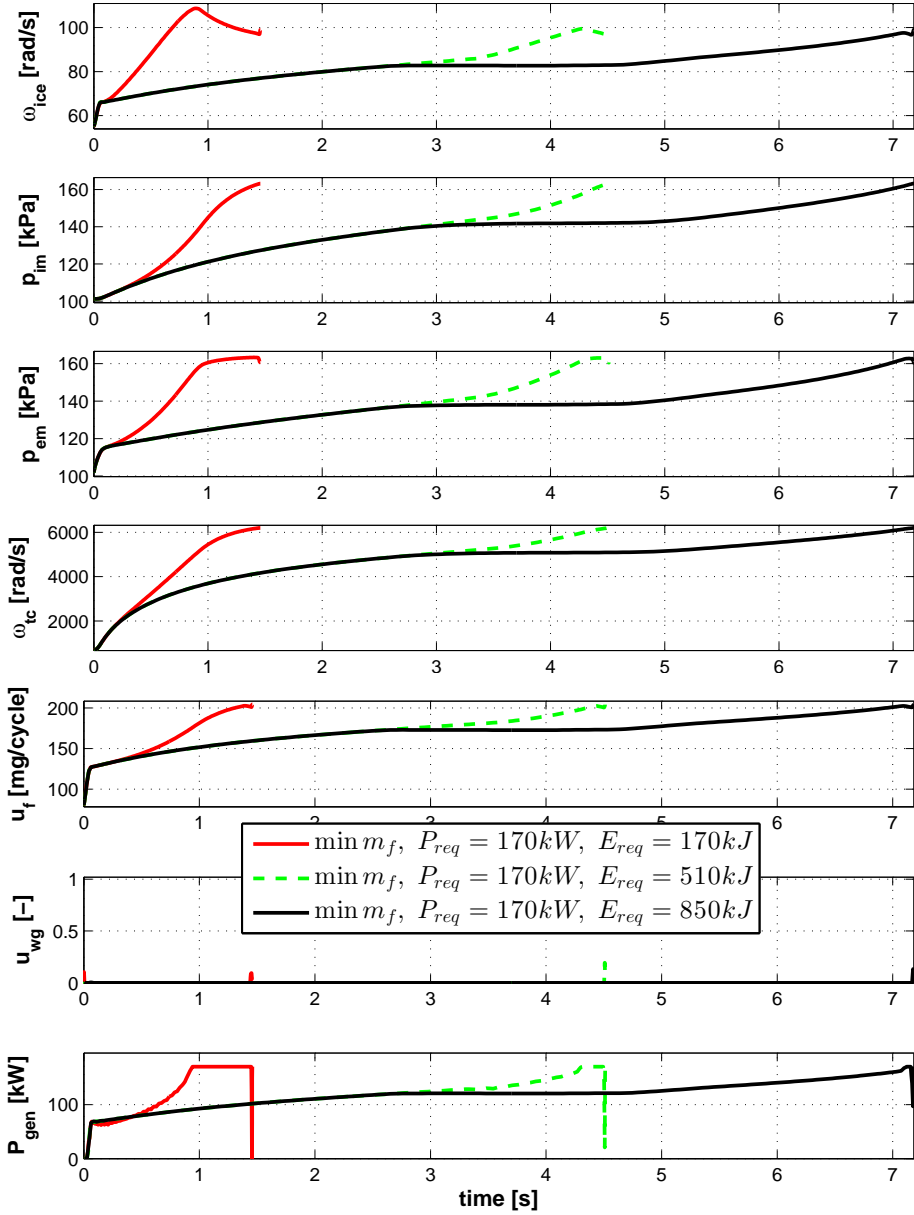


Figure 14: State and control trajectories for  $\min m_f$ ,  $P_{req} = 170 \text{ kW}$  for different  $E_{req}$ .

Table 2: The change in fuel consumption and duration of the different formulations compared to a power step to 170 kW.

$E_{req}(T)$		$\min m_f$	$\min m_{f2-phase}$	$\min T$	$\min T_{2-phase}$
-	$\Delta T[\%]$	0.9	-	0	-
	$\Delta m_f[\%]$	-2.1	-	0	-
170kJ	$\Delta T[\%]$	2.4	-1.7	-1.7	-1.7
	$\Delta m_f[\%]$	-11.5	-11.4	-11.4	-11.4
340kJ	$\Delta T[\%]$	15.3	-1.7	-1.7	-1.7
	$\Delta m_f[\%]$	-11.7	-11.4	-11.4	-11.4
510kJ	$\Delta T[\%]$	22.1	-1.7	-1.7	-1.7
	$\Delta m_f[\%]$	-11.8	-11.4	-11.4	-11.4
680kJ	$\Delta T[\%]$	27	-1.7	-1.7	-1.7
	$\Delta m_f[\%]$	-11.9	-11.4	-11.4	-11.4
850kJ	$\Delta T[\%]$	34.7	-1.7	-1.7	-1.7
	$\Delta m_f[\%]$	-12	-11.4	-11.4	-11.4

## 6.5 Energy transients: Results

For comparison  $P_{req} = 170$  kW is selected. To be able to compare the solutions to the different optimization problems and requested energies all controls are augmented so that they all produce 850 kJ, i.e. all shorter driving missions are extended, by maintaining the end point until the target energy is reached. These are then evaluated relative the power transients discussed in Section 5. The trajectories for the different problems are all compared in Fig. 15.

Since  $\min T$ ,  $\min T_{2-phase}$ , and  $\min m_{f2-phase}$  are insensitive to variations in  $E_{req}$  only  $E_{req} = 850$  kJ is shown. These three curves are also very similar ending up being plotted on top of each other. The  $\min m_f$  problem is thus the only problem where the characteristics change depending on  $E_{req}$ . The time and fuel consumptions for the different problems are shown in Table 2. Doing a fuel optimal power step to 170 kW and then staying there results in 2% better fuel economy compared to a time optimal power step. However, this comes at a price of 0.9% increase in duration.

With requirements on produced energy it is seen that the results are the same for all but  $\min m_f$  for the studied energies. The resulting consumption decrease is 11.4% and the duration decrease is 1.7%. For  $\min m_f$  the fuel economy increases with  $E_{req}$ , however the duration also increases with  $E_{req}$ . The control follows the maximum torque line and, if long enough, approaches the point of peak efficiency where  $P_{gen} \approx 120$  kW. The consumption decrease ranges from 11.4 to 12% and the duration increase from 15.3 to 34.7%. Interesting to note is that the minimum time solution only consumes up to 0.5 % more fuel but is up to 35 % faster.

## 7 More complex output profiles

So far the studied problems have been from idle to a specific  $P_{req}$  with different requirements on produced energy. That raises the question as to whether these

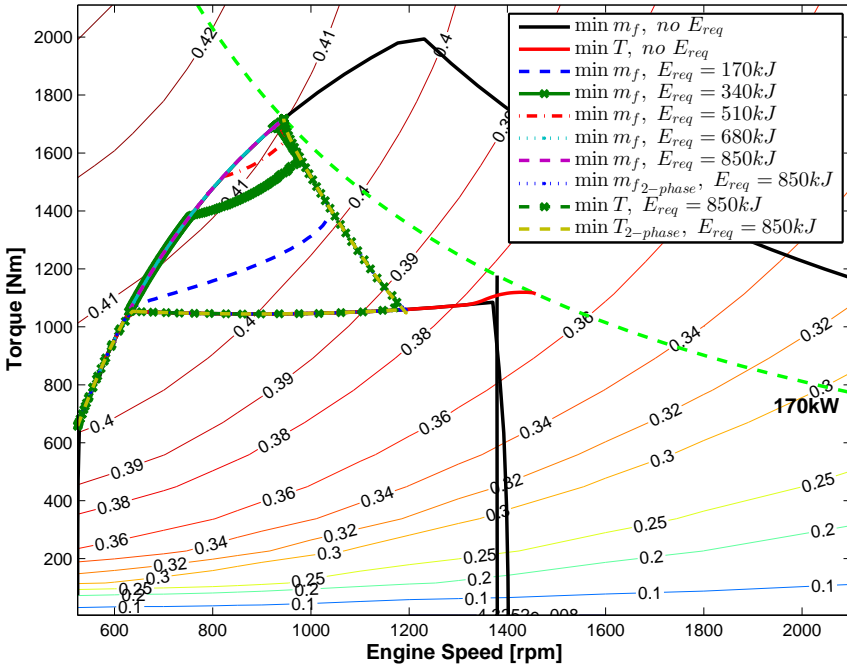


Figure 15: Torque vs engine speed for  $\min m_f/T$  one and two-phase solutions as well as for a step in power without requirements on produced energy.

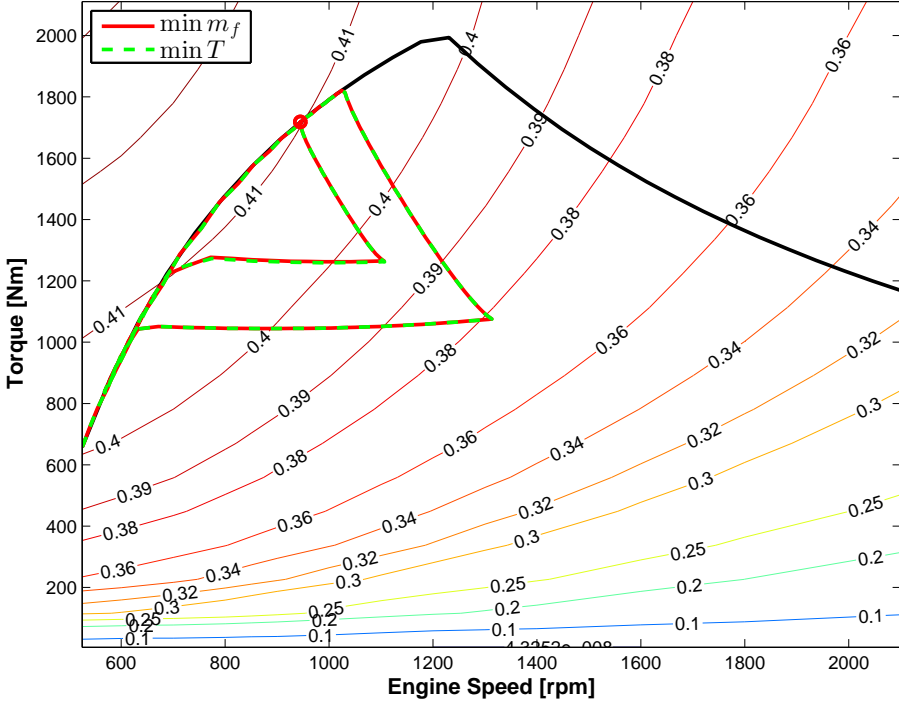


Figure 16: Engine speed and torque trajectories for  $\min T_{4\text{-phase}}$  and  $\min m_{f4\text{-phase}}$ . The solutions are similar despite different criteria.

results hold for more complex output profiles. In order to study this a problem is formulated where the generator is required to go from idle to 200 kW and produce 200 kJ, from there to 50 kW and produce 50 kJ and finally to 170 kW to produce 170 kJ and end in a stationary point. For  $\min m_f$  it is seen in Section 6.4 that the solution is dictated by the peak efficiency of the engine as well as the end constraints, and would therefore not follow the desired power trajectory. Therefore the problem is solved with fixed output power, implemented as a 4-phase problem where  $P_{gen} = 0$  kW in phase 1,  $P_{gen} = 200$  kW in phase 2,  $P_{gen} = 50$  kW in phase 3, and  $P_{gen} = 170$  kW in phase 4. This is solved both for minimum time and minimum fuel and the results are shown in Fig. 16-17. It is seen that both minimum fuel and minimum time produce similar solutions. The difference in fuel consumption is less than 0.04‰ and the difference in duration is less than one microsecond. Looking at Fig. 17 the controls follow the same characteristics as previously discussed. The engine accelerates to a higher engine speed, converting the kinetic energy to output power. When going from a higher output power to a lower the solution follows the maximum torque line. The only difference between the two criteria is the wastegate actuation, which qualitatively is the same, the time at which it opens and closes is however slightly different.

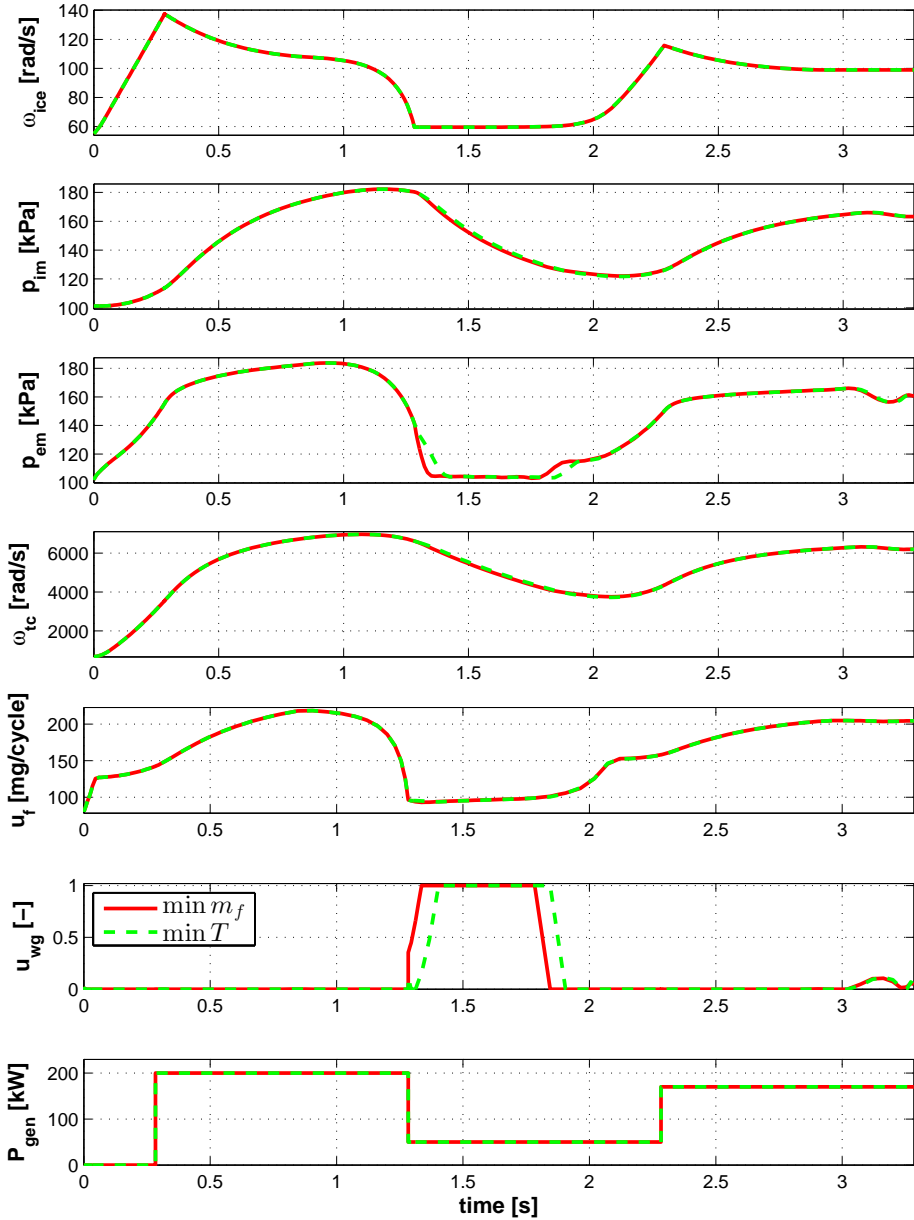


Figure 17: State and control trajectories for  $\min T_{4-phase}$  and  $\min m_{f4-phase}$ .

## 8 Discussion

The formulation and solution of optimal transients in a diesel-electric powertrain is studied. First the minimum fuel and minimum time control to steps in requested powers is formulated, solved, and discussed. The effects of the end constraints on the control trajectories have been studied through changing the end constraints of the optimization problem. It is shown that the optimal solutions are different for high and low requested powers. For high power transients the time and fuel optimal controls are very similar despite the criteria being different. The optimal control is to put as much energy as possible into the system, following the smoke-limiter and maximum torque line. The difference between the two criteria is which operating point they approach and also the fine tuning to get there. Whereas the time optimal control follows the smoke-limiter until the end, the fuel optimal control cuts off the fuel injection and ends near the operating point with highest efficiency obtainable without using the generator. This operating point requires more kinetic energy in the turbocharger which takes longer to build, but reduces the total amount of kinetic energy necessary to produce the requested power. It is also shown that without requiring a certain produced energy, it is not optimal to go to the fuel optimal operating point, due to the energy required to build enough kinetic energy in the turbocharger.

The power transient formulation is then extended to driving missions, defined as that the powertrain has to produce a certain amount of energy. This can be interpreted as how much freedom the optimization has when the operator applies a step in requested power before this power has to be produced. During which time the output power is allowed to vary. In order to also study fixed output driving missions the problem is also solved as a 2-phase problem with the output power fixed. This is then solved for both minimum time and minimum fuel.

For  $\min T$ ,  $\min m_{f_{2-phase}}$  and  $\min T_{2-phase}$  the characteristics of the solution are independent of requested energy and requested power. The optimal solution is to accelerate the engine, following the smoke-limiter, and then use the excess kinetic energy to produce power and approach the maximum efficiency point for the requested power. At which engine speed this step occurs does however depend on the requested power. The solutions to a sequence of steps in power are also seen to have the same characteristics. For  $\min m_f$  the solution changes with  $E_{req}$  and  $P_{req}$ . For lower requested energies the solution is to follow the maximum torque line, then accelerate the engine whilst producing power, and then finally approach the end operating point from a higher engine speed. For higher requested energies the engine accelerates along the maximum torque line and also has a stationary phase at the peak efficiency operating point, the end point is then approached following the maximum torque line.

The optimal controls are evaluated relative a time optimal power transient to 170 kW. The result shows that compared to just doing a time optimal power step and then holding the end controls large gains in fuel economy can be made. All evaluated controls offer roughly 11-12% reduction in consumption, but the time required differs. Interesting to note is that  $\min T$ ,  $\min m_{f_{2-phase}}$  and  $\min T_{2-phase}$  all produce roughly the same solution despite the criteria being

different. These strategies offer almost optimal fuel economy and are 15-35% faster, depending on amount of requested energy.

## 9 Conclusions

Time and fuel optimal transients in a diesel-electric system have been studied. From the performed studies and discussions a couple of conclusions can be drawn:

1. The turbocharger dynamics have a strong influence on the solution. This is seen from that the smoke-limiter is active in all studied transients.
2. The freedom to select engine speed can be used to improve response time of the powertrain. The time optimal solutions use the freedom to reduce turbocharger lag.
3. The stationary points of the solutions are, as expected, dictated by the efficiency map. The time and fuel optimal solutions have different stationary points.
4. The minimum time solution only consumes up to 0.5 % more fuel than the minimum fuel solution, but is up to 35 % faster.
5. Forcing the solution to follow a given output power trajectory yields the same solutions as the minimum time solution, regardless of criteria.

## References

- [1] Michael Benz, Markus Hehn, Christopher H. Onder, and Lino Guzzella. Model-based actuator trajectories optimization for a diesel engine using a direct method. *J Eng Gas Turb Power*, 133(3):298–312, 2011.
- [2] S Di Cairano, W Liang, I V Kolmanovsky, M L Kuang, and A M Phillips. Power smoothing energy management and its application to a series hybrid powertrain. *IEEE Transactions on Control Systems Technology*, 21(6):2091–2103, 2013.
- [3] Ximing Cheng, Fengchun Sun, and Minggao Ouyang. Novel load following control of an auxiliary power unit. In *Proceedings of the 6th World Congress on Intelligent Control and Automation*, Dalian, China, 2006.
- [4] Lars Eriksson. Modeling and control of turbocharged SI and DI engines. *Oil & Gas Science and Technology - Rev. IFP*, 62(4):523–538, 2007.
- [5] Anirudh Gautam and Avinash Kumar Agarwal. Comparative evaluation of turbochargers for high horsepower diesel-electric locomotives. In *SAE Technical Paper 2013-01-0930*, Detroit, Michigan, USA, 2013.

- [6] Jukka Halme and Jussi Suomela. Optimal efficiency based gen-set control for series hybrid work machine. In *IEEE VPPC 2012 – The 8th IEEE Vehicle Power and Propulsion Conference*, Seoul, Korea, October 2012.
- [7] B He and M Yang. Optimisation-based energy management of series hybrid vehicles considering transient behaviour. *Int. J. Alternative Propulsion*, 1(1):79–96, 2005.
- [8] Walter A. Hill, Greg Creelman, and Lothar Mischke. Control strategy for an icebreaker propulsion system. *IEEE Transactions on Industry Applications*, 28(4):887–892, 1992.
- [9] Boris Houska, Hans Joachim Ferreau, and Moritz Diehl. ACADO toolkit - an open source framework for automatic control and dynamic optimization. *Optimal Control Applications & Methods*, 32(3):298–312, 2011.
- [10] Sang-Min Kim and Seung-Ki Sul. Control of rubber tyred gantry crane with energy storage based on supercapacitor bank. *IEEE Transactions on Power Electronics*, 21(5):1420–1427, 2006.
- [11] Tae-Suk Kwon, Seon-Woo Lee, Seung-Ki Sul, Cheol-Gyu Park, Nag-In Kim, Byung il Kang, and Min-Seok Hong. Power control algorithm for hybrid excavator with supercapacitor. *IEEE Transactions on Industry Applications*, 46(4):1447–1455, 2010.
- [12] N P Kyrtatos, E I Tzanos, and C I Papadopoulos. Diesel engine control optimization for transient operation with lean/rich switches. *J Eng Gas Turb Power*, 4(3):219–232, 2003.
- [13] Tomas Nilsson, Anders Fröberg, and Jan Åslund. Optimal operation of a turbocharged diesel engine during transients. In *SAE Technical Paper 2012-01-0711*, Detroit, Michigan, USA, 2012.
- [14] C E Nino-Baron, A R Tariq, Guoming Zhu, and E G Strangas. Trajectory optimization for the engine-generator operation of a series hybrid electric vehicle. *IEEE Transactions on Vehicular Technology*, 60(6):2438–2447, 2011.
- [15] Constantine D Rakopoulos and Evangelos G Giakoumis. *Diesel engine transient operation - Principles of operation and simulation analysis*. Springer, 2009.
- [16] V Sezer, M Gokasan, and S Bogosyan. A novel ecms and combined cost map approach for high-efficiency series hybrid electric vehicles. *IEEE Transactions on Vehicular Technology*, 60(8):3557–3570, 2011.
- [17] Martin Sivertsson and Lars Eriksson. Time and fuel optimal power response of a diesel-electric powertrain. In *E-COSM'12 – IFAC Workshop on Engine and Powertrain Control, Simulation and Modeling*, Paris, France, October 2012.

- [18] Martin Sivertsson and Lars Eriksson. Optimal step responses in diesel-electric systems. In *Mechatronics'12 – The 13th Mechatronics Forum International Conference*, Linz, Austria, September 2012.
- [19] Martin Sivertsson and Lars Eriksson. Optimal transient control and effects of a small energy storage for a diesel-electric powertrain. In *AAC'13–The 7th IFAC Symposium on Advances in Automotive Control*, Tokyo, Japan, September 2013.
- [20] TOMLAB. PROPT - Matlab Optimal Control Software, "<http://www.tomdyn.com/>", 2012.
- [21] Johan Wahlström and Lars Eriksson. Modelling diesel engines with a variable-geometry turbocharger and exhaust gas recirculation by optimization of model parameters for capturing non-linear system dynamics. *Proceedings of the Institution of Mechanical Engineers, Part D, Journal of Automobile Engineering*, 225(7):960–986, 2011.
- [22] Fengjun Yan, Junmin Wang, and Kaisheng Huang. Hybrid electric vehicle model predictive control torque-split strategy incorporating engine transient characteristics. *IEEE Transactions on Vehicular Technology*, 61(6):2458–2467, 2012.
- [23] Hyunjae Yoo, Byung-Geuk Cho, Seung-Ki Sul, Sang-Min Kim, and Yongho Park. A power flow control strategy for optimal fuel efficiency of a variable speed engine-generator based series hybrid electric vehicle. In *IEEE ECCE'09 Energy Conversion Congress and Exposition*, pages 443–450, 2009.

## Appendix A: Model Data

Table 3: Nomenclature

Symbol	Description	Unit
$\omega_{ice}$	Engine speed	$rad/s$
$p_{im}$	Intake manifold pressure	$Pa$
$p_{em}$	Exhaust manifold pressure	$Pa$
$\omega_{tc}$	Turbocharger speed	$rad/s$
$u_f$	Injected fuel mass	$mg/cycle$
$u_{wg}$	Wastegate position	—
$P_{gen}$	Generator power	$W$
$P_{mech}$	Mechanical generator power	$W$
$P_{req}$	Requested power	$W$
$E_{req}$	Required energy	$J$
$\dot{m}_c$	Compressor massflow	$kg/s$
$\dot{m}_{c,corr}$	Corrected compressor massflow	$kg/s$
$\Pi_c$	Pressure ratio over compressor	—
$\Pi_{c,max}$	Pressure ratio for zero massflow	—
$P_c$	Compressor power	$W$
$\dot{m}_{ac}$	Massflow after compressor	$kg/s$
$\dot{m}_f$	Fuelflow	$kg/s$
$\lambda$	Air/fuel ratio	—
$\phi_\lambda$	Smoke-limiter	$kg/s$
$T_{ice}$	Engine torque	$Nm$
$T_{ig}$	Indicated gross torque	$Nm$
$T_{pump}$	Pumping torque	$Nm$
$T_{fric}$	Friction torque	$Nm$
$q_{in}$	Specific energy of the charge	$J/kg$
$x_p$	Pressure quotient from combustion	—
$T_{em}$	Exhaust manifold temperature	$K$
$\Pi_t$	Pressure ratio over turbine	—
$\Pi_t^*$	Usefull pressure ratio over turbine	—
$\Psi_t$	Massflow parameter	—
$\dot{m}_t$	Turbine massflow	$kg/s$
$P_t$	Turbine power	$W$
$\Pi_{wg}$	Pressure ratio over wastegate	—
$\Psi_{wg}$	Massflow parameter	—
$\dot{m}_{wg}$	Wastegate massflow	$kg/s$
$\eta_{gs,max}$	Maximum efficiency of the GenSet	—
$\eta_{gs,max}(P)$	Maximum efficiency for power $P$ of the GenSet	—

Table 4: Constants used

Symbol	Description	Value	Unit
$p_{amb}$	Ambient pressure	$1.011 \cdot 10^5$	$Pa$
$T_{amb}$	Ambient temperature	298.46	$K$
$p_{ref}$	Reference pressure	$1.011 \cdot 10^5$	$Pa$
$T_{ref}$	Reference temperature	298.46	$K$
$c_{pa}$	Spec. heat capacity of air, constant pressure	1011	$J/(kg \cdot K)$
$c_{va}$	Spec. heat capacity of air, constant volume	724	$J/(kg \cdot K)$
$\gamma_a$	Spec. heat capacity ratio of air	1.3964	-
$R_a$	Gas constant, air	287	$J/(kg \cdot K)$
$c_{pe}$	Spec. heat capacity of exhaust gas, constant pressure	1332	$J/(kg \cdot K)$
$\gamma_e$	Spec. heat capacity ratio of exhaust gas	1.2734	-
$R_e$	Gas constant, exhaust gas	286	$J/(kg \cdot K)$
$\gamma_{cyl}$	Spec. heat capacity ratio of cylinder gas	1.35004	-
$T_{im}$	Temperature intake manifold	300.6186	$K$
$p_{es}$	Pressure in exhaust system	$1.011 \cdot 10^5$	$Pa$
$(A/F)_s$	Stoichiometric oxygen-fuel ratio	14.57	-
$q_{HV}$	Heating value, diesel	$42.9 \cdot 10^6$	$J/kg$

Table 5: Parameters used

Symbol	Description	Value	Unit
$n_{cyl}$	Number of cylinders	6	-
$V_D$	Engine displacement	0.0127	$m^3$
$r_c$	Compression ratio	17.3	-
$J_{GenSet}$	Inertia of the engine-generator	3.5	$kg \cdot m^2$
$V_{is}$	Volume of intake system	0.0218	$m^3$
$R_c$	Compressor radius	0.04	$m$
$\Psi_{max}$	Max. compressor head parameter	1.5927	-
$\dot{m}_{c,corr,max}$	Max. corrected compressor mass-flow	0.5462	$kg/s$
$\eta_c$	Compressor efficiency	0.5376	-
$\eta_{vol}$	Volumetric efficiency	0.8928	-
$\eta_{ig,ch}$	Combustion chamber efficiency	0.6774	-
$c_{fr,1}$	Friction coefficient	$8.4100 \cdot 10^{-5}$	-
$c_{fr,2}$	Friction coefficient	$-5.6039 \cdot 10^{-3}$	-
$c_{fr,3}$	Friction coefficient	0.4758	-
$\eta_{sc}$	Non-ideal Seliger cycle compensation	1.0540	-
$x_{cv}$	Ratio of fuel burnt during constant volume	0.4046	-
$V_{em}$	Volume of exhaust manifold	0.0199	$m^3$
$J_{tc}$	Turbocharger inertia	$1.9662 \cdot 10^{-4}$	$kg \cdot m^2$
$w_{fric}$	Turbocharger friction	$2.4358 \cdot 10^{-5}$	$kg \cdot m^2/rad$
$A_{t,eff}$	Effective turbine area	$9.8938 \cdot 10^{-4}$	$m^3$
$\eta_t$	Turbine efficiency	0.7278	-
$c_{wg,1}$	Wastegate parameter	0.6679	-
$c_{wg,2}$	Wastegate parameter	5.3039	-
$A_{wg,eff}$	Effective wastegate area	$8.8357 \cdot 10^{-4}$	$m^3$
$\lambda_{min}$	Minimum air/fuel ratio, smoke-limit	1.2	-



# Optimal Transient Control Trajectories in Diesel-Electric Systems-Part 2: Generator and Energy Storage Effects<sup>†</sup>

Martin Sivertsson<sup>a</sup> and Lars Eriksson<sup>a</sup>

<sup>a</sup>*Vehicular Systems, Department of Electrical Engineering,  
Linköping University, SE-581 83 Linköping, Sweden.*

---

<sup>†</sup>This is a formatted version of “Optimal Transient Control Trajectories in Diesel-Electric Systems-Part 2: Generator and Energy Storage Effects” by Martin Sivertsson and Lars Eriksson, *Journal of Engineering for Gas Turbines and Power*, Volume 137, Number 2. ©ASME 2015. Reproduced with the permission of ASME. The original paper can be found at [asmedigitalcollection.asme.org](http://asmedigitalcollection.asme.org) <http://asmedigitalcollection.asme.org/>, and can be found using the Digital Object Identifier (DOI): 10.1115/1.4028360. The formatting is restricted to changing the article into a single-column format, adjusting sizes of figures and tables, and adjusting the referencing style.

## **Abstract**

The effects of generator model and energy storage on the optimal control of a diesel-electric powertrain in transient operation is studied. Two different types of problems are solved, minimum fuel and minimum time, with different generator models and limits as well as with an extra energy storage. For this aim a 4-state mean value engine model is used together with models for the generator and energy storage losses. In the optimization both the engines output power and speed are free variables. The considered transients are steps from idle to target power with different amounts of freedom, defined as requirements on produced energy, before the requested power has to be met. The main characteristics are seen to be independent of generator model and limits, they however shift the peak efficiency regions and therefore the stationary points. For minimum fuel transients the energy storage remains virtually unused for all requested energies, for minimum time it is used to reduce the response time. The generator limits are found to have the biggest impact on the fuel economy, whereas an energy storage could significantly reduce the response time. The possibility to reduce the response time is seen to hold for a large range of values of energy storage parameters. The minimum fuel solutions remain unaffected when changing the energy storage parameters, implying it is not beneficial to use an energy storage if fuel consumption is to be minimized. Close to the minimum time solution the fuel consumption with low required energy is quite sensitive to variations in duration, for larger energies it is not. Near the minimum fuel solution changes in duration have only minor effects on the fuel consumption.

# Introduction

A diesel-electric powertrain has no mechanical connection between the combustion engine and the wheels, introducing an extra degree of freedom since the engine speed can be controlled independently of the wheel speed. This offers the potential of both optimizing the performance and consumption since the operating point of the diesel engine can be controlled more freely than in a conventional powertrain. An open question is how to optimally control the engine-generator (GenSet) between two different outputs, especially when the diesel engine is turbocharged.

The literature regarding optimal control of diesel powertrains with the freedom of selecting engine speed is rather scarce. However two papers are found that explicitly study fuel or time optimal control of the diesel engine in transient operation, optimizing engine speed. [3] studies the control of a naturally aspirated diesel engine and use the stationary maps to model the efficiency. While [2] studies fuel optimal control of a turbocharged engine using a simple model and with the output trajectory fixed.

This paper is the second part of a two-part paper, studying fuel and time optimal control of a diesel electric powertrain with both engine speed and output power free variables in the optimization, using a model that incorporates both engine and turbocharger dynamics as well as emptying and filling of the manifolds. The first part, see [5], describes the model used and studies formulating the problem and solution of optimal transient control problems in diesel-electric powertrains. The focus of that study is the characteristics of the solution as a result of the engine properties, why the generator is lossless and considered ideal. This second part instead studies the effect of the generator model and limits as well as what effect adding an energy storage has on the optimal control trajectories.

The main contributions of the paper are: i) How a non-ideal generator changes the results from part 1. ii) A detailed study of how the energy storage efficiency influences the optimal solution. iii) Insights into optimal sizing of the energy storage, how it depends on the energy storage efficiency, and also what the limiting factors are. iv) A study on the trade-off between the minimum time and minimum fuel solutions, and how it changes with the presence of an energy storage.

## Outline

In Section 1 the additions to the model used in part 1 are presented. In Section 2 the problem is formulated and the solution procedure is described in Section 2.3. Section 3 discusses how the generator model affects the solution, whereas Section 4 summarizes the effects of the generator limits and Section 5 the effects of adding an energy storage, from [4]. In Section 7 the impact of energy storage properties is studied and in Section 8 the sensitivity of the minimum time solution is studied, before the paper is summarized with a concluding discussion in Section 9.

# 1 Model

The engine model used is the same as in part 1, but now considering both an energy storage and a model for the generator losses. The model is a nonlinear, four state, three input mean value engine model (MVEM), used together with models for the generator and energy storage losses, presented below. The states of the MVEM are engine speed,  $\omega_{ice}$ , inlet manifold pressure,  $p_{im}$ , exhaust manifold pressure,  $p_{em}$ , turbocharger speed,  $\omega_{tc}$ . The model is augmented with two summation states for the charge in the energy storage,  $q$ , and produced energy of the powertrain,  $E_{out}$  defined as:

$$\frac{dq}{dt} = -I_{batt} \quad (1)$$

$$\frac{dE_{out}}{dt} = P_{out} \quad (2)$$

The controls are injected fuel mass,  $u_f$ , wastegate position,  $u_{wg}$ , generator power,  $P_{gen}$ , and power from the energy storage,  $P_{batt}$ . For a complete description of the symbols used in this paper, see Table 3.

## 1.1 Energy Storage

The energy storage is modeled as an equivalent circuit according to:

$$I_{batt} = \frac{U_{oc} - \sqrt{U_{oc}^2 - 4R_i P_{batt}}}{2R_i} \quad (3)$$

The model for the energy storage has two tuning parameters,  $U_{oc}$  and  $R_i$ , with assumed reasonable values shown in Table 1. The impact of these values are studied in Section 7.

## 1.2 Generator

Inspired by eq. 4.15 in [1] the generator is modeled according to:

$$P_{loss} = P_{gen}^2 \left( \frac{c_{gen,1}}{\omega_{ice}^2} + c_{gen,2} \right) + \omega_{ice} c_{gen,3} + c_{gen,4} \quad (4)$$

$$P_{mech} = P_{gen} + P_{loss} \quad (5)$$

$$P_{out} = P_{gen} + P_{batt} \quad (6)$$

$P_{gen}$  is the electric power,  $P_{mech}$  the mechanical power of the generator, and  $P_{out}$  is the output power of the powertrain.  $P_{mech}$  has two limits, one for peak power and one for continuous power, seen in Fig. 2. The generator model has four tuning parameters,  $c_{gen,1-4}$ , with values tuned to fit the efficiency map of the generator, see Table 1.

## 1.3 Model validation

Adding a model for the generator losses decreases the efficiency of the powertrain compared to the model used in part 1. To ensure that the model still describes

Table 1: Parameters used in the generator and energy storage models

Symbol	Description	Value	Unit
$U_{oc}$	Open-Circuit Voltage	750	V
$R_i$	Internal Resistance	0.5	$\Omega$
$c_{gen,1}$	Generator parameter	$5.3727 \cdot 10^{-3}$	$rad/(sNm)$
$c_{gen,2}$	Generator parameter	$1.6537 \cdot 10^{-7}$	$1/W$
$c_{gen,3}$	Generator parameter	14.1957	$Nm$
$c_{gen,4}$	Generator parameter	$2.6887 \cdot 10^2$	$W$

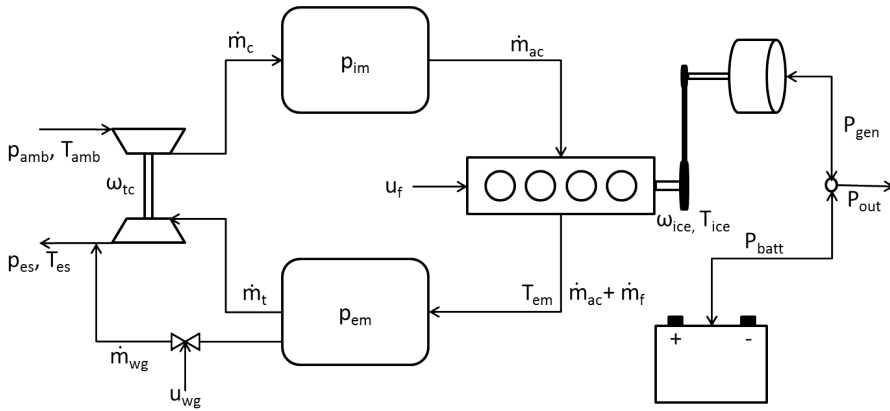


Figure 1: Structure of the MVEM. The modeled components as well as the connection between them.

Table 2: Relative error of the model vs. measurements

State	Mean	800 rpm	1000 rpm	1250 rpm	1500 rpm	1800 rpm
$p_{im}$	4.2	1.9	2.2	3.2	3.8	7.0
$p_{em}$	12.9	3.5	6.1	11.9	17.5	16.2
$\omega_{tc}$	6.4	5.8	5.0	4.0	6.0	10.5

the modeled powertrain the model including the generator losses is validated against five different datasets of measured data on the modeled powertrain. Each dataset is 100-270 s long and consists of 9-10 steps in generator power of different magnitudes as well as stationary phases in between for different constant engine speeds. Since engine output torque is not measured the torque model is inverted in the validation, resulting in almost no errors in the engine speed tracking. The relative model error vs. measurements for each dataset as well as the mean error over all datasets is shown in Table 2.

There it is seen that the mean relative error of the important intake manifold pressure dynamics are 4 % for all datasets, however the model fit increase with decreasing engine speed, being as low as 2 %.

## 2 Problem Formulation

This paper studies optimal transient control of a diesel-electric powertrain. The problem considered is the same as in part 1, i.e. minimum time and minimum fuel control from idle to a target power and energy. The problem is defined as:

$$\begin{aligned}
 \min_{u(t)} \quad & \int_0^T \dot{m}_f(x(t), u(t)) dt \quad \text{or} \quad \min_{u(t)} T \\
 \text{s.t.} \quad & \dot{x}(t) = f(x(t), u(t)) \\
 & (x(t), u(t)) \in \Omega(t)
 \end{aligned} \tag{7}$$

where  $x$  is the state vector of the MVEM,  $\dot{x}$  is the state equations defined in part 1 together with Eqs. (1)-(2), and  $u = [u_f, u_{wg}, P_{gen}, P_{batt}]$ .

The studied transients from idle to a target power and energy are also subject to time varying constraints imposed by the components, such as maximum torque and minimum speed, as well as environmental constraints, i.e. a limit on  $\phi_\lambda$  set by the smoke-limiter, and also a requirement that the control has to end

Table 3: Nomenclature

Symbol	Description	Unit
$\omega_{ice}$	Engine speed	$rad/s$
$p_{im}$	Intake manifold pressure	$Pa$
$p_{em}$	Exhaust manifold pressure	$Pa$
$\omega_{tc}$	Turbocharger speed	$rad/s$
$q$	Charge in energy storage	–
$E_{out}$	Produced energy	$J$
$u_f$	Injected fuel mass	$mg/cycle$
$u_{wg}$	Wastegate position	–
$P_{gen}$	Generator power	$W$
$P_{batt}$	Energy storage power	$W$
$I_{batt}$	Energy storage current	$A$
$P_{mech}$	Mechanical generator power	$W$
$P_{loss}$	Loss power in generator and power electronics	$W$
$P_{out}$	Output power	$W$
$P_{req}$	Requested power	$W$
$E_{req}$	Required energy	$J$
$\dot{m}_c$	Compressor massflow	$kg/s$
$\dot{m}_{ac}$	Massflow after compressor	$kg/s$
$\dot{m}_f$	Fuelflow	$kg/s$
$\lambda$	Air/fuel ratio	–
$\phi_\lambda$	Smoke-limiter	$kg/s$
$T_{ice}$	Engine torque	$Nm$
$T_{em}$	Exhaust manifold temperature	$K$
$\dot{m}_t$	Turbine massflow	$kg/s$
$\dot{m}_{wg}$	Wastegate massflow	$kg/s$
$\eta_{gs,max}$	Maximum efficiency of the GenSet	–
$\eta_{gs,max}(P)$	Maximum efficiency for power $P$ of the GenSet	–

in a stationary point. The time varying constraints  $(x(t), u(t)) \in \Omega(t)$  are:

$$\begin{aligned}
x(0) &= x_0, & \dot{x}(T) &= 0 \\
u_{min} &\leq u(t) \leq u_{max}, & x_{min} &\leq x(t) \leq x_{max} \\
T_{ice}(x(t), u(t)) &\leq T_{ice,max}(\omega_{ice}(t)) \\
P_{out}(t) &= P_{gen}(t) + P_{batt}(t), & \phi_\lambda(x(t), u(t)) &\geq 0 \\
0 &\leq P_{out}(t) \leq P_{req}, & P_{out}(T) &= P_{req} \\
P_{batt} &= 0 \text{ or } P_{batt}(T) = 0, & P_{batt}(t) &\leq \frac{\alpha U_{oc}^2}{4R_i} \\
q(T) &= q(0) = 0, & E_{out}(T) &= E_{req}
\end{aligned} \tag{8}$$

where  $\alpha$  is a parameter set to 0.98 to avoid complex numbers in the iterations.  $E_{req} = -$  kJ means that the constraint  $E_{out}(T) = E_{req}$  is removed.

Here the accelerator position is interpreted as a power request. The problem defined by Eqs. (7)-(8) is thus how to control the GenSet in order to be able to satisfy the operators power request, either as fast as possible, or as fuel efficiently as possible. The initial state values,  $x_0$ , correspond to idle, that is an

Table 4: The different generator limits used.

<u>Standard-lim</u>	
$P_{mot,peak}(\omega_{ice}(t)) \leq P_{mech}(P_{gen}(t), \omega_{ice}(t)) \leq P_{gen,peak}(\omega_{ice}(t))$	$P_{mot,cont}(\omega_{ice}(T)) \leq P_{mech}(P_{gen}(T), \omega_{ice}(T)) \leq P_{gen,cont}(\omega_{ice}(T))$
<u>Cont-lim</u>	
$P_{mot,cont}(\omega_{ice}(t)) \leq P_{mech}(P_{gen}(t), \omega_{ice}(t)) \leq P_{gen,cont}(\omega_{ice}(t))$	
<u>Peak-lim</u>	
$P_{mot,peak}(\omega_{ice}(t)) \leq P_{mech}(P_{gen}(t), \omega_{ice}(t)) \leq P_{gen,peak}(\omega_{ice}(t))$	
<u>Power-lim</u>	
$-300 \text{ kW} \leq P_{gen}(t) \leq 300 \text{ kW}$	

engine speed of 525 rpm and  $P_{gen} = 0$  W with the wastegate open, i.e.  $u_{wg} = 1$ . To solve these nonlinear optimal control problems Tomlab/PROPT is used, see [6]. This commercial software uses pseudospectral collocation methods to solve optimal control problems. Such methods only guarantee a local minimum. Care has therefore been taken to ensure that the resulting solutions are at least good local minima.

## 2.1 Generator power and limits

The generator has two limits on mechanical power,  $P_{mech}(P_{gen}(t), \omega_{ice}(t))$ , one for continuous operation and one for peak power, denoted *cont* and *peak*. In order to study how these constraints affect the solution the problem is solved for four different cases. The cases are listed in Table 4, where *mot* refers to motoring mode and *gen* generating mode.

In the first case the generator is allowed to exceed the continuous limit, but not the peak, and also has to end in a stationary point, below the continuous limit. In the second case the generator is never allowed to exceed the continuous limit. In the third case it is only limited by the peak limit and in the fourth only limits on the power electronics are enforced. The different limits as well as the maximum torque line can be seen in Fig. 7, where  $T_{mech} = P_{mech}/\omega_{ice}$ .

## 2.2 Energy storage

In order to study the effects of adding a small energy storage to assist during the transients the problem is solved with both  $P_{batt} = 0$  and with  $P_{batt}$  as a free variable. In order to ensure stationarity in charge,  $q$ , in the final time step  $P_{batt}(T) = 0$  in both cases. Since  $U_{oc}$  and  $R_i$  are independent of  $q$  only the relative depletion is of interest, the initial  $q$ -level is thus set to zero. To also be able to study optimal size of the energy storage, the size is not fixed. The influence of storage parameters is also studied in Section 7.

## 2.3 Numerical solution path

Since the tool supports integral constraints and the computational complexity of the problem increases with the number of states, the summation states for

charge in the battery as well as produced energy, defined in Eqs. (1)-(2) are reformulated as constraints according to Eq. (9).

$$\int_0^T I_{batt} dt = 0, \text{ and } \int_0^T P_{out} dt = E_{req} \quad (9)$$

## 2.4 Oscillating solutions and non-unique solutions

In order to receive smooth solutions the integral of the squared state derivatives is, as in part 1, added to the cost function with a weighting factor that is iteratively decreased,

$$\min m_f + w \int_0^T \dot{x}^T \dot{x} dt \quad (10)$$

and the lowest weight that gives a smooth solution is then used. The worst case change from this technique is less than 0.15 %<sub>00</sub> in fuel consumption and 0.4 % in time.

To handle that the minimum time solution is non-unique above a certain  $E_{req}$  the same reformulation as in part 1 is used. I.e. time is first minimized and then a second problem is solved where fuel is minimized, according to the strategy discussed in Section 2.4, with  $T \leq \min T + \epsilon$ , where  $\epsilon$  means that the minimum time is rounded up. How much the time needs to be rounded up to obtain a smooth solution differs slightly, but the largest increase in duration from this technique is less than a tenth of a permil. The obtained solution is both smooth and with lower fuel consumption without any significant effects on the duration, see Fig. 2. For a closer study on the impact of this strategy, see Section 8.

## 2.5 Initial guess and control intervals

The problem defined in Section 2 is first solved without requirements on produced energy for the different cases, i.e. for the two criteria, with and without energy storage. This then becomes a step from idle to a terminal power,  $P_{req} = 170$  kW, referred to as a power transient. Since the solutions to the power transients don't have the problems discussed in Section 2.4 those techniques are not used. For each generator limit the first initial guess is a simulated trajectory representing idle, without energy storage. The number of control intervals used for the power transients is set to 50.

The solution process with requirements on produced energy, denoted energy transients, is then started with these results as initial guess and a small required energy. For higher energies the solution for the nearest lower  $E_{req}$  is used as initial guess. The problem is then solved with an increasing number of collocation points until good accuracy has been obtained. The shown trajectories all have 125 control intervals, regardless of duration.

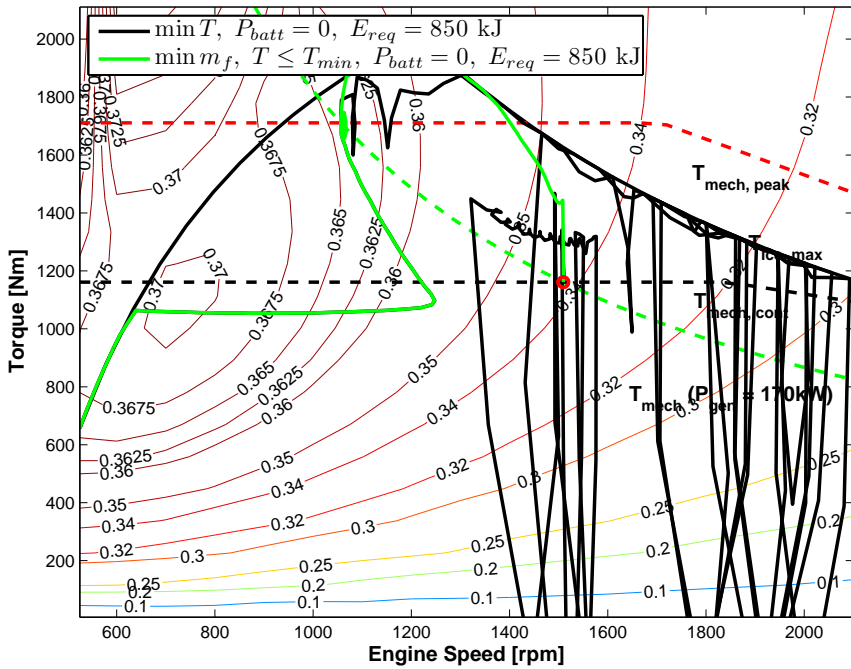


Figure 2: Two trajectories that are both time optimal, but the fuel consumption differs by 10.6%. For higher  $E_{req}$  the minimum time solution is not unique.

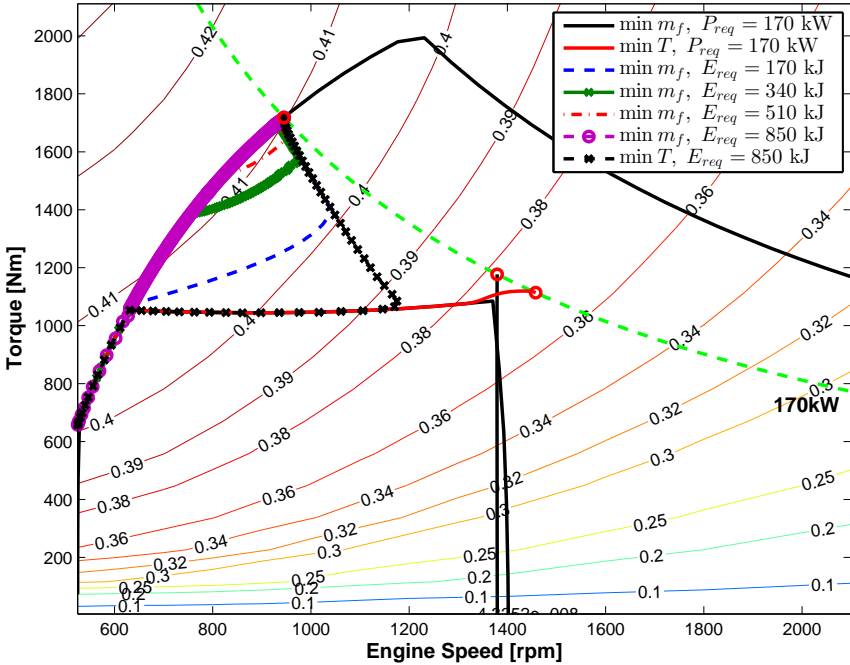


Figure 3: Torque vs engine speed for  $\min m_f$  and  $\min T$  and different requirements on produced energy with the generator considered ideal. Red circles mark the end operating point.

### 3 Effect of generator losses

Adding a model for the generator losses changes the efficiency contours of the powertrain, seen when comparing Fig. 2 and Fig. 3. The maximum efficiency of the powertrain,  $\eta_{gs,max}$  is no longer on the maximum torque line. To study how the change in efficiency affects the optimal controls the case with ideal generator model is compared to the results when generator losses are added, corresponding to Power-lim without energy storage. The corresponding trajectories for different  $E_{req}$  are shown in Fig. 4.

The addition of a model for the generator losses does not change the characteristics of the solution. For minimum time the solution is still to overshoot the engine speed of the final operating point and use this excess kinetic energy to produce output power. The main difference is that both the engine speed when the step in power occurs, as well as that of the stationary point, at  $\eta_{gs,max}(P_{req})$ , increases with generator losses. For trajectories in torque and engine speed, see Fig. 3 and Fig. 7.

For minimum fuel the trajectories appear to be different, this is related to the change in efficiency of the powertrain. With generator losses the peak efficiency is no longer on the maximum torque line of the engine. The control is still to

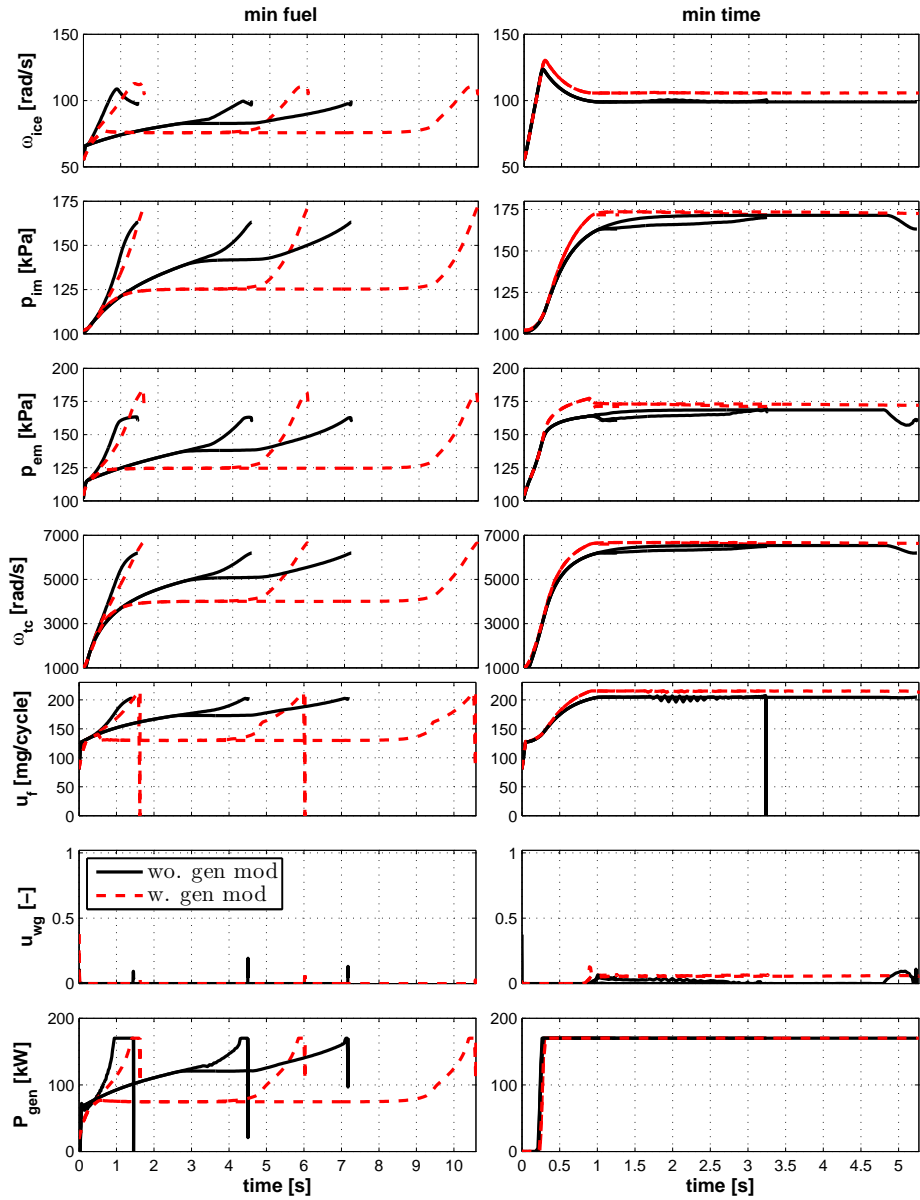


Figure 4: Minimum fuel and minimum time solutions for  $E_{req} = [170, 510, 850]$  kJ with and without a model for the generator losses.

accelerate whilst producing power and if  $E_{req}$  is large enough, have a stationary phase at  $\eta_{gs,max}$ , before a final acceleration to meet the end constraints, see Fig. 8.

## 4 Effects of generator limits

The addition of a model for the generator losses has shifted the region of peak efficiency away from the maximum torque line. Imposing different generator limits shifts the engine speed for which the peak efficiency for  $P_{gen} = P_{req}$ ,  $\eta_{gs,max}(P_{req})$ , is obtained. The state and control trajectories for the different limits are shown in Fig. 5.

### 4.1 Minimum fuel

Changing the generator limits does not change the characteristics of the solution. The control is still to accelerate whilst producing power, following the maximum torque line and smoke-limit, towards  $\eta_{gs,max}$  and since this is below the continuous limit this applies to all the cases. For larger  $E_{req}$  the control then stays there before the engine is accelerated to  $\eta_{gs,max}(P_{req})$  for the given case, see Fig. 8. The only exceptions are  $E_{req} = 85$  kJ for Peak and Power-lim. This is since  $E_{req}$  is so small that the solution is mainly dictated by fulfilling the end constraints. Instead the engine is accelerated to a higher engine speed and then decelerated by the generator, converting the kinetic energy to output power.

Standard-lim and Cont-lim are very similar, as well as Peak-lim and Power-lim. For Standard and Cont-lim this is because the generator hardly exceeds the continuous limit. For Peak and Power-lim this similarity is due to that their  $\eta_{gs,max}(P_{req})$  are close.

### 4.2 Minimum time

The minimum time solutions have similar characteristics. The optimal control is to accelerate the engine with wastegate closed up to roughly 130rad/s and then a step in generator power  $P_{gen} = 0 \rightarrow P_{req}$  is applied. The engine then wanders towards  $\eta_{gs,max}(P_{req})$ , within the given generator limits. This means that for Cont-lim the step is not to  $P_{req}$ , since that power is above the continuous limit, instead  $P_{gen}$  follows the continuous limit up to the stationary point.

When the end point is approached the wastegate is actuated to bring the engine to stationary conditions. For all limits except Standard-lim the stationary point is the same as the end point, at  $\eta_{gs,max}(P_{req})$ . For Standard-lim the control is slightly different. This is since  $\eta_{gs,max}(P_{req})$  is on the peak limit but the control has to end below the continuous limit. For larger  $E_{req}$  it first wanders to the peak limit where it has a stationary phase before it accelerates to the end point, but for low  $E_{req}$  it instead accelerates to the end point, without a stationary phase.

The initial phase of these solutions is qualitatively similar to the results with an ideal generator model discussed in part 1. With generator limits the

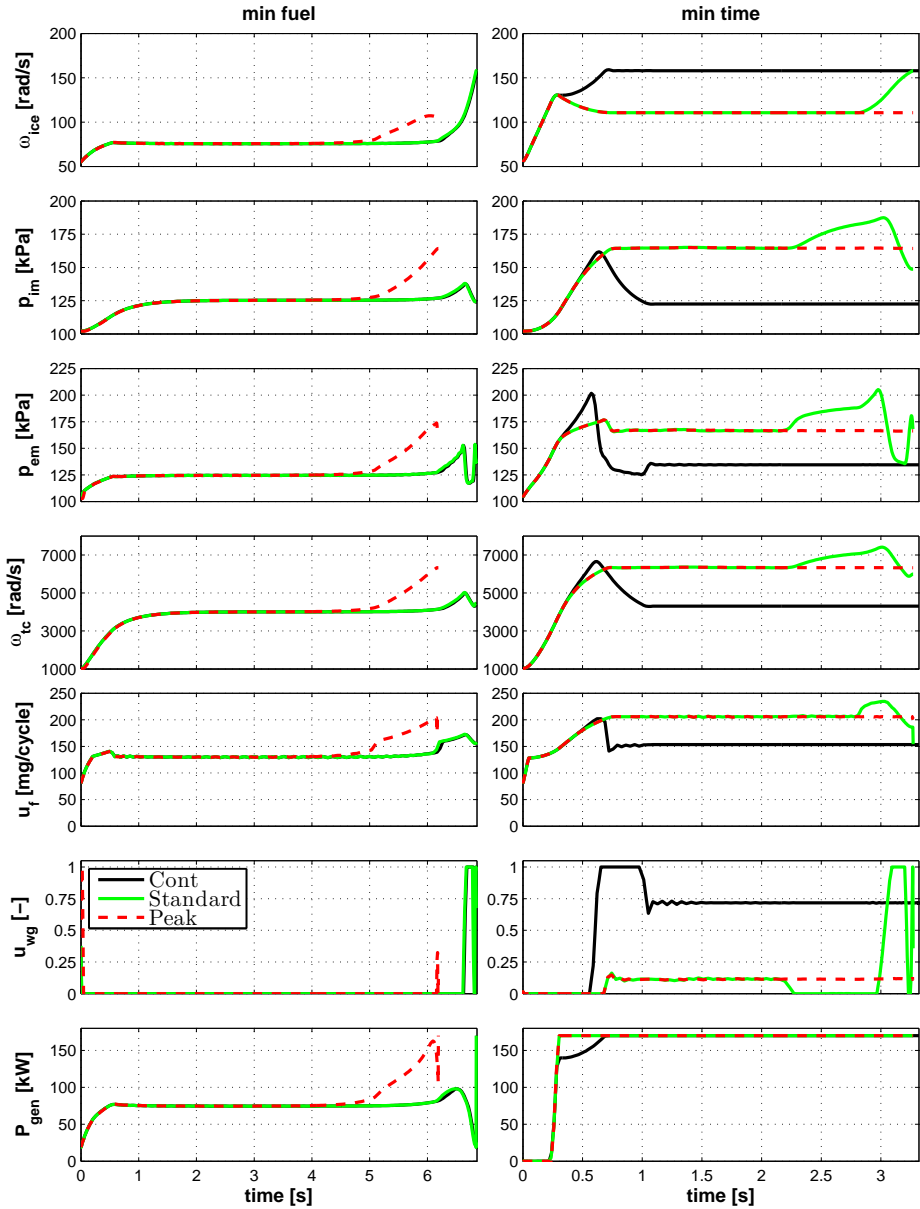


Figure 5: Effects of generator limits. Minimum fuel and minimum time solutions for  $E_{req} = 510$  kJ for the different generator limits.

peak efficiency region is shifted relative the previous results, thus changing the trajectory after the initial acceleration, see Fig. 7.

## 5 Effects of energy storage

To study the effects of adding an energy storage the problem defined in Section 2 is solved with  $P_{req} = 170$  kW and  $E_{req} = [-, 85, 510, 850]$  kJ and  $P_{batt}$  as a free variable for all generator limits. The results for Standard-lim are shown in Fig. 6, for comparison the case without energy storage is also shown. For comparison between the different cases see Fig. 7-8. For state and control trajectories for the other limits see [4].

### 5.1 Minimum fuel

None of the solutions with Standard and Cont-lim use the energy storage, the solution is thus unaffected. With Peak-lim only  $E_{req} = 85$  kJ uses the energy storage, but with Power-lim all the solutions use the energy storage. Without energy storage these transients all approach the end operating point from a higher engine speed. This is also the case with energy storage but now since  $P_{out} \leq P_{req}$  and  $P_{out} = P_{gen} + P_{batt}$ ,  $P_{gen} > P_{req}$  and the control can brake the engine harder, energy that can be used earlier in the transient to reduce the output power of the generator. The energy storage usage is however very slight.

### 5.2 Minimum time

When minimizing time the energy storage is used, but how it is used depends on  $E_{req}$ . For  $E_{req} = 85$  kJ the generator is used in motoring mode for the first 0.17-0.19 s, depending on generator limit, before it goes over into generator mode. The energy storage continues to produce output power, for all cases except Cont-lim, until approximately the maximum engine speed is reached. The generator power is then ramped up to the generator limit, which it follows until the end, whereas the engine follows the maximum torque line. During this phase the wastegate is actuated to maintain the engine torque within the limits while being on the smoke-limit. The transient then ends with actuation in all controls to meet the end constraints.

For  $E_{req} \geq 510$  kJ the energy storage output is controlled so that the response time is immediate, i.e.  $P_{out} = P_{req}$  from  $t=0$ . For all but Cont-lim the generator is ramped up with a slight overshoot in engine speed before it approaches a stationary point recharging the energy storage. Cont-lim instead follows the generator limit to a stationary point. The stationary point for all cases is limited either by the generator limit, or engine max torque. At the stationary point the wastegate is actuated so the component limit and smoke-limit coincide. The engine speed of the stationary point is  $E_{req}$  dependent, the higher the  $E_{req}$  the closer  $P_{gen}$  is to  $P_{req}$  and thus the higher the efficiency, controlling the rate of charge of the energy storage. For larger energies there is more time to recharge the energy storage, which yields lower  $P_{batt}$  and thus better efficiency of both

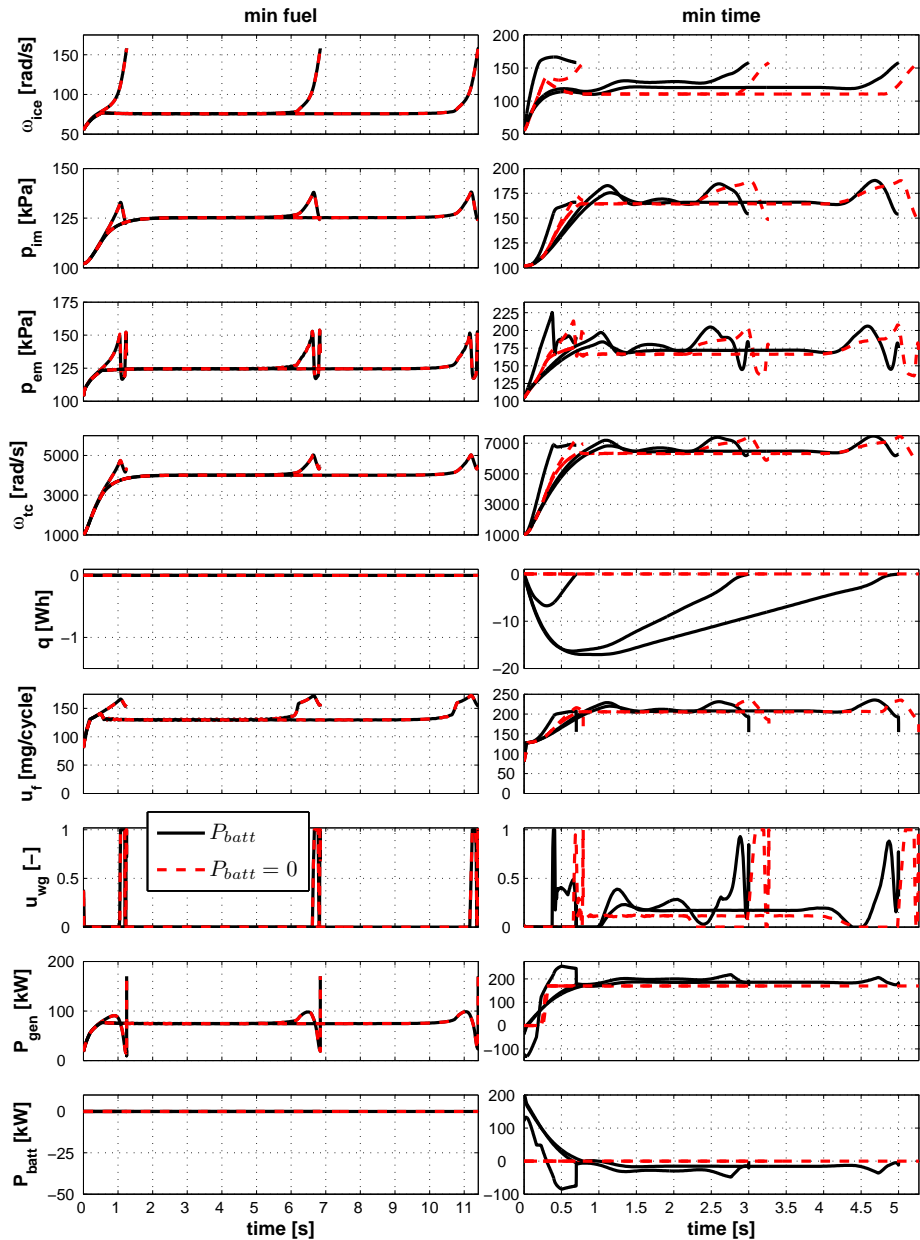


Figure 6: Effects of energy storage. Minimum fuel and minimum time solutions for  $E_{req} = [85, 510, 850]$  kJ. Standard-lim. As a reference the case without energy storage is also shown.

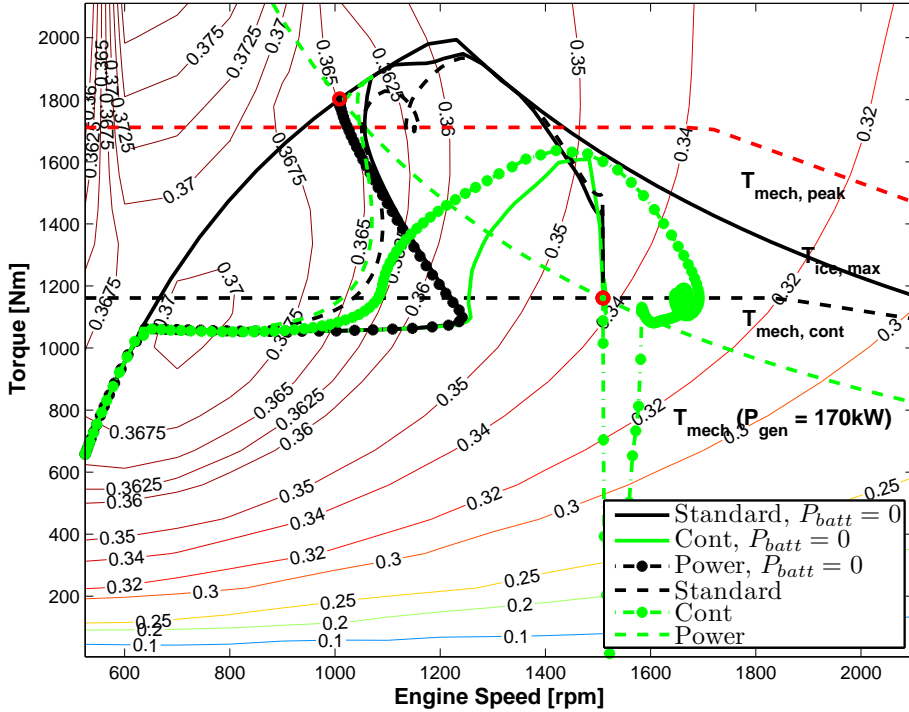


Figure 7: Torque and Engine speed plot for the different limits,  $\min T$ ,  $E_{req} = 850$  kJ, with and without energy storage.

the genset and the energy storage. The transient ends with the genset being controlled to end in the region of peak efficiency within the given limits.

## 6 Discussion

The different criteria and limits, as well as the effects of the energy storage, are compared in Table 5 and Fig. 7-8. In order for the results to be comparable, all results are augmented by holding the final controls until 850 kJ has been produced. There it is seen that even though the energy storage is used in some of the minimum fuel transients, the effect on the fuel consumption is negligible. The biggest effect comes from changing the generator limits. Both the fuel economy and decrease in duration improves with increasing limits and if the entire range of the engine is allowed the improvement in both is roughly 10%. Even though all longer minimum fuel transients have a stationary phase at the peak efficiency of the genset, the decrease in fuel consumption of this is small. The increase in duration is however substantial.

For minimum time the decrease in fuel consumption without energy storage is almost as high as for minimum fuel for Peak and Power-lim, following the conclusion in part 1. For the other two limits the fuel economy potential is

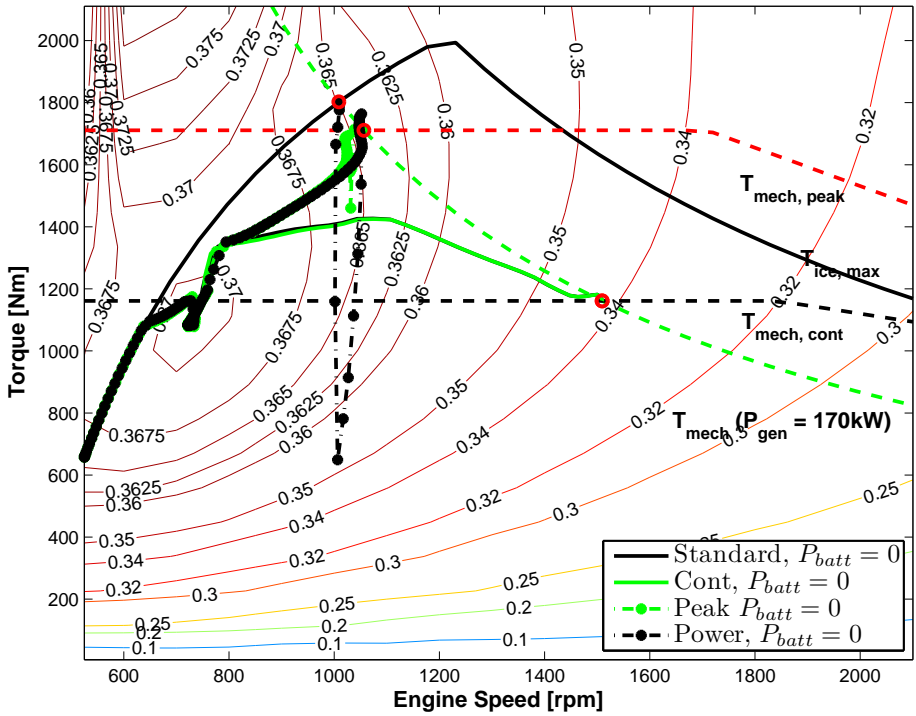


Figure 8: Torque and Engine speed plot for the different limits,  $\min m_f$ ,  $P_{batt} = 0$ ,  $E_{req} = 850$  kJ.

Table 5: Change in fuel consumption and duration of the different strategies compared to the reference trajectory.  $\Delta = [\Delta T \text{ [%]}, \Delta m_f \text{ [%]}, \Delta q_{max} \text{ [Wh]}]$ ,  $\Delta q_{max} = \max q - \min q$ .

$E_{req}(T)$		min $m_f$			min $T$	
		$P_{batt} = 0$	$P_{batt}$	$P_{batt} = 0$	$P_{batt}$	
<u>Standard-lim</u>						
-	$\Delta$	[0.2 -0.7 0.0]	[-0.1 -0.7 0.5]	[0.0 0.0 0.0]	[-0.9 -0.5 2.8]	
85kJ	$\Delta$	[7.3 -1.6 0.0]	[7.2 -1.6 0.0]	[-1.3 -0.2 0.0]	[-3.0 1.1 6.7]	
510kJ	$\Delta$	[65.0 -5.2 0.0]	[65.0 -5.2 0.0]	[-1.7 -4 0.0]	[-6.7 -2.5 16.3]	
850kJ	$\Delta$	[112.7 -8.2 0.0]	[112.7 -8.2 0.0]	[-1.7 -6.5 0.0]	[-6.7 -5.3 17.1]	
<u>Cont-lim</u>						
85kJ	$\Delta$	[7.3 -1.6 0.0]	[7.3 -1.6 0.0]	[-0.8 -0.8 0.0]	[-1.7 7.8 3.5]	
510kJ	$\Delta$	[65.2 -5.3 0.0]	[64.8 -5.3 0.0]	[-0.8 -1.2 0.0]	[-6.7 2.3 17.6]	
850kJ	$\Delta$	[112.8 -8.2 0.0]	[112.8 -8.2 0.0]	[-0.8 -1.1 0.0]	[-6.7 1.8 18.2]	
<u>Peak-lim</u>						
-	$\Delta$	[0.8 -2.1 0.0]	[1.3 -3.6 2.7]	[0.0 0.0 0.0]	[-1.5 -2.9 4.4]	
85kJ	$\Delta$	[0.0 -8.8 0.0]	[0.1 -8.8 0.4]	[-1.7 -8.7 0.0]	[-3.2 -2.2 6.1]	
510kJ	$\Delta$	[52.8 -9.7 0.0]	[52.8 -9.7 0.0]	[-1.7 -8.7 0.0]	[-6.7 -7.2 16.3]	
850kJ	$\Delta$	[100.4 -10.3 0.0]	[100.5 -10.3 0.0]	[-1.7 -8.7 0.0]	[-6.7 -7.5 17.0]	
<u>Power-lim</u>						
85kJ	$\Delta$	[-0.5 -8.8 0.0]	[-0.9 -8.9 1.2]	[-1.7 -8.7 0.0]	[-4.0 -7.1 9.1]	
510kJ	$\Delta$	[49.8 -9.8 0.0]	[49.9 -9.8 0.1]	[-1.7 -8.9 0.0]	[-6.7 -7.8 16.9]	
850kJ	$\Delta$	[97.5 -10.4 0.0]	[97.6 -10.4 0.1]	[-1.7 -8.9 0.0]	[-6.7 -7.9 17.7]	

however a bit more limited. Adding an energy storage decreases the fuel gains but instead it improves the response time. For  $E_{req} \geq 510$  kJ the response time is immediate, regardless of generator limit, and this with an energy storage of only up to 18Wh $\approx$ 65 kJ.

## 7 Impact of energy storage properties

Defining the energy storage efficiency as  $\eta_{batt} = (\frac{P_{batt}}{P_{ech}})^{\text{sign}(P_{batt})}$  and  $P_{ech} = U_{oc}I_{batt}$  and inserting Eq. (3) yields:

$$\eta_{batt} = \left( \frac{P_{batt}}{\frac{1}{2} \frac{U_{oc}^2}{R_i} - \sqrt{\frac{1}{4} (\frac{U_{oc}^2}{R_i})^2 - \frac{U_{oc}^2}{R_i} P_{batt}}} \right)^{\text{sign}(P_{batt})} \quad (11)$$

The efficiency of the energy storage is thus a function of  $\frac{U_{oc}^2}{R_i}$  and  $P_{batt}$ . Since both  $U_{oc}$  and  $R_i$  are implemented as constants the impact of the efficiency of the energy storage on the optimal solution can be expressed as a function of  $R_i$  alone.

### 7.1 Impact of internal resistance

To study how the internal resistance of the energy storage,  $R_i$ , affects the optimal solution the resistance is varied between 0 and 10000  $\Omega$  and the problem is

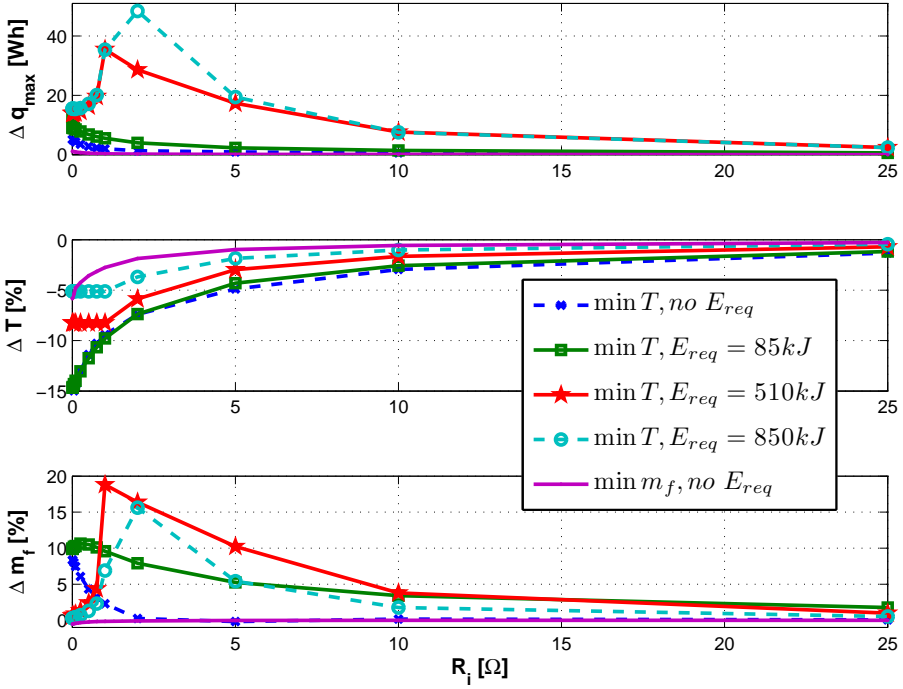


Figure 9: Change in energy storage usage and fuel and time consumption as a function of internal resistance. All consumption changes relative the case without energy storage,  $P_{batt} = 0$ .

solved for  $\min T$  and  $\min m_f$  with  $E_{req} = [-, 85, 510, 850]$  kJ using Standard-lim. Neither 0 nor 10000  $\Omega$  can be considered realistic values but to fully study the impact of the parameters the problem is solved for these extremes. In the resulting figures only the  $\Omega$ -region where the solution is affected is shown. The resulting energy storage usage as well as the change in fuel and time consumption, relative the case without energy storage, are shown in Fig. 9. For  $\min m_f$  only the results for the case without requirements on produced energy are shown. This is since even with  $R_i = 0 \Omega$  the change in fuel consumption from adding an energy storage is negligible for the studied required energies (savings in the order 0.01 %).

For  $E_{req} \leq 85$  kJ  $\Delta q_{max}$  decreases with increasing internal resistance, approaching the solution without energy storage. For  $E_{req} \geq 510$  kJ  $\Delta q_{max}$  is no longer monotone in  $R_i$ . For  $R_i \leq 1 \Omega$  the response is immediate and the depth of discharge thus increases as a function of  $R_i$  to provide the required output power. From  $R_i \geq 1 \Omega$   $P_{batt}$  is limited by the constraint that the square root in Eq. (3) needs to be positive, and for  $R_i \geq 2 \Omega$  this has the effect that the response is no longer immediate. The powers of the generator and engine are also limited, this together with the fact that  $E_{req}$  has to be met limits the power available to recharge the energy storage. These effects lead to that for larger  $E_{req}$  and  $R_i$  the

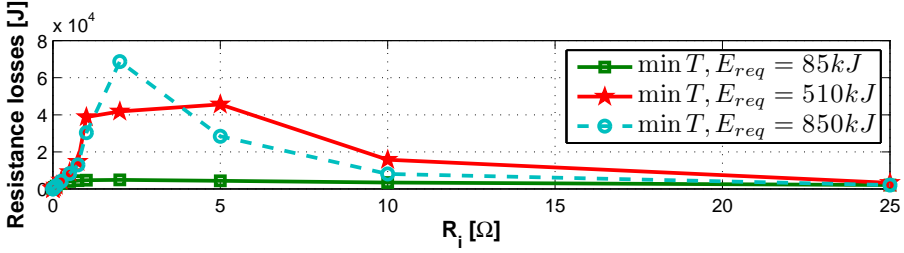


Figure 10: The losses in the energy storage as a function of internal resistance for  $E_{req} = [85, 510, 850]$  kJ.

depth of discharge decreases. This is also seen in Fig. 10. Despite the increase in  $R_i$  the amount of energy lost in the resistance decreases. However, even with  $R_i = 10 \Omega$ , the potential decrease in duration is between 1-3% depending on  $E_{req}$ , showing that an energy storage could really be beneficial for reducing the response time.

## 7.2 Optimal size of the energy storage

In the problems studied so far it is seen that the size of the energy storage, necessary for the time optimal transients, increases with  $E_{req}$ . This raises the question of how large the energy storage needs to be to not limit the solution even for very large  $E_{req}$ .

### Solution method for long durations

A problem in studying this is that since  $P_{out} \leq P_{req}$  the duration in time also increases, and with the strategy previously used, using a fixed number of control intervals regardless of duration, there is a risk that the number of control intervals per second limits the solution. Increasing the number of collocation points on the other hand makes solving the problems both slower and more difficult. Studying the time optimal solutions for larger  $E_{req}$  and  $R_i = [0.001, 0.5, 1] \Omega$  and Standard-lim it is seen that they all have the same characteristic. First there is an acceleration phase, where the energy storage is discharged. Then there is a stationary phase on the peak-limit of the generator, recharging the energy storage, and finally an acceleration to meet the end constraints, ending at the continuous limit. To avoid the problem with long optimizations, but still be able to approximate the solution, the problem is reformulated as a 3-phase problem. In the 3-phase problem the first phase and last phase are with the same constraints as before, but in the second phase the constraint  $P_{mech} = P_{mech,peak}$  is added. The durations of the first and last phases are also limited. With this formulation, since it is known that the second phase is rather stationary, the number of collocation points can be reduced, so the control interval density is high during the transient phases but low in the stationary. This method is found to give a good approximation of the optimal solution in the interval 850-2550 kJ.

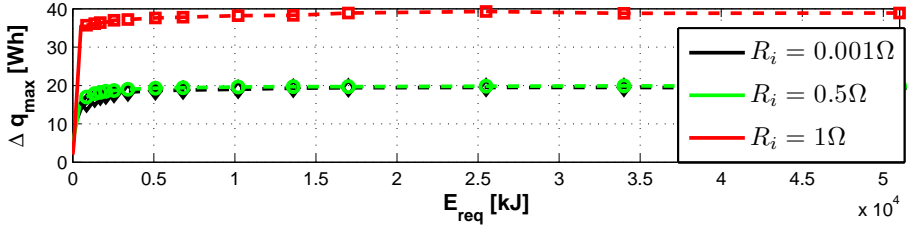


Figure 11: Optimal energy storage size as a function of  $E_{req}$  for different values of  $R_i$ .

## Results

The method described in Section 7.2 is used to solve the problem for a set of  $E_{req}$  up to 51 MJ, corresponding to a minimum duration of 300 s. The result is shown in Fig. 11. Looking at Fig. 11 it is apparent that the optimal size is a function of both  $R_i$  and  $E_{req}$ , however  $E_{req}$  only seems to influence the solution up to a certain point. This is reasonable since the energy storage is used to compensate for the time it takes to reach the efficient operating region. The maximum size seems to be between 20-40 Wh depending on  $R_i$ . Using average values from [1] for a high power Li-ion battery (100 Wh/kg, 1800 W/kg) as well as a super capacitor (2.6 Wh/kg, 5250 W/kg) the necessary weight is found to be in the range 19-38 kg (super-cap) and 56-111 kg (Li-ion) depending on internal resistance. Important to note is that in all cases it is the specific power that is limiting, for just specific energy the weight would be in the 0.2-0.4 kg range (Li-ion).

## 8 Trade-off between $\min T$ and $\min m_f$

The strategy for solving minimum time problems, discussed in Section 2.3, has negligible effect on the duration of the solution. It however raises the question on how sensitive the fuel consumption is to changes in duration from the minimum time solution. To study this the strategy is reformulated according to Eq. (12).

$$\min m_f, T \leq (1 + \epsilon)T_{min} \quad (12)$$

The problem is then solved for several values of  $\epsilon \in [0, 1.5]$  and  $E_{req} = [85, 510, 850]$  kJ both with and without energy storage using Standard-lim. The resulting Pareto fronts, in Fig. 12, show the trade-off between the two criteria, expressed relative the minimum values.

For  $E_{req} = 85$  kJ the solution is rather sensitive to  $\epsilon$  near zero, especially with an energy storage. With energy storage an increase in duration of just 1 % lowers the fuel consumption with 4.8 % (0.6 % without energy storage). It is also relatively flat for larger  $\epsilon$ , the last 30 % increase in duration only lowers the consumption with 0.3 % (with energy storage). For larger  $E_{req}$  the Pareto front is flatter, meaning that the duration needs to be increased substantially to

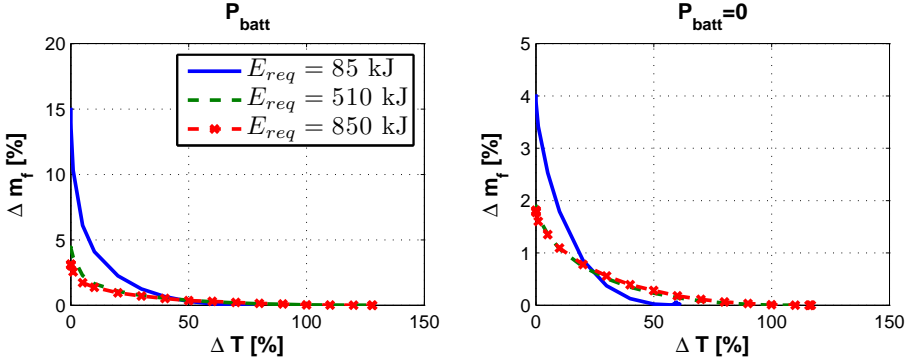


Figure 12: The effect on the fuel consumption of increasing the minimum time.

have significant effects on the fuel consumption. This is also visible in Table 5 which shows that the minimum time solution is almost as fuel efficient as the minimum fuel solution but substantially faster.

## 9 Concluding discussion

The effect of adding a generator model and its limits, as well as the effects of adding an energy storage, on the optimal control of a diesel-electric powertrain during transients is studied. The studied transients are steps from idle to a terminal power and energy. The results show that the characteristics remain unchanged by the addition of a generator model, supporting the previous assumption that the dynamics of the diesel-engine are dominant. The generator model and limits do however shift the locations of the peak efficiency regions, affecting the stationary points.

Adding an energy storage to assist in the transients is shown to be beneficial to reduce the response time, but it cannot improve the fuel economy. For minimum fuel the energy storage remains virtually unused, for minimum time the energy storage is used both to accelerate the engine and to produce output power. The solutions are relatively insensitive to energy storage parameters. Decreasing internal resistance does not have significant effects on the minimum fuel solution with requirements on produced energy. For minimum time it is seen that even when increasing the internal resistance 20 times, there are still duration benefits to be made regardless of required energy. The resistance and required energy influence the optimal size of the energy storage, a size that is found to be in the range of 20-40 Wh.

The relative fuel economy for the minimum fuel formulation improves with increasing  $E_{req}$ , regardless of generator limits, but the time penalty for this quite quickly becomes relatively large. The minimum fuel solutions produce power from the start, accelerating towards the peak efficiency region of the GenSet, where it then stays for a large part of the transient. This leads to that the time penalty increases with the a model for the generator losses since the peak

efficiency of the GenSet is shifted to a lower output power. The minimum time solutions first accelerate the engine before it starts to produce power. Adding a small energy storage can reduce this delay, and even remove it for larger requested energies, regardless of generator limits. Also even with a generator losses the minimum time formulation not only decreases the duration of the transients, it is also almost as efficient as the minimum fuel solution. For the case without energy storage, and Peak or Power-lim, the minimum time controls just increase the consumption with roughly 1 % compared to minimum fuel, despite being substantially faster.

This implies that for energy transients the fuel optima is relatively flat, something that is confirmed when studying the trade-off between minimum time and minimum fuel. Close to the minimum time solution the fuel consumption with low required energy is quite sensitive to variations in duration. A small increase in fuel results in substantial decrease in duration. For larger energies the difference is not that large, and especially near the minimum fuel solution large increases in duration have only slight effects on the fuel consumption.

## 10 Conclusion

Time and fuel optimal transients of a diesel-electric powertrain, with and without an energy storage, are studied. From the performed studies and discussions the following general conclusions can be drawn.

1. The characteristics of the optimal control mainly depend on the engine properties, the stationary points are however affected by generator model and limits.
2. An energy storage can help reduce the response time, but not the fuel consumption, for steps to higher output powers. This property is insensitive to the efficiency of the energy storage.
3. The optimal energy storage size is small in terms of energy, but large in terms of power which is the limiting factor.

## References

- [1] Lino Guzzella and Antonio Sciarretta. *Vehicle Propulsion Systems - Introduction to Modeling and Optimization*. Springer, 3rd edition, 2013.
- [2] Tomas Nilsson, Anders Fröberg, and Jan Åslund. Optimal operation of a turbocharged diesel engine during transients. In *SAE Technical Paper 2012-01-0711*, Detroit, Michigan, USA, 2012.
- [3] C E Nino-Baron, A R Tariq, Guoming Zhu, and E G Strangas. Trajectory optimization for the engine-generator operation of a series hybrid electric vehicle. *IEEE Transactions on Vehicular Technology*, 60(6):2438–2447, 2011.

- [4] Martin Sivertsson and Lars Eriksson. Generator effects on the optimal control of a power assisted diesel-electric powertrain. In *IEEE VPPC 2013 – The 9th IEEE Vehicle Power and Propulsion Conference*, Beijing, China, October 2013.
- [5] Martin Sivertsson and Lars Eriksson. Optimal transient control trajectories in diesel-electric systems-part 1: Modeling, problem formulation and engine properties. *Accepted for publication in J Eng Gas Turb Power*, 2014.
- [6] TOMLAB. PROPT - Matlab Optimal Control Software, "<http://www.tomdyn.com/>", 2012.



# Turbocharger dynamics influence on optimal control of diesel engine powered systems<sup>†</sup>

Vaheed Nezhadali<sup>a</sup>, Martin Sivertsson<sup>a</sup>, and Lars Eriksson<sup>a</sup>

<sup>a</sup>*Vehicular Systems, Department of Electrical Engineering,  
Linköping University, SE-581 83 Linköping, Sweden.*

---

<sup>†</sup>This is a formatted version of “Turbocharger dynamics influence on optimal control of diesel engine powered systems” by Vaheed Nezhadali, Martin Sivertsson, and Lars Eriksson, SAE International Journal of Engines, Volume 7, Number 1. ©SAE 2014. Reproduced with the permission of SAE. The original paper can be found at [papers.sae.org](http://papers.sae.org) <http://papers.sae.org/>, and can be found using the Digital Object Identifier (DOI): 10.4271/2014-01-0290. The formatting is restricted to changing the article into a single-column format, adjusting sizes of figures and tables, and adjusting the referencing style.

## **Abstract**

The importance of including turbocharger dynamics in diesel engine models are studied, especially when optimization techniques are to be used to derive the optimal controls. This is done for two applications of diesel engines where in the first application, a diesel engine in wheel loader powertrain interacts with other subsystems to perform a loading operation and engine speed is dictated by the wheel speed, while in the second application, the engine operates in a diesel-electric powertrain as a separate system and the engine speed remains a free variable. In both applications, mean value engine models of different complexities are used while the rest of system components are modeled with the aim of control study. Optimal control problems are formulated, solved, and results are analyzed for various engine loading scenarios in the two applications with and without turbocharger dynamics. It is shown that depending on the engine loading transients, fuel consumption and operation time can widely vary when the turbocharger dynamics are considered in the diesel engine model. Including these, have minor effects on fuel consumption and operation time at minimum fuel operations of the first application ( $\approx 0.1\%$ ) while the changes are considerable in the second application (up to 60%). In case of minimum time operations however, fuel consumption and operation time are highly affected in both applications implying that not considering turbocharger dynamics in the diesel engine models may lead to overestimation of the engine performance especially when the results are going to be used for control purposes.





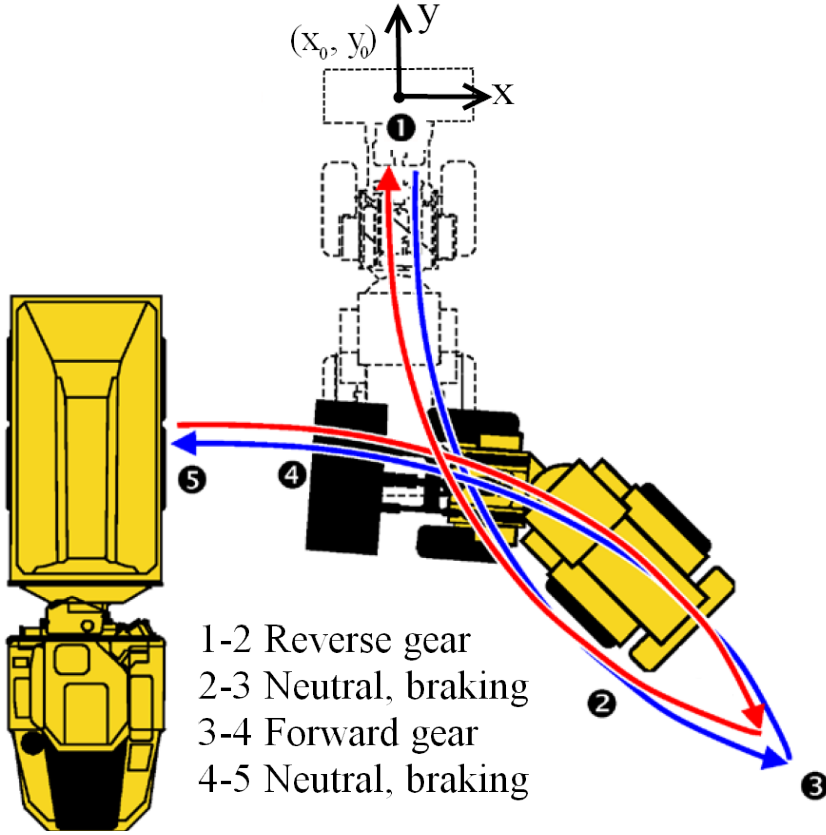


Figure 3: WL trajectory and the numbered sequence of actions in the short loading cycle, picture from [7]

## 1 Model

### 1.1 Application 1, Wheel Loader

The WL model consists of three main subsystems namely powertrain, lifting and steering where a 6-cylinder 12.7-liter diesel engine produces the power required in other subsystems. The detailed version of the WL model as a nonlinear system with nine states and four control inputs is available in [4]. The states in the system, as seen in Figure 1, are engine speed  $\omega_{ice}$ , intake manifold pressure  $p_{im}$ , vehicle speed  $v$ , bucket lifting speed  $v_{buc}$ , bucket height  $h_{buc}$ , vehicle positions in  $xy$  plane, vehicle heading angle  $\theta$  and steering angle  $\delta$ . The four control inputs are fuel injection per combustion cycle of engine  $u_{mf}$ , bucket acceleration  $u_{ab}$ , braking torque signal  $u_b$  and derivative of steering angle  $u_{str}$ . The engine model is presented once as a full model ( $FM_{WL}$ ) including the turbocharger dynamics and then with no turbocharger dynamics called reduced model ( $RM_{WL}$ ). Figure 3 shows a WL and its trajectory while operating in the short loading cycle.

## Full Model, Wheel Loader

The  $FM_{WL}$  diesel engine is represented by a simplified version of the MVEM in [1] where engine speed,  $\omega_{ice}$ , and intake manifold pressure,  $p_{im}$ , are states and injected fuel mass,  $u_{mf}$  is the control input. The turbocharger dynamics are represented by a first order system with a time constant that describes the intake manifold pressure. Engine power is consumed in order to lift the loaded bucket and perform steering,  $P_{lift}$  and  $P_{str}$  respectively, while consuming power for vehicle transportation  $P_{trans}$ . Dynamics of engine speed are then calculated by Newton's second law as:

$$\frac{d\omega_{ice}}{dt} = \frac{1}{J_{ice}} \left( T_{ice} - \frac{P_{lift} + P_{str} + P_{trans}}{\omega_{ice}} \right) \quad (1)$$

where  $J_{ice}$  is engine inertia and  $T_{ice}$  the engine torque. Intake manifold pressure is related to a static pressure model,  $p_{model}$ , by a first order system according to:

$$\frac{dp_{im}}{dt} = \frac{1}{\tau} (p_{model} - p_{im}), \quad \tau = c_{\tau 1} \omega_{ice}^{c_{\tau 2}} \quad (2)$$

where  $\tau$  is the time constant in the intake manifold pressure buildup due to turbocharger dynamics, and the static pressure map is calculated as follows

$$p_{model} = c_{p,1} T_{ice} + c_{p,2} \omega_{ice}^2 + c_{p,3} (T_{ice} \omega_{ice})^2 + c_{p,4} \quad (3)$$

with  $c_{p1,2,3,4}$  and  $c_{\tau 1,2}$  tuned to correspond to the stationary intake manifold pressure values at different engine loads and speeds, and the response time during intake manifold pressure transients at different engine speeds respectively. The net engine torque  $T_{ice}$  is modeled as the subtraction of the friction torque  $T_{fric}$  from the gross indicated torque  $T_{ig}$  according to:

$$T_{ice} = T_{ig}(u_{mf}) - T_{fric}(\omega_{ice}) \quad (4)$$

The air mass flow to the engine,  $\dot{m}_a$  calculated using a constant volumetric efficiency,  $\eta_{vol}$ , and mass of injected fuel,  $\dot{m}_f$  are calculated as follows:

$$\dot{m}_a = \frac{\eta_{vol} V_D \omega_{ice} p_{im}}{4 \pi R_a T_{amb}}, \quad \dot{m}_f = \frac{10^{-6}}{4 \pi} u_{mf} \omega_{ice} n_{cyl} \quad (5)$$

where  $V_D$ ,  $R_a$ ,  $T_{amb}$  and  $n_{cyl}$  are respectively engine displacement volume, gas constant, ambient temperature and number of engine cylinders.

The minimum relative air to fuel ratio according to the environmental limits on smoke generation is denoted by  $\lambda_{min}$ , and a parameter  $\phi_\lambda$  representing the smoke generation during the engine operation is defined as:

$$\phi_\lambda = \dot{m}_a - \dot{m}_f (A/F)_s \lambda_{min} \quad (6)$$

where  $(A/F)_s$  is the stoichiometric air to fuel ratio of the fuel.

## Reduced Model, Wheel Loader

The  $RM_{WL}$  for the diesel engine does not include the intake manifold pressure dynamics in (2) and has only the engine speed as state determined by (1) while the only control input to the diesel engine as in the  $FM_{WL}$  is injected fuel mass  $u_{mf}$ . All other system states and control inputs mentioned in section 1.1 are left without any change and the net engine torque is calculated by (4) similar to the  $FM_{WL}$  case.

## 1.2 Application 2, Diesel-Electric

The modeled powertrain consists of a 6-cylinder 12.7-liter SCANIA diesel engine with a fixed-geometry turbine and a wastegate for boost control, equipped with a generator. To study the effects and importance of including a turbocharger model in the optimization, two different models are used where the full and reduced models are denoted by  $FM_{DE}$  and  $RM_{DE}$  respectively. The first model,  $FM_{DE}$ , models the physics of the powertrain, incorporating the nonlinear nature and turbocharger dynamics. In the second model,  $RM_{DE}$ , only the stationary efficiency map of the engine is modeled, neglecting turbocharger dynamics.

### Full Model, Diesel-Electric

The model is a nonlinear, four state, three input MVEM, used together with models for the generator losses. The diesel engine model is the same as the one used in [8], augmented with a model for the generator losses as in [9].

The states of the MVEM are engine speed,  $\omega_{ice}$ , inlet manifold pressure,  $p_{im}$ , exhaust manifold pressure,  $p_{em}$  and turbocharger speed,  $\omega_{tc}$ . The controls are injected fuel mass,  $u_{mf}$ , wastegate position,  $u_{wg}$ , and generator power,  $P_{gen}$ . The engine model consists of two control volumes, intake and exhaust manifold, and four restrictions, compressor, engine, turbine, and wastegate. The control volumes are modeled with the standard isothermal model, using the ideal gas law and mass conservation. The engine and turbocharger speeds are modeled using Newton's second law. The governing differential equations of the MVEM are:

$$\frac{d\omega_{ice}}{dt} = \frac{1}{J_{genset}} \left( T_{ice} - \frac{P_{mech}}{\omega_{ice}} \right) \quad (7)$$

$$\frac{dp_{im}}{dt} = \frac{R_a T_{im}}{V_{im}} (\dot{m}_c - \dot{m}_{ac}) \quad (8)$$

$$\frac{dp_{em}}{dt} = \frac{R_e T_{em}}{V_{em}} (\dot{m}_{ac} + \dot{m}_f - \dot{m}_t - \dot{m}_{wg}) \quad (9)$$

$$\frac{d\omega_{tc}}{dt} = \frac{P_t - P_c}{\omega_{tc} J_{tc}} - w_{fric} \omega_{tc}^2 \quad (10)$$

where  $\dot{m}$  denotes massflows,  $T_{im/em}$  manifold temperatures,  $J_{genset/tc}$  inertias,  $V_{im/em}$  manifold volumes,  $R_e$  gas constant,  $P_{t/c}$  turbine/compressor powers,  $T_{ice}$  engine torque, and  $P_{mech}$  mechanical generator power, with connections

between the components as in Figure 2. There is also a summation state, to keep track of the produced energy:

$$\frac{dE_{gen}}{dt} = P_{gen} \quad (11)$$

The model consists of eight submodels, connected as seen in Figure 2. The submodels are models for compressor massflow and power, intake manifold pressure, engine torque and exhaust temperature, exhaust manifold pressure, wastegate massflow, turbine massflow and power, and generator losses. The diesel engine smoke generation is represented by  $\phi_\lambda$  parameter similar to (6).

### Reduced Model, Diesel-Electric

The  $RM_{DE}$  is a one state, two control model, MVEM with a model for the generator losses, similar to the models used in [3] and [12] where transient operation of naturally aspirated diesel engines are studied. The model corresponds to the  $FM_{DE}$  with the last three states left out:

$$\frac{d\omega_{ice}}{dt} = \frac{1}{J_{genset}} \left( T_{ice} - \frac{P_{mech}}{\omega_{ice}} \right) \quad (12)$$

The net engine torque,  $T_{ice}$ , is as in the  $FM_{DE}$  modeled as:

$$T_{ice} = T_{ig} - T_{fric} - T_{pump} \quad (13)$$

$$T_{pump} = \frac{V_D}{4\pi} (p_{em} - p_{im}) \quad (14)$$

Since the  $RM_{DE}$  does not have the states  $p_{im}$ ,  $p_{em}$ ,  $T_{pump}$  is instead modeled according to:

$$T_{pump} = (c_{Tp,1}\omega_{ice} + c_{Tp,2})u_{mf} + c_{Tp,3}\omega_{ice} + c_{Tp,4} \quad (15)$$

with parameters tuned to correspond to the pumping torque of the stationary efficiency map of  $FM_{DE}$ .

## 2 Problem Formulation

Optimal control problems are formulated for both applications using the  $FMs$  and  $RM$ s described in the previous section. Engine loading cycles and requirements together with the component specific limitations are described in terms of boundary conditions and time varying path constraints in the problem formulation. Considering the complexity and detail level of the models, using methods such as dynamic programming is computationally expensive, instead PROPT [13] which is a solver engine using pseudospectral collocation method is used for solving the optimal control problems.

## 2.1 Problem Formulation, Wheel Loader

To study the importance of the turbocharger dynamics, two optimal control problems are formulated,  $\min T$  and  $\min m_f$ , as follows:

$$\begin{aligned} \min_{u(t)} \quad & \int_0^T \dot{m}_f(s(t), u(t)) dt \quad \text{or} \quad \min_{u(t)} T \\ \text{s.t.} \quad & \dot{s}(t) = f(s(t), u(t)) \\ & (s(t), u(t)) \in \Omega(t) \end{aligned} \quad (16)$$

where  $s$  is the state vector of the model,  $\dot{s}$  is defined by dynamic equations of the state variables in lifting and steering subsystems [4], plus (1), (2) in  $FM_{WL}$  case or only (1) in  $RM_{WL}$  case. The control inputs vector  $u = [u_{mf}, u_{ab}, u_b, u_{str}]$  is the same for both  $FM_{WL}$  and  $RM_{WL}$ .

The WL operation, see Figure 3, in the short loading cycle starts from an initial WL position  $(x_0, y_0)$  and the loaded bucket is lifted to a desired final level while the WL travels first in backward direction from the loading point until a point where it stops, and then starts the forward move towards the load receiver. The gear shifts during this operation introduce discontinuities into the problem and in order to avoid these, the optimal control problem is divided and solved in four phases with constant gearbox gear ratios during each, which in time order begin with first reversing  $[0, t_1]$ , then braking with neutral gear  $[t_1, t_2]$ , then forwarding  $[t_2, t_3]$ , and finally braking with neutral gear  $[t_3, T]$ .

The fuel consumption  $\dot{m}_f$  in (16) is then calculated as the sum of consumed fuel during each of the phases as follows:

$$\dot{m}_f = \int_0^{t_1} \dot{m}_{f,1} dt + \int_{t_1}^{t_2} \dot{m}_{f,2} dt + \int_{t_2}^{t_3} \dot{m}_{f,3} dt + \int_{t_3}^T \dot{m}_{f,4} dt \quad (17)$$

In order to ensure the continuity of the states and physical properties during WL operation, the successive phases are concatenated by constraints as follows:

$$\begin{aligned} u_{ab}, u_{str}, s_j \text{ at phase } (i+1)_{init} &= u_{ab}, u_{ab}, s_j \text{ at phase } (i)_{end} \\ j \in \{1, 2, 3, 4, 5, 6, 7, 8, 9\}, i \in \{1, 2, 3\} \end{aligned} \quad (18)$$

Time varying constraints,  $(s(t), u(t)) \in \Omega(t)$ , imposed by the components, such as maximum torque and minimum speed, and also a requirement that the control has to end in a stationary point are:

$$\begin{aligned} s(0) &= s_0, & \dot{s}(T) &= 0 \\ u_{min} &\leq u(t) \leq u_{max}, & s_{min} &\leq s(t) \leq s_{max} \\ T_{ice}(s(t), u(t)) &\leq T_{ice,max}(s(t)), & R_{min} &\geq R \\ P_{h cyl}(s(t), u(t)) &\leq P_{h cyl,max}, & decc_{lim} &\leq \dot{v} \end{aligned} \quad (19a)$$

where  $R$  is the turning radius of the WL during the operation,  $P_{hycl}$  is the pressure in the hydraulic lift cylinders of the WL's boom and  $decc_{lim}$  is a lower limit on the braking deceleration which ensures the stability of WL structure by avoiding harsh braking. For the  $FM_{WL}$  with turbocharger dynamics, there is also an environmental constraint, i.e. a limit on  $\phi_\lambda$  set by the smoke-limiter, equivalent to a lower limit on the air-fuel ratio:

$$\phi_\lambda(\dot{m}_a, \dot{m}_f) \geq 0 \quad (19b)$$

## 2.2 Problem Formulation, Diesel-Electric

In case of the diesel-electric powertrain, the  $\min T$  and  $\min m_f$  optimal control problems have the same structure as in (16) with the difference being that  $\dot{s}$  is defined by (7)-(10) and  $u = [u_{mf}, u_{wg}, P_{gen}]$  ( $FM_{DE}$ ), or (12) and  $u = [u_{mf}, P_{gen}]$  ( $RM_{DE}$ ). The considered problem is a step from idle to a requested output power,  $P_{req}$ , augmented with that a certain amount of energy,  $E_{req}$  has to be produced.  $E_{req}$  can be interpreted as a short driving mission, and also as a measure on the amount of freedom given to the powertrain, in terms of produced energy, before the operators power request has to be met.

The studied transients from idle to a target power and energy are subjected to time varying constraints as those of the 1st application which are imposed by the components and also the requirement to end up in a stationary point. The time varying constraints  $(s(t), u(t)) \in \Omega(t)$  in the diesel-electric problem formulation are:

$$\begin{aligned} s(0) &= s_0, & \dot{s}(T) &= 0 \\ u_{min} &\leq u(t) \leq u_{max}, & s_{min} &\leq s(t) \leq s_{max} \\ T_{ice}(s(t), u(t)) &\leq T_{ice,max}(s(t)), & P_{gen}(T) &= P_{req} \\ 0 &\leq P_{gen}(t) \leq P_{req}, & E_{gen}(T) &= E_{req} \end{aligned} \quad (20a)$$

and for  $FM_{DE}$  also:

$$\phi_\lambda(\dot{m}_a, \dot{m}_f) \geq 0 \quad (20b)$$

## 3 Results

The optimal control problems formulated in the previous section are solved for different engine loading scenarios and the effect of not including turbocharger dynamics in the diesel engine models are analyzed for both applications.

### 3.1 Wheel Loader Application

In order to investigate the effect of turbocharger dynamics under various loading conditions, the optimal control problems defined in section 2.1, are first solved for WL loading cycles of different lengths by defining various final position values at  $t = T$  for states  $x$  and  $y$ . Figure 4 shows the increase in the fuel consumption and cycle duration in  $\min m_f$  (top) and  $\min T$  transients (bottom). As it is

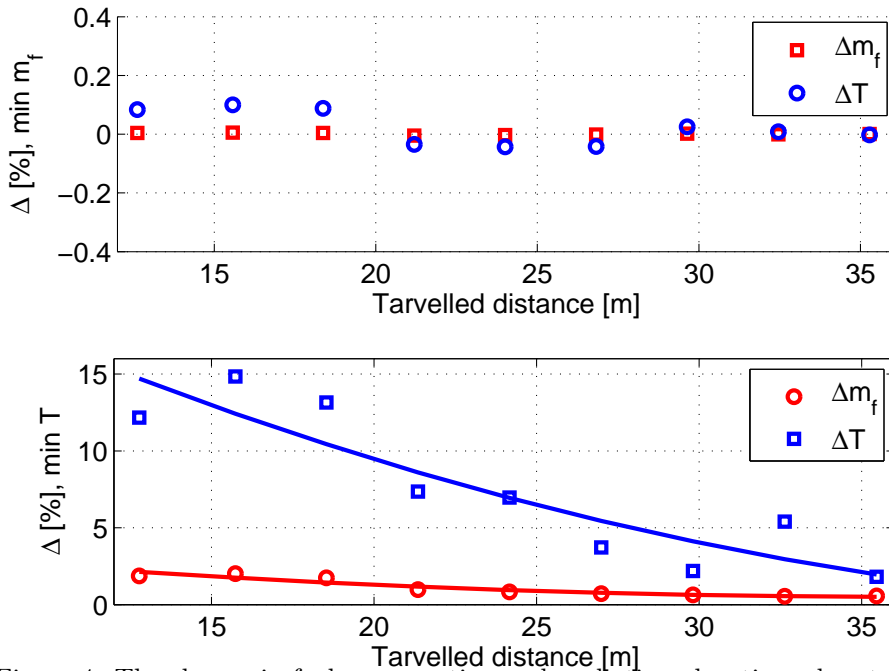


Figure 4: The change in fuel consumption and cycle time duration when turbochargers dynamics are not included. Second order polynomials are fitted to the results in the bottom subplot for better visualization.

seen, the changes in the fuel consumption or cycle duration are less than 0.1% in  $\min m_f$  transients when the turbocharger dynamics are not included in the diesel engine model. The engine operating points corresponding to the cycle with the shortest traveling distance in the top section of Figure 4, are depicted in Figure 5 (top) for the  $FM_{WL}$  and  $RM_{WL}$ . It is seen that neglecting the turbocharger dynamics in the  $RM_{WL}$  does not have a considerable effect on the engine operation during  $\min m_f$  transients. In both  $FM_{WL}$  and  $RM_{WL}$  cases, the engine is controlled in the low engine speed region of the engine map since lower fuel consumption is the main objective. Mostly no rapid engine acceleration takes place and therefore smoke generation constraint due to the boost limit becomes active only during a short interval at the beginning of the loading operation, shown by X in Figure 5, where the vehicle starts from stand still and engine speed is low.

On the other hand, in the  $\min T$  operations, as seen in the bottom plot of Figure 4, when turbocharger dynamics are not included, the operation time can be underestimated up to 15%. Lower fuel consumptions are also obtained without turbocharger dynamics. The trend is such that the fuel consumption and operation time are underestimated more in the shorter traveling distances. This is due to the fact that in the cycles with shorter traveling distance, the lifting and vehicle acceleration which are the major engine power consumers are fulfilled almost simultaneously (lifting and acceleration) resulting in higher loads

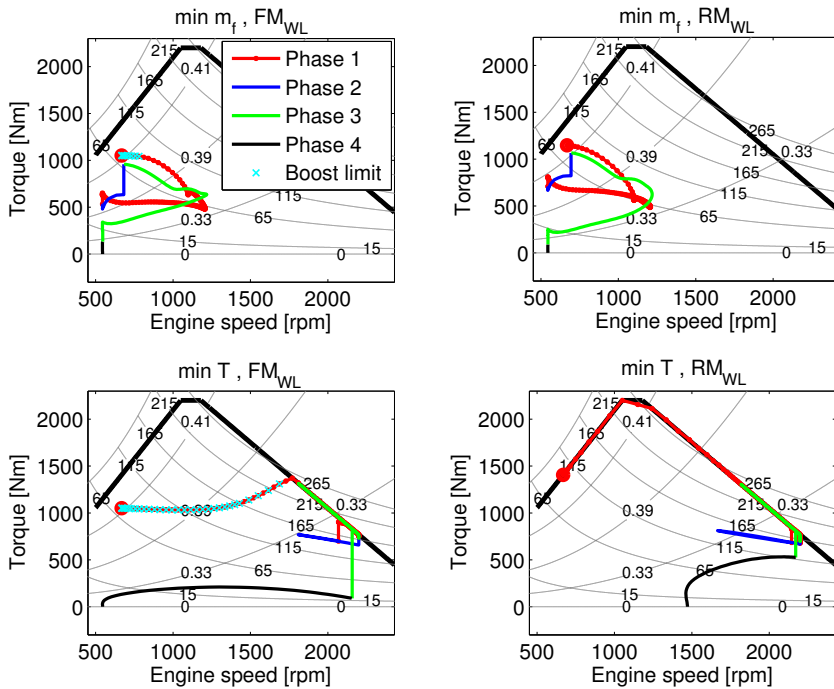


Figure 5: Engine operating points using  $FM_{WL}$ (left) and  $RM_{WL}$ (right) in  $\min m_f$  (top) and  $\min T$  (bottom) transients. The red circle denotes the engine operation starting point.

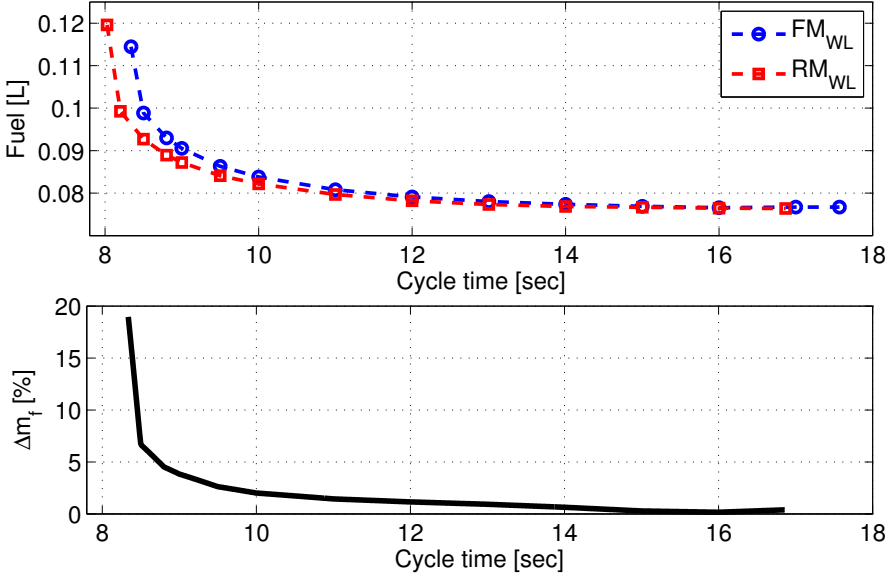


Figure 6: Top: Trade-off between fuel consumption and cycle duration for same loading cycle. Bottom: The increase in fuel consumption during same loading cycle at different cycle durations when turbocharging dynamics are included.

on engine compared to the cycles with longer travel distance where the load lifting and vehicle acceleration are performed in almost separate periods of the loading cycle (first vehicle acceleration, then load lifting). The details of this shift in power distribution pattern are studied deeper in [4], [5] and [6]. Looking at the engine operating points corresponding to the cycles with the shortest travel distance at the bottom of Figure 4, it is seen that when turbocharger dynamics are not included in the model, Figure 5 bottom-right, the engine operation is mainly limited by the maximum torque production limits when the WL starts the operation at phase one, however in case of including turbocharger dynamics, Figure 5 bottom-left, engine operation at the beginning of operation, is limited by the boost limit and cannot produce large torques due to insufficient intake manifold pressure.

The trade-off between fuel consumption and cycle operation time is informative for WL operators as it is useful to select a compromise between the two and achieve a higher productivity [11]. To investigate how this trade-off is affected for a certain loading cycle when turbocharger dynamics are not included, optimal control problems in (16) are reformulated as:

$$\begin{aligned}
 \min_{u(t)} \quad & w_1 \left( \int_0^T \dot{m}_f(s(t), u(t)) dt \right) + w_2 T \\
 \text{s.t.} \quad & \dot{s}(t) = f(s(t), u(t)) \\
 & (s(t), u(t)) \in \Omega(t) \\
 & w_1 + w_2 = 1
 \end{aligned} \tag{21}$$

The problem is solved for several  $w_1$  and  $w_2$  values using the same set of

constraints as in section 2.1 using  $FM_{WL}$  and  $RM_{WL}$  for diesel engine. The results are presented in Figure 6 where the selected WL operating cycle is selected to be the one with shortest travel distance in Figure 4. The results imply that not including the turbocharger dynamics, underestimates the fuel consumption more in the shorter operations which is as already discussed, due to higher load demands from the engine during the shorter cycles where the engine operation is affected by the smoke-limiter constraint more severely. The importance of turbocharger dynamics on fuel consumption decrease as the operation becomes less engine load demanding for the longer cycles.

### 3.2 Diesel-Electric Application

The problem formulated in (16) and (20), how to control the diesel-electric powertrain in order to be able to satisfy the operators power and energy request, either as fast as possible, or as fuel efficient as possible, is solved for  $P_{req} = 170$  kW and  $E_{req} = [0 - 850]$  kJ with the two different models.  $E_{req} = 0$  means that there are no requirements on produced energy, just power, i.e. the  $E_{gen}(T) = E_{req}$  constraint is removed. A comparison between the different models and problems is shown in Figure 7. For a deeper analysis of the results with  $FM_{DE}$ , see [10].

For  $RM_{DE}$ , the  $\min T$  and  $\min m_f$  solutions to  $E_{req} = 0$  are equivalent. The solution is to accelerate along the maximum torque line to the point of peak efficiency for  $P_{gen} = 170$  kW, denoted  $\eta_{max}(P_{req})$ . For  $\min T$   $E_{req}$  has no effect on the characteristics of the solution, the acceleration phase is the same, the duration spent at the stationary point does however increase. For  $\min m_f$ , a requirement on produced energy means that the solution will accelerate along the maximum torque line towards the peak efficiency of the GENSET, denoted  $\eta_{max}$ , have a stationary phase there, and then accelerate towards  $\eta_{max}(P_{req})$ .  $E_{req}$  thus only affects the time spent at the peak efficiency of the GENSET.

With turbocharger dynamics the resulting trajectories differ substantially compared to  $RM_{DE}$ , see Figure 7. Whereas the results with  $RM_{DE}$  are mainly dictated by the maximum torque line and stationary efficiencies, the results with  $FM_{DE}$  are mainly dictated by the smoke-limiter and ability to generate enough turbocharger speed to reach the efficient operating regions. So for  $E_{req} = 0$  kJ this has the effect that the end operating point is nowhere near  $\eta_{max}(P_{req})$ . For the solution to actually end at  $\eta_{max}(P_{req})$ ,  $E_{req} \geq 170$  for both  $\min T$  and  $\min m_f$ , compared to  $E_{req} \geq 0$  kJ for  $RM_{DE}$ . For  $\min T$  this means that with  $E_{req} > 170$  kJ the characteristic is unaffected. Also for  $\min m_f$  to have a stationary phase at  $\eta_{max}$ ,  $E_{req} \geq 340$  kJ, below that the solution does not have any stationary phases, compared to  $E_{req} \geq 42.5$  kJ for  $RM_{DE}$ . This means that when the operator requests  $P_{req}$ , this request has to be held for 1-2s for it to be optimal to approach the optimal stationary point, something that is not captured without including turbocharger dynamics in the model.

Looking at the trajectories, they are qualitatively very different. In Figure 8, the relative change in duration and consumption of neglecting the turbocharger dynamics,  $RM_{DE}$  vs  $FM_{DE}$ , is shown. For  $E_{req} = 0$  kJ,  $RM_{DE}$  underestimates both the fuel consumption and duration with over 60 % both for  $\min m_f$  and  $\min T$ . The difference then decreases as  $E_{req}$  increases, since above a certain  $E_{req}$

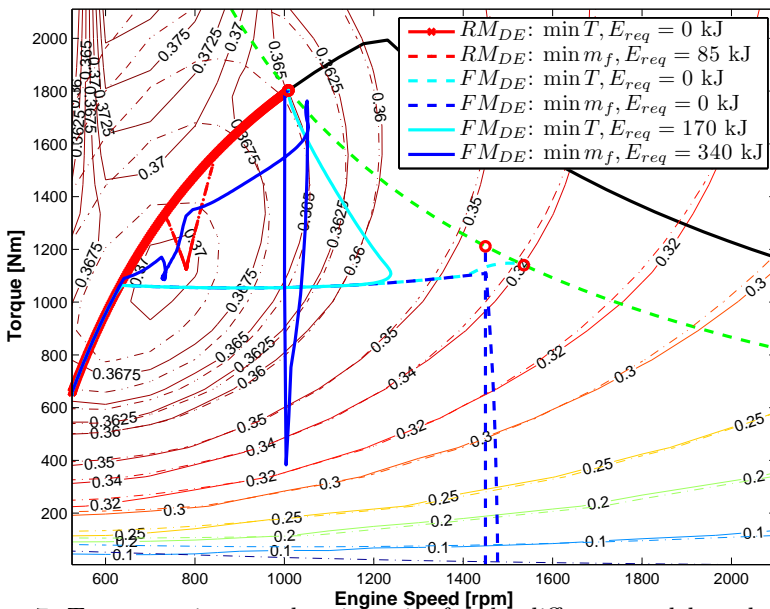


Figure 7: Torque-engine speed trajectories for the different models and problems. Efficiency contours are for the GENSET.

the stationary points are similar, and for larger  $E_{req}$  the transient contribution to the fuel consumption and duration decreases.

## 4 Conclusions

The importance of incorporating turbocharger dynamics in the optimization of transient control is studied for two different applications of diesel engines. In the first application, the transients are studied for a diesel engine operating as a component in a wheel loader where engine transients are affected by the power requirements in the lifting, steering and transportation subsystems while the engine speed is affected by the wheel speed during the operation.

The minimum time and minimum fuel transients of the diesel engine are analyzed for wheel loader loading cycles of different length with and without turbocharger dynamics in the diesel engine model. It is shown that by not considering the turbocharger dynamics, fuel consumption and cycle duration are not affected considerably during minimum fuel transients since the engine is controlled to operate at low engine speed and torque where there is no demand for high intake manifold pressure, thus lowering the importance of turbocharger dynamics. In the minimum time transients however, it is shown that the required operation times can be underestimated by up to 15% when turbocharger dynamics are not considered and fuel consumption is also calculated to be up to 2% lower. This is due the higher torque demand on the diesel engine which calls for higher intake manifold pressure in order to satisfy the smoke

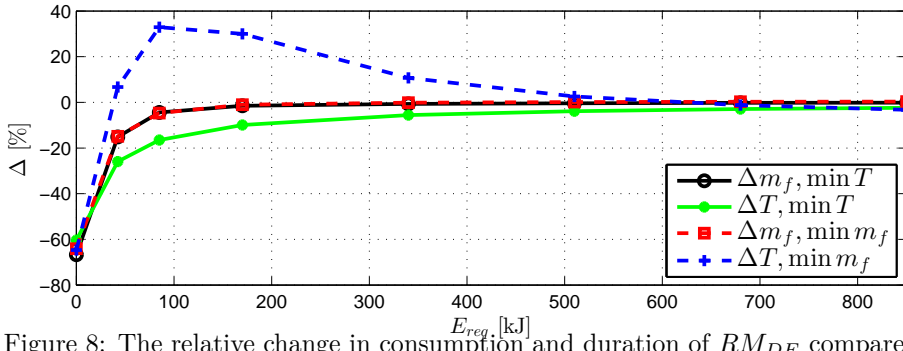


Figure 8: The relative change in consumption and duration of  $RM_{DE}$  compared to  $FM_{DE}$ .

generation limit which in turn takes longer times when turbocharger dynamics are included. Underestimation of fuel consumption and cycle time duration in minimum time transients are more severe during wheel loader loading cycles with shorter traveling distance since load lifting and vehicle transportation have to be performed simultaneously. The engine has to then deliver larger amounts of power in a shorter time calling for faster rise in the intake manifold pressure which is constrained by the turbocharger dynamics.

In the second application, the diesel engine transients are studied while the engine operates in a diesel-electric powertrain. For this aim two different models are used, a four state, three control MVEM, and a one state, two control MVEM. The considered problem is a step from idle to target power and energy, which is solved both for minimum time and minimum fuel. The results show that the optimal trajectories differ substantially and that neglecting the turbocharger dynamics can underestimate the optimal duration and consumption by over 60%. Also the amount of energy required for it to be optimal to go to the optimal operating points differ with 170 – 300 kJ, meaning for the considered case the same power has to be requested for 1-2s, something that is not captured when the dynamics are neglected.

## References

- [1] Walström, J., Eriksson, L.: Modeling engines with a variable-geometry turbocharger and exhaust gas recirculation by optimization of model parameters for capturing non-linear system dynamics. In *Journal of Automobile Engineering* 225, 960–986 (2011).
- [2] Rakopoulos, C. D., Giakoumis, E. G., : Diesel engine transient operation - Principles of operation and simulation analysis. In *Springer*, 2009.
- [3] Tomas Nilsson, T., Fröberg, A., Åslund, J., : Optimized engine transients. In *7th IEEE Vehicle power and propulsion conference*, Chicago, Illinois, USA, 2011.
- [4] Nezhadali, V., and Eriksson, L., : Optimal lifting and path profile for a

- wheel loader considering engine and turbo limitations. In *Optimization and Optimal Control in Automotive Systems*, Springer Lecture Notes in Control Science, 2014.
- [5] Nezhadali, V., Eriksson, L. : Modeling and optimal control of a wheel loader in the lift-transport section of the short loading cycle. In *AAC'13 - The 7th IFAC Symposium on Advances in Automotive Control*, Tokyo, Japan, September 2013.
- [6] Filla, R.: Quantifying Operability of Working Machines. Linköping University, Dissertation, NO. 1390 (2011).
- [7] Filla, R.: Optimizing the trajectory of a wheel loader working in short loading cycles. In *SICFP2013 - The 13th Scandinavian International Conference on Fluid Power*. Linköping, Sweden, 2013.
- [8] Sivertsson, M., Eriksson, L., : Time and fuel optimal power response of a diesel-electric powertrain. In *E-COSM'12-IFAC Workshop on Engine and Power-train Control, Simulation and Modeling*, Paris, France, October 2012.
- [9] Sivertsson, M., Eriksson, L., : Optimal transient control and effects of a small energy storage for a diesel-electric powertrain. In *AAC'13 - The 7th IFAC Symposium on Advances in Automotive Control*, Tokyo, Japan, September 2013.
- [10] Sivertsson, M., Eriksson, L., : Generator effects on the optimal control of a power assisted diesel-electric powertrain. In *IEEE VPPC 2013 - The 9th IEEE Vehicle Power and Propulsion Conference*, Beijing, China, October 2013.
- [11] Frank, B., Skogh, L., Filla, R., Fröberg, A., Alaküla, M. : On increasing fuel efficiency by operator assistant systems in a wheel loader. In *The International Conference on Advanced Vehicle Technologies and Integration*, 155-161 (2012).
- [12] C E Nino-Baron, C. E., Tariq, A. R., Zhu, G., Strangas, E. G. : In Trajectory optimization for the engine-generator operation of a series hybrid electric vehicle. In *IEEE Transactions on Vehicular Technology*, 60(6):2438-2447, 2011.
- [13] TOMLAB 7.9 : <http://www.tomdyn.com/>.



# Optimal and real-time control potential of a diesel-electric powertrain<sup>†</sup>

Martin Sivertsson<sup>a</sup> and Lars Eriksson<sup>a</sup>

<sup>a</sup>*Vehicular Systems, Department of Electrical Engineering,  
Linköping University, SE-581 83 Linköping, Sweden.*

4

---

<sup>†</sup>This is a formatted version of “Optimal and real-time control potential of a diesel-electric powertrain” by Martin Sivertsson and Lars Eriksson, IFAC World Congress 2014, Cape Town, South Africa. ©IFAC 2014. Reproduced with the permission of IFAC. The original version was published in [ifac-papersonline.net](http://ifac-papersonline.net), <http://ifac-papersonline.net>, and can be found using the Digital Object Identifier (DOI): 10.3182/20140824-6-ZA-1003.01969. The formatting is restricted to changing the article into a single-column format, adjusting sizes of figures and tables, and adjusting the referencing style.

## Abstract

Real-time control strategies and their performance related to the optimal control trajectories for a diesel-electric powertrain in transient operation are studied. The considered transients are steps from idle to target power. A non-linear four state-three input mean value engine model, incorporating the important turbocharger dynamics, is used for this study. The strategies are implemented using the SAE J1939-standard for engine control and evaluated compared to both the optimal solution and the solution when the engine is restricted to follow its stationary optimal line. It is shown that with the control parameters tuned for a specific criteria both engine control strategies in the SAE J1939-standard, speed control and load control, can achieve almost optimal results, where engine load controlled shows a better trade-off between fuel economy and duration. The controllers are then extended and it is shown that it is possible to control the powertrain in a close to optimal way using the SAE J1939-standard, both with the engine speed and load controlled. However the mode where the engine is load controlled is seen to be more robust.

## Introduction

The diesel-electric powertrain, such as the BAE Systems TorqE™, see Fig. 1, offers the potential to increase the performance and lower the fuel consumption, since it decouples the diesel engine from the wheels. Through this electrification of the powertrain the engine speed can be chosen freely which also enables the powertrain to produce maximum power from standstill. This in combination with the torque characteristics of the electric motors can thus increase performance and potentially lower the fuel consumption.

During stationary operation the desired operating point can be found from the combined efficiency map of the engine-generator (GENSET). An open question is how to optimally control the GENSET between two different outputs, especially when the diesel engine is turbocharged. In transient operation the turbocharger dynamics limit the changes in load and speed that can be achieved, often referred to as turbocharger lag, see [5]. The absence of an energy storage also makes the system more restricted and difficult to manage, compared to a series hybrid, that can use the energy storage to compensate for the dynamics of the engine, since all power consumed has to be produced by the GENSET. Therefore efficient transient control is of high importance, any delay in power response of the GENSET will also result in delay in power at the wheels.

Previous papers have studied how to best exploit the extra degree of freedom available in a diesel-electric and optimally control the engine-generator (GENSET) from idle to target power and energy, see [9, 10]. The main contribution of this paper is the study of the potential performance of different control strategies using the control principles used in industry, i.e. the SAE J1939-standard for engine control, see [6]. Two main approaches are discussed and implemented with the control parameters tuned for minimum fuel or minimum time. This is then performed for several cases and the results are related to the previous optimal results, investigating the potential for optimal control. As a further contribution the controllers are extended and it is shown that it is possible to control the GENSET in an optimal manner using the SAE J1939-standard.

The literature regarding diesel-electric powertrains is rather scarce. For series hybrids on the other hand, where the GENSET is augmented with an energy storage, there are several publications. A common approach is to use the stationary map to generate setpoints for the GENSET, see [11, 1, 7]. This optimization does not consider the transient effects of the GENSET and therefore raises the question if the optimal setpoint actually is the operating point with highest efficiency. Another approach is to limit the change in requested power from the GENSET so the controller can maintain the GENSET operating close to its stationary optimal line, see [1, 11]. This means that the energy storage needs provide a larger part of the requested power, but it also assumes that it is optimal to follow the stationary optimal line in transients. Whether these assumptions are true or not for turbocharged GENSETs is also studied in this paper.

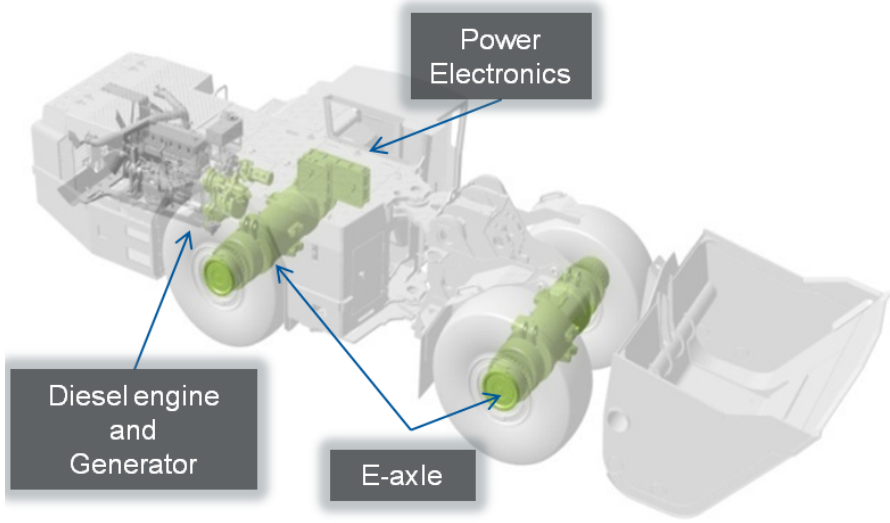


Figure 1: BAE Systems TorqE™ powertrain.

## 1 Model

The modeled powertrain consists of a 6-cylinder 12.7-liter SCANIA diesel engine with a fixed-geometry turbine and a wastegate for boost control, equipped with a generator. The model is a nonlinear, four state, three input mean value engine model (MVEM), used together with models for the generator losses. The diesel engine model is the same as the one used in [8], augmented with a model for the generator losses as in [9].

The states of the MVEM are engine speed,  $\omega_{ice}$ , inlet manifold pressure,  $p_{im}$ , exhaust manifold pressure,  $p_{em}$ , turbocharger speed,  $\omega_{tc}$ . The controls are injected fuel mass,  $u_f$ , wastegate position,  $u_{wg}$ , and generator power,  $P_{gen}$ . The engine model consists of two control volumes, intake and exhaust manifold, and four restrictions, compressor, engine, turbine, and wastegate. The control volumes are modeled with the standard isothermal model, using the ideal gas law and mass conservation. The engine and turbocharger speeds are modeled using Newton's second law. The governing differential equations of the MVEM

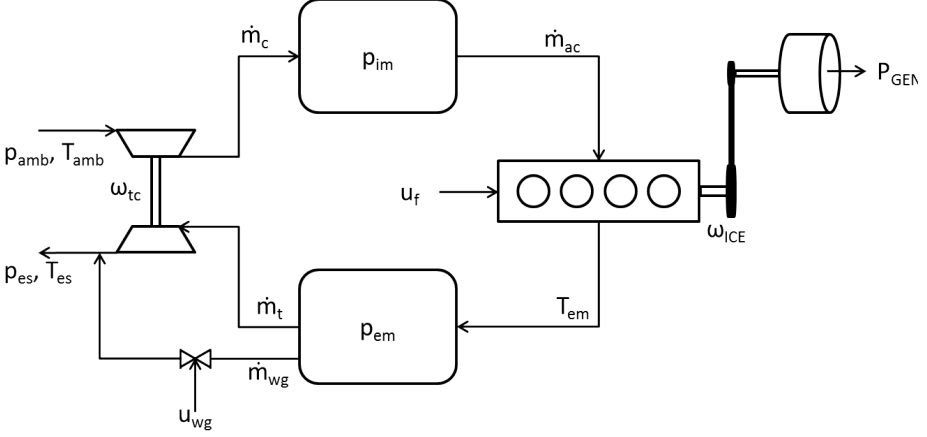


Figure 2: Structure of the MVEM. The modeled components as well as the connection between them.

are:

$$\frac{d\omega_{ice}}{dt} = \frac{1}{J_{genset}} \left( T_{ice} - \frac{P_{mech}}{\omega_{ice}} \right) \quad (1)$$

$$\frac{dp_{im}}{dt} = \frac{R_a T_{im}}{V_{im}} (\dot{m}_c - \dot{m}_{ac}) \quad (2)$$

$$\frac{dp_{em}}{dt} = \frac{R_e T_{em}}{V_{em}} (\dot{m}_{ac} + \dot{m}_f - \dot{m}_t - \dot{m}_{wg}) \quad (3)$$

$$\frac{d\omega_{tc}}{dt} = \frac{P_t - P_c}{\omega_{tc} J_{tc}} - w_{fric} \omega_{tc}^2 \quad (4)$$

Where  $\dot{m}_x$  denote massflows,  $T_{im/em}$  manifold temperatures,  $J_{genset/tc}$  inertias,  $V_{im/em}$  manifold volumes,  $R_{a/e}$  gas constants,  $P_{t/c}$  turbine/compressor powers,  $T_{ice}$  engine torque, and  $P_{mech}$  mechanical generator power, with connections between the components as in Fig 2. For further explanation of the symbols, see Table 2 in the appendix. There is also a summation state, to keep track of the produced energy:

$$\frac{dE_{gen}}{dt} = P_{gen} \quad (5)$$

The model consists of ten submodels, connected as seen in Fig. 2. The submodels are models for compressor massflow and power, intake manifold pressure, engine torque and exhaust temperature, exhaust manifold pressure, wastegate massflow, turbine massflow and power,, generator losses, and engine and turbocharger speed.

## 2 Problem Formulation

The considered problem is that the GENSET is at idle when the operator requests a step in power. Previous papers have studied how to best exploit the

extra degree of freedom available in a diesel-electric and optimally control the GENSET from idle to target power and energy by solving the two optimization problems:

$$\begin{aligned} \min_{u(t)} \quad & \int_0^T \dot{m}_f(x(t), u(t)) dt \quad \text{or} \quad \min_{u(t)} T \\ \text{s.t.} \quad & \dot{x}(t) = f(x(t), u(t)) \\ & (x(t), u(t)) \in \Omega(t) \end{aligned} \quad (6a)$$

where  $x$  is the state vector of the model,  $\dot{x}$  and is defined by (1)-(4) and  $u = [u_f, u_{wg}, P_{gen}]$ . The considered problem is a step from idle to a requested output power,  $P_{req}$ , augmented with that a certain amount of energy,  $E_{req}$  has to be produced.  $E_{req}$  can be interpreted as a short driving mission, and also as a measure on the amount of freedom given to the powertrain, in terms of produced energy, before the operators power request has to be met.

The studied transients from idle to a target power and energy are also subject to time varying constraints imposed by the components, such as maximum torque and minimum speed, and also a requirement that the control has to end in a stationary point. The time varying constraints  $(x(t), u(t)) \in \Omega(t)$  are:

$$\begin{aligned} x(0) &= x_0, & \dot{x}(T) &= 0 \\ u_{min} &\leq u(t) \leq u_{max}, & x_{min} &\leq x(t) \leq x_{max} \\ T_{ice}(x(t), u(t)) &\leq T_{ice,max}(x(t)), & P_{gen}(T) &= P_{req} \\ 0 &\leq P_{gen}(t) \leq P_{req}, & E_{gen}(T) &= E_{req} \\ \phi_\lambda(x(t), u(t)) &\geq 0 \end{aligned} \quad (6b)$$

For all problems studied in this paper  $P_{req} = 170$  kW.

### 3 Optimal control trajectories

The resulting engine torque-engine speed trajectories to (6) for  $E_{req} = 340$  kJ and  $E_{req} \geq 0$  kJ, are shown in Fig. 3. Also shown is the minimum fuel solution for fixed output power, denoted  $\min m_{f,2-phase}$ . In  $\min m_{f,2-phase}$  the problem is solved using two phases with the added constraints that in phase 1  $P_{gen} = 0$  and in phase 2  $P_{gen} = P_{req}$ . For a more thorough discussion on the optimal results, see [9, 10].

With  $E_{req} \geq 0$  the solutions for the two criteria are very similar. The optimal control puts as much energy as possible into the system, following the smoke-limiter and maximum torque line. The difference between the solutions to the two criteria is which operating point they approach and also the fine tuning to get there.

When  $E_{req} > 0$  the solutions differ. For  $\min T$  and  $\min m_{f,2-phase}$  the characteristics are the same, and also independent of  $E_{req}$ . The optimal solution is to accelerate the engine, following the smoke-limiter, and then use the excess kinetic energy to produce power and approach the maximum efficiency point for the requested power. At which engine speed this step occurs does however depend on the requested power.

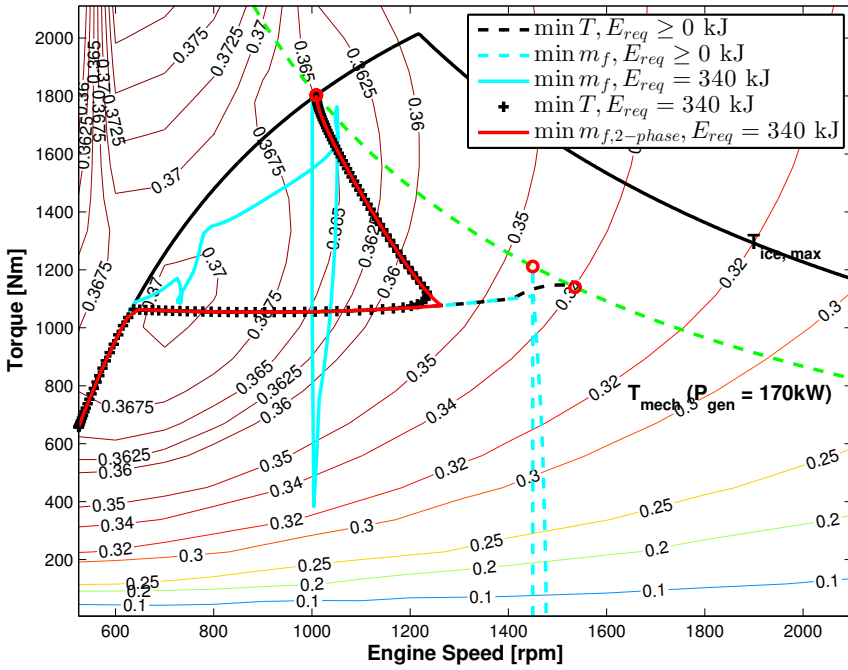
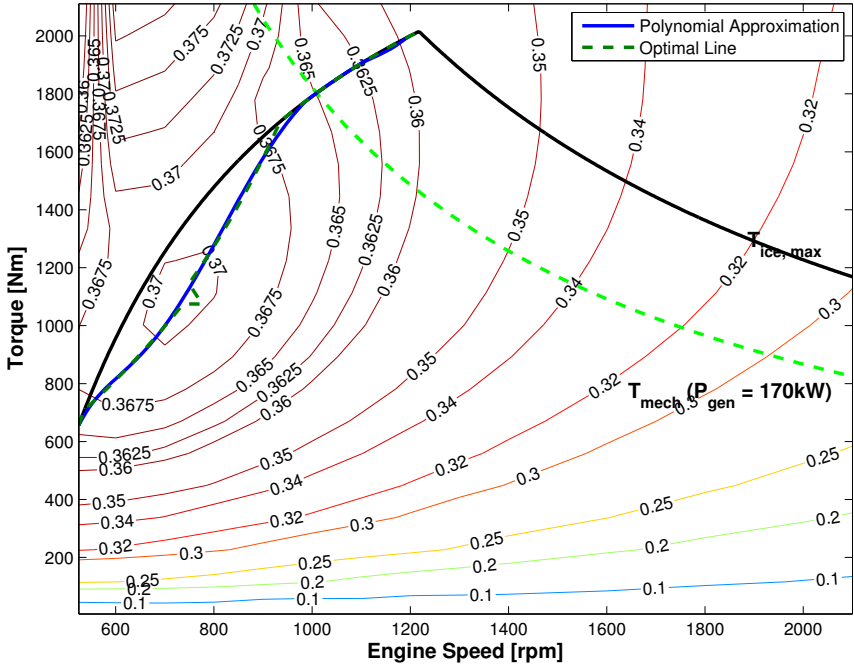


Figure 3: The fuel and time optimal trajectories for different  $E_{req}$ .



control to follow the optimal line the control cannot reach a point where it can sustain  $P_{gen} = 170$  kW without producing output power, since the control needs to build turbocharger speed and intake manifold pressure without accelerating the GENSET. In order to reach the final operating point the produced energy is  $E_{gen} = [305, 320]$  kJ for  $\min T$  and  $\min m_f$  respectively. This means that the operator or controller has to request  $P_{req} = 170$  kW for 2.7-2.8s for this power to be realizable, a problem the optimal control does not have. However to make the comparison fair the strategies are evaluated using  $E_{req} = 340$  kJ, and the results are expressed relative the time optimal solution for  $E_{req} = 340$  kJ, shown in Table 1. There it is seen that even though the optimal trajectories do not follow the stationary optimal line, following the optimal line gives almost optimal fuel economy, the difference is just 0.3-0.4% depending on criteria. Following the optimal line is also substantially faster than the  $\min m_f$  solution. However, the  $\min T$  solution consumes just 1.4-1.7% more fuel than the  $\min m_f$  and optimal line strategies but is 27.7-65.2% faster.

## 5 Control using SAE J1939

In the optimization it is assumed that the actuators in the GENSET can be individually controlled, this is commonly not the case. A common approach in GENSET control is to split the control in two parts, engine and generator control. The engine is controlled using the SAE J1939-standard, following either a speed or torque reference. The controller parameters are tuned first by iterating through a large set of possible candidates and then selecting the best one as initial guess for an optimization problem solved with *fmincon* in Matlab to fine tune the performance. In the following control strategies the wastegate is assumed fully closed throughout the transient, i.e.  $u_{wg} = 0$ .

### 5.1 Strategy 1: Engine Speed Controlled

The normal GENSET control is that the engine tries to follow a reference speed, see [3, 2, 4]. From talks with the industry the standard generator control scheme for propulsion applications is to reduce the produced power from the desired power based on the speed error of the engine. The scheme can be summarized as:

$$\omega_{ice,err} = \omega_{ice,ref} - \omega_{ice} \quad (8)$$

$$u_f = \text{sat} \left( k_{p,\omega} \omega_{ice,err} + k_{i,\omega} \int_0^T \omega_{ice,err} dt \right) \quad (9)$$

$$P_{gen} = \text{sat} (P_{gen,ref} - k_{p,gen} \omega_{red}) \quad (10)$$

$$\omega_{red} = \begin{cases} \omega_{ice,err} - \omega_d & \text{if } \omega_{ice,err} - \omega_d \geq 0 \\ 0 & \text{otherwise} \end{cases} \quad (11)$$

Where  $\omega_d$  is a dead-zone to circumvent the drawback that the speed error has to be zero for the requested power to be produced.  $\text{sat}(u_x)$  means that the

control is saturated to comply with the constraints. For  $u_f$  this means both smoke-limited, max torque-limited as well as being limited by the maximum possible fuel injection. Here the gains for the engine speed controller,  $k_p$  and  $k_i$ , are tuned to correspond to the speed controller of the modeled engine. The Strategy 1 (S1) control thus has three parameters/setpoints.

## 5.2 Strategy 2: Engine Load Controlled

Instead of using the speed request of the SAE J1939-standard to control the engine, one could use the load request and instead use the generator to control the speed of the GENSET. From a  $P_{req}$  this strategy then requires two setpoints, desired torque and speed. From a  $P_{req}$  and  $\omega_{ice,ref}$  the mechanical torque of the generator,  $T_{mech}$ , is calculated. This torque is then sent to the engine control system. In simulation the torque model is inverted to calculate the fuel control. The generator power is set by a PI-controller from the engine speed error. A drawback is that  $P_{gen}$  is not allowed to exceed  $P_{req}$ , since that would require a consumer being able to accept the excess power. This means that the generator cannot control the engine speed if  $\omega_{ice,err} < 0$  since potentially  $\omega_{ice}T_{ice} > P_{mech}(\omega_{ice}, P_{req})$ . A solution to this problem is to instead decrease the desired torque proportional to the unavailable torque desired from the generator by the controller.

The suggested strategy is then summarized as:

$$P_{gen,sp} = k_{p,P}\omega_{ice,err} + k_{i,P} \int_0^T \omega_{ice,err} dt \quad (12)$$

$$P_{gen} = sat(P_{gen,sp}) \quad (13)$$

$$T_{red} = \begin{cases} \frac{P_{gen,sp} - P_{gen}}{\omega_{ice}} & \text{if } P_{gen,sp} - P_{gen} \geq 0 \\ 0 & \text{otherwise} \end{cases} \quad (14)$$

$$T_{ref} = \frac{P_{mech}(P_{req}, \omega_{ice,ref})}{\omega_{ice,ref}} - k_{p,T}T_{red} \quad (15)$$

$$u_f = sat(f(\omega_{ice}, T_{ref}, p_{im}, p_{em})) \quad (16)$$

The Strategy 2 (S2) controller then has three tuning parameters,  $k_{p,P}$ ,  $k_{i,P}$ , and  $k_{p,T}$ .

## 5.3 Results and Discussion

To investigate the potential for optimal control, the gains in the two different controllers are tuned for the different criteria,  $P_{req}$  and  $E_{req}$ . The previously solved optimal control problem, (6), requires the end point to be stationary,  $P_{gen}(T) = P_{req}$ ,  $E_{gen}(T) = E_{req}$ , as well as component and environmental constraints to be fulfilled. To request stationarity and that the power and energy should be met is infeasible for lower  $E_{req}$  when using PI-controllers due to the turbocharger dynamics, since  $E_{req}$  will be met before the target speed and stationary conditions are reached. For S1 the stationarity requirement is

therefore removed, since the generator power is decreased if the speed error increases. For S2 it is replaced with the requirement  $0 \leq \omega_{ice,err}(T) \leq 0.52 \text{ rad/s}$ .

In Fig. 5 the resulting torque-speed trajectories for the two different controllers are shown. The gains are tuned for  $E_{req} = [170, 340]$  kJ but for S2 both  $E_{req}$  have the same solution why  $E_{req} = 340$  kJ is left out. For S1 the controller is also simulated and plotted for for  $E_{req} = 8.5$  MJ to show how  $\omega_{ice,ref}$  is used.

With S1 it is not optimal to request the speed of peak efficiency, something also seen in Fig. 5 that  $\omega_{ice,ref}$ , marked by red stars, is quite far from the peak efficiency region. This since the requested engine speed cannot be met unless  $E_{req}$  is very large and for low  $\omega_{ice,ref}$   $P_{req}$  cannot be met without exceeding  $E_{req}$ , since it is necessary to build turbocharger speed to be able to produce the high torques required. For  $\min m_f$  the parameters are instead such that the GENSET stays in the high efficiency region, for  $\min T$  the ability to meet  $P_{req}$  dominates.

With S2 it is both fuel and time optimal to set  $\omega_{ice,ref}$  in the peak efficiency region. For  $\min m_f$  the end point is approached with very little overshoot in engine speed, whereas for  $\min T$  the overshoot is larger, similar to the time optimal trajectories.

In Table 1 the fuel consumption and duration are related to the time optimal results. These controllers are not far from fuel optimal when tuned for  $\min m_f$ , and not far from time optimal when tuned for  $\min T$ . For S1 the punishment in the metric it is not tuned for is substantial, i.e. the fuel consumption increases with 8% when the controller is tuned for  $\min T$  and the duration increases with 25% when tuned for  $\min m_f$ . With S2 this is avoided with and the controller performs well in both metrics regardless for which it is tuned. However the potential fuel economy of S1 is higher than S2, whereas S2 is faster than S1. Worth noting is that S2  $\min T$  is very close to the time optimal solution in both metrics, and the trajectory is also qualitatively similar seen when comparing Fig. 4 and 5.

## 6 Optimal control using SAE J1939

Even though the implemented strategies S1 and S2 can come close to the optimal solutions the gains of the controllers end up quite extreme, tuned for a specific criteria. The question whether or not the optimal trajectories are implementable using the SAE J1939-standard is still open. To evaluate this  $\min m_{f,2-phase}$  is selected since it represents a good trade-off between fuel and duration, and also since it is rather simple. First it accelerates along the smoke-limiter up to a certain engine speed,  $\omega_{step}$ , and then applies a step in generator power from zero to  $P_{req}$ , a power that is then held until the end. The wastegate is used to maintain the engine on the smoke-limit. Here the wastegate is ignored and again assumed closed throughout the transient.

### 6.1 Optimal control with the engine speed controlled (S1)

For S1 this means that first a  $\omega_{ice,ref,1}$  higher than  $\omega_{step}$  is sent to the engine speed controller. Since  $P_{gen}$  should be zero the  $P_{gen}$  control has to be

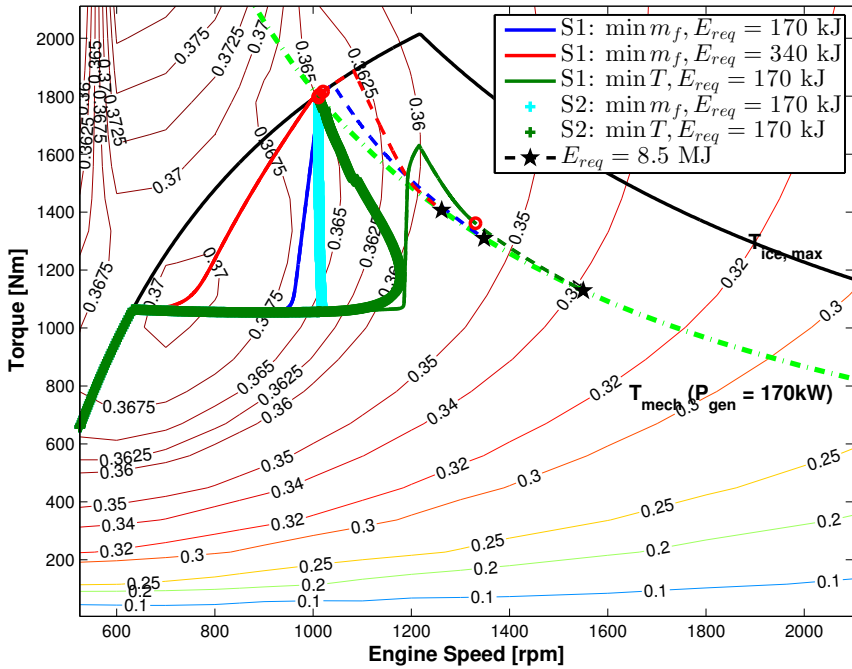


Figure 5: The resulting engine torque-engine speed trajectories for the two control strategies, with gains optimized for  $E_{req} = [170, 340]$  kJ but also simulated for  $E_{req} = 8.5$  MJ. Solid and + are optimized results with red circles marking the end points, dashed are simulated until  $E_{req} = 8.5$  MJ with pentagrams marking the end points.

disconnected. When  $\omega_{ice} = \omega_{step}$ ,  $P_{gen} = P_{req}$  and this power should then be maintained and if  $\omega_{step}$  is correct the engine speed should decrease. When  $\frac{d\omega_{ice}}{dt} \geq 0$  the speed reference is set to  $\omega_{ice,ref}$ . For this to work the integrator in the engine speed controller needs to be reset to a value fitting the target operating point, which makes the control sensitive to errors and integral wind-up. When this shift of reference occurs the generator control can be activated since now the reference speed is the target for control, not just a value to ensure that the control follows the smoke-limiter. This control increases the number of control parameters with one, since  $\omega_{ice,ref,1}$  is just set to a value higher than  $\omega_{step}$ , which means that only  $\omega_{step}$  and  $\omega_{ice,ref}$  need to be decided.

## 6.2 Optimal control with the engine Load controlled (S2)

Using S2 the torque reference is calculated using  $\omega_{ice,ref}$  and  $P_{req}$ . The difference here compared to S2 is that the generator is not activated by exceeding  $\omega_{ice,ref}$ , but by exceeding  $\omega_{step}$ . When this speed is exceeded  $P_{gen} = sat(P_{gen,sp})$  calculated according to (12) with the integrator part set to  $P_{req}$ . To avoid integral wind-up this is reset to  $P_{req}$  when  $\omega_{ice,err} = 0$ . To avoid decreasing the reference when it is not necessary  $T_{red} = 0$  and only activated if the step has occurred and  $\frac{d\omega_{ice}}{dt} > 0$ . When  $\omega_{ice,err} = 0$  it is then reset to zero. This scheme then only has one extra parameter,  $\omega_{step}$ .

## 6.3 Results and discussion

For both strategies  $\omega_{step}$  and  $\omega_{ice,ref}$  need to be decided.  $\omega_{ice,ref}$  can be found from stationary measurements, however  $\omega_{step}$  is not as easily defined. To investigate the controllers sensitivity to error in this parameter it is varied  $\omega_{opt} \pm 10\%$  where  $\omega_{opt}$  is the speed where the step occurs in the optimal min  $m_{f,2-phase}$  solution shown in Fig. 4.  $\omega_{ice,ref}$  is decided as the end operating point from that solution. The results are shown in Fig. 6 and in Table 1.

For both strategies it is possible to control the GENSET in an optimal manner, both controllers end up being as fast and roughly as fuel efficient as the optimal solution. For S1 the control is however quite sensitive to errors in  $\omega_{step}$ . It also has the drawback that the integrator of the engine speed controller needs to be reset, something that is not available in the SAE J1939 standard. In Fig. 6 the used gains are in the same range as for S1:  $\min m_f, E_{req} = 340$  kJ. With 10% error in  $\omega_{step}$  the control ends up with the engine stalling, indicating that this control strategy is not very robust. For S2 the gains are set to reasonable values, not tuned for a specific criteria. S2 does not have the drawback of changing reference as with S1, looking at Fig. 6 is also robust to errors in  $\omega_{step}$ . Despite errors of 10% the control manages to bring the GENSET to stationarity in speed and power within 1.5s.

# 7 Conclusion

In this paper the performance of several different control strategies for a diesel-electric powertrain in transient operation are discussed and evaluated compared

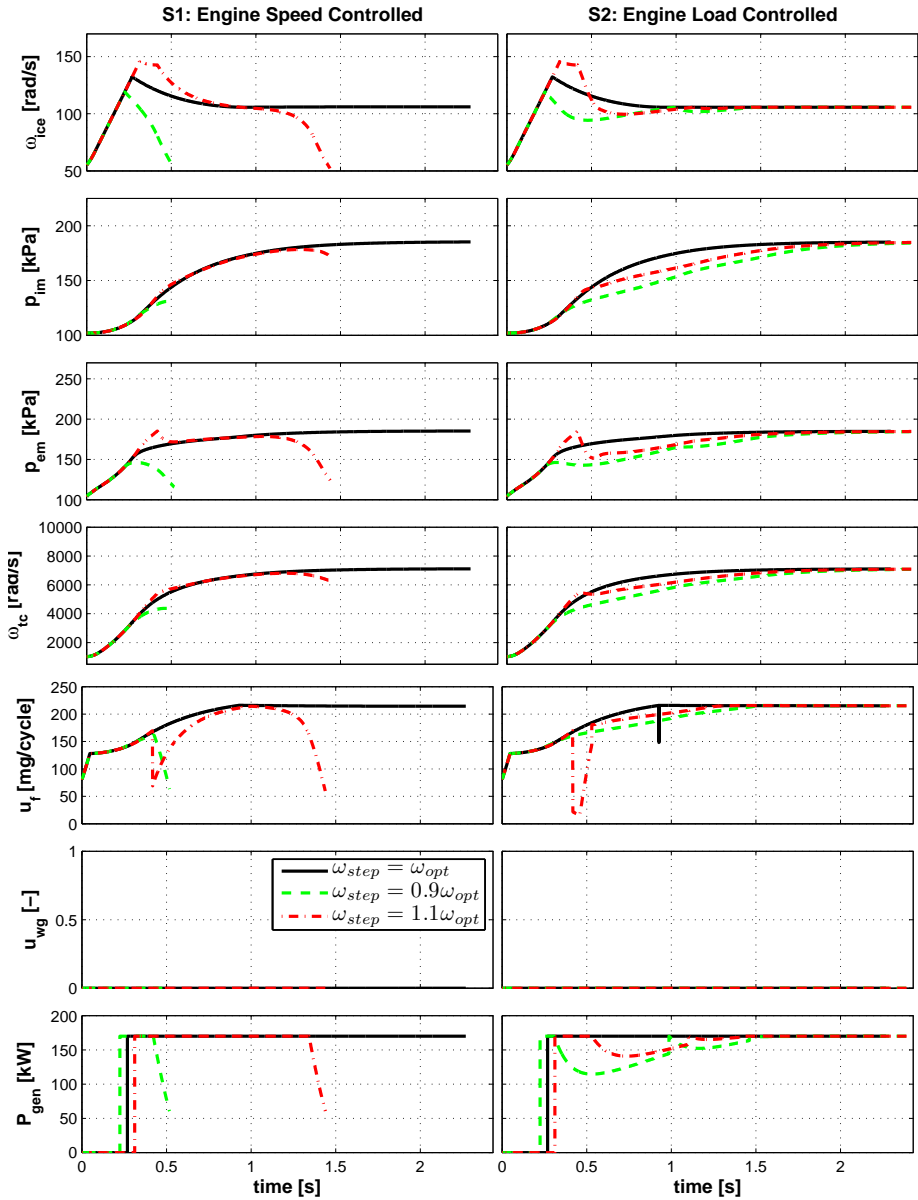


Figure 6: Optimal control using S1 and S2. S2 is robust to errors in  $\omega_{step}$ , S1 is not.

Table 1: Change in fuel and time compared to  $\min T$ ,  $E_{req} = 340$  kJ.

	$\Delta m_f$ [%]	$\Delta T$ [%]
$\min T$	0.0	0.0
$\min m_f$	-1.7	65.2
$\min m_{f,2-phase}$	0.1	0.0
$\min T_{opt-line}$	-1.4	27.7
$\min m_{f,opt-line}$	-1.5	38.3
S1: $\min T$	8.0	0.8
S1: $\min m_f$	-1.2	25.2
S2: $\min T$	0.0	0.3
S2: $\min m_f$	-0.1	3.8
S1: Opt-control	0.2	0.0
S2: Opt-control	0.1	0.0

to the optimal control trajectories. The considered problem is that the GENSET starts at idle and the operator requests a certain power,  $P_{req}$  a power that should be met either as fast or as fuel efficient as possible. To make the controllers comparable this is augmented with that a certain amount of energy has to be produced. The controllers are then evaluated in terms of duration and fuel economy compared to the minimum fuel and minimum time solutions.

First a strategy where the control is limited to follow the stationary optimal line is evaluated. It is seen to provide almost optimal fuel economy, it however takes almost 3s to reach the requested output power, regardless of criteria.

Then two basic PI control strategies using the same structure as used in industry are studied. The engine is controlled using the SAE J1939-standard which has the options of using speed control or load control to control the engine. The gains of the PI controllers are then tuned for minimum time or minimum fuel. With the engine speed controlled, a strategy called S1, the controller is seen to give almost optimal performance in the metric for which it was tuned, for the other metric the performance is not as good. With the engine load controlled, called S2, the resulting solutions represents a better trade-off between the two metrics, while still being close the optimal results.

Finally it is shown that the optimal trajectories could be implemented using the SAE J1939-standard, both with the engine speed controlled and with the engine load controlled. With the engine speed controlled this involves switching speed reference and resetting of the internal speed controller of the engine, something that may not be possible. It is also seen that the control is not robust to errors in one of the parameters describing the optimal solution. With the engine load controlled on the other hand the reference sent to the engine is in the ideal case constant throughout the transient and even with errors it is changed in a less dramatic way. The resulting controller is also seen to be robust to errors and to able to bring the engine speed and output power to stationarity within 1.5s.

## References

- [1] S Di Cairano, W Liang, I V Kolmanovsky, M L Kuang, and A M Phillips. Power smoothing energy management and its application to a series hybrid powertrain. *IEEE Transactions on Control Systems Technology*, 21(6): 2091–2103, 2013.
- [2] A. R. Cooper, D.J. Morrow, and K. D R Chambers. A turbocharged diesel generator set model. In *Universities Power Engineering Conference (UPEC), 2009 Proceedings of the 44th International*, pages 1–5, 2009.
- [3] Joon-Hwan Lee, Seung-Hwan Lee, and Seung-Ki Sul. Variable speed engine generator with super-capacitor; isolated power generation system and fuel efficiency. In *Industry Applications Society Annual Meeting, 2008. IAS '08. IEEE*, pages 1–5, 2008.
- [4] J. Leuchter, V. Refucha, Z. Krupka, and P. Bauer. Dynamic behavior of mobile generator set with variable speed and diesel engine. In *Power Electronics Specialists Conference, 2007. PESC 2007. IEEE*, pages 2287–2293, 2007.
- [5] Constantine D Rakopoulos and Evangelos G Giakoumis. *Diesel engine transient operation - Principles of operation and simulation analysis*. Springer, 2009.
- [6] SAE J1939 Standard. "[http://standards.sae.org/j1939/71\\_201002/](http://standards.sae.org/j1939/71_201002/)", 2013. Read 2013-10-04.
- [7] V Sezer, M Gokasan, and S Bogosyan. A novel ecms and combined cost map approach for high-efficiency series hybrid electric vehicles. *IEEE Transactions on Vehicular Technology*, 60(8):3557–3570, 2011.
- [8] Martin Sivertsson and Lars Eriksson. Time and fuel optimal power response of a diesel-electric powertrain. In *E-COSM'12 – IFAC Workshop on Engine and Powertrain Control, Simulation and Modeling*, Paris, France, October 2012.
- [9] Martin Sivertsson and Lars Eriksson. Optimal transient control and effects of a small energy storage for a diesel-electric powertrain. In *AAC'13–The 7th IFAC Symposium on Advances in Automotive Control*, Tokyo, Japan, September 2013.
- [10] Martin Sivertsson and Lars Eriksson. Generator effects on the optimal control of a power assisted diesel-electric powertrain. In *IEEE VPPC 2013 – The 9th IEEE Vehicle Power and Propulsion Conference*, Beijing, China, October 2013.
- [11] Hyunjae Yoo, Byung-Geuk Cho, Seung-Ki Sul, Sang-Min Kim, and Yongho Park. A power flow control strategy for optimal fuel efficiency of a variable speed engine-generator based series hybrid electric vehicle. In *IEEE ECCE'09 Energy Conversion Congress and Exposition*, 2009.

# A Nomenclature

Table 2: Model nomenclature

Symbol	Description
$\omega_{ice}$	Engine Speed
$p_{im}$	Intake manifold pressure
$p_{em}$	Exhaust manifold pressure
$\omega_{tc}$	Turbocharger speed
$u_f$	Injected fuel per cycle
$u_{wg}$	Wastegate position
$P_{gen}$	Electrical generator power
$P_{mech}$	Mechanical generator power
$T_{ice}$	Engine torque
$\dot{m}_c$	Compressor massflow
$\dot{m}_{ac}$	Air massflow into the cylinders
$\dot{m}_f$	Fuel massflow
$\dot{m}_t$	Turbine massflow
$\dot{m}_{wg}$	Wastegate massflow
$T_{em}$	Exhaust manifold temperature
$P_c$	Compressor power
$P_t$	Turbine power
$J_{genset}$	GENSET inertia
$J_{tc}$	Turbocharger inertia
$T_{im}$	Intake manifold temperature
$R_{a/e}$	Gas constant air/exhaust gas
$V_{is}$	Volume of intake system
$V_{em}$	Volume of exhaust manifold
$w_{fric}$	Friction coefficient, turbocharger



# Modeling for Optimal Control: A Validated Diesel-Electric Powertrain Model<sup>†</sup>

Martin Sivertsson<sup>a</sup> and Lars Eriksson<sup>a</sup>

<sup>a</sup>*Vehicular Systems, Department of Electrical Engineering,  
Linköping University, SE-581 83 Linköping, Sweden.*

---

<sup>†</sup>This is a formatted version of “Modeling for Optimal Control: A Validated Diesel-Electric Powertrain Model” by Martin Sivertsson and Lars Eriksson, SIMS 2014 - 55th International Conference on Simulation and Modelling, Aalborg, Denmark. The original version can be found at LiU Electronic Press, [http://www.ep.liu.se/ecp\\_home/index.en.aspx?issue=108](http://www.ep.liu.se/ecp_home/index.en.aspx?issue=108). The formatting is restricted to changing the article into a single-column format, adjusting sizes of figures and tables, and adjusting the referencing style.

## **Abstract**

An optimal control ready model of a diesel-electric powertrain is developed, validated and provided to the research community. The aim of the model is to facilitate studies of the transient control of diesel-electric powertrains and also to provide a model for developers of optimization tools. The resulting model is a four state three control mean value engine model that captures the significant nonlinearity of the diesel engine, while still being continuously differentiable.

# Nomenclature

Table 1: Symbols used

Symbol	Description	Unit
$p$	Pressure	Pa
$T$	Temperature	K
$\omega$	Rotational speed	rad/s
$N$	Rotational speed	rpm
$\dot{m}$	Massflow	kg/s
$P$	Power	W
$M$	Torque	Nm
$\Pi$	Pressure ratio	-
$V$	Volume	$m^3$
$\eta$	Efficiency	-
$A$	Area	$m^2$
$\Psi$	Head parameter	-
$\Phi$	Flow parameter	-
$\gamma$	Specific heat capacity ratio	-
$c_p$	Specific heat capacity constant pressure	J/(kg · K)
$c_v$	Specific heat capacity constant volume	J/(kg · K)
$R$	Gas Constant	J/(kg · K)
$r_c$	Compression ratio	-
$n_{cyl}$	Number of cylinders	-
$(A/F)_s$	Stoichiometric air/fuel-ratio	-
$q_{HV}$	Lower heating value of fuel	J/kg
$u_f, u_{wg}, P_{gen}$	Control signals	mg/cycle, -, W
$J$	Inertia	$kg \cdot m^2$
$BSR$	Blade speed ratio	-
$R$	Radius	m
$\lambda$	Air/fuel equivalence ratio	-
$\phi$	Fuel/air equivalence ratio	-

## Introduction

Optimal control can be an important tool to gain insight into how to control complex nonlinear multiple-input multiple-output systems. However for the model to be analyzable and also for the results to be relevant, higher demands are set on model quality. This relates both to differentiability of the model, for efficient solution processes of the optimal control problem, and also its extrapolation properties since the obtained solutions are often on the border to or outside the nominal operating region. This paper presents the modeling and final model of a diesel-electric powertrain to be used in the study of transient operation. This optimal control ready model will also be made available to the research community to further encourage optimal control studies.

Table 2: Subscripts used

Index	Description	Index	Description
<i>amb</i>	Ambient	<i>c</i>	Compressor
<i>im</i>	Intake manifold	<i>em</i>	Exhaust manifold
01	Compressor inlet	02	Compressor outlet
<i>eo</i>	Engine out	<i>a</i>	Air
<i>e</i>	Exhaust	<i>ac</i>	After Compressor
<i>f</i>	Fuel	<i>ice</i>	Engine
<i>GenSet</i>	Engine-Generator	<i>t</i>	Turbine
<i>wg</i>	Wastegate	<i>es</i>	Exhaust System
<i>vol</i>	Volumetric	<i>d</i>	Displaced
<i>fric</i>	Friction	<i>pump</i>	Pumping
<i>ig</i>	Indicated gross	<i>mech</i>	Mechanical
<i>tc</i>	Turbocharger	<i>ref</i>	Reference

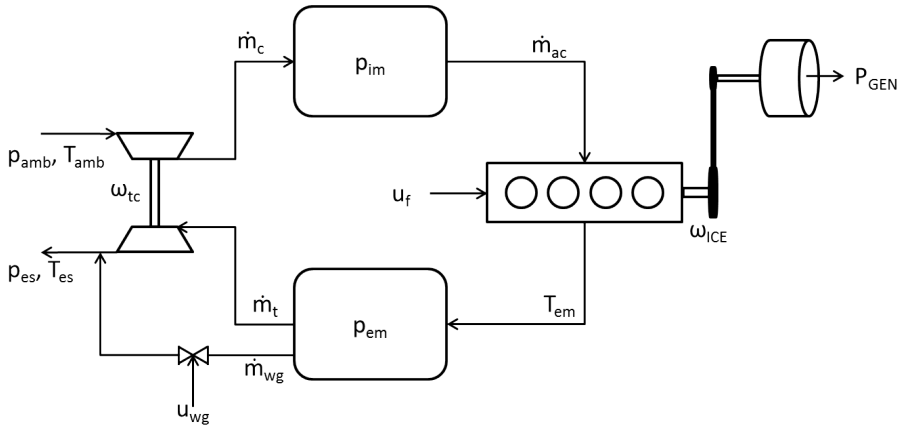


Figure 1: Structure of the model

The resulting model is a four state, three control, mean value engine model (MVEM) that consists of 10 submodels that are all continuously differentiable, and suitable for automatic differentiation, in the region of interest in order to enable the nonlinear program solvers to use higher order search methods.

In engine simulation the component efficiencies are often implemented as maps. In an optimal control framework such strategies are undesirable, instead the developed model includes analytically differentiable efficiency models for the compressor, turbine, cylinder massflow, engine torque and generator power. The efficiency map of the measured production engine is highly nonlinear, see Fig. 3-left, something that is well captured by the developed model, as seen in Fig. 2-left. The resulting mean relative model errors are less than 2.9% for the states and less than 5.4% for the component models.

A typical internal combustion engine normally has an efficiency "island" located near the maximum torque line where its peak efficiency is obtained,

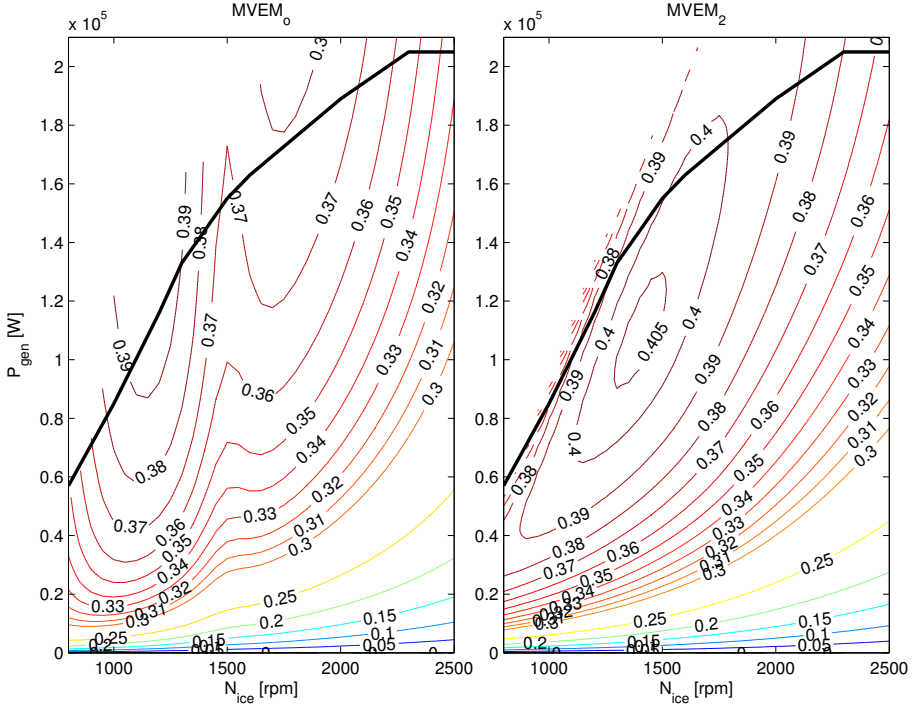


Figure 2: Efficiency of the two models,  $MVEM_0$ : a model trying to capture the characteristics of the modeled engine (left) and  $MVEM_2$ : a model representing a typical engine (right).

see [4, 5, 1]. Due to the special nature of the efficiency map of the measured engine the model is also provided with a second torque model, yielding a more typical efficiency map, see Fig. 2-right.

## 1 Contributions

The contributions of the paper are three-fold: 1) A methodology how to model and parametrize a model of a diesel-electric powertrain is presented. The measurements are conducted without a dynamometer, the only requirements are a diesel-electric powertrain and sensors. 2) A model structure and modeling approach with provided equations, enabling researchers to adjust the parameters of the model to represent their own powertrain. 3) It also provides researchers without engine models or data a relevant and validated open source model on which control design or optimization can be performed.

Measured	Implemented	Measured	Implemented
$\omega_{ice}$	State	$T_{amb}$	Constant
$p_{im}$	State	$T_{01}$	$T_{amb}$
$p_{em}$	State	$T_{02}$	not used
$\omega_{tc}$	State	$T_{im}$	Constant
$\dot{m}_f$	Control ( $u_f$ )	$T_{em}$	Static model
$u_{wg}$	Control	$p_{amb}$	Constant
$P_{gen}$	Control	$p_{01}$	$p_{amb}$
$\dot{m}_c$	Static model	$p_{02}$	$p_{im}$
$p_{es}$	Constant	$\lambda$	Static model

Table 3: Measured variables and their implementation in the model.

## 2 Model structure

The aim of the model is control systems design and optimization. This imposes the requirement that the model has to be detailed, but at the same time computationally fast. This leads to a 0-D or MVEM approach. Within MVEM there are two different approaches, one is black box modelling or standard system identification techniques, another is physical modelling where the engine is described using standard physical relations. Due to that one of the model aims is optimization and the solution of optimization problems often are on the border to or outside the nominal operating region the physical modeling approach is selected for its extrapolation properties. For more information about engine modelling as well as the state of the art of engine models the reader is referred to [4, 5].

## 3 Modeling

The measured and modeled engine-generator combination (GenSet) consists of a generator mounted on the output shaft of a medium-duty tier 3 diesel-engine. The engine is equipped with a charge air cooled wastegated turbocharger. The states of the developed MVEM are engine speed,  $\omega_{ice}$ , inlet manifold pressure,  $p_{im}$ , exhaust manifold pressure,  $p_{em}$ , turbocharger speed,  $\omega_{tc}$ . The controls are injected fuel mass,  $u_f$ , wastegate position,  $u_{wg}$ , and generator power,  $P_{gen}$ .

The submodels are models for compressor massflow and power, engine out and exhaust manifold temperatures, cylinder massflow, turbine massflow and power, wastegate massflow, engine torque and generator power, with connections between the components as in Fig 1. The signals measured and also how they are implemented in the model are listed in Table 3. The data sets used are described in Appendix and listed in Table 5-7.

The tuning process is that first the component models are tuned to stationary measurements. Then the dynamic models are tuned using the results from the component tuning, and finally the whole model is tuned to both dynamic and stationary measurements. In the dynamic and full model tuning all measured signals except the states and  $\dot{m}_f$  are used.

### 3.1 Error measure

In the modeling the following relative error is used:

$$e_{\text{rel}}(k) = \frac{y_{\text{mod}}(k) - y_{\text{meas}}(k)}{\frac{1}{M} \sum_{l=1}^M |y_{\text{meas,stat}}(l)|} \quad (1)$$

i.e. regardless of whether it is dynamic or stationary measurements that are considered the error is normalized by the mean absolute value from the stationary measurements. In the tuning it is the euclidean norm of this relative error that is minimized.

### 3.2 Dynamic Models

There are four dynamic models, two rotational states and two manifolds. The rotational states,  $\omega_{ice}$  and  $\omega_{tc}$  are modelled using Newton's second law

$$J_{GenSet} \frac{d\omega_{ice}}{dt} = \frac{P_{ice} - P_{mech}}{\omega_{ice}} \quad (2)$$

$$J_{tc} \frac{d\omega_{tc}}{dt} = \frac{P_t \eta_{tm} - P_c}{\omega_{tc}} \quad (3)$$

and the manifolds are modelled using the standard isothermal model [7]

$$\frac{dp_{im}}{dt} = \frac{R_a T_{im}}{V_{im}} (\dot{m}_c - \dot{m}_{ac}) \quad (4)$$

$$\frac{dp_{em}}{dt} = \frac{R_e T_{em}}{V_{em}} (\dot{m}_{ac} + \dot{m}_f - \dot{m}_t - \dot{m}_{wg}) \quad (5)$$

where in the tuning the measured intake manifold temperature,  $T_{im}$  is used but in the final model the intercooler is assumed to be ideal, i.e. no pressure loss and  $T_{im}$  constant. The dynamic models have four tuning parameters,  $J_{GenSet}$ ,  $J_{tc}$ ,  $V_{im}$  and  $V_{em}$ .

### 3.3 Compressor

The compressor model consists of two sub-models, one for the massflow and one for efficiency. In order to avoid problems for low turbocharger speeds and transients with pressure ratios  $\Pi_c < 1$  a variation of the physically motivated  $\Psi$   $\Phi$  model in [4] is used. The idea is that  $\Psi$  approaches a maximum at zero flow and that the maximum flow in the region of interest is quadratic in  $\omega_{tc}$ .

#### Massflow model

The pressure quotient over the compressor:

$$\Pi_c = \frac{p_{02}}{p_{01}} \quad (6)$$

Pressure ratio for zero flow:

$$\Pi_{c,max} = \left( \frac{\omega_{tc}^2 R_c^2 \Psi_{max}}{2c_{p,a} T_{01}} + 1 \right)^{\frac{\gamma_a}{\gamma_a - 1}} \quad (7)$$

Corrected and normalized turbocharger speed:

$$\omega_{tc,corr,norm} = \frac{\omega_{tc}}{15000\sqrt{T_{01}/T_{ref}}} \quad (8)$$

Maximum corrected massflow:

$$\begin{aligned} \dot{m}_{c,corr,max} = \\ c_{\dot{m}_{c,1}}\omega_{tc,corr,norm}^2 + c_{\dot{m}_{c,2}}\omega_{tc,corr,norm} + c_{\dot{m}_{c,3}} \end{aligned} \quad (9)$$

Corrected massflow:

$$\dot{m}_{c,corr} = \dot{m}_{c,corr,max} \sqrt{1 - \left( \frac{\Pi_c}{\Pi_{c,max}} \right)^2} \quad (10)$$

The massflow is then given by:

$$\dot{m}_c = \frac{\dot{m}_{c,corr} p_{01} / p_{ref}}{\sqrt{T_{01}/T_{ref}}} \quad (11)$$

The surge-line is modeled using the lowest massflows for each speedline from the compressor map and is well described by the linear relationship:

$$\Pi_{c,surge} = c_{\dot{m}_{c,surge,1}} \dot{m}_{c,corr} + c_{\dot{m}_{c,surge,2}} \quad (12)$$

In an optimization context surge is undesirable why this is implemented as a constraint according to:

$$\Pi_c \leq \Pi_{c,surge} \quad (13)$$

### Efficiency model

The efficiency of the compressor is modeled using a quadratic form in the flow parameter  $\Phi$  and speed  $\omega_{tc}$  following [4]. The dimensionless flow parameter is defined as:

$$\Phi = \frac{\dot{m}_c R_a T_{01}}{\omega_{tc} 8 R_c^3 p_{01}} \quad (14)$$

Deviation from optimal flow and speed:

$$d\Phi = \Phi - \Phi_{opt} \quad (15)$$

$$d\omega = \omega_{tc,corr,norm} - \omega_{opt} \quad (16)$$

The compressor efficiency is given by:

$$\eta_c = \eta_{c,max} - \begin{bmatrix} d\Phi \\ d\omega \end{bmatrix}^T \begin{bmatrix} Q_1 & Q_3 \\ Q_3 & Q_2 \end{bmatrix} \begin{bmatrix} d\Phi \\ d\omega \end{bmatrix} \quad (17)$$

The consumed power is calculated as the power from consumed in an isentropic process divided by the efficiency:

$$P_c = \frac{\dot{m}_c c_{p,a} T_{01} \left( \Pi_c^{\frac{\gamma_a-1}{\gamma_a}} - 1 \right)}{\eta_c} \quad (18)$$

### Initialization

The compressor has 10 tuning parameters,  $\Psi_{max}$ ,  $c_{\dot{m}_{c,1-3}}$ ,  $\Phi_{opt}$ ,  $\eta_{c,max}$  and  $\omega_{opt}$ ,  $Q_{1-3}$ . The model is first fitted to the compressor map then to the stationary measurements, using data set A, but then  $\dot{m}_c$  is measured and  $\eta_c$  and  $P_c$  are calculated according to:

$$\eta_c = \frac{T_{01}(\Pi_c^{1-1/\gamma_a} - 1)}{T_{02} - T_{01}} \quad (19)$$

$$P_c = \dot{m}_c c_{p,a} (T_{02} - T_{01}) \quad (20)$$

The results are mean/max absolute errors of [2.4/8.2, 2.3/23.2, 1.4/7.8] % for [ $\dot{m}_c$ ,  $\eta_c$ ,  $P_c$ ] respectively.

### 3.4 Cylinder Gas Flow

The cylinder gas flow models are models for the air and fuel flow in to the cylinder. The airflow model is a model for the volumetric efficiency of the engine. The model used is the same as in [9] according to:

$$\eta_{vol} = c_{vol,1}\sqrt{p_{im}} + c_{vol,2}\sqrt{\omega_{ice}} + c_{vol,3} \quad (21)$$

$$\dot{m}_{ac} = \frac{\eta_{vol} p_{im} \omega_{ice} V_d}{4\pi R_a T_{im}} \quad (22)$$

The control signal  $u_f$  is injected fuel mass in mg per cycle and cylinder and the total fuel flow is thus given by:

$$\dot{m}_f = \frac{10^{-6}}{4\pi} u_f \omega_{ice} n_{cyl} \quad (23)$$

The air-fuel equivalence ratio  $\lambda$  is computed using:

$$\lambda = \frac{\dot{m}_{ac}}{\dot{m}_f} \frac{1}{(A/F)_s} \quad (24)$$

In diesel engines a lower limit on  $\lambda$  is usually used in order to reduce smoke. However in fuel cut, i.e.  $u_f = 0$ ,  $\lambda = \infty$  which is undesirable in optimization. Instead the fuel-air equivalence ratio  $\phi$  is used and the lower limit on  $\lambda$  can be expressed as:

$$\phi = \frac{\dot{m}_f}{\dot{m}_{ac}} (A/F)_s \quad (25)$$

$$0 \leq \phi \leq \frac{1}{\lambda_{min}} \quad (26)$$

### Initialization

The tuning parameters of the gas flow models are  $c_{vol,1-3}$ . The model is initialized using all stationary measurements, i.e. set A using that at stationary conditions  $\dot{m}_{ac} = \dot{m}_c$ . The volumetric efficiency model corresponds well to measurements with a mean/max absolute relative error of [0.9/3.7] %.

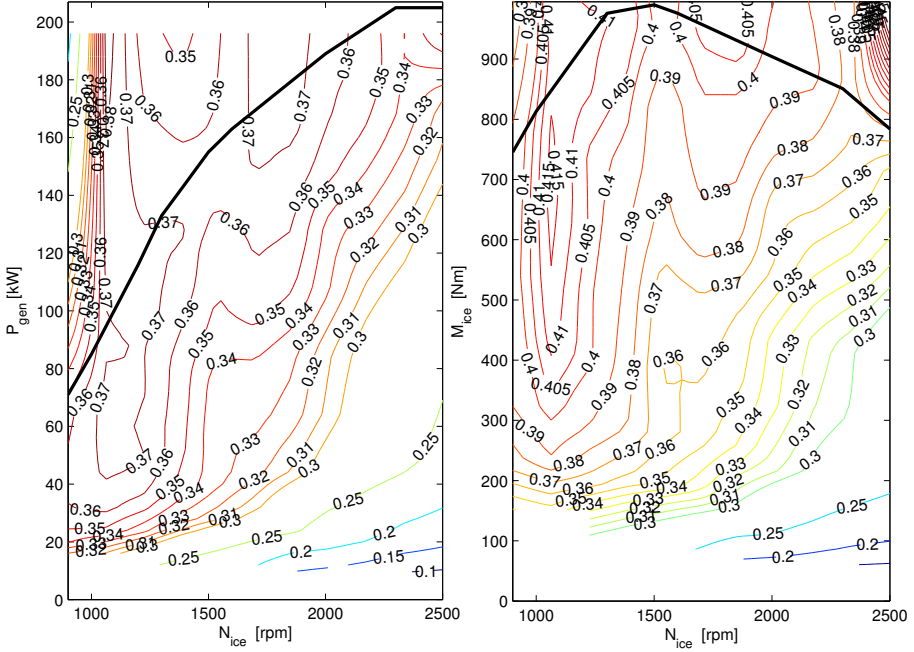


Figure 3: Efficiency of the powertrain (left) and efficiency of the engine (right)

### 3.5 Engine torque and generator

The engine torque is not measured so the tuning of the torque models have to rely on the DC-power out from the power electronics. Then there are actually three efficiencies that should be modeled, the power electronics, the generator, and the engine efficiencies. In Fig. 3-left the total efficiency of the powertrain is shown, with the maximum power line.

First the engine torque model is tuned. In the tuning the engine torque is calculated using the stationary efficiency map of the generator, provided by the manufacturer. The efficiency of the power electronics is lumped with the generator efficiency and is here assumed to be 0.98. Then the generator model is tuned, first using the stationary map and then measurements but with the torque calculated using the efficiency map.

#### Engine torque model

In Fig. 3-right the efficiency of the engine is shown, with  $M_{ice}$  calculated using the generators efficiency map and 2% losses in the power electronics assumed. The engine torque is modeled using three components, see [7], i.e. friction torque,  $M_{fric}$ , pumping torque  $M_{pump}$  and gross indicated torque,  $M_{ig}$ . The torque consumption of the high pressure pump is not modeled on it's own, but lumped in to the following models. The net torque of the engine can then be computed.

$$M_{ice} = M_{ig} - M_{fric} - M_{pump} \quad (27)$$

The pumping torque is proportional to the pressure quotient over the cylinder:

$$M_{pump} = \frac{V_d}{4\pi} (p_{em} - p_{im}) \quad (28)$$

The friction torque is modeled as a quadratic shape in engine speed:

$$M_{fric} = \frac{V_d}{4\pi} 10^5 (c_{fr1}\omega_{ice}^2 + c_{fr2}\omega_{ice} + c_{fr3}) \quad (29)$$

The indicated gross torque is proportional to the fuel energy:

$$M_{ig} = \frac{u_f 10^{-6} n_{cyl} q_{HV} \eta_{ig}}{4\pi} \quad (30)$$

Where the indicated gross efficiency is defined as:

$$\eta_{ig} = \eta_{ig,t} \left(1 - \frac{1}{r_c^{\gamma_{cyl} - 1}}\right) \quad (31)$$

The torque model in (27)-(31) is fairly common, and if  $\eta_{ig,t}$  is implemented as a constant maximum brake torque (MBT)-timing is assumed. A typical internal combustion engine normally has an efficiency "island" located near the maximum torque line where its peak efficiency is obtained, see [4, 5, 1]. However looking at Fig. 3-right this is clearly not the case. Therefore the model is provided with two different torque models, seen in Fig. 4.

Torque model 1 (TM1) is used in the model tuning and validation and is designed to capture the nonlinear nature seen in Fig. 3. TM1 consists of two second order polynomials and a switching function:

$$\eta_{ig,t} = M_{f,1} + g_f (M_{f,2} - M_{f,1}) \quad (32)$$

$$g_f = \frac{1 + \tanh(0.1(\omega_{ice} - 1500\pi/30))}{2} \quad (33)$$

$$M_{f,1} = c_{M_{f,1,1}}\omega_{ice}^2 + c_{M_{f,1,2}}\omega_{ice} \quad (34)$$

$$M_{f,2} = c_{M_{f,2,1}}\omega_{ice}^2 + c_{M_{f,2,2}}\omega_{ice} + c_{M_{f,2,3}} \quad (35)$$

Torque model 2 (TM2) is designed and provided to represent a "typical" engine with an efficiency island, to be used for optimal control studies, and is thus not used in the tuning or validation. TM2 is quadratic in  $\frac{u_f}{\omega_{ice}}$  and expressed as

$$\eta_{ig,t} = \eta_{ig,ch} + c_{u_f,1} \left(\frac{u_f}{\omega_{ice}}\right)^2 + c_{u_f,2} \frac{u_f}{\omega_{ice}} \quad (36)$$

The maximum power line is implemented as a limit on the net power of the engine,  $P_{ice} = T_{ice}\omega_{ice}$ , which is well approximated by two quadratic functions and a maximum value:

$$P_{ice} \leq P_{ice,max} \quad (37)$$

$$P_{ice} \leq c_{P_1}\omega_{ice}^2 + c_{P_2}\omega_{ice} + c_{P_3} \quad (38)$$

$$P_{ice} \leq c_{P_4}\omega_{ice}^2 + c_{P_5}\omega_{ice} + c_{P_6} \quad (39)$$

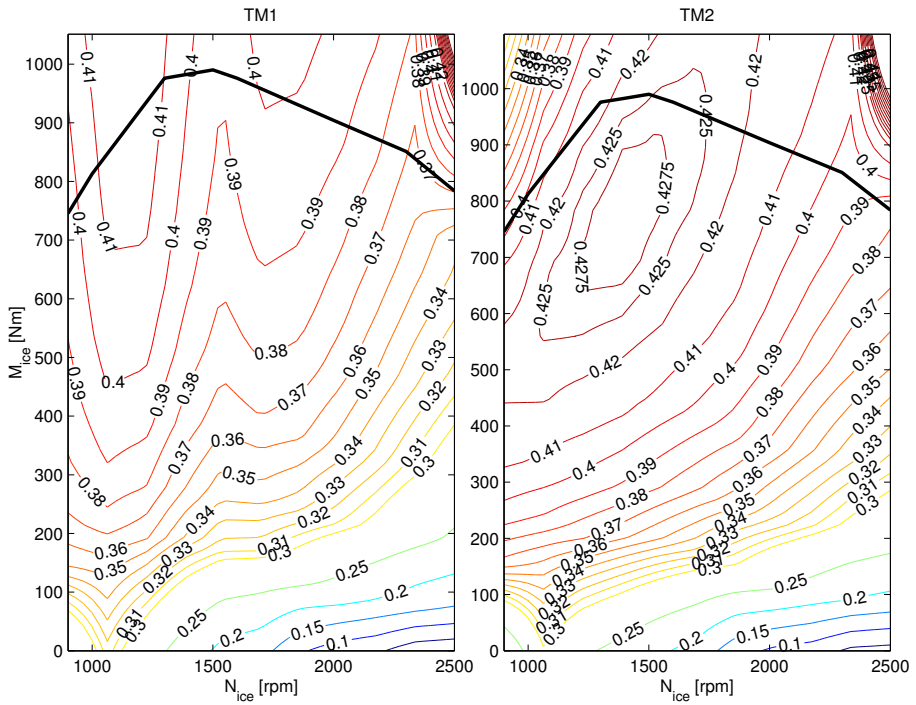


Figure 4: The two different torque models. Left: (32) certification speed . Right: (36) "Typical"

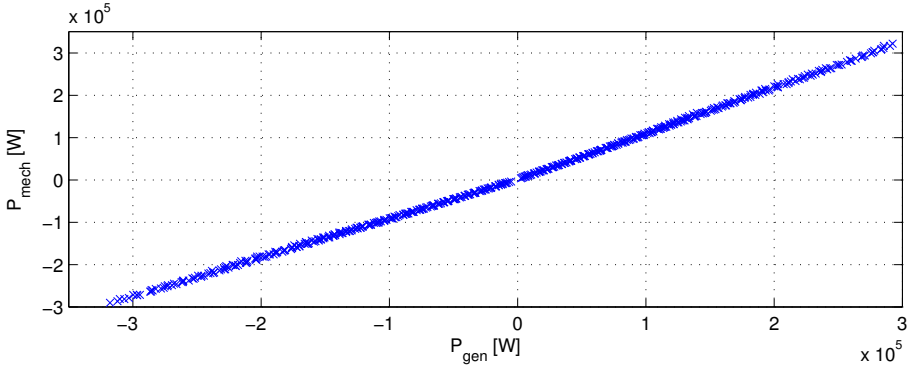


Figure 5: Mechanical generator power as a function of electrical power

### Initialization

The two torque models have eight and six tuning parameters respectively. The tuning parameters are  $c_{fr1-3}$ , and  $c_{Mf,1,1-2}$ ,  $c_{Mf,2,1-3}$ , or  $\eta_{ig,ch}$  and  $c_{uf,1-2}$ . The models are fitted using set C. For (32) it is rather straightforward. For model (36) the "island" is not visible in the measured data, therefore the parameters of  $\eta_{ig,ch}$  are manually tuned and the  $M_{fric}$  model is tuned assuming MBT-timing. The mean/max absolute relative errors of TM1 are [2.2/10.9] %.

### Generator model

Looking at Fig. 5 a reasonable first approximation of the relationship between mechanical and electrical power of the generator is two affine functions, something normally denoted willans line, [6], where the slope of the line depends on whether the generator is in generator or motor mode.

$$P_{mech}^+ = e_{gen,1}P_{gen} + P_{gen,0}, \quad \text{if } P_{gen} \geq 0 \quad (40)$$

$$P_{mech}^- = e_{gen,2}P_{gen} + P_{gen,0}, \quad \text{if } P_{gen} < 0 \quad (41)$$

This model is not continuously differentiable so therefore to smoothen it out a switching function is used. The model is then given by:

$$P_{mech} = P_{mech}^- + \frac{1 + \tanh(0.005P_{gen})}{2} (P_{mech}^+ - P_{mech}^-) \quad (42)$$

$e_{gen,1-2}$  are seen to have a quadratic dependency on  $\omega_{ice}$ , a reasonable addition to the willans line is thus to model  $e_{gen,1-2}$  as:

$$e_{gen,x} = e_{gen,x-1}\omega_{ice}^2 + e_{gen,x-2}\omega_{ice} + e_{gen,x-3} \quad (43)$$

which constitutes the full model.

### Initialization

The generator model has seven tuning parameters,  $P_{gen,0}$  and  $e_{gen,1/2,1-3}$ . The model is first fitted to the generator map and secondly to measurement data,

using set C. The mean/max absolute relative errors of the generator model are [0.7/2.5] %.

### 3.6 Exhaust temperature

The cylinder out temperature model is based on ideal the Seiliger cycle and is a version of the model found in [9]. The model consists of the pressure quotient over the cylinder:

$$\Pi_e = \frac{p_{em}}{p_{im}} \quad (44)$$

The specific charge:

$$q_{in} = \frac{\dot{m}_f q_{HV}}{\dot{m}_f + \dot{m}_{ac}} (1 - x_r) \quad (45)$$

The combustion pressure quotient:

$$x_p = \frac{p_3}{p_2} = 1 + \frac{q_{in} x_{cv}}{c_{v,a} T_1 r_c^{\gamma_a - 1}} \quad (46)$$

The combustion volume quotient:

$$x_v = \frac{v_3}{v_2} = 1 + \frac{q_{in} (1 - x_{cv})}{c_{p,a} \left( \frac{q_{in} x_{cv}}{c_{v,a}} + T_1 r_c^{\gamma_a - 1} \right)} \quad (47)$$

The residual gas fraction:

$$x_r = \frac{\Pi_e^{1/\gamma_a} x_p^{-1/\gamma_a}}{r_c x_v} \quad (48)$$

Temperature after intake stroke:

$$T_1 = x_r T_{eo} + (1 - x_r) T_{im} \quad (49)$$

The engine out temperature:

$$T_{eo} = \eta_{sc} \Pi_e^{1-1/\gamma_a} r_c^{1-\gamma_a} x_p^{1/\gamma_a - 1} \left( q_{in} \left( \frac{1 - x_{cv}}{c_{p,a}} + \frac{x_{cv}}{c_{v,a}} \right) + T_1 r_c^{\gamma_a - 1} \right) \quad (50)$$

To account for the cooling in the pipes the model from [2] is used, where  $V_{pipe}$  is the total pipe volume:

$$T_{em} = T_{amb} + (T_{eo} - T_{amb}) e^{-\frac{h_{tot} V_{pipe}}{(\dot{m}_f + \dot{m}_{ac}) c_{p,e}}} \quad (51)$$

The model equations described in (45)-(50) are nonlinear and depend on each other and need to be solved using fixed point iterations. In [9] it is shown that it suffices with one iteration to get good accuracy if the iterations are initialized using the solution from last time step. In an optimization context remembering the solution from last time step is difficult and also using a model that uses an unknown number of iterates is undesirable. However the loss in model precision of assuming no residual gas, i.e.  $x_r = 0$ , is negligible therefore this is assumed. Further, the addition of heat loss in the pipe through (51) drives  $x_{cv}$  to zero.

The reduced model is then given by:

$$q_{in} = \frac{\dot{m}_f q_{HV}}{\dot{m}_f + \dot{m}_{ac}} \quad (52)$$

$$T_{eo} = \eta_{sc} \Pi_e^{1-1/\gamma_a} r_c^{1-\gamma_a} \left( \frac{q_{in}}{c_{p,a}} + T_{im} r_c^{\gamma_a-1} \right) \quad (53)$$

$$T_{em} = T_{amb} + (T_{eo} - T_{amb}) e^{-\frac{h_{tot} V_{pipe}}{(\dot{m}_f + \dot{m}_{ac}) c_{p,e}}} \quad (54)$$

### Initialization

The used temperature model has two tuning parameters,  $\eta_{sc}$  and  $h_{tot}$ . The first step of the initialization assumes that there is no heat loss in the manifold before the sensors. Then the complete model is fitted using the results from  $T_{em} = T_{eo}$ . The nominal set is used in the fitting. The mean/max absolute relative error of the temperature model is [1.9/5.4] % and the error increase from assuming  $x_r = 0$  is [0.014/0.06] %.

### 3.7 Turbine and Wastegate

Since the massflow is not measured on the exhaust side, the models for wastegate and turbine have to be fitted together.

$$\Pi_t = \frac{p_{es}}{p_{em}} \quad (55)$$

#### Turbine

The massflow is modeled with the standard restriction model, using that half the expansion occurs in the stator and half in the rotor, see [3]:

$$\Pi_t^* = \max\left(\sqrt{\Pi_t}, \left(\frac{2}{\gamma_e + 1}\right)^{\frac{\gamma_e-1}{\gamma_e}}\right) \quad (56)$$

$$\Psi_t(\Pi_t^*) = \sqrt{\frac{2\gamma_e}{\gamma_e - 1} \left( (\Pi_t^*)^{\frac{2}{\gamma_e}} - (\Pi_t^*)^{\frac{\gamma_e+1}{\gamma_e}} \right)} \quad (57)$$

$$\dot{m}_t = \frac{p_{em}}{\sqrt{R_e T_{em}}} \Psi_t A_{t,eff} \quad (58)$$

The turbine efficiency is modeled as a quadratic shape in blade-speed ratio (BSR), as used in [10, 3].

$$BSR = \frac{R_t \omega_{tc}}{\sqrt{2c_{p,e} T_{em} (1 - \Pi_t^{\frac{\gamma_e-1}{\gamma_e}})}} \quad (59)$$

$$\eta_{tm} = \eta_{tm,max} - c_m (BSR - BSR_{opt})^2 \quad (60)$$

The power to the turbocharger is then:

$$P_t \eta_m = \dot{m}_t c_{p,e} T_{em} \eta_{tm} \left( 1 - \Pi_t^{\frac{\gamma_e-1}{\gamma_e}} \right) \quad (61)$$

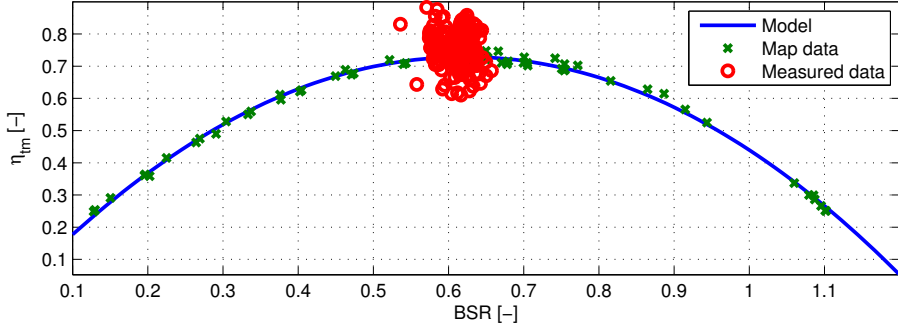


Figure 6: BSR model and its fit to map and measured data

Due to uncertainty of the behaviour outside the mapped region, and to avoid problems with negative turbine efficiency, a reasonable constraint is to restrict BSR to the maximum and minimum values provided in the map, i.e.  $BSR_{min} \leq BSR \leq BSR_{max}$ .

### Wastegate

The wastegate massflow is modeled with the standard restriction model and an effective area that changes linearly in  $u_{wg}$ .

$$\Pi_{wg}^* = \max(\Pi_t, \left(\frac{2}{\gamma_e + 1}\right)^{\frac{\gamma_e}{\gamma_e - 1}}) \quad (62)$$

$$\Psi_{wg} = \sqrt{\frac{2\gamma_e}{\gamma_e - 1} \left( (\Pi_{wg}^*)^{\frac{2}{\gamma_e}} - (\Pi_{wg}^*)^{\frac{\gamma_e + 1}{\gamma_e}} \right)} \quad (63)$$

$$\dot{m}_{wg} = \frac{p_{em}}{\sqrt{R_e T_{em}}} \Psi_{wg} u_{wg} A_{wg,eff} \quad (64)$$

### Initialization

The initialization uses data set C. The massflow models need to be fitted together and the turbine efficiency cannot be calculated from measurements since none of the massflows are measured. Looking at the nominal data set the quadratic shape in BSR is not observed since the measurements are rather constant in BSR, see Fig. 6. Since this shape is nonexistent in the measurements the efficiency model of the turbine is locked to the map fit since otherwise it would converge to an arbitrary shape trying to capture as much as the cloud nature of the measured data as possible. One could consider adding pulse compensation factors for the massflow and efficiency but the resulting improvements are small.

The massflow models are fitted together using  $\dot{m}_{ac} + \dot{m}_f = \dot{m}_t + \dot{m}_{wg} = \dot{m}_{exh}$ . Friction losses according to  $P_c = P_t \eta_m - w_{fric} \omega_{tc}^2$  can be added, however the parameter  $w_{fric}$  becomes small in the optimization.

The final turbine and wastegate models have three tuning parameters,  $A_{t,eff}$ ,  $\eta_{tm,max}$  and  $A_{wg,eff}$ . The results are mean/max relative errors of [2.3/5.4, 4.7/17.0] % for [ $\dot{m}_{exh}$ ,  $P_t\eta_{tm}$ ] respectively.

### Exhaust flow models

Using the standard restriction model a max-expression is necessary under the square root to keep the flow real, representing choking which occurs at  $\Pi_t^{-1} \approx [3.3, 1.8]$  for the turbine and wastegate. However such expressions are undesirable when using optimization tools. Instead the following expressions are used:

$$\Psi_t = c_{t,1} \sqrt{1 - \Pi_t^{c_{t,2}}} \quad (65)$$

$$\Psi_{wg} = c_{wg,1} \sqrt{1 - \Pi_t^{c_{wg,2}}} \quad (66)$$

The flow models are fitted to produce the same flow profile as the standard restriction models in (57), (63), where  $c_{t,1-2}$  and  $c_{wg,1-2}$  are tuning parameters.

## 3.8 Dynamic models

So far the models are tuned using stationary measurements. The next step is to tune the parameters of the dynamic models in (2)-(5). Since torque is not measured  $J_{GenSet}$  is fixed to it's real value and only  $V_{im}$ ,  $V_{em}$  and  $J_{tc}$  are tuned. Since torque and eventual torque errors might lead to engine stalling the torque model is inverted to track the real engine speed trajectory. This will lead to that there will be almost no errors in engine speed. To fit the dynamic models data set D-I are used but only the transients in the measurements, plus a couple of seconds before and after. As in [9] the transient is also normalized to 0-1 so that the stationary point has no effect on the dynamics.

## 3.9 Full models

The full models are tuned using both dynamic and stationary measurements, using a similar cost function as in [9]. If the same cost function is used the model will not be able to reach the same maximum torque as the real engine for low engine speeds without  $\lambda$  being excessively low. Therefore to ensure that the model is able to span the entire operating range of the engine an addition is made. The model is simulated with  $\lambda = \lambda_{min}$  for  $N_{ice} = 800$  rpm and the models maximum torque is added to the cost function according to:

$$V_{M_{max}} = w_{M_{max}} \left( \frac{M_{ice,max,mod}(800rpm)}{M_{ice,max,meas}(800rpm)} - 1 \right) \quad (67)$$

(67) assumes that the engine is smoke-limited at 800 rpm and maximum torque and thus tries to force the max torque of the model to coincide with that of the real engine, where  $w_{M_{max}}$  is a weighting parameter.

To ensure reasonable behaviour also when the generator is in motoring mode this side is fitted using the efficiency map from the manufacturer with an assumed

Table 4: Mean relative errors of the complete model. Bold marks variables used in the tuning and T, V, are the errors relative tuning and validation sets respectively.

	$\omega_{ice}$		$\mathbf{p}_{im}$		$\mathbf{p}_{em}$		$\omega_{tc}$	
	T	V	T	V	T	V	T	V
Dyn.	0.0	0.0	2.8	2.2	2.8	2.9	2.9	2.9
	<b><math>\dot{m}_c</math></b>	<b><math>P_c</math></b>	<b><math>\dot{m}_{ac}</math></b>	<b><math>T_{em}</math></b>	<b><math>\dot{m}_{exh}</math></b>	<b><math>P_t</math></b>	<b><math>P_{mech}^+</math></b>	<b><math>P_{mech}^-</math></b>
Stat.	2.5	1.8	2.5	2.4	3.3	5.4	3.4	1.4

power electronics efficiency of 98%. For the stationary tuning set C is used and for the dynamics sets D-I are used. The full cost function is given by:

$$\begin{aligned}
 V_{tot}(\theta) = & \frac{1}{y_{dyn} M_{dyn}} \sum_{k=1}^{M_{dyn}} \sum_{y_n=1}^{y_{dyn}} \sum_{l=1}^{N_{dyn}} \frac{(e_{rel,dyn}^{y_n}(l))^2}{N_{dyn}} \\
 & + \frac{1}{y_{stat}} \sum_{y_s=1}^{y_{stat}} \sum_{m=1}^{N_{stat}} \frac{(e_{rel,stat}^{y_s}(m))^2}{N_{stat}} \\
 & + V_{M_{max}}^2
 \end{aligned} \tag{68}$$

where  $y$  is the number of outputs,  $M$  the number of datasets and  $N$  the number of operating points in each dataset.

The models are also, as in [9], validated using only dynamic measurements and in particular all load transients, i.e. set  $J_{0.1, 1, 2-N_{0.1, 1, 2}}$ .

## 4 Results

The resulting fit to both tuning data and validation data is shown in Table 4. The variables used in the tuning are written in bold in the resulting tables. Table 4 shows that the model is a good mathematical representation of the measured system with state errors less than 3% and stationary errors in the same range. In Fig. 7 the state trajectories of the model are compared to measurements. There it is also seen that the agreement is good.

The pressure dynamics, and in particular the exhaust pressure, are faster than the speed dynamics therefore the resulting model is moderately stiff. This is also seen when selecting ode-solvers. In matlab ode23t and ode15s are twice as fast as the standard ode45 when simulating the model. When the states are normalized with their maximum values the relative and absolute tolerances [1e-4, 1e-7] are found to be good trade-offs between accuracy and performance.

## 5 Conclusion

In this paper a validated optimization ready model of a diesel-electric powertrain is presented. The resulting model is four state-three control mean value engine model, available for download in the **LiU-D-El**-package from [8]. The model is

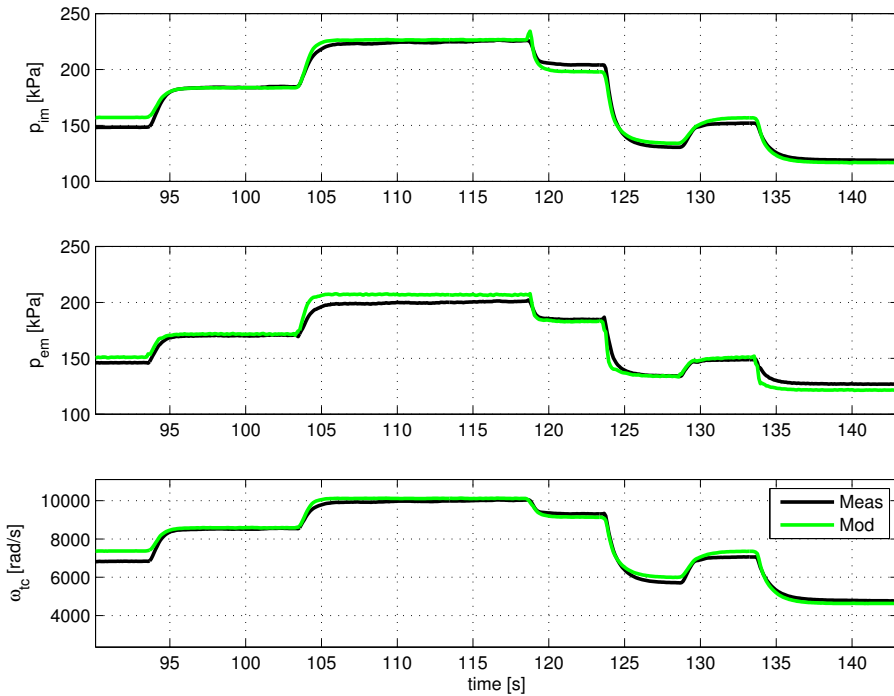


Figure 7: Model vs. measurements

able to capture the highly nonlinear nature of the turbocharger diesel engine, and is at the same time continuously differentiable in the region of interest, to comply with optimal control software. The model is provided with two torque models to be used for optimal control studies. The first model, called  $MVEM_o$  with a torque model representing the actual engine, as well as a model with a more general torque model aimed to represent a typical engine, called  $MVEM_2$ .

Both  $MVEM_o$  and  $MVEM_2$  are included in the **LiU-D-EI**-package together with a small example that can be downloaded fully parametrized from [8] implemented in matlab.

## References

- [1] Michael Ben-Chaim, Efraim Shmerling, and Alon Kuperman. Analytic modeling of vehicle fuel consumption. *Energies*, 6(1):117–127, 2013.
- [2] Lars Eriksson. Mean value models for exhaust system temperatures. *SAE 2002 Transactions, Journal of Engines*, 2002-01-0374, 111(3), September 2003.
- [3] Lars Eriksson. Modeling and control of turbocharged SI and DI engines. *Oil & Gas Science and Technology - Rev. IFP*, 62(4):523–538, 2007.

- [4] Lars Eriksson and Lars Nielsen. *Modeling and Control of Engines and Drivelines*. John Wiley & Sons, 2014.
- [5] L. Guzzella and C.H. Onder. *Introduction to Modeling and Control of Internal Combustion Engine Systems*. Springer, 1st edition, 2004.
- [6] Lino Guzzella and Antonio Sciarretta. *Vehicle Propulsion Systems - Introduction to Modeling and Optimization*. Springer, 2nd edition, 2007.
- [7] John B. Heywood. *Internal Combustion Engine Fundamentals*. McGraw-Hill Book Co., 1988.
- [8] Vehicular systems software. "<http://www.fs.isy.liu.se/Software/>", 2014.
- [9] Johan Wahlström and Lars Eriksson. Modelling diesel engines with a variable-geometry turbocharger and exhaust gas recirculation by optimization of model parameters for capturing non-linear system dynamics. *Proceedings of the Institution of Mechanical Engineers, Part D, Journal of Automobile Engineering*, 225(7):960–986, 2011.
- [10] N. Watson. Transient performance simulation and analysis of turbocharged diesel engines. In *SAE Technical Paper 810338*, 1981.

## A Data used

There are a total of 192 stationary points measured. Of those 192, 53 are with the wastegate locked in a fixed position. Since injection timing is not measured those points are only used when fitting the gas flow models since there are some questions about what the engine control unit does when the wastegate control is altered. Nominal refers to unaltered wastegate, see Table 5

The dynamic data set consists of 21 measurements. The first six, D-I, are engine speed transients with constant (as close as the generator control can track) generator power and a sequence of steps in reference speed that the engine speed controller tries to track, see Table 6.

The last 15 sets are with constant reference speed, and different load steps, see Table 7. As with the speed transients the ECU controls the engine speed and the generator acts as a disturbance. The load transients are conducted at different engine speeds and then a programmed sequence of 23 power steps is performed with varying rise time, or rate at which the power changes. The first five,  $J_{0.1} - N_{0.1}$  are with a ramp duration of 0.1s and the other are with 1s and 2s respectively. The total length of each set is approximately 300s.

Table 5: Stationary Data

Data Set	A	B	C
Delimiter	all	nominal	nominal & $P_{gen} > 0$
Nr. of points	192	139	127

Table 6: Speed transients

Data Set	D	E	F	G	H	I
$P_{gen}$ [kW]	30	60	90	130	160	180
Nr. of steps	22	22	22	22	21	21

Table 7: Load transients

Data Set	$J_{0.1, 1, 2}$	$K_{0.1, 1, 2}$	$L_{0.1, 1, 2}$	$M_{0.1, 1, 2}$	$N_{0.1, 1, 2}$
Speed [rpm]	1100	1500	1800	2000	2200
Nr. of steps	23	23	23	23	23



# An Optimal Control Benchmark: Transient Optimization of a Diesel-Electric Powertrain<sup>†</sup>

Martin Sivertsson<sup>a</sup> and Lars Eriksson<sup>a</sup>

<sup>a</sup>*Vehicular Systems, Department of Electrical Engineering,  
Linköping University, SE-581 83 Linköping, Sweden.*

---

<sup>†</sup>This is a formatted version of “An Optimal Control Benchmark: Transient Optimization of a Diesel-Electric Powertrain” by Martin Sivertsson and Lars Eriksson, SIMS 2014 - 55th International Conference on Simulation and Modelling, Aalborg, Denmark. The original version can be found at LiU Electronic Press, [http://www.ep.liu.se/ecp\\_home/index.en.aspx?issue=108](http://www.ep.liu.se/ecp_home/index.en.aspx?issue=108). The formatting is restricted to changing the article into a single-column format, adjusting sizes of figures and tables, and adjusting the referencing style.

## **Abstract**

An optimal control benchmark is presented and discussed. The benchmark is optimal transient control of a nonlinear four state three control model of a diesel-electric powertrain and constructed in such a manner that it is available in several versions to be of interest for developers of optimal control tools at different levels of development. This includes with and without time as a parameter as well as with and without time varying constraints.

# Nomenclature

Table 1: Symbols used

Symbol	Description	Unit
$p$	Pressure	Pa
$T$	Temperature	K
$\omega$	Rotational speed	rad/s
$\dot{m}$	Massflow	kg/s
$P$	Power	W
$M$	Torque	Nm
$E$	Energy	J
$\Pi$	Pressure ratio	-
$V$	Volume	$m^3$
$R$	Gas Constant	J/(kg · K)
$u_f, u_{wg}, P_{gen}$	Control signals	mg/cycle, -, W
$J$	Inertia	kg · $m^2$
$BSR$	Blade speed ratio	-
$\phi$	Fuel-air equivalence ratio	-
$\lambda_{min}$	Air-fuel smoke-limit	-

Table 2: Subscripts used

Index	Description	Index	Description
$ice$	Engine	$Gen.Set$	Engine-Generator
$im$	Intake manifold	$em$	Exhaust manifold
$c$	Compressor	$ac$	After compressor
$t$	Turbine	$wg$	Wastegate
$f$	Fuel	$tc$	Turbocharger
$a$	Air	$e$	Exhaust
$gen$	Generator-electrical	$mech$	Generator-mechanical
$req$	Requested	$c, surge$	Compressor surge-limit

## Introduction

In this paper a benchmark for optimal control tools is suggested and presented. The current state of computer technology has enabled a rise in the development of optimal control packages that can handle models of complex systems. However to evaluate the performance of the tools developers often have to rely on relatively small problems that do not reflect the purpose for which the tools were developed.

This paper presents a benchmark on which to evaluate developed optimal control tools. The benchmark problem is the optimization of the control of a diesel-electric powertrain from idle to a target output power and energy. The benchmark relies on the validated model of a diesel-electric powertrain described

in [2]. The model is a nonlinear four state, three controls mean value engine model (MVEM), that consists of 10 submodels that describe the individual components of the powertrain. Due to the complex and nonlinear nature of the modeled system the resulting optimization problem is non-convex and the optimization tools can therefore only guarantee local optima. The model is continuously differentiable in the desired operating region and is implemented using only analytical expressions. The motivation for this is to enable the solvers to use higher order search methods in the optimization. It also makes the model suitable for automatic differentiation (AD), enabling developers to also evaluate AD routines versus computing gradients and Hessians using finite differences.

In the paper the solutions to the problems using two different solvers, the ACADO Toolkit, see [1], TOMLAB/PROPT, see [6], is presented and discussed. The model and the resulting optimal trajectories, as well as the corresponding initial guesses, are available for research community. Two types of problems are considered, time and fuel minimization. To make the benchmark problem suitable for optimal control tools at different stages of development the problems are solved both with duration as a parameter to be optimized as well as for a fixed duration and also with and without path constraints.

## 1 Contributions

The contribution of this paper is the formulation and solution of an optimal control problem to serve as a benchmark on which to evaluate optimal control. The intention of the benchmark is to provide the research community with a relevant problem of reasonable complexity on which to benchmark optimal control tools. The benchmark is provided together with a simultaneously developed model, both available for download. To ensure that the benchmark is relevant for tools at different stages of development the problem is provided both with and without path constraints as well as with and without time as a parameter.

## 2 Model

The model used can be downloaded from [5] and is described in detail as *MVEM<sub>2</sub>* in [2], and provided either on its own, in the **LiU-D-El**-package, or together with the benchmark in the **LiU-D-El+Benchmark**-package. The modeled diesel-electric powertrain consists of a 6-cylinder diesel engine with a fixed-geometry turbine and a wastegate for boost control, with a generator mounted on the output shaft. The states of the MVEM are engine speed,  $\omega_{ice}$ , inlet manifold pressure,  $p_{im}$ , exhaust manifold pressure,  $p_{em}$ , and turbocharger speed,  $\omega_{tc}$ . The controls are injected fuel mass,  $u_f$ , wastegate position,  $u_{wg}$ , and generator power,  $P_{gen}$ . The engine model consists of two control volumes, intake and exhaust manifold, and four restrictions, compressor, engine, turbine, and wastegate. The control volumes are modeled with the standard isothermal model, using the ideal gas law and mass conservation. The engine and turbocharger speeds are modeled using Newton's second law. The governing differential equations of the

MVEM are:

$$\frac{d\omega_{ice}}{dt} = \frac{P_{ice} - P_{mech}}{\omega_{ice} J_{GenSet}} \quad (1)$$

$$\frac{dp_{im}}{dt} = \frac{R_a T_{im}}{V_{im}} (\dot{m}_c - \dot{m}_{ac}) \quad (2)$$

$$\frac{dp_{em}}{dt} = \frac{R_e T_{em}}{V_{em}} (\dot{m}_{ac} + \dot{m}_f - \dot{m}_t - \dot{m}_{wg}) \quad (3)$$

$$\frac{d\omega_{tc}}{dt} = \frac{P_t \eta_{tm} - P_c}{\omega_{tc} J_{tc}} \quad (4)$$

The MVEM is extended with two summation states to keep track on produced and consumed energy. The summation states are defined as:

$$\frac{dm_f}{dt} = \dot{m}_f \quad (5)$$

$$\frac{dE_{gen}}{dt} = P_{gen} \quad (6)$$

### 3 Problem Formulation

The proposed benchmark problem is the same problem as is studied in [3, 4]. The problem is that the GenSet is at idle when the operator requests a step in output power,  $P_{gen}$ , that should be met either as fuel efficient or time efficient as possible. The requested power is also augmented with an energy requirement,  $E_{gen}$ , that has to be produced before the GenSet reaches stationary conditions. This problem is mathematically expressed as:

$$\begin{aligned} \min_{u(t)} \quad & \int_0^T \dot{m}_f(x(t), u(t)) dt \quad \text{or} \quad \min_{u(t)} T \\ \text{s.t.} \quad & \dot{x}(t) = f(x(t), u(t)) \\ & (x(t), u(t)) \in \Omega(t) \end{aligned} \quad (7)$$

where  $x$  is the state vector of the MVEM,  $\dot{x}$  is the state equations (1)-(4) together with the summation states in (5)-(6), and  $u = [u_f, u_{wg}, P_{gen}]$ .

The constraints of the optimization problems,  $(x(t), u(t)) \in \Omega(t)$ , can be divided into two categories, time independent and time varying constraints. The first category, time independent constraints, are bounds on states and controls as well as initial and final conditions expressed as:

$$\begin{aligned} x(0) &= x_0, & \dot{x}(T) &= 0 \\ u_{min} &\leq u(t) \leq u_{max}, & x_{min} &\leq x(t) \leq x_{max} \\ 0 &\leq P_{gen}(t) \leq 100 \text{ kW}, & P_{gen}(T) &= 100 \text{ kW} \\ E_{gen}(T) &\geq 100 \text{ kJ} \end{aligned} \quad (8)$$

The time varying constraints are constraints imposed by the components, such as maximum power of the engine, surge-limit of the compressor, blade speed

ratio-limit of the turbine, as well as environmental constraints, i.e. an upper limit on  $\phi$  set by the smoke-limiter:

$$\begin{aligned} P_{ice}(x(t), u(t)) &\leq P_{ice,max}(x(t)) \\ \Pi_c &\leq \Pi_{c,surge} \\ BSR_{min} &\leq BSR(x(t), u(t)) \leq BSR_{max} \\ 0 &\leq \phi(x(t), u(t)) \leq \frac{1}{\lambda_{min}} \end{aligned} \quad (9)$$

To be relevant for software developers at different stages of development the benchmark problems defined in (7)-(9) are also available as a minimum fuel problem with fixed end time, as well as without the time varying constraints in (9).

## 4 Solution accuracy

To ensure that the solutions are at least good local minima both benchmark problems,  $\min T$  and  $\min m_f$ , are solved using PROPT and two different initial guesses, see Fig. 2-right). The first initial guess is a hard acceleration with  $\phi = \frac{1}{\lambda_{min}}$  from idle followed by a step in load power to  $P_{gen} = 100$  kW, and the second one is the GenSet at idle. Both initial guesses produce the same solution, although they are very different, indicating that the solutions are at least a good local minima. All solutions shown are with 125 control intervals/collocation points. In the following the initial guess from idle to 100kW is used.

## 5 With time varying constraints

The benchmark problems defined by (7)-(9) are solved using ACADO and PROPT, and the solutions from the two solvers are shown and compared in Fig. 1, where  $\omega_{ice/tc}$  is engine speed and turbocharger speed,  $p_{im/em}$  intake and exhaust manifold pressure,  $u_f/u_{wg}/P_{gen}$  are the controls, i.e. injected fuel mass per cycle, wastegate position, and output power from the generator. The  $\min m_f$  problem is also solved with fixed end time,  $T$ . For this a duration between the time optimal and fuel optimal durations is selected,  $T = 1.33$ . The solution with fixed end time is shown in Fig. 2-left).

Both solvers produce qualitatively the same solutions, there are however some differences owing to discretization technique employed as well as solution method. The resulting consumptions are shown in Table. 3. For further comparison all three solutions using PROPT are shown in torque-engine speed domain in Fig. 3.

Looking at Fig. 1 the trajectories for  $\min m_f$  and  $\min T$  are a bit different. For  $\min T$   $u_f$  follows the smoke-limit, i.e.  $\phi = \frac{1}{\lambda_{min}}$ , during the entire transient, whereas for  $\min m_f$  it is only smoke-limited  $0.17 \leq t \leq 0.91$  and  $t = T$ . During the initial acceleration engine efficiency is instead maximized, clearly seen in Fig. 3. The  $\min T$  solutions apply a step in  $P_{gen}$  from  $0 \rightarrow 100$  kW whereas the  $\min m_f$   $P_{gen}$  actuation is a slightly later and not in a step from  $0 \rightarrow 100$  kW.

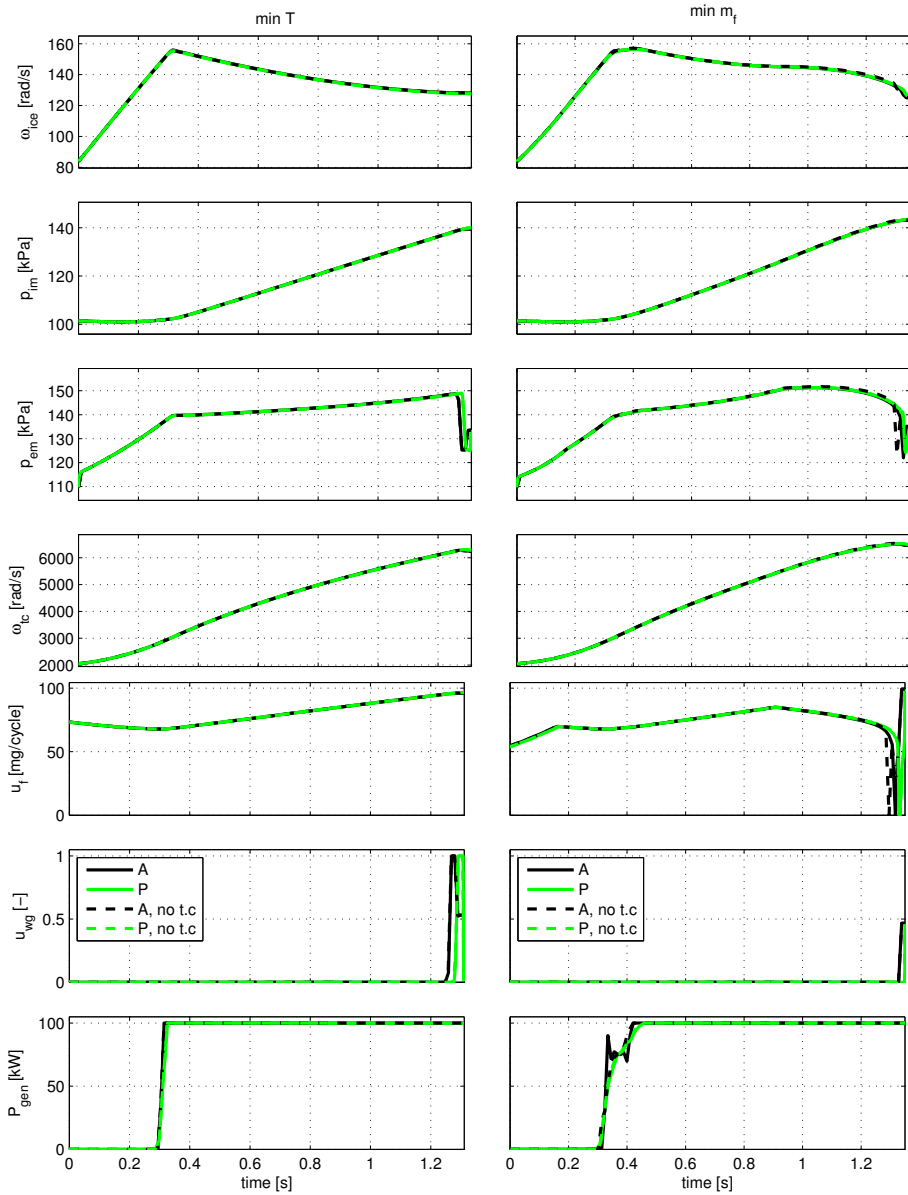


Figure 1: Minimum time (left) and minimum fuel (right) solutions to the benchmark problem using PROPT (P) and ACADO (A) with and without (no t.c) time varying constraints.

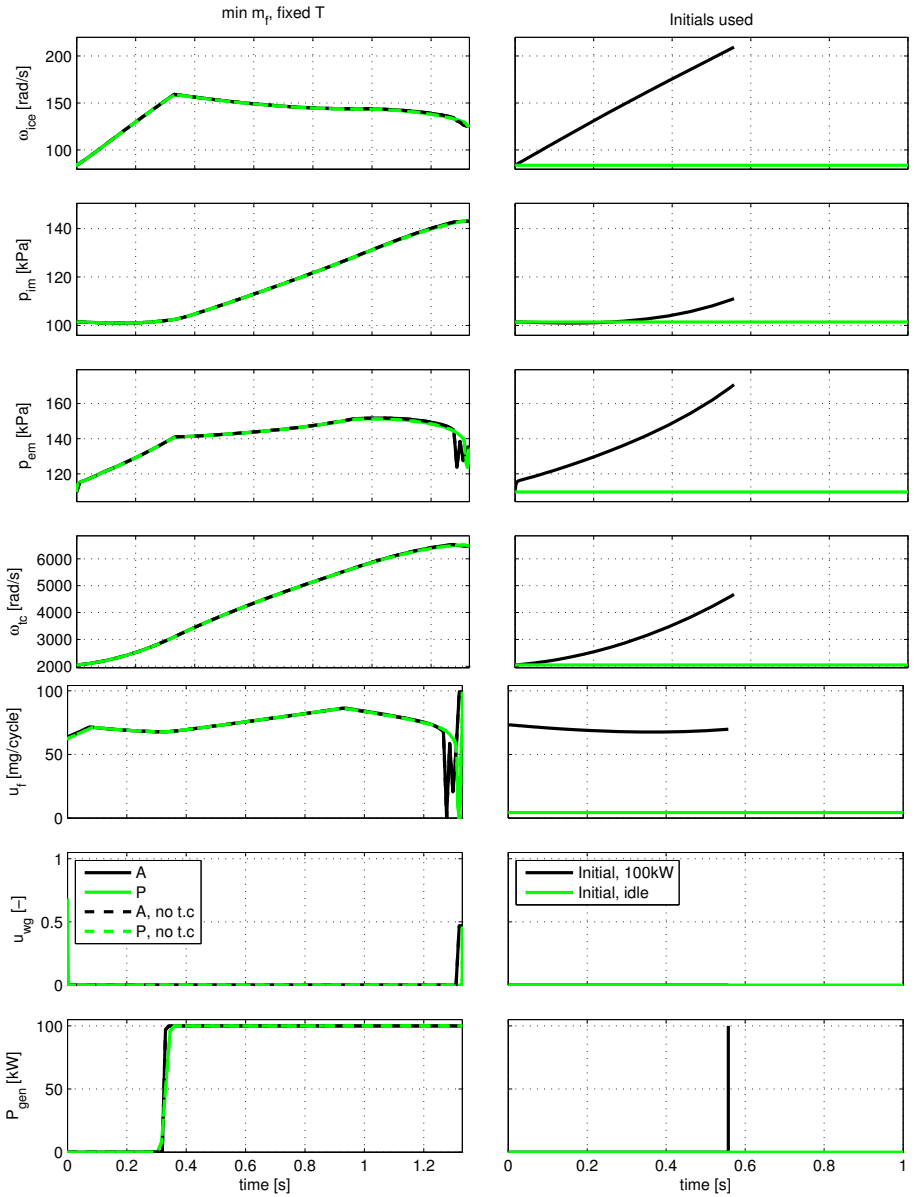


Figure 2: The fixed time solutions using PROPT (P) and ACADO (A) (left) with and without(no t.c) time varying constraints, as well as the different initial guesses used (right).

Table 3: Time and fuel consumption to the benchmark problems using both PROPT (P) and ACADO (A).

Criteria	Tool	$m_f$	$T$
$\min m_f$	P	6.5917398e-03	1.3498815e+00
	A	6.5977572e-03	1.3497437e+00
$\min T$	P	6.6392313e-03	1.3103439e+00
	A	6.6466370e-03	1.3110366e+00
$\min m_f, \text{ fixed } T$	P	6.5933240e-03	1.3300000e+00
	A	6.6005188e-03	1.3300000e+00

At the end of the transient the  $\min m_f$  use both  $u_f$  and  $u_{wg}$  to bring the states to stationarity whereas  $\min T$  only uses  $u_{wg}$ . Noteworthy is that none of the solutions end in the peak efficiency operating point, neither of the GenSet nor of the ICE.

The  $\min m_f$ , fixed time, solutions are as expected a mix between the  $\min T/m_f$  solutions. The  $P_{gen}$  actuation follows that of  $\min T$  but  $u_f$  and  $u_{wg}$  are more similar to  $\min m_f$ .  $u_f$  during the initial acceleration does however not follow the maximum efficiency trajectory but instead follows a trajectory between this and the smoke-limit, see Fig.1.

## 6 Without time varying constraints

In the problems solved in Section 5 the only time varying constraint that is active is the smoke-limiter, i.e. the constraint on  $\phi$ . The others can therefore be removed without affecting the solution. For the problem without (9) to be relevant, i.e. the problem defined by (7)-(8), the smoke-limiter needs to be included. To achieve this without state-dependent time varying constraints the model is reformulated so that  $\phi$  is a control signal and  $u_f$  calculated from it. Since  $\phi = \frac{\dot{m}_f}{\dot{m}_{ac}}(A/F)_s$  and  $\dot{m}_f = \frac{10^{-6}}{4\pi}u_f\omega_{ice}n_{cyl}$  the model can be reformulated to:

$$\dot{m}_f = \frac{\phi\dot{m}_{ac}}{(A/F)_s} \quad (10)$$

$$u_f = \frac{4\pi}{10^{-6}} \frac{\dot{m}_f}{\omega_{ice}n_{cyl}} \quad (11)$$

and with  $\phi$  replacing  $u_f$  as control signal all the time varying constraints are removed. The solutions to the problem without time varying constraints follow, as expected, the same discussion as with time varying constraints. The results are also shown in Fig. 1-2 but the trajectories end up on top of each other. The fuel and time consumptions are shown in Table 4. The reformulation leads to slightly different numerical values but the difference is negligible.

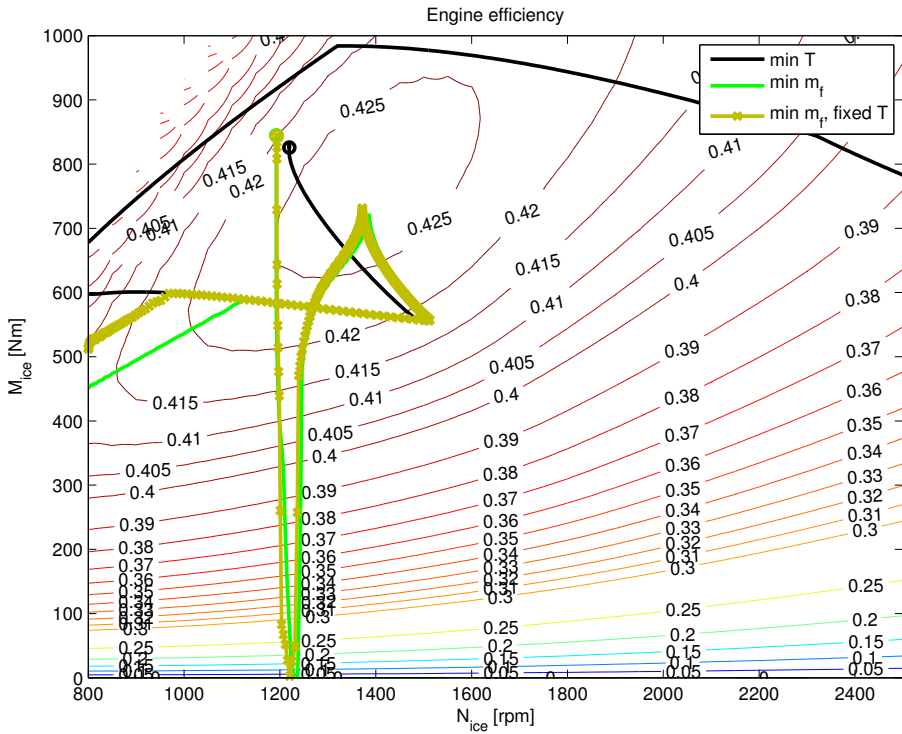


Figure 3: Torque-engine speed trajectories for the three benchmark problems.

Table 4: Time and fuel consumption to the benchmark problems without time varying constraints using both PROPT (P) and ACADO (A).

Criteria	Tool	$m_f$	$T$
min $m_f$	P	6.5916926e-03	1.3497981e+00
	A	6.5985144e-03	1.3493627e+00
min $T$	P	6.6394831e-03	1.3103321e+00
	A	6.6468526e-03	1.3104947e+00
min $m_f$ , fixed $T$	P	6.5930972e-03	1.3300000e+00
	A	6.6000832e-03	1.3300000e+00

## 7 Conclusion

In this paper an optimal control benchmark is suggested and presented. The benchmark concerns transient optimization of a diesel-electric powertrain, from idle to a target power and energy. The benchmark makes use of a freely available four state-three control nonlinear model of a diesel-electric powertrain. Both the model and the initial guesses used are available for download in the **LiU-D-El+Benchmark**-package from [5]. The benchmark is available in several versions, both with and without time varying constraints, as well as with and without time as a parameter.

## References

- [1] Boris Houska, Hans Joachim Ferreau, and Moritz Diehl. ACADO toolkit - an open source framework for automatic control and dynamic optimization. *Optimal Control Applications & Methods*, 32(3):298–312, 2011.
- [2] Martin Sivertsson and Lars Eriksson. Modeling for optimal control: A validated diesel-electric powertrain model. In *SIMS'14 - 55th International Conference on Simulation and Modelling*, Aalborg, Denmark, 2014.
- [3] Martin Sivertsson and Lars Eriksson. Optimal transient control trajectories in diesel-electric systems-part 1: Modeling, problem formulation and engine properties. *Journal of Engineering for Gas Turbines and Power*, 137(2), February 2015.
- [4] Martin Sivertsson and Lars Eriksson. Optimal transient control trajectories in diesel-electric systems-part 2: Generator and energy storage effects. *Journal of Engineering for Gas Turbines and Power*, 137(2), February 2015.
- [5] Vehicular systems software. "<http://www.fs.isy.liu.se/Software/>", 2014.
- [6] TOMLAB. PROPT - Matlab Optimal Control Software, "<http://www.tomdyn.com/>", 2012.



# Model and discretization impact on oscillatory optimal control for a diesel-electric powertrain<sup>†</sup>

Martin Sivertsson<sup>a</sup> and Lars Eriksson<sup>a</sup>

<sup>a</sup>*Vehicular Systems, Department of Electrical Engineering,  
Linköping University, SE-581 83 Linköping, Sweden.*

---

<sup>†</sup>This is a formatted version of “Model and discretization impact on oscillatory optimal control for a diesel-electric powertrain” by Martin Sivertsson and Lars Eriksson, submitted to IFAC Workshop on Engine and Powertrain Control Simulation and Modeling 2015, Columbus, Ohio. The formatting is restricted to changing the article into a single-column format, adjusting sizes of figures and tables, and adjusting the referencing style.

## **Abstract**

A mean value engine model is used to study optimal control of a diesel-electric powertrain. The resulting optimal controls are shown to be highly oscillating for certain operating points, raising the question whether this is an artifact of discretization, modeling choices or a phenomenon available in real engines. Several model extensions are investigated and their corresponding optimal control trajectories are studied. It is shown that the oscillating controls cannot be explained by the implemented extensions to the previously published model, nor by the discretization, showing that for certain operating points the optimal solution is periodic.

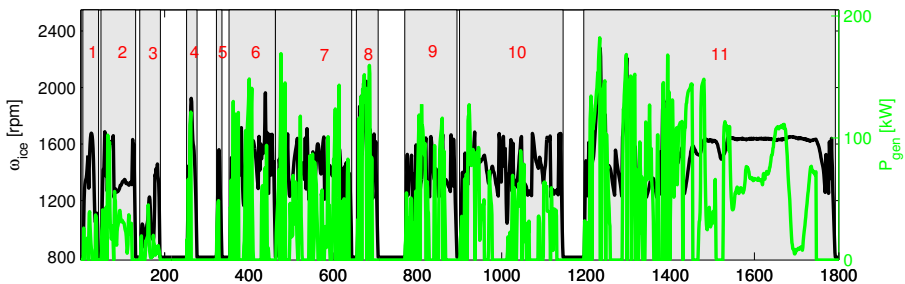


Figure 1: The WHTC and its traction phases.

## Introduction

The engine speed of a conventional vehicle is normally decided by the wheel speed and the gear ratio. In a diesel-electric powertrain this mechanical path between the combustion engine and the wheels is replaced by an electric path instead. This introduces an extra degree of freedom since the engine speed can be controlled independently of the wheel speed, which offers the potential of both optimizing the performance and consumption since the operating point of the diesel engine can be controlled more freely than in a conventional powertrain. This of course raises the question of how to use this extra degree of freedom.

Previously it has been studied how to optimally control the powertrain between two different power levels, see [12, 13]. For off-highway machinery the driving patterns are normally very transient, something that is captured in the World Harmonized Transient Cycle (WHTC), see [17], shown in Fig. 1. The WHTC can be divided into 11 traction phases, defined as the period between two idle periods, where idle is assumed to occur when the engine speed is the idle speed and no power is required. Here the phases where the engine is motored, i.e.  $P_{gen} < 0$  are ignored and  $P_{gen}$  is in those cases set to zero. To investigate the potential of the diesel-electric powertrain and how to best exploit the extra degree of freedom introduced by the electrification of the powertrain, minimizing fuel for the WHTC is cast as an optimal control problem (OCP). In a conventional powertrain WHTC prescribes both engine speed and output power, but here engine speed is a degree of freedom and also optimized. If this OCP is solved for phase 8 in the WHTC the resulting controls are very oscillatory, see Fig. 1,  $t \in [670, 678], [684, 687]$ . It is mentioned in [12] that the optimal solutions in transient optimal control of a diesel-electric powertrain are often oscillatory and in [2] the unconfirmed hypothesis is that the oscillations seen in the optimal variable geometry turbine (VGT) control of a diesel engine are due to decrease in the gas exchange losses. This is due to that the exhaust manifold pressure oscillates with the VGT position whereas the intake manifold pressure remains unaffected due to the slower turbocharger dynamics. This could indicate that the optimal solution is in fact periodical as described in [5], [6].

Other possible explanations are either that the solution is along a singular arc and that the controls are therefore oscillatory, as discussed in [10], or that it is an integration error exploited by the algorithm to decrease the criteria as

shown in [7]. In both these cases it would be suspected that the frequency of the oscillations depend on the discretization. To test this hypothesis a single operating point is selected and studied using a very fine time discretization.

## 1 Contributions

The contributions of this paper is a deeper study of the occurrence of oscillating controls for diesel-electric powertrains as a solution for optimal control problems. More specifically it studies whether the observed oscillations are an artifact of the discretization. It also investigates if the oscillations can be explained by the models used and whether or not extending the model impacts the oscillating solutions. The paper also presents a fast and accurate residual gas model suitable for use in an optimal control context.

Table 1: Symbols used

Symbol	Description	Unit
$p$	Pressure	Pa
$T$	Temperature	K
$\omega$	Rotational speed	rad/s
$\dot{m}$	Massflow	kg/s
$P$	Power	W
$M$	Torque	Nm
$E$	Energy	J
$\Pi$	Pressure ratio	-
$V$	Volume	$m^3$
$\gamma$	Specific heat capacity ratio	-
$c_p$	Specific heat capacity constant pressure	J/(kg · K)
$c_v$	Specific heat capacity constant volume	J/(kg · K)
$R$	Gas Constant	J/(kg · K)
$u_f, u_{wg}, P_{gen}$	Control signals	mg/cycle, -, W
$J$	Inertia	kg · m <sup>2</sup>
$BSR$	Blade speed ratio	-
$\phi$	Fuel-air equivalence ratio	-
$\lambda_{min}$	Air-fuel smoke-limit	-
$x_r$	Residual gas fraction	-
$MFR$	Fuel to mass ratio	-
$q_{HV}$	Lower heating value	J/kg
$r_c$	Compression ratio	-

## 2 Model

The basic model used can be downloaded in the **LiU-D-El**-package from [14] and is described in detail as  $MVEM_o$  in [11]. The modeled diesel-electric powertrain consists of a 6-cylinder diesel engine with a fixed-geometry turbine and a wastegate for boost control, with a generator mounted on the output shaft.

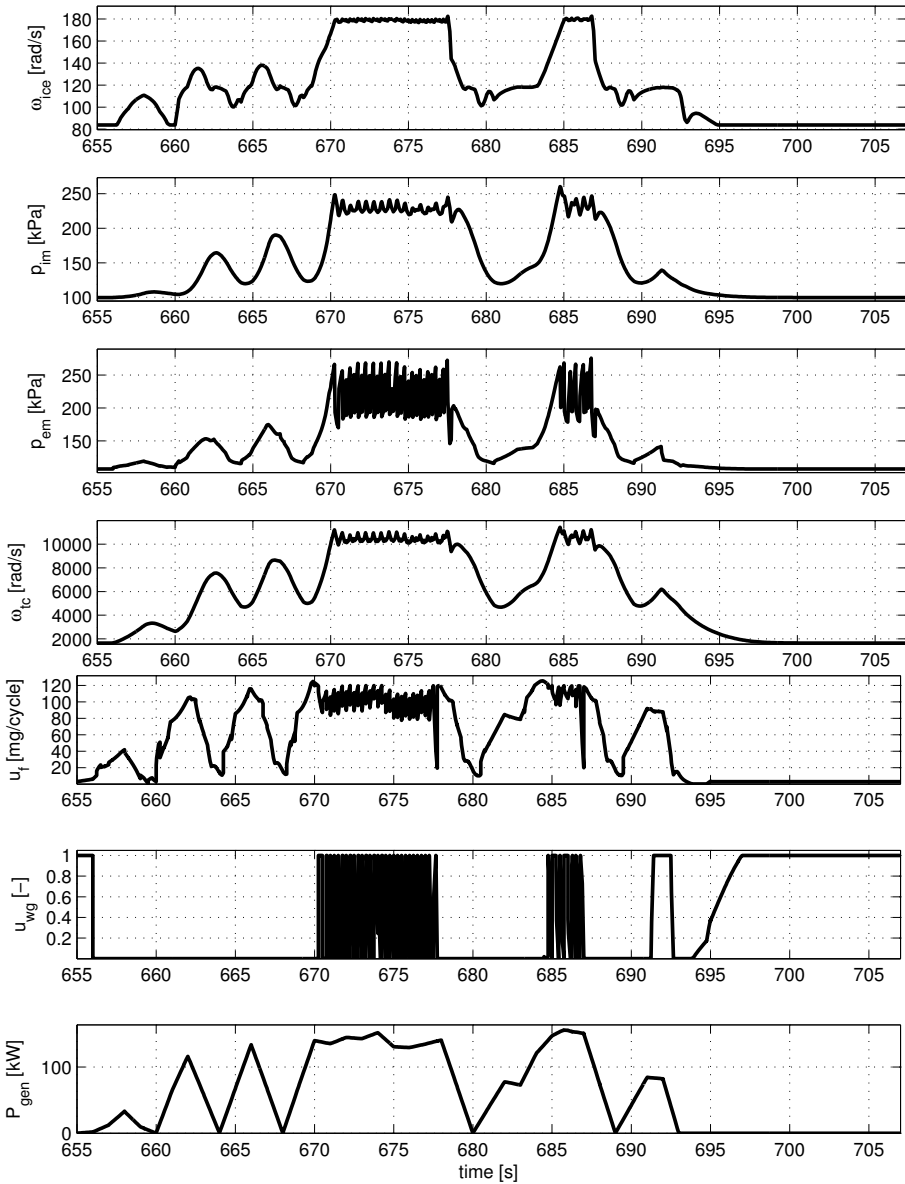


Figure 2: The optimal solution to phase 8 of the WHTC, with  $\omega_{ice}$  as a degree of freedom. The resulting controls are highly oscillatory, see  $t \in [670, 678]$ ,  $[684, 687]$

Table 2: Subscripts used

Index	Description	Index	Description
<i>ice</i>	Engine	<i>GenSet</i>	Engine-Generator
<i>im</i>	Intake manifold	<i>em</i>	Exhaust manifold
<i>c</i>	Compressor	<i>ac</i>	After compressor
<i>t</i>	Turbine	<i>wg</i>	Wastegate
<i>f</i>	Fuel	<i>tc</i>	Turbocharger
<i>a</i>	Air	<i>e</i>	Exhaust
<i>gen</i>	Generator-electrical	<i>mech</i>	Generator-mechanical
<i>ref</i>	Reference	<i>c, surge</i>	Compressor surge-limit
<i>vol</i>	Volumetric	<i>d</i>	Displaced
<i>fric</i>	Friction	<i>pump</i>	Pumping
<i>ig</i>	Indicated gross	<i>eo</i>	Engine out
<i>amb</i>	Ambient		

The states of the MVEM are engine and turbocharger speeds,  $\omega_{ice/tc}$ , and inlet and exhaust manifold pressures,  $p_{im/im}$ . The controls are injected fuel mass,  $u_f$ , wastegate position,  $u_{wg}$ , and generator power,  $P_{gen}$ . The engine model consists of two control volumes, intake and exhaust manifold, and four restrictions, compressor, engine, turbine, and wastegate. The governing differential equations of the MVEM are:

$$\frac{d\omega_{ice}}{dt} = \frac{P_{ice} - P_{mech}}{\omega_{ice} J_{GenSet}} \quad (1)$$

$$\frac{dp_{im}}{dt} = \frac{R_a T_{im}}{V_{im}} (\dot{m}_c - \dot{m}_{ac}) \quad (2)$$

$$\frac{dp_{em}}{dt} = \frac{R_e T_{em}}{V_{em}} (\dot{m}_{ac} + \dot{m}_f - \dot{m}_t - \dot{m}_{wg}) \quad (3)$$

$$\frac{d\omega_{tc}}{dt} = \frac{P_t \eta_{tm} - P_c}{\omega_{tc} J_{tc}} \quad (4)$$

For a complete list of the symbols used in the paper, see Table 4-5.

### 3 Problem Formulation

This paper uses the MVEM to study optimal stationary operation, or lack of it in the case of oscillating controls.

#### 3.1 Stationary optimization

As a reference for the dynamic optimization, three stationary optimization problems are first solved, to find the following three stationary points for the given  $\omega_{ref}, P_{ref}$ -combination: The maximum efficiency,  $\phi_{max}$ , the maximum fuel/air-ratio,  $\eta_{max}$ , and the minimum fuel/air-ratio,  $\phi_{min}$ .  $\eta = \frac{P_{gen}}{\dot{m}_f q_{HV}}$  is the efficiency of the powertrain and  $\phi$  is the fuel/air-ratio. These problems are solved

to find the optimal operating point for stationary operation and also the limits for stationary operation.

### 3.2 Dynamic optimization

The main optimal control problem studied is:

$$\begin{aligned} \min_{u(t)} \quad & \int_0^T \dot{m}_f \\ \text{s.t.} \quad & \dot{x}(t) = f(x(t), u(t)) \\ & (x(t), u(t)) \in \Omega(t) \end{aligned} \quad (5)$$

where  $x$  is the state vector of the MVEM,  $\dot{x}$  is the state equations (2)-(5), and  $u = [u_f, u_{wg}, P_{gen}]$ . The optimal control problems are also subject to a set of constraints, namely:

$$\begin{aligned} x(0) = x(T) = x(\eta_{max}), \quad & \dot{x}(T) = 0 \\ u_{min} \leq u(t) \leq u_{max}, \quad & x_{min} \leq x(t) \leq x_{max} \\ \omega_{ice}(T) = \omega_{ref} \text{ or } \omega_{ice}(t) = \omega_{ref}, \quad & P_{gen}(t) = P_{ref} \\ P_{ice}(x(t), u(t)) \leq P_{ice,max}(x(t)), \quad & \phi(x(t), u(t)) \leq \frac{1}{\lambda_{min}} \\ BSR_{min} \leq BSR(x(t), u(t)) \leq BSR_{max}, \quad & \Pi_c \leq \Pi_{c,surge} \end{aligned} \quad (6)$$

The constraints are actuator and state limits, as well as constraints imposed by the components, such as maximum power of the engine,  $P_{ice}$ , surge-limit of the compressor,  $\Pi_{c,surge}$ , blade speed ratio-limit of the turbine,  $BSR$ , as well as environmental constraints, i.e. an upper limit on  $\phi$  set by the smoke-limiter.

The driving mission-constraints are that the powertrain starts in the operating point of maximum efficiency  $\eta_{max}$ , a point it should also end in, with the added requirement that the end operating point should be stationary. The generator power is also fixed to the reference value. Two types of problems are then studied, one where the engine speed is fixed to the reference speed, denoted  $\omega_{ice} = \text{fix}$ , and one where it is allowed to depart from this as long as it starts and ends in  $\omega_{ice} = \omega_{ref}$ , denoted  $\omega_{ice} = \text{free}$ .

## 4 Numerical Solution

The software package that is used to solve the optimal control problem numerically is CasADi [1]. First the problem is discretized using Radau collocation with three collocation points in each control interval. The states are thus approximated with a third order polynomial, whereas the controls are approximated by a second order polynomial in each control interval. The states are required to be continuous over each control interval boundary, whereas the controls are allowed to be discontinuous. The resulting nonlinear program(NLP) is solved using IPOPT, [15], with the MA57 linear solver from the HSL package, [9]. For the wastegate oscillation study 200 control intervals have been used.

## 5 Oscillating controls

The stationary point of interest here is the one seen with oscillating controls in Fig. 1 namely  $P_{gen} = 140$  kW and  $\omega_{ice} = 1700$  rpm. The three stationary OCPs (OSS) described in Section 3.1 and the two dynamic OCPs (OSD),  $\omega_{ice} = \text{fix}$  and  $\omega_{ice} = \text{free}$ , described in Section 3.2 are solved using CasADi/IPOPT/HSL and the results are shown in Fig. 3. Looking at Fig. 3 it is clearly visible that both OSDs result in a periodic oscillation. If the engine speed is free the amplitude and frequency changes slightly, however the nature of the oscillation remains the same. The nature of the opening and closing goes against the hypothesis that this should be oscillations due to a singular arc or an effect of the integration error since the wastegate only opens 9-11 times despite 200 control intervals with a three controls in each interval, yielding an optimal period of 90-110ms which is approximately 20 times the control interval length. This indicates that the oscillations are in fact optimal.

This is especially interesting for the case with fixed engine speed, since then the effect can be isolated since all torque losses only depend on engine speed except the pumping torque,  $M_{pump}$ , see Appendix A.1. This means that the oscillating control actually decreases the pumping torque, as hypothesised in [2]. Looking at Fig. 3 the low pass filtering effect of the turbocharger can be clearly seen since the wastegate opening and closing results in a  $p_{em}$  span of 60-100 kPa depending on if  $\omega_{ice} = \text{free/fix}$ , whereas the effect on  $p_{im}$  is only 4-5 kPa. In Fig. 4 the pumping power,  $P_{pump} = \omega_{ice} M_{pump}$ , are shown relative  $P_{pump}(\eta_{max})$ . Both  $x(\phi_{min})$  and  $x(\phi_{max})$  increase  $P_{pump}$  compared to  $x(\eta_{max})$ , as expected. The oscillation changes  $P_{pump}$  several hundred percent away from what is stationary optimal.

In Table 3 the gains of oscillating controls are quantified.  $x(\phi_{max})$  and  $x(\phi_{min})$  both increase the pumping energy  $E_{pump}$  with 50% which also leads to a relative efficiency decrease of 0.5% (0.2% absolute). The oscillating control with fixed  $\omega_{ice}$  decreases  $E_{pump}$  with 2.4% and  $\omega_{ice}$  free with 4.1%. Since the friction losses are quadratic in engine speed,  $\omega_{ice}$ -free, increases the friction losses, but it is still beneficiary since the relative efficiency increase is 0.52‰ vs. 0.24‰ for  $\omega_{ice}$ -fix (0.2‰ vs. 0.09‰ absolute).

The gains are small but nevertheless surprising since it's a dynamic phenomenon. Looking at Fig. 5 the wastegate's effect on the stationary efficiency as well as pumping torque is shown. The efficiency is a convex function in  $u_{wg}$  whereas  $M_{pump}$  is concave, which if the analysis was performed for stationary conditions would lead to the conclusion that oscillating controls would increase the pumping torque and consequently decrease the efficiency. However the result is actually the opposite, oscillating between the two worst controls from a stationary perspective, increases the efficiency dynamically.

## 6 Model extensions

To investigate whether the oscillating controls are results of a modeling assumption a set of different model extensions are considered. The extensions and their motivation are:

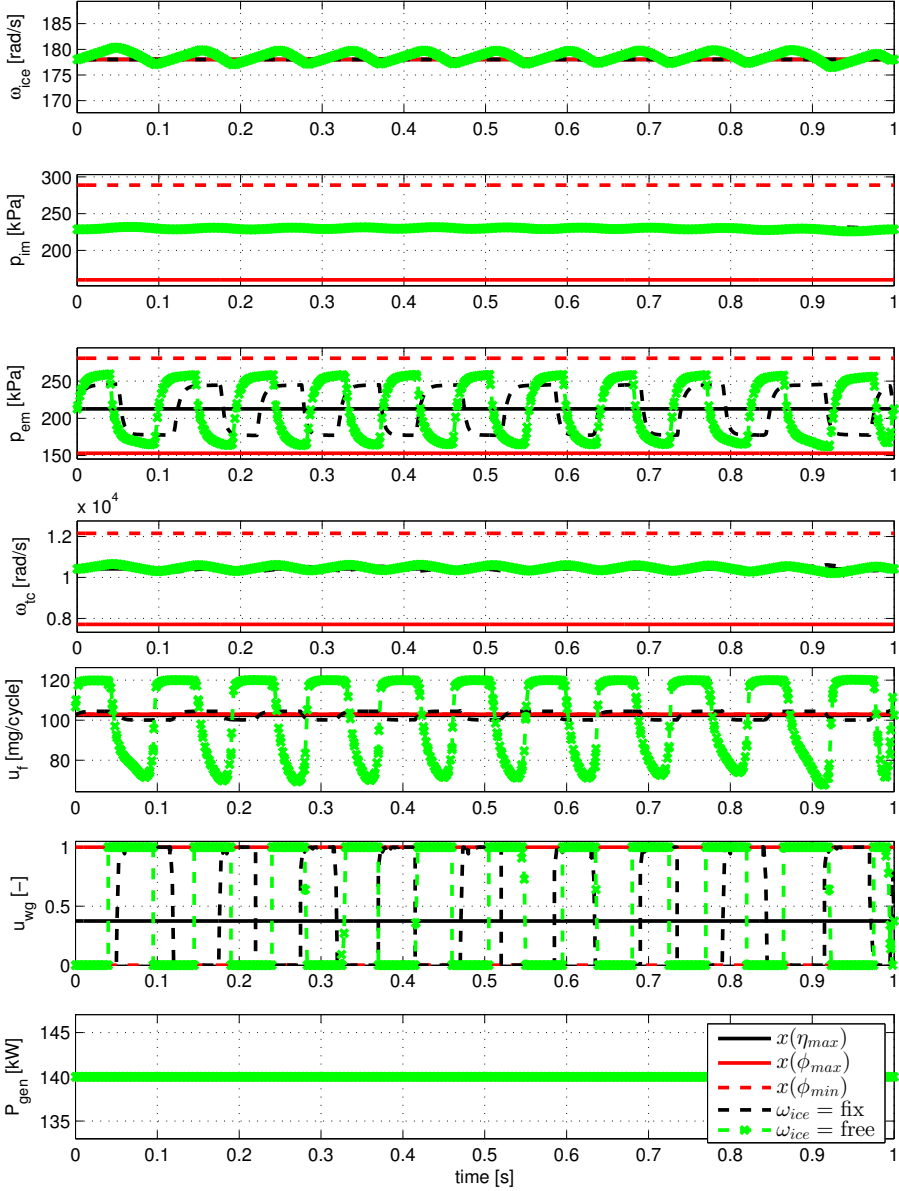


Figure 3: Optimal states and controls for constant output power, both stationary and dynamic. The dynamic solutions are highly oscillatory.

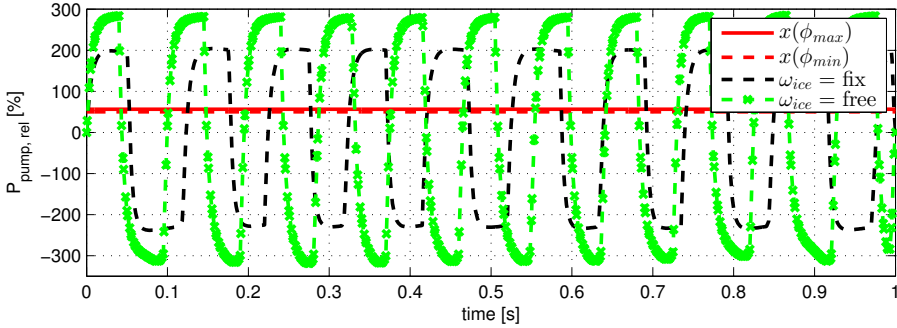


Figure 4: Pumping power relative the stationary optimal point.

	$\Delta\eta$	$\Delta E_{fric}$	$\Delta E_{pump}$	$\Delta E_{ig}$
$x(\phi_{max})$	-0.542	0.0	56.3782	0.5448
$x(\phi_{min})$	-0.482	0.0	50.1279	0.4844
$\omega_{ice} = \text{fix}$	0.024	0.0	-2.4073	-0.0223
$\omega_{ice} = \text{free}$	0.052	0.8797	-4.0869	-0.0263

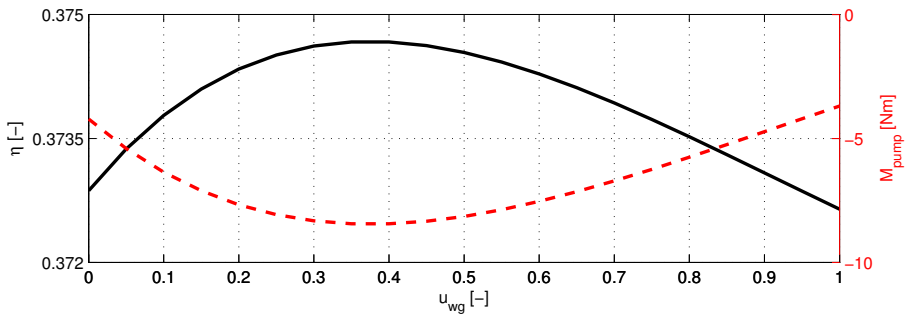
Table 3: Changes in efficiency and energies relative  $x(\eta_{max})$  in percent,  $E_x = \int_0^T P_x dt$ .

Figure 5: Wastegate position's effect on the efficiency and pumping torque during stationary conditions.

- $x_r$ : Model for residual gas: In [11] it is shown that mean/max absolute relative error increase of assuming  $x_r = 0$  is  $[0.014/0.06]$  % versus measurements. However in the oscillating controls the exhaust pressure changes very rapidly, something that might have a significant effect on the amount of residual gas trapped in the cylinder.
- $\eta_{vol,2}$ : Pressure ratio dependent volumetric efficiency model. In the volumetric efficiency model used, see Appendix A.2, only the dependence of the intake manifold pressure and engine speed are modeled. Of course the changing pressure ratio over the engine could have effects on the volumetric efficiency.
- Adiabatic: The isothermal exhaust manifold model used, see Appendix A.3, neglects energy conservation since it assumes that the gases flowing in and out of the control volume have the same temperature, therefore an adiabatic exhaust manifold model that satisfies both conservation of mass and energy is implemented.

The basic model is  $MVEM_o$ , which is then extended with different combinations of these three models. The model fit for the different models versus both dynamic(Dyn.) and stationary measurements(Stat) are shown in Table 4. None of the model extensions have any significant effects on the model fit versus measurements.

## 6.1 Residual gas

In [16] the engine out temperature model is based on an ideal Seiliger cycle model, incorporating residual gas. The model is formulated as:  $x_{r,0} = 0, T_{eo,0} = 800$ . While  $\|T_{eo,k+1} - T_{eo,k}\| > 1e-6$

$$\begin{aligned}
 q_{in} &= \frac{\dot{m}_f q_{HV}}{\dot{m}_f + \dot{m}_{ac}} (1 - x_{r,k}) \\
 x_p &= 1 + \frac{q_{in} x_{cv}}{c_{v,a} T_1 r_c^{\gamma_a - 1}} \\
 x_v &= 1 + \frac{q_{in} (1 - x_{cv})}{c_{p,a} \left( \frac{q_{in} x_{cv}}{c_{v,a}} + T_1 r_c^{\gamma_a - 1} \right)} \\
 x_{r,k+1} &= \frac{\Pi_e^{1/\gamma_a} x_p^{-1/\gamma_a}}{r_c x_v} \\
 T_1 &= x_{r,k+1} T_{eo,k} + (1 - x_{r,k+1}) T_{im} \\
 T_{eo,k+1} &= \eta_{sc} \Pi_e^{1-1/\gamma_a} r_c^{1-\gamma_a} x_p^{1/\gamma_a - 1} \\
 &\quad \left( q_{in} \left( \frac{1 - x_{cv}}{c_{p,a}} + \frac{x_{cv}}{c_{v,a}} \right) + T_1 r_c^{\gamma_a - 1} \right)
 \end{aligned} \tag{7}$$

The equations in (7) are nonlinear and depend on each other and need to be solved using fixed point iterations. In [16] it is shown that if the solution from the previous time step is known, one iteration suffices to get a good approximation

of the engine out temperature. In an optimization context it is difficult to keep track of the solution form the previous time step since the time steps are solved simultaneously. Also a submodel that is evaluated for a varying number of iterations is undesirable, especially since it complicates the computation of derivatives. Therefore this type of model is not implementable in an optimization context and a new model is developed.

$x_r$  is modeled as a function of both pressure ratio over the engine and the fuel to mass ratio. defined as:

$$MFR = \frac{\dot{m}_f}{\dot{m}_f + \dot{m}_{ac}} \quad (8)$$

$$x_r = \frac{x_{r,mod1}}{x_{r,mod2}} = \frac{c_{x_{r1}}\Pi_e^2 + c_{x_{r2}}\Pi_e + c_{x_{r3}}}{1 + c_{x_{r4}}MFR} \quad (9)$$

In Fig. 6-top this gives a good agreement to the iterative model, resulting in mean/max relative errors of [0.92/4.52] %. Using that  $x_{cv}$  becomes zero in the optimization for this particular engine  $T_{eo}$  can be computed according to

$$T_{eo} = \frac{(1 - x_r) \left( \frac{q_{HV} MFR}{c_{p,a}} + T_{im} r_c^{\gamma_a - 1} \right)}{\frac{1}{\eta_{sc} \Pi_e^{1-1/\gamma_a} r_c^{1-\gamma_a}} - x_r r_c^{\gamma_a - 1}} \quad (10)$$

$T_{eo}$  and  $x_r$  could be used as starting values and then one iteration of the fixed point iteration can be performed. However it turns out that not only is it more computations, the model fit is actually worse. When simulated over the entire WHTC the mean/max absolute relative error of exhaust gas temperature,  $T_{eo}$  for the model in (8)-(10) relative the model in (7) are [0.025/0.22]%. If in addition to (8)-(10) one fixed point iteration is used the errors increase to [0.045/0.34] %. The model used is therefore the one without iterations. In Fig. 6-bottom the fit vs. the model in (7) is shown.

## 6.2 $\eta_{vol,2}$ : Modified volumetric efficiency

The  $\eta_{vol,2}$  model implemented is a modified version of the model found in [4], consisting of an ideal part and two polynomials, in  $\omega_{ice}$  and  $p_{im}$  respectively.

$$\eta_{vol,ideal} = \frac{r_c - \left( \frac{p_{em}}{p_{im}} \right)^{1/\gamma_a}}{r_c - 1}$$

$$\eta_{vol,\omega_{ice}} = c_{\eta_{vol,1}} \omega_{ice}^2 + c_{\eta_{vol,2}} \omega_{ice} + c_{\eta_{vol,3}}$$

$$\eta_{vol} = \eta_{vol,\omega_{ice}} \eta_{vol,ideal} + c_{\eta_{vol,4}} p_{im} + c_{\eta_{vol,5}}$$

The component model fit for stationary measurements are slightly better than the model in (20), with mean/max absolute relative errors of 0.62/2.68 % vs. 0.9/3.7 % for (20), which is to be expected since the number of tuning parameters increases from three to five.

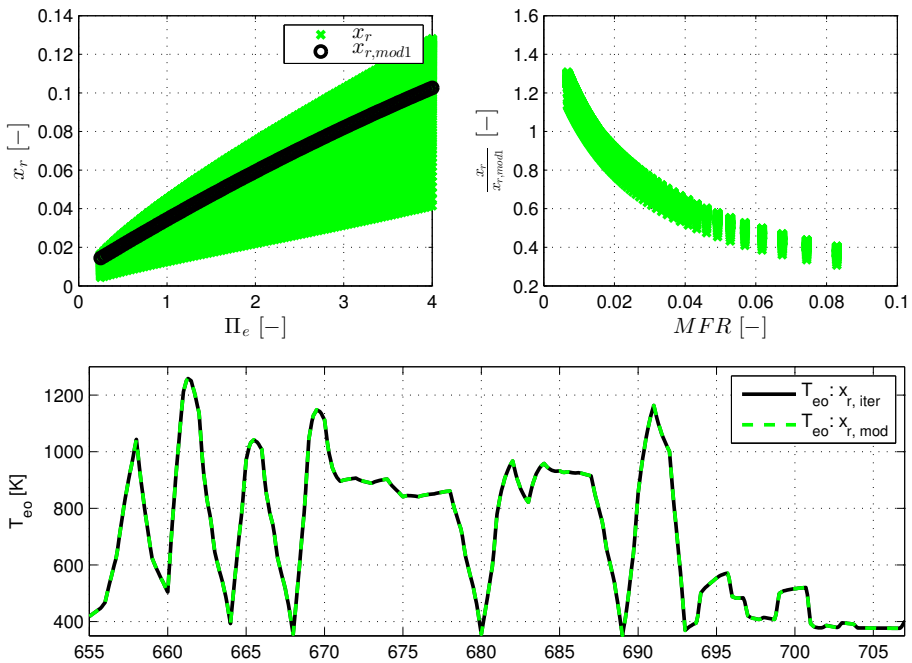


Figure 6: Top: Residual gas,  $x_r$ , vs. pressure ratio,  $\Pi_e$ , and how this dependence is modeled (Left). The  $x_r$  error's dependence on MFR (Right). Bottom: Fit of the new residual gas model for phase 8 of the WHTC.

Table 4: Mean absolute relative errors for the different models versus measurements. T=tuning set, V=validation set.

Dyn.	$\omega_{ice}$		$P_{im}$		$P_{em}$		$\omega_{tc}$	
	T	V	T	V	T	V	T	V
$MVEM_o$	0.0	0.0	2.8	2.2	2.8	2.9	2.9	2.9
$x_r$	0.0	0.0	2.8	2.2	2.8	2.9	2.9	2.9
$x_r$ +adiabatic	0.0	0.0	2.8	2.2	2.8	3.0	2.9	3.0
$\eta_{vol,2}$	0.0	0.0	2.8	2.3	2.9	3.0	3.0	3.2
$\eta_{vol,2}$ + $x_r$ +adiabatic	0.0	0.0	2.9	2.3	2.9	3.0	3.1	3.2
Stat.	$\dot{m}_c$	$P_c$	$\dot{m}_{ac}$	$T_{em}$	$\dot{m}_{exh}$	$P_t$	$P_{mech}^+$	$P_{mech}^-$
$MVEM_o$	2.5	1.8	2.5	2.4	3.3	5.4	3.4	1.4
$x_r$	2.5	1.8	2.4	2.5	3.3	5.5	3.3	1.5
$x_r$ +adiabatic	2.5	1.8	2.5	2.7	3.1	4.9	3.1	1.5
$\eta_{vol,2}$	2.5	2.0	2.7	2.3	3.2	5.5	5.1	1.4
$\eta_{vol,2}$ + $x_r$ +adiabatic	2.5	1.9	2.7	2.6	3.0	4.9	4.4	1.6

### 6.3 Adiabatic exhaust manifold model

The adiabatic model, as described in [3, 8] is implemented according to:

$$\begin{aligned} \frac{dp_{em}}{dt} &= \frac{R_e \gamma_e}{V_{em}} (T_{em,k} (\dot{m}_{ac} + \dot{m}_f) - T_{em} (\dot{m}_t + \dot{m}_{wg})) \\ \frac{dT_{em}}{dt} &= \frac{R_e T_{em}}{p_{em} V_{em}} \left( \gamma_e \left( T_{em,k} (\dot{m}_{ac} + \dot{m}_f) - T_{em} (\dot{m}_t + \dot{m}_{wg}) \right) \right. \\ &\quad \left. - T_{em} (\dot{m}_{ac} + \dot{m}_f - \dot{m}_t - \dot{m}_{wg}) \right) \end{aligned}$$

This means extending the model with an additional state,  $T_{em}$ .  $T_{em,k}$ , i.e. the temperature of the gases flowing into the manifold are computed according to (23), that is temperature after heat loss.

## 7 Results

The two OSDs defined in Section 3.2 are solved for the different models and the resulting optimal pumping power,  $P_{pump}$  is plotted relative the stationary optimal in Fig. 7. The oscillations cannot be explained by any of the model extensions. The periodic nature of the solution is present for all model extensions and the changes in frequency and amplitude of the oscillations are minor. In Table 5 the changes in energies and efficiency are shown, which confirms the results seen in Fig. 7. The decrease in pumping energy,  $\Delta E_{pump}$ , increases for each model extension for  $\omega_{ice} = \text{fix}$ , indicating that given a standard mean value engine model it actually is optimal to use periodic wastegate control in order to decrease the pumping torque.

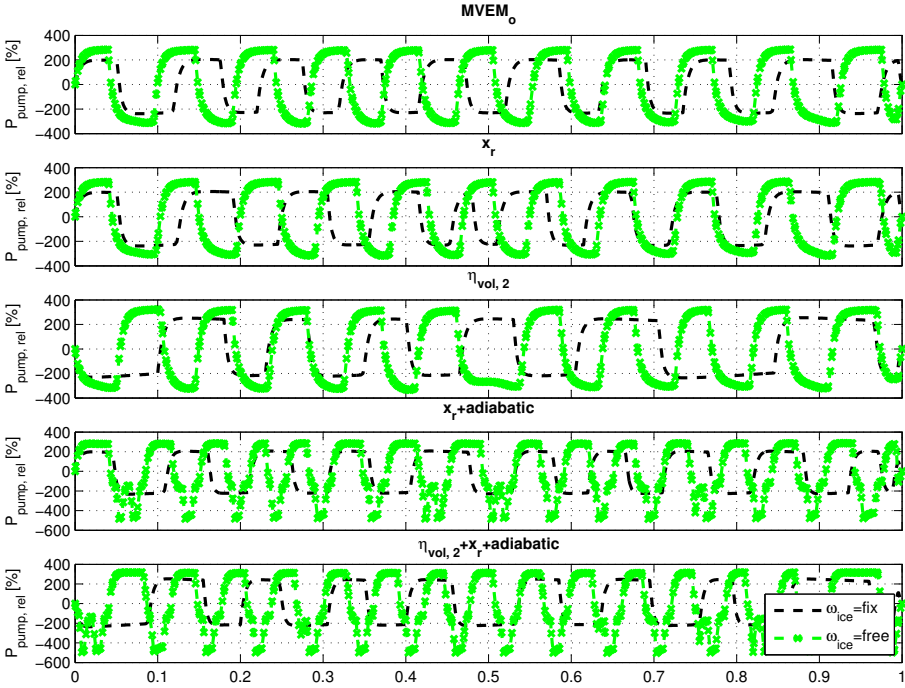


Figure 7: Relative pumping power of the optimal solutions to the two OSDs for the different models, relative the stationary optimal operating point. The oscillatory solution can not be explained by any of the model extensions.

Table 5: Changes in efficiency and energies of the two OSDs,  $\omega_{ice} = \text{fix}$  and  $\omega_{ice} = \text{free}$ , relative  $x(\eta_{max})$ , for the different models.

		$\Delta\eta$	$\Delta E_{fric}$	$\Delta E_{pump}$	$\Delta E_{ig}$
$MVEM_o$	fix	0.024	0.0	-2.41	-0.02
	free	0.052	0.88	-4.09	-0.03
$x_r$	fix	0.024	0.0	-2.52	-0.02
	free	0.054	1.32	-3.64	0.02
$x_r+$ adiabatic	fix	0.024	0.0	-2.58	-0.02
	free	0.068	1.74	-3.7	0.19
$\eta_{vol,2}$	fix	0.029	0.0	-3.14	-0.03
	free	0.070	-2.23	-10.16	-0.31
$\eta_{vol,2} + x_r+$ adiabatic	fix	0.030	0.0	-3.23	-0.03
	free	0.080	-1.99	-10.21	-0.22

## 8 Conclusions

Optimal control of a diesel-electric powertrain is studied. It is shown that the oscillatory solutions seen for certain operating points are not directly discretization dependent. Instead the solution is periodic with a period much greater than the control interval length. Further it is seen that the pumping work of the engine decreases as a result of the oscillations. To study if this effect is a result of over-simplification in the previously published mean value engine model, several model extensions are investigated and their corresponding optimal control problems are solved. Furthermore a new residual gas model, suitable for optimal control, is presented. It is shown that the oscillating controls cannot be explained by the implemented extensions to the previously published model, showing that for certain operating points for mean value engine models the optimal solution is actually periodic.

## References

- [1] Joel Andersson. *A General-Purpose Software Framework for Dynamic Optimization*. PhD thesis, Arenberg Doctoral School, KU Leuven, Department of Electrical Engineering (ESAT/SCD) and Optimization in Engineering Center, Kasteelpark Arenberg 10, 3001-Heverlee, Belgium, October 2013.
- [2] Jonas Asprión, Oscar Chinellato, and Lino Guzzella. Optimal control of diesel engines: Numerical methods, applications, and experimental validation. *Mathematical Problems in Engineering*, 2014.
- [3] Alain Chevalier, Martin Müller, and Elbert Hendricks. On the validity of mean value engine models during transient operation. In *SAE Technical Paper 2000-01-1261*. SAE International, 1992.
- [4] Lars Eriksson and Lars Nielsen. *Modeling and Control of Engines and Drivelines*. John Wiley & Sons, 2014.
- [5] Elmer G. Gilbert. Vehicle cruise: Improved fuel economy by periodic control. *Automatica*, 12:159–166, 1976.
- [6] Elmer G. Gilbert. Optimal periodic control: A general theory of necessary conditions. *SIAM Journal of Control and Optimization*, 15(5):717–746, 1977.
- [7] Erik Hellström, Jan Åslund, and Lars Nielsen. Design of an efficient algorithm for fuel-optimal look-ahead control. *Control Engineering Practice*, 18(11):1318–1327, 2010.
- [8] Elbert Hendricks. Isothermal vs. adiabatic mean value SI engine models. In *AAC'01 – 3rd IFAC Symposium on Advances in Automotive Control*, Karlsruhe, Germany, 2001.
- [9] HSL. A collection of fortran codes for large scale scientific computation. <http://www.hsl.rl.ac.uk>, 2013.

- [10] Adam Lowell Schwartz. *Theory and implementation of numerical methods based on Runge-Kutta integration for solving optimal control problems*. PhD thesis, University of Berkeley, California, 1996.
- [11] Martin Sivertsson and Lars Eriksson. Modeling for optimal control: A validated diesel-electric powertrain model. In *SIMS 2014 - 55th International Conference on Simulation and Modelling*, Aalborg, Denmark, 2014.
- [12] Martin Sivertsson and Lars Eriksson. Optimal transient control trajectories in diesel-electric systems-part 1: Modeling, problem formulation and engine properties. *Journal of Engineering for Gas Turbines and Power*, 137(2), February 2015.
- [13] Martin Sivertsson and Lars Eriksson. Optimal transient control trajectories in diesel-electric systems-part 2: Generator and energy storage effects. *Journal of Engineering for Gas Turbines and Power*, 137(2), February 2015.
- [14] Vehicular Systems Software. LiU D-El. "<http://www.fs.isy.liu.se/Software/>", 2014.
- [15] Andreas Wächter and Lorenz T. Biegler. On the implementation of an interior-point filter line-search algorithm for large-scale nonlinear programming. *Mathematical Programming*, 106:25–57, 2006.
- [16] Johan Wahlström and Lars Eriksson. Modelling diesel engines with a variable-geometry turbocharger and exhaust gas recirculation by optimization of model parameters for capturing non-linear system dynamics. *Proceedings of the Institution of Mechanical Engineers, Part D, Journal of Automobile Engineering*, 225(7):960–986, 2011.
- [17] WHDC Working Group. Worldwide harmonized heavy duty emissions certification procedure. "<http://www.unece.org/fileadmin/DAM/trans/doc/2005/wp29grpe/TRANS-WP29-GRPE-50-inf04r1e.pdf>", 2005. GRPE-50-4-Rev.1, Read 2/2-2015.

## A Excerpts from original model

### A.1 Torque model

$$M_{ice} = M_{ig} - M_{fric} - M_{pump} \quad (11)$$

$$M_{pump} = \frac{V_d}{4\pi} (p_{em} - p_{im}) \quad (12)$$

$$M_{fric} = \frac{V_d}{4\pi} 10^5 (c_{fr1}\omega_{ice}^2 + c_{fr2}\omega_{ice} + c_{fr3}) \quad (13)$$

$$M_{ig} = \frac{u_f 10^{-6} n_{cyl} q_{HV} \eta_{ig}}{4\pi} \quad (14)$$

$$\eta_{ig} = \eta_{ig,t} \left(1 - \frac{1}{r_c^{\gamma_{cyl} - 1}}\right) \quad (15)$$

$$\eta_{ig,t} = M_{f,1} + g_f (M_{f,2} - M_{f,1}) \quad (16)$$

$$g_f = \frac{1 + \tanh(0.1(\omega_{ice} - 1500\pi/30))}{2} \quad (17)$$

$$M_{f,1} = c_{M_{f,1},1}\omega_{ice}^2 + c_{M_{f,1},2}\omega_{ice} \quad (18)$$

$$M_{f,2} = c_{M_{f,2},1}\omega_{ice}^2 + c_{M_{f,2},2}\omega_{ice} + c_{M_{f,2},3} \quad (19)$$

### A.2 Volumetric efficiency

$$\eta_{vol} = c_{vol,1}\sqrt{p_{im}} + c_{vol,2}\sqrt{\omega_{ice}} + c_{vol,3} \quad (20)$$

### A.3 Exhaust pressure and temperature

$$q_{in} = \frac{\dot{m}_f q_{HV}}{\dot{m}_f + \dot{m}_{ac}} \quad (21)$$

$$T_{eo} = \eta_{sc} \Pi_e^{1-1/\gamma_a} r_c^{1-\gamma_a} \left( \frac{q_{in}}{c_{p,a}} + T_{im} r_c^{\gamma_a - 1} \right) \quad (22)$$

$$T_{em} = T_{amb} + (T_{eo} - T_{amb}) e^{-\frac{h_{tot} V_{pipe}}{(\dot{m}_f + \dot{m}_{ac}) c_{p,e}}} \quad (23)$$

$$\frac{dp_{em}}{dt} = \frac{R_e T_{em}}{V_{em}} (\dot{m}_{ac} + \dot{m}_f - \dot{m}_t - \dot{m}_{wg}) \quad (24)$$

# Optimal stationary control of diesel engines using periodic control<sup>†</sup>

Martin Sivertsson<sup>a</sup> and Lars Eriksson<sup>a</sup>

<sup>a</sup>*Vehicular Systems, Department of Electrical Engineering,  
Linköping University, SE-581 83 Linköping, Sweden.*

---

<sup>†</sup>This is a formatted version of “Optimal stationary control of diesel engines using periodic control” by Martin Sivertsson and Lars Eriksson, submitted to Control Engineering Practice. The formatting is restricted to changing the article into a single-column format, adjusting sizes of figures and tables, and adjusting the referencing style.

## **Abstract**

Measurements and optimal control are used to study whether the fuel economy of a diesel engine can be improved through periodic control of the wastegate. The measurements show that the pumping torque of the engine is changed when the wastegate is controlled in a periodic manner versus stationary even if the mean position is the same. If this decreases the fuel consumption or not is seen to be frequency and operating point dependent. The measurements indicate that the phenomenon occurs in the time scales capturable by mean value engine models (MVEM). The operating points are further analyzed using a MVEM and optimal control. It is shown that whether the optimal solution exhibits periodic oscillations or not is operating point dependent, but is not due to the instantaneous nature of the controls. Even if an actuator model is added the oscillations persist for reasonable time constants, the frequency of the oscillations is however affected. Further it is shown that the periodic control can be predicted by optimal periodic control theory and that the frequency of the control affects the resulting efficiency.

## Introduction

Numerical optimal control is a powerful tool to study how to best utilize the available controls to get a desired output from complex systems. The resulting optimal controls may however be oscillatory, as seen Fig. 1 where the optimal state and control trajectories to a prescribed output power profile of a diesel-electric powertrain is shown. These oscillations can be divided into four categories: a) the algorithm is stuck in a local minima, b) the algorithm exploits numerical errors to decrease the criteria to be minimized, c) the optima is not unique and the oscillations do not affect the criteria, or d) the oscillations are actually optimal given the model and maybe even for the physical system.

The problem with local minima is algorithm and/or initial guess dependent and inherent in numerical optimal control of nonconvex problems. With good knowledge of the problem it can normally be ensured that the received solutions are at least good local minima, for instance using fundamentally different initial guesses and see that they converge to the same solution.

In [14] it is shown that along singular arcs the resulting controls are often highly oscillatory and that the oscillations are artifacts of the numerical method and not the solution itself. It is also claimed that the problem gets worse in the presence of active trajectory constraints. In [9] it is shown that oscillations can be produced as a result of that the optimizer uses the integrator error to decrease the objective.

In [17] it is shown that under certain circumstances the minimum time solution for a step in output power and energy of a diesel-electric powertrain is not unique. There the problem is solved by first minimizing time and then using the optimal time as a constraint and minimize fuel.

For certain problems the optimal steady state solution (OSS) is not the same as the optimal dynamic solution (ODS) of the problem, even when a steady state solution would have been expected. This is the case when the optimal solution is periodic. Two examples where it is shown that the optimal solution is periodic are [8] and [12] who both deal with the topic of vehicle speed optimization. There also exist some theory on how to test whether a stationary solution can be improved by periodically varying control, see [4, 5, 3, 6].

For physical systems oscillating controls are often undesirable, since it might increase wear in components and also be perceived as strange by the operator. In optimization oscillating controls also have the problem that they impair convergence of the algorithm. Further if a fixed step integrator is used and the system has fast dynamics the oscillations will also demand a very fine grid to guarantee the integration accuracy, which will increase the memory usage and further slow down the algorithm.

One technique commonly used to get rid of oscillations is regularisation. The idea is to add a penalty term to the cost function to remove the oscillations. In [14] adding the piecewise derivative variation of the control to the cost function to penalize oscillating controls is suggested, a strategy also used in [2]. In [17, 18] the integral of the squared state derivatives is added to the cost function to accomplish the same thing. Another technique is to reformulate the problem to remove the gain of oscillating controls. In [9] a change in formulation, going

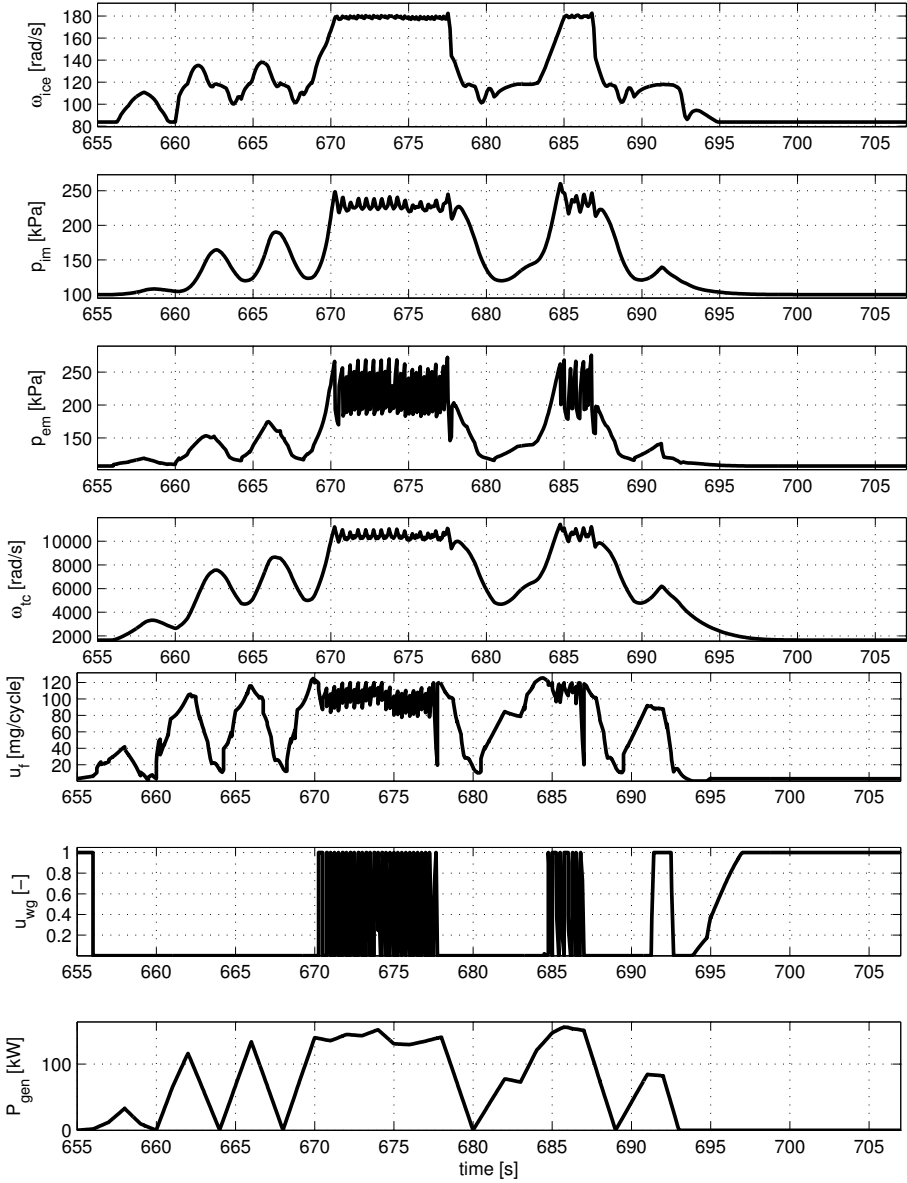


Figure 1: The optimal state and control trajectories to the prescribed output power trajectory,  $P_{gen}$ , for a diesel-electric powertrain. The resulting controls are highly oscillatory, see  $t \in [670, 678]$ ,  $[684, 687]$

from velocity to kinetic energy as state variable, solves the problem of oscillatory controls.

In previous works by the authors optimal control of a diesel-electric powertrain in transient operation is studied, see [17, 18]. It has been seen and noted that the resulting solutions are oscillatory, and the oscillations are especially severe in the wastegate control. These oscillatory solutions have been seen both with TOMLAB/Propt, using pseudospectral collocation and sequential quadratic programming (SQP), see [19], as well as with ACADO Toolkit, using multiple shooting and SQP, see [10], suggesting that the problem should not be an artifact of the integration routine/solver. In [2] the unconfirmed hypothesis is that the oscillations seen in the optimal variable geometry turbine (VGT) control of a diesel engine are due to decrease in the gas exchange losses. This is due to that the exhaust manifold pressure oscillates with the VGT position whereas the intake manifold pressure remains unaffected due to the slow turbocharger dynamics.

In [16] it is shown that it actually is optimal to oscillate the wastegate, that it actually decreases the pumping torque of the engine and that this phenomenon does not disappear when the model is extended, and that the period time is fundamentally different from the discretization step length, suggesting that it might be a property of the physical system itself. This paper continues this study using both measurements and further simulation and optimization to study if the oscillating solutions seen are a result of the optimal solution being periodic, and also if this applies to the real engine.

## 1 Contributions

The contributions of this paper is a study of whether or not gains can be made by controlling the wastegate in a periodic manner in an otherwise stationary operation of a diesel engine. More specifically the paper contributes with a novel experimental investigation of whether the stationary operation of a real engine can be improved by controlling the wastegate periodically, and whether these dynamic effects occur in the time scales captured by mean value engine models (MVEM) or not. Further, using simulation and optimization techniques, the paper extends the study in [16] to see if the nature of the oscillating optimal solutions are operating point dependent. It also verifies the optimality of the periodic control using optimal periodic control theory, as well as shows that this can be used to predict the period of the oscillations. Finally it studies if the optimal oscillatory solution is affected by including an actuator model for the wastegate and how it is affected by the time constant of the actuator.

## 2 Measurements

The measurements are conducted on the diesel engine-generator combination (GenSet) of a diesel-electric powertrain. The measurements are conducted on a complete powertrain equipped with extra sensors, and not a test bench. The GenSet consists of a generator mounted on the output shaft of a medium-duty

Table 1: Measured operating points

Engine Speed [rpm]	1100	1500	1800	2000	2200
Generated Power [kW]	80	120	120	160	130

tier 3 diesel-engine. The engine is equipped with a charge air cooled wastegated twin-scroll turbocharger. To model the powertrain 192 stationary points are measured together with 21 dynamic data sets that consist of either a sequence of power transients with constant engine speed or a sequence of engine speed transients under constant power. These measurements are used to build a mean value engine model of the powertrain in [15]. The measured signals, sensors used, as well as measured rate is shown in Table 6 in Appendix B.

To investigate the impact of the wastegate control five operating points are selected. These points are different constant engine speeds and output powers, see Table 1, that are measured with:

- Nominal wastegate control as on the production engine
- The wastegate locked in several fixed positions
- The wastegate controlled by an external pneumatic actuator. With this actuator the wastegate can be opened and closed in a pulsating manner to investigate how the system behaves in the presence of oscillating controls.

## 2.1 Stationary measurements

In this paper the focus is on stationary optimal control, or absence of stationarity in the case of oscillating controls. For all stationary measurements the engine is run in speed control mode of the SAEJ1939 standard, see [13], which means that a speed reference,  $\omega_{ref}$ , is sent to the engine control unit (ECU), a speed reference the ECU tries to track. The generator acts as a load on the engine and the generator controller tries to produce the prescribed output power,  $P_{ref}$ . This operating point is then held until the pressures, temperatures and turbocharger speed have reached stationarity. The main measurement rate is 10kHz that is then downsampled and stored. In this paper the measurements are further downsampled to 200, 50, and 10Hz respectively, using combinations of 2, 4 and 5th order FIR filters. The main metrics used in this paper from these measurements are the average efficiency of the powertrain,  $\eta$  and the average pumping torque of the engine,  $M_{pump}$ , defined according to:

$$\eta = \frac{\bar{P}_{gen}}{\bar{m}_f q_{HV}} \quad (1)$$

$$M_{pump} = \frac{\bar{P}_{pump}}{\bar{\omega}_{ice}}$$

where  $\bar{\cdot}$  means average,  $P_{gen}$  is the output power of the generator,  $\dot{m}_f$  the fuel flow,  $P_{pump}$  the pumping power,  $q_{HV}$  the lower heating value of the fuel, and  $\omega_{ice}$  the engine speed. For a full list of symbols used see Appendix A.

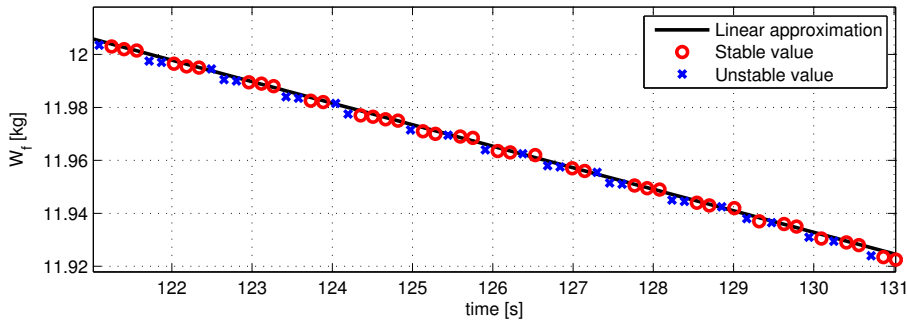


Figure 2: Measured fuel weight and the linear approximation.

## 2.2 Calculating fuel flow

The fuel flow is not measured, instead the fuel weight in the tank is measured. Due to recirculating flow and response time of the scale and system itself, this technique is only suitable for stationary points. Further the scale reports whether the measurement is stable or unstable. To get an accurate approximation of the fuel flow a first order polynomial is fitted with the least squares method, using only the stable measurements and the slope of this polynomial is the fuel flow in  $kg/s$ , see Fig. 2. It turns out that the relative difference in slope if all measured points are used instead of only the stable measurements is negligible but still only the stable points are used.

## 2.3 Output power

As described in [15] the efficiency of the power electronics is lumped together with the generator efficiency. Meaning that the produced output power of the powertrain is  $P_{gen} = I_{DC}U_{DC}$ .

## 2.4 Measurements with pulsating wastegate

The measurements start in stationary conditions with closed wastegate, the ECU controlling engine speed, and the generator control set to a fixed output power. The wastegate is then opened and closed in a pulsating manner using the external pneumatic actuator and different periods and opening lengths, see Table 2. Since the fuel flow is measured using a scale and only stationary points are of interest, the pressures are then allowed to stabilize and the analysis is conducted on the last 30s of the pulsating part, the exact duration is adjusted slightly to include an integer number of periods for the wastegate pulsation, see Fig. 3.

## 2.5 Results

In Fig. 4 the measured signals, downsampled to 200Hz, are shown. The exhaust pressures seem noisy due to pulsations from the cylinders. If instead the

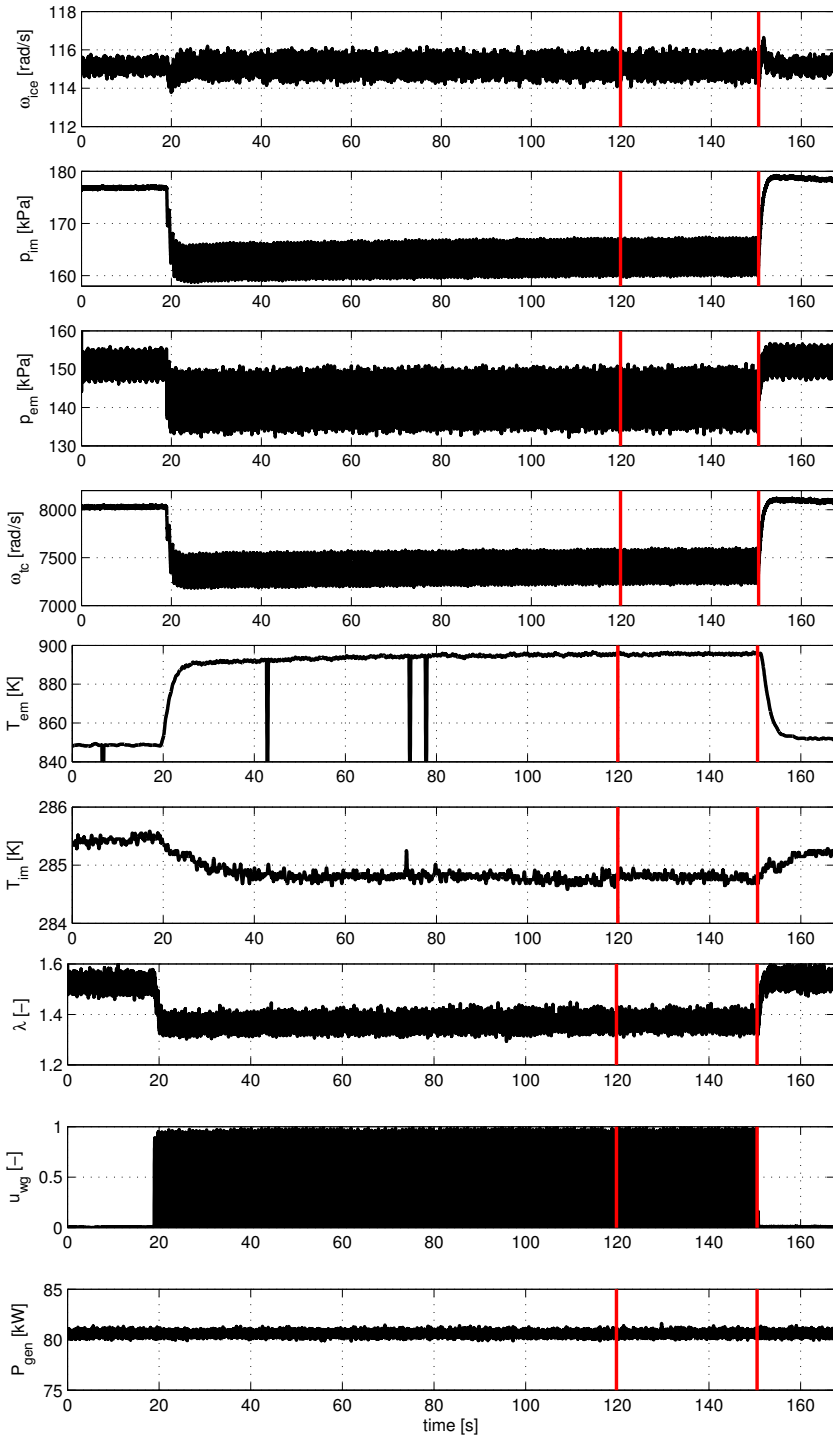


Figure 3: Measurement using pulsating wastegate position, 1100rpm, 80kW, 200Hz. Only the stationary part between the red lines is used in the analysis.

measurements are downsampled to 50Hz the pulsations in the exhaust pressures are removed and it can be clearly seen that the wastegate only affects the front bank of the exhaust manifold, while still accurately capturing the dynamics in  $p_{im}$  and  $u_{wg}$ .  $p_{em,f}$ , controlled by the wastegate, is seen to be a lot faster than  $p_{im}$  indicating that this could be used to decrease the pumping torque. If the data is downsampled to 10Hz the accuracy starts to drop, smearing out the peaks in both pressure and wastegate position. The analysis is therefore conducted using the measurements downsampled to 50Hz.

In Fig. 6 the mean efficiency and pumping torque (1) is plotted as a function of mean wastegate position for the different operating points, with fixed, normal and pulsated wastegate position. For the fixed and nominal wastegate controls the efficiency of the powertrain correlates strongly with the pumping torque. The only exception is 160kW, 2000rpm, where  $M_{pump}$  is monotonic in  $u_{wg}$  whereas the efficiency has a clear peak around  $u_{wg} = 0.2$ .

From the measurements it is clear that even though  $\bar{u}_{wg}$  is the same,  $M_{pump}$  and  $\eta$  change depending on whether the wastegate is opened and closed in a pulsating manner or kept at the same position. The pulsating measurements with small opening times, i.e.  $\bar{u}_{wg} \leq 0.1$  increases the pumping torque for all operating points. For  $\bar{u}_{wg} > 0.1$   $M_{pump}$  decreases for 80kW, 1100rpm and 120kW, 1500rpm and increases for the other three operating points, with some exceptions for 120kW, 1800rpm. Looking at the efficiency the trend is similar, if the pulsations decrease the pumping torque, the efficiency increases, and conversely, if the pumping torque increases the efficiency decreases. There are however some exceptions, especially for  $\bar{u}_{wg} \leq 0.1$  and also for several of the points for 120kW, 1800rpm, but in general the measurements show that pulsating wastegate can be used to alter both the pumping torque and the efficiency of the powertrain. Here the pulsations are performed in open loop control, with a few selected periods and opening times, there could be a potential for closed loop control.

The analysis is performed using measurements downsampled to 50Hz. To investigate if the conclusions depends on the sampling rate, an analysis is performed for different sampling rates. In Fig. 7 the relative error in pumping torque and wastegate position is shown relative the measurements at 200Hz. 50Hz seems to be an adequate sampling time to capture these effects, as indicated in Fig. 5, with a maximum relative error in  $M_{pump}$  of 1.3‰ indicating that this phenomenon occurs within the range of, and could be captured by, a mean value engine model [7].

Table 2: Pulse periods and opening durations used. \* means duration only used with 1.5s and 2.25s period, \*\* only with 0.75s period.

Period [s]	0.75	1.5	2.25		
Duration [s]	0.125	0.25**	0.375	0.75*	1.125*

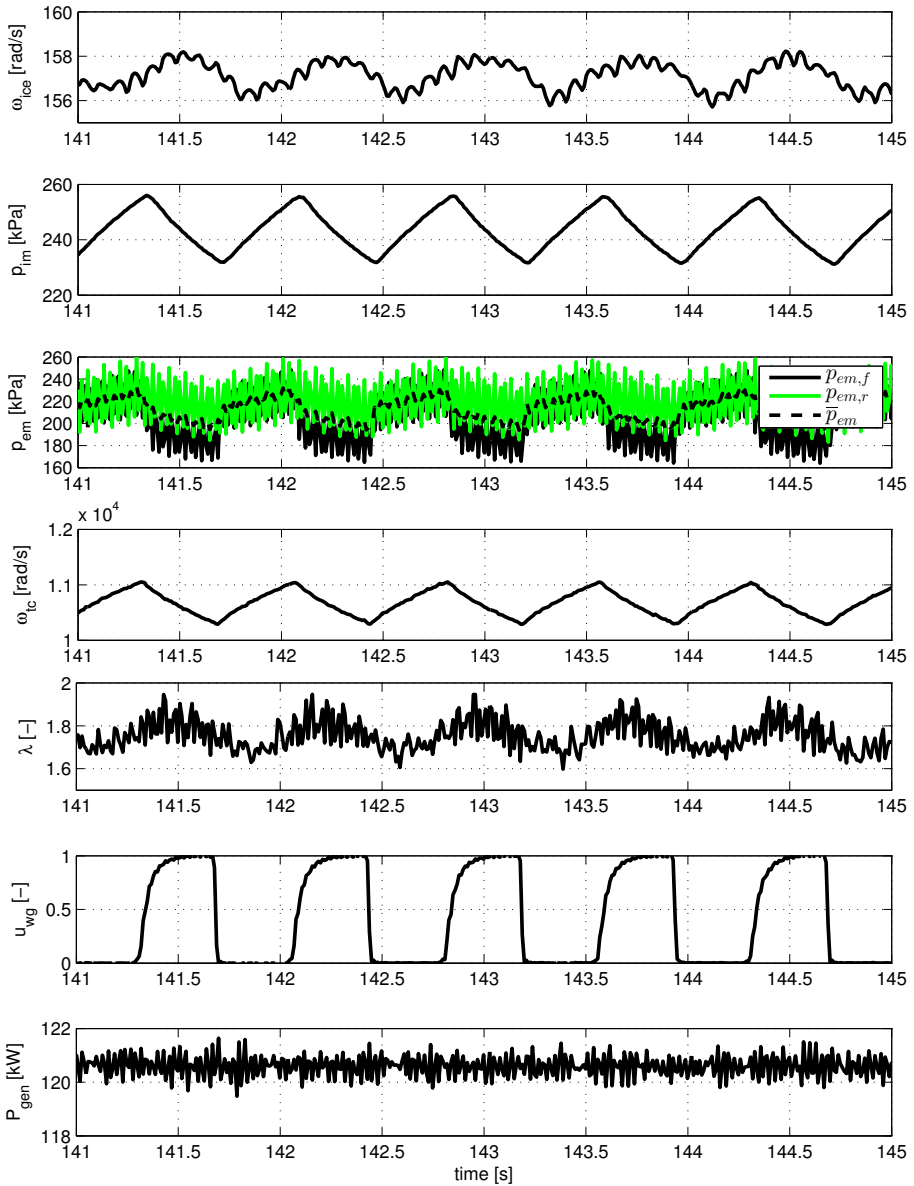


Figure 4: Measured signals for 120kW, 1500rpm, with pulsating wastegate downsampled to 200Hz. The exhaust pressures appear to be noisy, but this is due to individual pulsations from the cylinders.

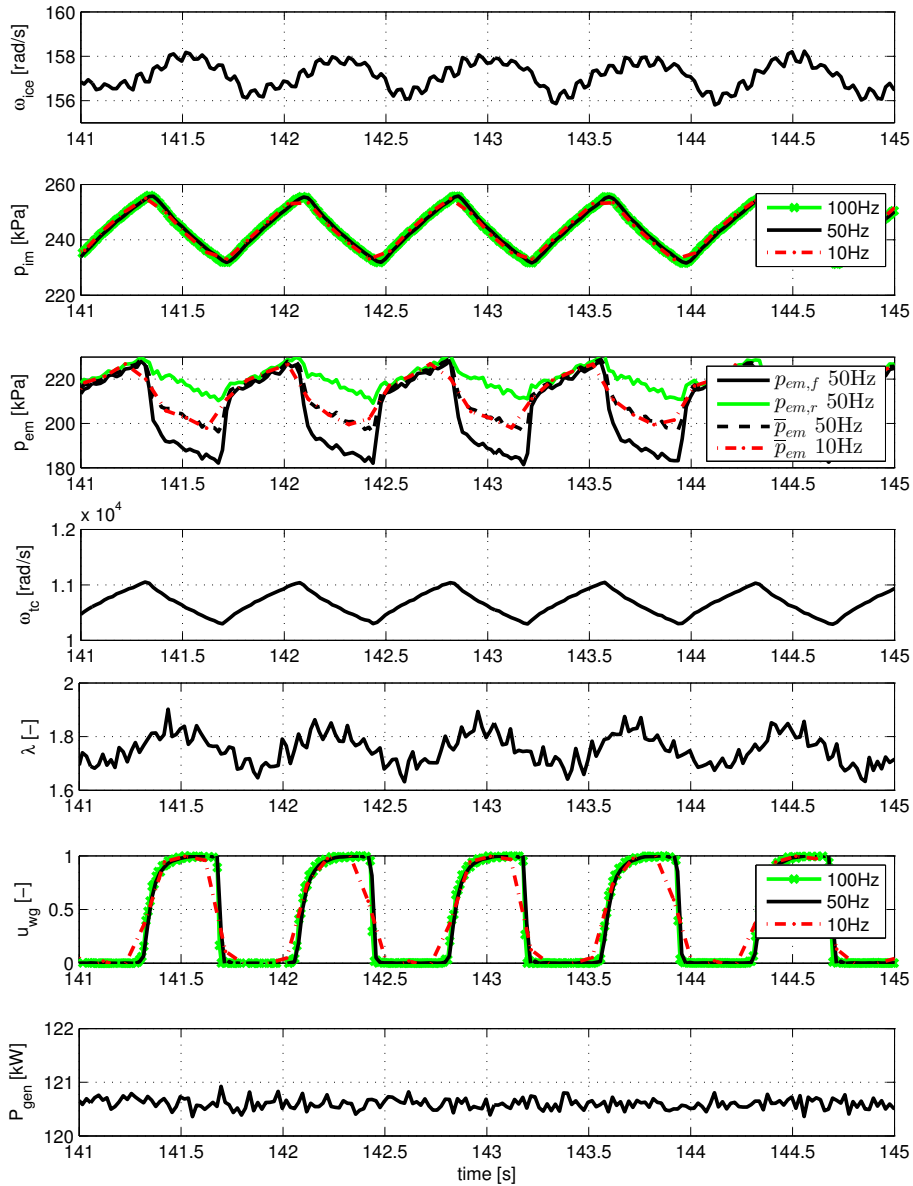


Figure 5: Measured signals for 120kW, 1500rpm, with pulsating wastegate downsampled to 50Hz. The individual pulsations in exhaust pressures are removed while still capturing the dynamics in  $p_{im}$  and  $u_{wg}$ . Downsampling to 10Hz appears to be too slow.

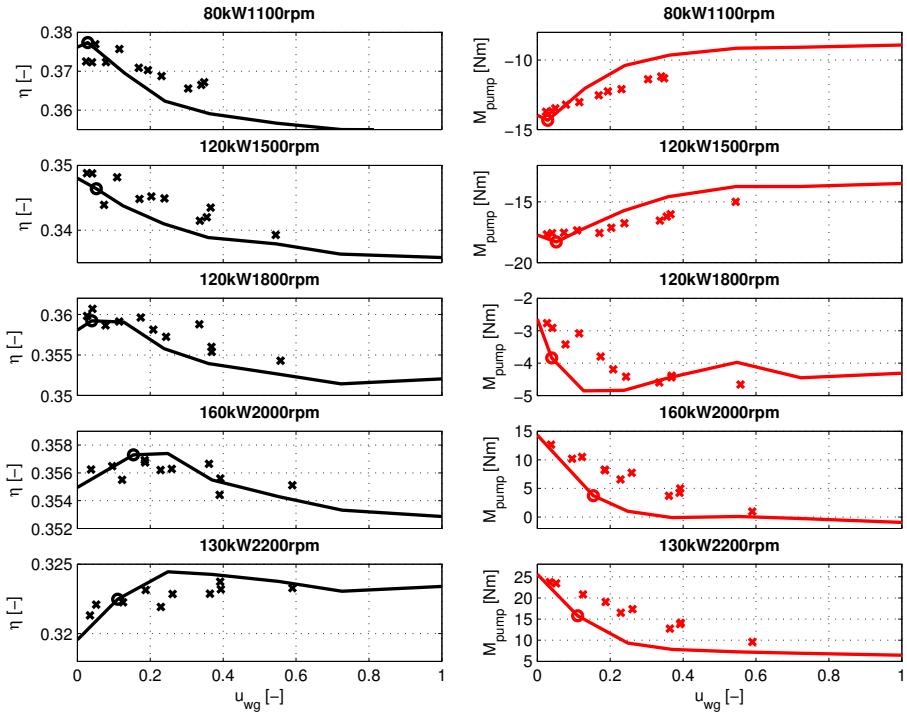


Figure 6: The effect of the wastegate on the efficiency and pumping torque during constant engine speed and generator power. Solid line is wastegate in a fixed position, circle is nominal wastegate control, and x marks pulsed wastegate. 50Hz measurements are used.

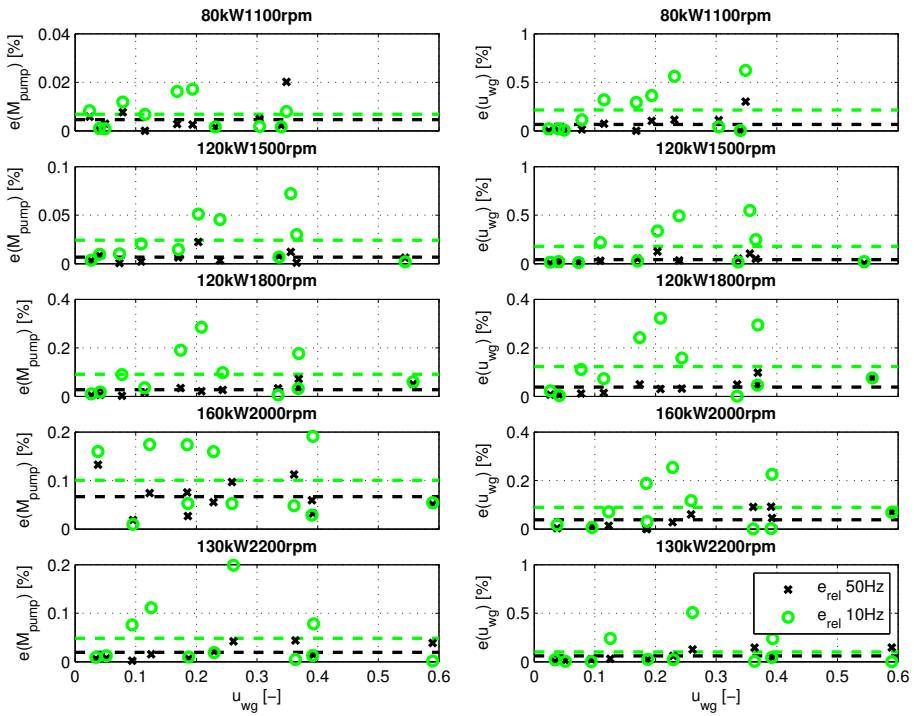


Figure 7: Relative errors in pumping torque and wastegate position if the study is conducted using 50Hz and 10Hz measurements, vs. 200Hz. Dashed lines mark the average error

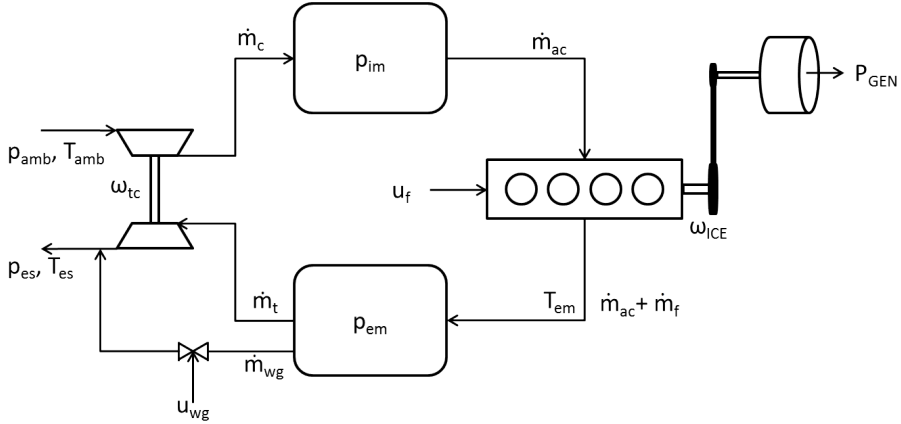


Figure 8: Structure of the MVEM. The modeled components as well as the connection between them.

### 3 Simulation and Optimization

To analyze the effects and results more analytically a mean value engine model of the system is used in an optimal control study to investigate whether or not it is optimal to oscillate in the measured points.

#### 3.1 Model

The model used can be downloaded in the **LiU-D-El**-package from [20] and is parameterized and validated against measurement data in [15] as *MVEM<sub>o</sub>*. The states of the MVEM are engine speed,  $\omega_{ice}$ , inlet manifold pressure,  $p_{im}$ , exhaust manifold pressure,  $p_{em}$ , and turbocharger speed,  $\omega_{tc}$ . The controls are injected fuel mass,  $u_f$ , wastegate position,  $u_{wg}$ , and generator power,  $P_{gen}$ . The engine model consists of two control volumes, intake and exhaust manifold, and four restrictions, compressor, engine, turbine, and wastegate, with connections between the components according to Fig. 8. The control volumes are modeled with the standard isothermal model, using the ideal gas law and mass conservation. The engine and turbocharger speeds are modeled using Newton's second law. The governing differential equations of the MVEM are:

$$\frac{d\omega_{ice}}{dt} = \frac{P_{ice} - P_{mech}}{\omega_{ice} J_{GenSet}} \quad (2)$$

$$\frac{dp_{im}}{dt} = \frac{R_a T_{im}}{V_{im}} (\dot{m}_c - \dot{m}_{ac}) \quad (3)$$

$$\frac{dp_{em}}{dt} = \frac{R_e T_{em}}{V_{em}} (\dot{m}_{ac} + \dot{m}_f - \dot{m}_t - \dot{m}_{wg}) \quad (4)$$

$$\frac{d\omega_{tc}}{dt} = \frac{P_t \eta_{tm} - P_c}{\omega_{tc} J_{tc}} \quad (5)$$

### 3.2 Problem Formulation

First an optimal control problem (OCP) is solved to find the optimal steady state controls (OSS) for the studied operating points, i.e. the controls that maximize  $\eta = \frac{P_{gen}}{\dot{m}_f H_{LHV}}$  given that  $\dot{x} = 0$  and  $P_{gen} = P_{ref}$ . These controls are then used as input and comparison for the following OCP:

$$\begin{aligned} \min_{u(t)} \quad & \int_0^T \dot{m}_f \\ \text{s.t.} \quad & \dot{x}(t) = f(x(t), u(t)) \\ & (x(t), u(t)) \in \Omega(t) \end{aligned} \quad (6)$$

where  $x$  is the state vector of the MVEM,  $\dot{x}$  is the state equations (2)-(5) and  $u = [u_f, u_{wg}, P_{gen}]$ . The optimal control problems are also subject to a set of constraints, namely:

$$\begin{aligned} x(0) = x(T) = x(\eta_{max}), \quad & \dot{x}(T) = 0 \\ u_{min} \leq u(t) \leq u_{max}, \quad & x_{min} \leq x(t) \leq x_{max} \\ \omega_{ice}(t) = \omega_{ref}, \quad & P_{gen}(t) = P_{ref} \\ \Pi_c \leq \Pi_{c,surge} \quad & \phi(x(t), u(t)) \leq \frac{1}{\lambda_{min}} \\ BSR_{min} \leq BSR(x(t), u(t)) \leq BSR_{max} \\ P_{ice}(x(t), u(t)) \leq P_{ice,max}(x(t)) \end{aligned} \quad (7)$$

The constraints are actuator and state limits, as well as constraints imposed by the components, such as maximum power of the engine,  $P_{ice}$ , surge-limit of the compressor,  $\Pi_{c,surge}$ , blade speed ratio-limit of the turbine,  $BSR$ , as well as environmental constraints, i.e. an upper limit on  $\phi$  set by the smoke-limiter. The driving mission-constraints are that the powertrain starts in the operating point of maximum efficiency,  $x(0) = x(\eta_{max})$ , a point it should also end in, with the added requirement that the end operating point should be stationary. The generator power and engine speed are fixed to their reference values. Since the modeled losses in the torque model are only speed dependent, except for the pumping torque, that depend on the intake and exhaust manifold pressures, this formulation ensures that if the results are oscillatory, it is actually optimal and it does actually decrease the pumping torque.

### 3.3 Numerical Solution

The software package that is used to solve the optimal control problem numerically is CasADi [1]. First the problem is discretized using Radau collocation with three collocation points in each control interval. The states are thus approximated with a third order polynomial, whereas the controls are approximated by a second order polynomial in each control interval. The states are required to be continuous over each control interval boundary, whereas the controls are allowed to be discontinuous. The resulting nonlinear program(NLP) is solved using IPOPT, [21], with the MA57 linear solver from the HSL package, [11]. In this study 200 control intervals per second is used.

### 3.4 Results

The OCP defined in (6)-(7) is solved for the different operating points in Table 1. In Fig. 9-left the stationary efficiency as well as pumping torque of the model for the points in Table 1 is shown. In Fig. 9-right the OSD wastegate actuation to the solved OCP is compared to the OSS. Comparing the efficiency and pumping torque curves between the model, Fig. 9-left and the measurements, Fig. 6, it can be seen that for both the measurement and model the efficiency goes from convex to concave in wastegate position, whereas the pumping torque goes from concave to convex. For which operating point this transition occurs differs slightly. In general the peak efficiency occurs for a smaller wastegate opening for the measurements than for the model, see for instance 130kW, 2200rpm. This might indicate that the effective wastegate area in the model is too small, however it's value is actually 2% larger than the measured wastegate size. In any case the agreement is considered good as the model is a global MVEM for the engine with no special tuning for these operating points.

The resulting wastegate controls from the solution to the OCP exhibit oscillations for all operating points except 80kW, 1100rpm. This seems to be due to that the OSS control in that case is with wastegate fully closed. The closer to the boundaries the stationary optima is, the longer the period of the oscillation, but in all solutions the wastegate control is switching between zero and one, which according to a pure stationary analysis should increase the pumping torque. Whether it is optimal or not and where the optima is attained thus seems to depend on the matching of the engine and turbocharger.

In Fig. 10 the relative pumping torque vs. the stationary optima is shown for the different operating points. Through the oscillations the pumping torque is changed several hundred percent away from what is stationary optimal. The operating point with the oscillations with the shortest period also has the largest relative benefit, see Table. 3, where the change in efficiencies and energies relative the stationary optima is shown. The relative efficiency increase of oscillating the wastegate is for the studied operating points up to 0.3%, which is small, but in an optimization context, clear.

Looking at Fig. 11 the low pass filtering effect of the turbocharger, as hypothesised by [2], can be clearly seen since the wastegate opening and closing results in a  $p_{em}$  span of 60 kPa, whereas the effect on  $p_{im}$  is only 4-6 kPa.

Relating the optimal results to the measurements, the solutions exhibit faster oscillations than used in the experiments, with periods as short as 0.1s. Also in the experiments the wastegate is open at most 75% of the period, whereas for 160kW, 2000rpm and 130kW, 2200rpm the optimal solution is with wastegate open 88-95% of the time.

### 3.5 $\Pi$ -test and periodic control

The  $\Pi$ -test, [4, 3], is a sufficient condition to determine if a periodic OCP is proper, i.e. if the OSS solutions can be improved by a suitable periodic operation. To simplify the problem,  $P_{gen}$  and  $\omega_{ice}$  are implemented as constants, the engine torque is computed from the mechanical generator power and engine speed, and

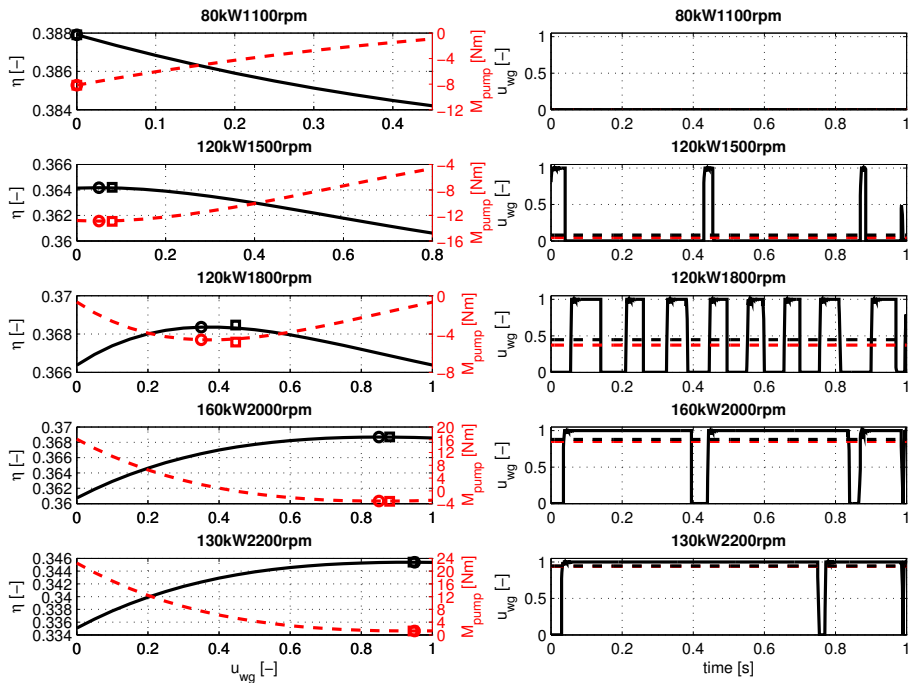


Figure 9: Left: Wastegate position's effect on the efficiency and pumping torque during stationary conditions, circles mark  $\eta_{max}$  and  $M_{pump,min}$  of OSS, squares average value of OSD. Right: Optimal wastegate actuation both for the OSD (solid), OSS (red dashed), as well as average value of OSD (black dashed).

Table 3: Changes in efficiency and energies for the OSD relative  $x(\eta_{max})$  in percent, where  $E_x = \int_0^T P_x dt$ .

	$\Delta\eta$	$\Delta E_{fric}$	$\Delta E_{pump}$	$\Delta E_{ig}$
80kW, 1100rpm	0.000	0.0	0.0	0.0
120kW, 1500rpm	0.006	0.0	-0.37	-0.006
120kW, 1800rpm	0.027	0.0	-4.43	-0.027
160kW, 2000rpm	0.007	0.0	-1.93	-0.007
130kW, 2200rpm	0.003	0.0	-1.69	-0.003

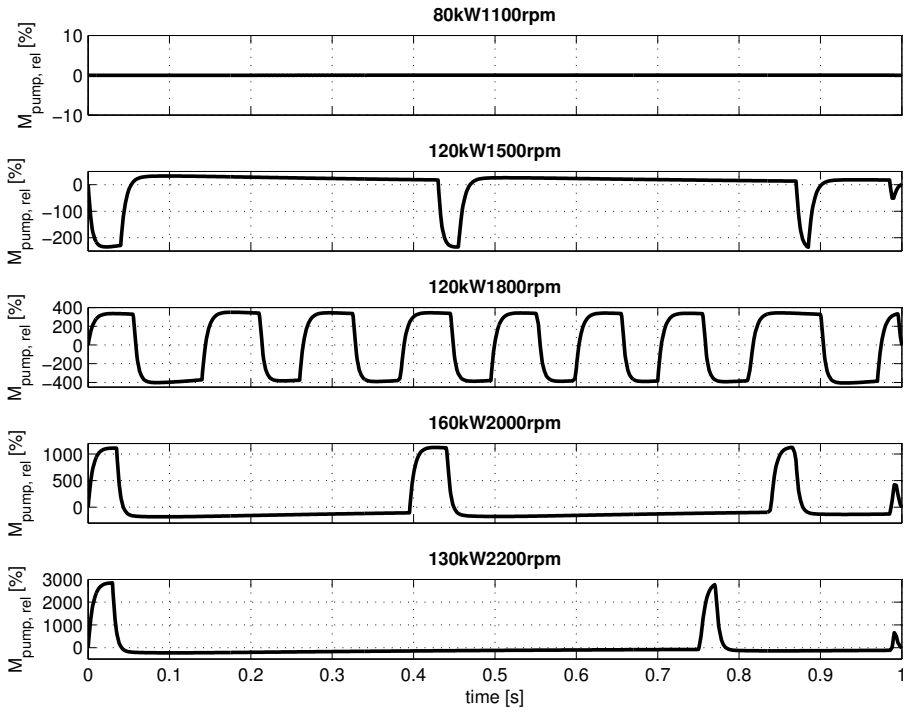


Figure 10: Pumping torque of the OSD relative the OSS.

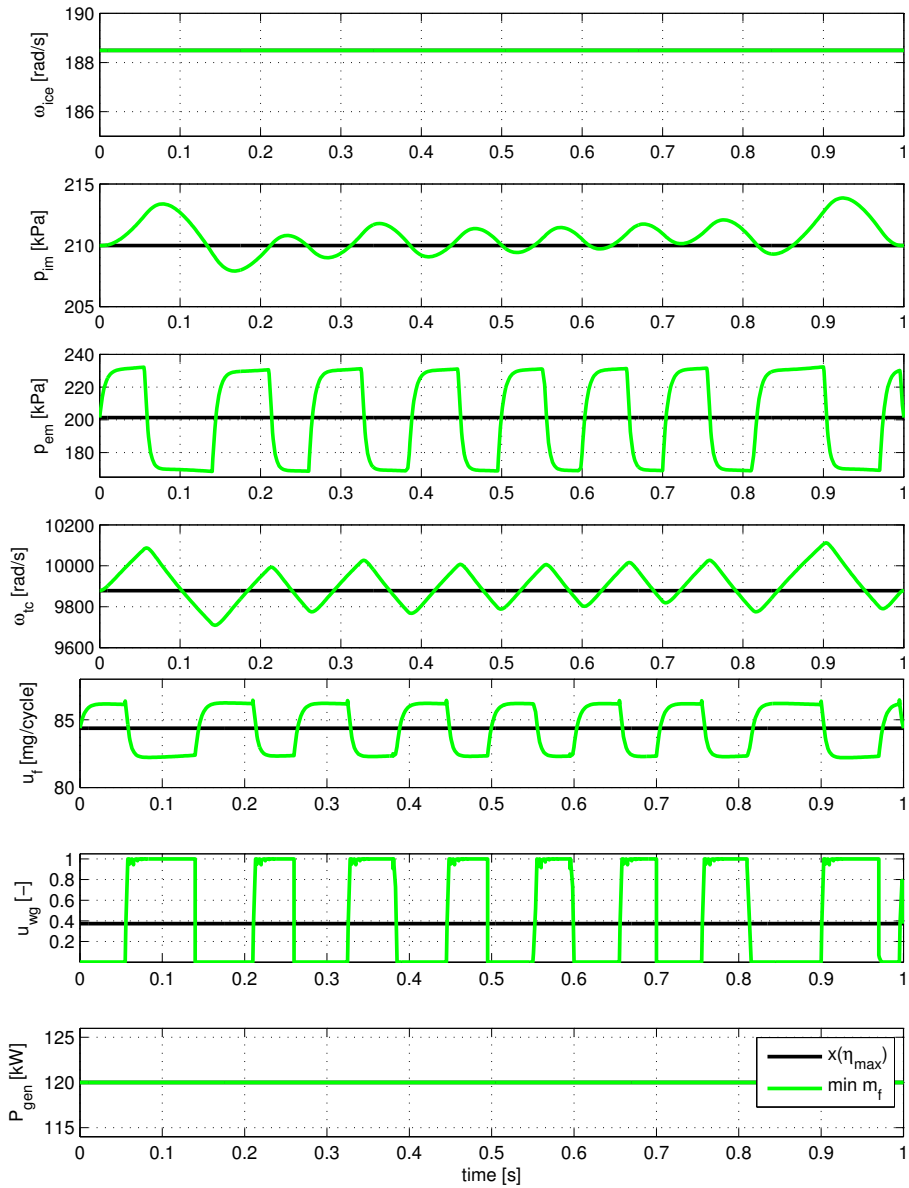


Figure 11: States and control trajectories for the OSD, 120kW,1800rpm. The solution is highly oscillatory.

the fuel flow is computed by inverting the engine torque model. The model is then reduced to a three-state, one-control, MVEM.

For the operating points considered where oscillations occur, i.e. all points except 80kW, 1100rpm, no constraints are active in the OSS-solution except the power constraint, engine speed constraint and stationarity constraints. These constraints, except the stationarity constraints, are thus implemented within the model. Two problems are considered using the reduced model, one stationary and one periodic, defined as:

$$\text{OSS}_r : \begin{cases} \min_{u_{wg}(t)} \int_0^T \dot{m}_f \\ \text{s.t.} \quad 0 = f(x, u_{wg}) \end{cases} \quad (8)$$

$$\text{OSD}_r : \begin{cases} \min_{u_{wg}(t)} \frac{1}{T} \int_0^T \dot{m}_f \\ \text{s.t.} \quad \dot{x} = f(x(t), u_{wg}(t)) \\ x(0) = x(T) \end{cases} \quad (9)$$

The idea is that the solution to (8), denoted  $x^*, u^*$ , is also a solution to (9), however not necessarily the optimal one. If the optimal control from (8) can be improved by a periodic variation around  $u^*$  for (9), (9) is proper, if not then the solutions are the same.

Defining the hamiltonian as:

$$H(x, u, \lambda) = \dot{m}_f(x) + \Lambda^\top f(x, u) \quad (10)$$

The II-test is defined as:

$$\begin{aligned} A &= f'_x(x^*, u^*), \quad B = f'_u(x^*, u^*), \quad R = H''_{uu}(x^*, u^*) \\ Q &= H''_{xu}(x^*, u^*), \quad P = H''_{xx}(x^*, u^*) \\ G(j\omega) &= (j\omega I - A)^{-1} B \\ \Pi(\omega) &= G(-j\omega)^\top P G(j\omega) + Q^\top G(j\omega) + G^\top(-j\omega) Q \end{aligned} \quad (11)$$

where  $H'_x$  means partial derivative with respect to  $x$ , and  $\Pi(\omega)$  is an  $m \times m$  hermitian matrix, where  $m$  is the number of controls. If for some  $\omega$ ,  $\Pi(\omega)$  is not positive semi-definite, and (9) is normal at  $x^*, u^*$ , then (9) is proper. Here there are no active constraints and A is non-singular, the normality condition is therefore automatically satisfied. Since  $m = 1$   $\Pi(\omega)$  is scalar and the requirement translates to if  $\Pi(\omega)$  is negative for any  $\omega$  then (9) is proper.

The problem in (8) is solved using `fmincon` in Matlab, which also provides the optimal lagrange multipliers  $\Lambda$ , for 120kW, 1800rpm,  $\Pi(\omega)$  is computed using (11) and plotted as a function of  $\omega$  in Fig. 12-top. The figure shows that for frequencies  $\omega \geq 9$  rad/s (9) is proper. Hence a weak variation of the  $u^*$  control of sinusoidal type should decrease the consumption for all frequencies larger than 9 rad/s. Defining a periodic control signal according to:

$$u_{wg} = u_{wg}^* + \epsilon \sin \omega t \quad (12)$$

The reduced model is then simulated using this control, for different  $\omega$  and  $\epsilon$  and compared to  $u^*$ . To make the comparison fair, the model is simulated

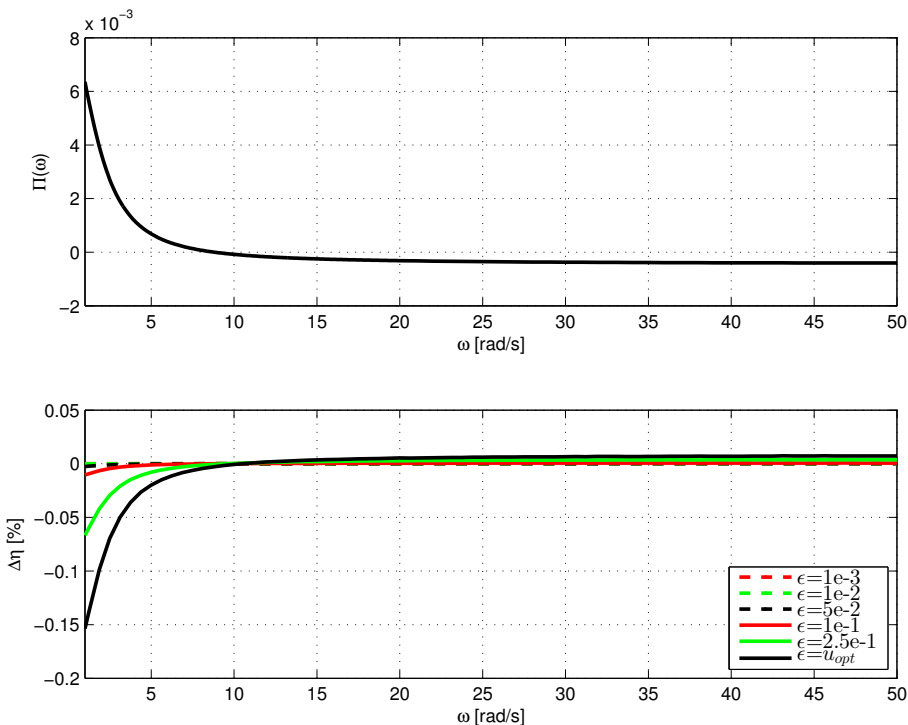


Figure 12: Top:  $\Pi(\omega)$  for 120kW, 1800rpm. Bottom: The change in efficiency for the periodic control vs.  $u^*$  for different frequencies and amplitudes.

until the oscillations in the states have reached their final amplitude, and then restarted using this as initial conditions. The change in efficiency is shown in Fig. 12-bottom. The results confirm the results of the  $\Pi$ -test. For  $\omega \geq 9$  rad/s the periodic control improves the efficiency, the improvement increases with  $\epsilon$ . Worth noting is also that  $\epsilon$  acts as an amplification and that a periodic control with  $\omega < 9$  rad/s decreases the efficiency. It turns out that for the operating points in Table 1 the frequencies,  $\omega_p$ , above which  $OSD_r$  is proper is in the range 7-11 rad/s. The only exception is 80kW, 1100rpm where  $\omega_p = 0$ , however this is hardly valid since  $u^* = 0$  which means that all periodic variations would lead to negative wastegate positions, i.e. massflow into the manifold which would be free energy.  $\omega_p \geq 7$ -11 rad/s translates to a period  $T \leq 0.6$ -0.9s. This supports the results from Section 2.5 that pulsating control with  $\bar{u}_{wg} \geq 0.1$  increases the pumping torque. This is since the lowest  $\bar{u}_{wg}$  are achieved with the two longest periods in Table 2 which are well above the found  $\omega_p$ .

### 3.6 Including an actuator model

One of the assumptions in the current MVEM is that the actuators are infinitely fast. This is of course not the case, however it is of interest to investigate the limit of optimal control, i.e. to see what would be possible *if* the actuators were

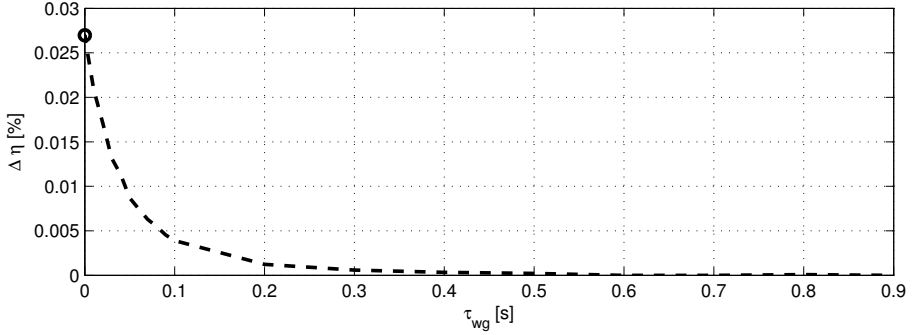


Figure 13: Change in efficiency of the OSD relative  $x(\eta_{max})$  as a function of the wastegate actuator time constant,  $\tau_{wg}$ . Circle marks the solution without actuator model.

that fast. To investigate if the oscillations seen here are only possible due to the instantaneous nature of the controls the model is extended with a wastegate actuator model. This is modeled using a first order model according to:

$$\frac{dx_{wg}}{dt} = \frac{1}{\tau_{wg}}(u_{wg} - x_{wg}) \quad (13)$$

This of course introduces the question for which  $\tau_{wg}$  the OSDs result in oscillatory solutions. Therefore the OCPs are solved for a set of time constants between  $1\mu s$  and  $1s$  and the relative change in efficiency is shown in Fig. 13. As expected the potential gain decreases with increasing time constant. With the pneumatic actuator used in the measurements the time constant is  $70ms$  when opening and  $20ms$  when closing, why  $50ms$  is considered a reasonable value. In Fig. 14 the solution with  $\tau_{wg} = 50ms$  is shown.  $50ms$  is chosen as a reasonable time constant, even if it depends on way of actuation, electrical or pneumatic. As can be seen in Fig. 14 both the frequency and the amplitude of the oscillations change when an actuator model is added. The wastegate control signal follows the same pattern as before, however the slower actuator dynamics prevent the wastegate from reaching it's fully open or fully closed position. The amplitude of the pressure oscillations are still a lot higher in the exhaust manifold than in the intake manifold, through the lowpass-filtering effect of the turbocharger. The span of the pressures during the oscillations are  $60$  vs.  $11kPa$  ( $p_{em}$  vs.  $p_{im}$ ) allowing for the pumping torque to be optimized.

## 4 Results and discussion

The measurements on a diesel-electric powertrain in Section 2 show that the pumping torque of a system where the wastegate is periodically controlled differs from when it is controlled in a stationary manner, even if the mean wastegate position is the same. This effect occurs in the time scales captured by mean value engine models but whether the pulsating control is beneficiary or not is

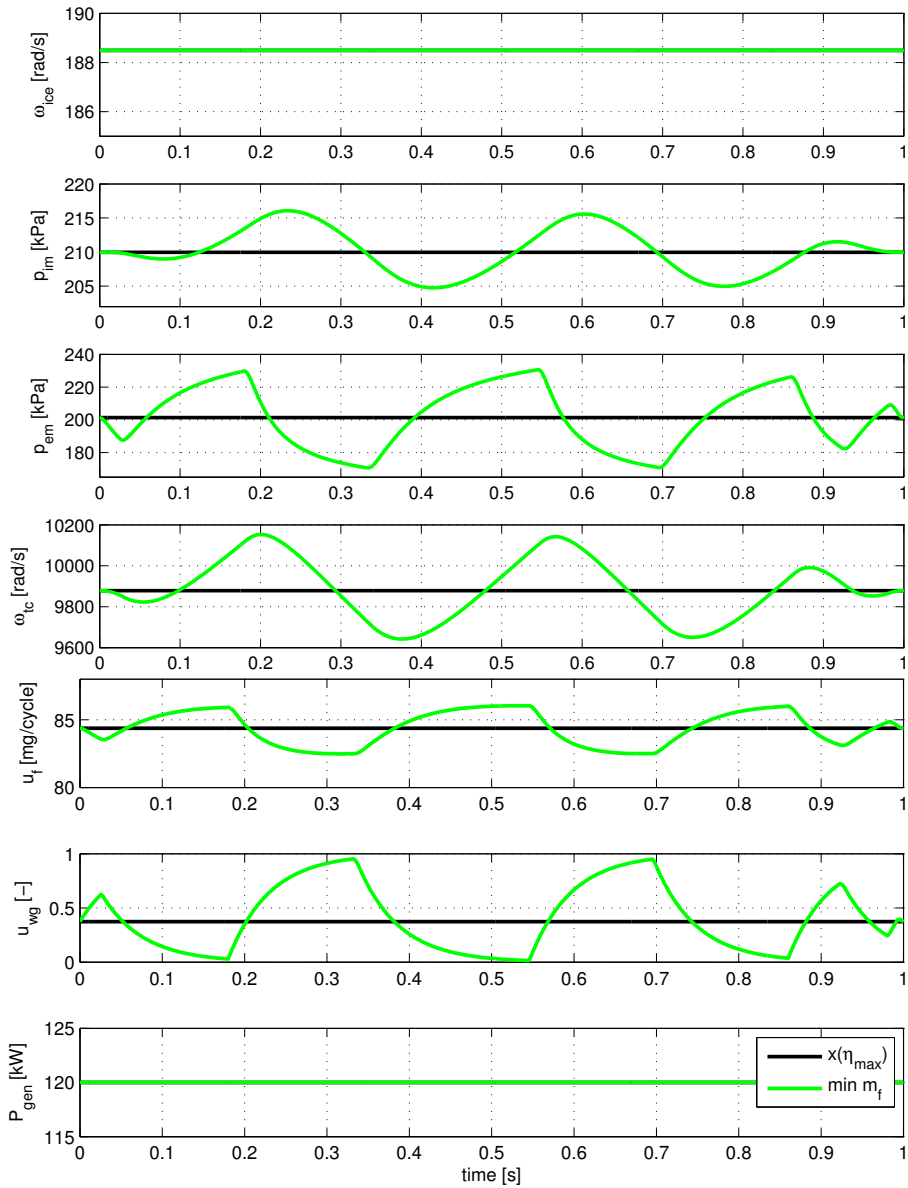


Figure 14: States and control trajectories for the OSD with wastegate actuator model, 120kW, 1800rpm. The oscillations persist, however the period increases.

shown to be operating point and period dependent, for some cases it increases the efficiency and for others not.

This is also confirmed in simulation in Section 3. The optimal control is not periodic for all the investigated operating points, this seems to be due to whether the optimal steady state solution lies on the boundary or not which indicates that it depends on the matching of the turbocharger and engine. The optimal periods and opening times are however different from the ones used in the measurements for all operating points but one. For that operating point the model predicts the stationary optima to be within the control set whereas the measurements show it to be on the boundary. Optimal periodic control theory confirms that the steady state solutions can be improved by periodic control. It also predicts well for which frequencies this is true, explaining why some measured points increase and some decrease the pumping torque. In general the periods used in measurements are too long, both compared to what the optimization in Section 3.4 shows, and to what the  $\Pi$ -test in Section 3.5 predicts.

Further it is shown in Section 3.6 that the oscillating nature of the controls is not a result of instantaneous nature of the controls in the model. When an actuator model is added for the wastegate the optimal control is still periodic, however the time constant of the actuator has a direct impact on the optimal frequency of the solution.

## 5 Conclusions

Optimal control of diesel engines in stationary operation is studied and more specifically if gains can be made from controlling the wastegate in a periodic manner. Measurements show that the pumping torque can be changed from its stationary value and even decreased using periodic control, for certain operating points. Using optimal control techniques as well as optimal periodic control theory it is shown that whether periodic control can improve the efficiency of the engine or not, depends on both the operating point as well as the frequency of the control. This does not change when an actuator model is added.

## References

- [1] Joel Andersson. *A General-Purpose Software Framework for Dynamic Optimization*. PhD thesis, Arenberg Doctoral School, KU Leuven, Department of Electrical Engineering (ESAT/SCD) and Optimization in Engineering Center, Kasteelpark Arenberg 10, 3001-Heverlee, Belgium, October 2013.
- [2] Jonas Asprion, Oscar Chinellato, and Lino Guzzella. Optimal control of diesel engines: Numerical methods, applications, and experimental validation. *Mathematical Problems in Engineering*, 2014.
- [3] Dennis S. Bernstein and Elmer G. Gilbert. Optimal periodic control: The  $\pi$  test revisited. *IEEE Transactions on Automatic Control*, AC-25(4):673–684, 1980.

- [4] Sergio Bittanti, Giorgio Fronza, and Guido Guardabassi. Periodic control: A frequency domain approach. *IEEE Transactions on Automatic Control*, AC-18(1):33–38, 1973.
- [5] Sergio Bittanti, Giorgio Fronza, and Guido Guardabassi. Optimal steady-state versus periodic operation in discrete systems. *Journal of Optimization Theory and Applications*, 18(4):521–536, 1976.
- [6] W. L. Chan and S. K. Ng. Normality and proper performance improvement in periodic control. *Journal of Optimization Theory and Applications*, 29(2):215–229, 1979.
- [7] Lars Eriksson and Lars Nielsen. *Modeling and Control of Engines and Drivelines*. John Wiley & Sons, 2014.
- [8] Elmer G. Gilbert. Vehicle cruise: Improved fuel economy by periodic control. *Automatica*, 12:159–166, 1976.
- [9] Erik Hellström, Jan Åslund, and Lars Nielsen. Design of an efficient algorithm for fuel-optimal look-ahead control. *Control Engineering Practice*, 18(11):1318–1327, 2010.
- [10] Boris Houska, Hans Joachim Ferreau, and Moritz Diehl. ACADO toolkit - an open source framework for automatic control and dynamic optimization. *Optimal Control Applications & Methods*, 32(3):298–312, 2011.
- [11] HSL. A collection of fortran codes for large scale scientific computation. <http://www.hsl.rl.ac.uk>, 2013.
- [12] Kevin McDonough, Ilya Kolmanovsky, Dimitar Filev, Diana Yanakiev, Steve Szwabowski, and John Micheline. Stochastic dynamic programming control policies for fuel efficient vehicle following. In *American Control Conference*, Washington DC, 2013.
- [13] SAE J1939 Standard. "[http://standards.sae.org/j1939/71\\_201002/](http://standards.sae.org/j1939/71_201002/)", 2013. Read 2013-10-04.
- [14] Adam Lowell Schwartz. *Theory and implementation of numerical methods based on Runge-Kutta integration for solving optimal control problems*. PhD thesis, University of Berkeley, California, 1996.
- [15] Martin Sivertsson and Lars Eriksson. Modeling for optimal control: A validated diesel-electric powertrain model. In *SIMS 2014 - 55th International Conference on Simulation and Modelling*, Aalborg, Denmark, 2014.
- [16] Martin Sivertsson and Lars Eriksson. Model and discretization impact on oscillatory optimal control for a diesel-electric powertrain. In *Submitted to E-COSM'15 - IFAC Workshop on Engine and Powertrain Control, Simulation and Modeling*, Columbus, Ohio, August 2015.

- [17] Martin Sivertsson and Lars Eriksson. Optimal transient control trajectories in diesel-electric systems-part 1: Modeling, problem formulation and engine properties. *Journal of Engineering for Gas Turbines and Power*, 137(2), February 2015.
- [18] Martin Sivertsson and Lars Eriksson. Optimal transient control trajectories in diesel-electric systems-part 2: Generator and energy storage effects. *Journal of Engineering for Gas Turbines and Power*, 137(2), February 2015.
- [19] TOMLAB. PROPT - Matlab Optimal Control Software, "<http://www.tomdyn.com/>", 2012.
- [20] Vehicular Systems Software. LiU D-El. "<http://www.fs.isy.liu.se/Software/>", 2014.
- [21] Andreas Wächter and Lorenz T. Biegler. On the implementation of an interior-point filter line-search algorithm for large-scale nonlinear programming. *Mathematical Programming*, 106:25–57, 2006.

## A Nomenclature

Table 4: Symbols used

Symbol	Description	Unit
$p$	Pressure	Pa
$T$	Temperature	K
$\omega$	Rotational speed	rad/s
$\dot{m}$	Massflow	kg/s
$\Pi$	Pressure ratio	-
$P$	Power	W
$M$	Torque	Nm
$E$	Energy	J
$V$	Volume	$m^3$
$R$	Gas Constant	J/(kg · K)
$u_f, u_{wg}, P_{gen}$	Control signals	mg/cycle, -, W
$J$	Inertia	kg · $m^2$
$BSR$	Blade speed ratio	-
$\eta$	Fuel-air equivalence ratio	-
$\phi$	Fuel-air equivalence ratio	-
$\lambda$	Air-fuel equivalence ratio	-
$q_{HV}$	Lower heating value	J/kg

Table 5: Subscripts used

Index	Description	Index	Description
<i>ice</i>	Engine	<i>GenSet</i>	Engine-Generator
<i>im</i>	Intake manifold	<i>em</i>	Exhaust manifold
<i>c</i>	Compressor	<i>ac</i>	After compressor
<i>t</i>	Turbine	<i>wg</i>	Wastegate
<i>f</i>	Fuel	<i>tc</i>	Turbocharger
<i>a</i>	Air	<i>e</i>	Exhaust
<i>gen</i>	Generator-electrical	<i>mech</i>	Generator-mechanical
<i>ref</i>	Reference	<i>c, surge</i>	Compressor surge-limit
<i>fric</i>	Friction	<i>pump</i>	Pumping
<i>ig</i>	Indicated gross	<i>tm</i>	Turbo, mechanical
<i>amb</i>	Ambient	<i>es</i>	Exhaust system

## B Measured signals and sensors

Table 6: Measured signals and sensors. \* means that the signal is asynchronous and the rate refers to an average

Name	Description	Sensor	Base rate
$p_{amb}$	Ambient pressure	Dynisco PT130-50 Pressure Transducer	500Hz
$p_{im}$	Pressure intake manifold	Dynisco PT130-50 Pressure Transducer	500Hz
$p_{em,f}$	Pressure exhaust manifold, front	Dynisco PT130-50 Pressure Transducer	2kHz
$p_{em,r}$	Pressure exhaust manifold, rear	Dynisco PT130-50 Pressure Transducer	2kHz
$p_{es}$	Pressur eafter turbine	Dynisco PT130-50 Pressure Transducer	2kHz
$p_{c,b}$	Pressure before compressor	Dynisco PT130-50 Pressure Transducer	500Hz
$p_{c,a}$	Pressure after compressor	Dynisco PT130-50 Pressure Transducer	500Hz
$T_{amb}$	Ambient temperature	TC 1.5mm mineral insulated type K thermocouple	12-13Hz*
$T_{im}$	Temperature intake manifold	TC 1.5mm mineral insulated type K thermocouple	12-13Hz*
$T_{em,f}$	Temperature exhaust manifold, front	TC 1.5mm mineral insulated type K thermocouple	12-13Hz*
$T_{em,r}$	Temperature exhaust manifold, rear	TC 1.5mm mineral insulated type K thermocouple	12-13Hz*
$T_{es}$	Temperature after turbine	TC 1.5mm mineral insulated type K thermocouple	12-13Hz*
$T_{c,b}$	Temperature before compressor	TC 1.5mm mineral insulated type K thermocouple	12-13Hz*
$T_{c,a}$	Temperature after compressor	TC 1.5mm mineral insulated type K thermocouple	12-13Hz*
$n_{tc}$	Turbine rotational speed	PicoTurn PT2G Turbocharger Speed Sensor	500Hz
$u_{wg}$	Wastegate position	Firstmark Controls Series 170 Subminiature Position Transducer	1kHz*
$\dot{m}_c$	Massflow through compressor	ABB FMT500 Thermal Massflow Meter	500Hz
$I_{DC}$	Measured DC current	LEM IT 1000-S High Performance Current Transducer	2kHz
$U_{DC}$	Measured DC voltage	Tektronix P5200 High-voltage Differential Probe	2kHz
$\lambda$	Air-fuel ratio	ETAS636 Lambda module	2kHz
$W_f$	Fuel weight	Kern IFS60K0,5DL Counting scale	6-7Hz*
$n_e$	Engine rotational speed	CAN-signal	50Hz



# Adaptive Control of a Hybrid Powertrain with Map-based ECMS<sup>†</sup>

Martin Sivertsson, Christofer Sundström, and Lars Eriksson

*Vehicular Systems, Department of Electrical Engineering,  
Linköping University, SE-581 83 Linköping, Sweden.*

---

<sup>†</sup>This is a formatted version of “Adaptive Control of a Hybrid Powertrain with Map-based ECMS” by Martin Sivertsson, Christofer Sundström, and Lars Eriksson, IFAC World Congress 2011, Milano, Italy. ©IFAC 2011. Reproduced with the permission of IFAC. The original version was published in [ifac-papersonline.net](http://ifac-papersonline.net), <http://ifac-papersonline.net>, and can be found using the Digital Object Identifier (DOI): 10.3182/20110828-6-IT-1002.02091. The formatting is restricted to changing the article into a single-column format, adjusting sizes of figures and tables, and adjusting the referencing style.

## Abstract

To fully utilize the fuel reduction potential of a hybrid powertrain requires a careful design of the energy management control algorithms. Here a controller is created using map-based equivalent consumption minimization strategy and implemented to function without any knowledge of the future driving mission. The optimal torque distribution is calculated offline and stored in tables. Despite only considering stationary operating conditions and average battery parameters, the result is close to that of deterministic dynamic programming. Effects of making the discretization of the tables sparser are also studied and found to have only minor effects on the fuel consumption. The controller optimizes the torque distribution for the current gear as well as assists the driver by recommending the gear that would give the lowest consumption. Two ways of adapting the control according to the battery state of charge are proposed and investigated. One of the adaptive strategies is experimentally evaluated and found to ensure charge sustenance despite poor initial values.

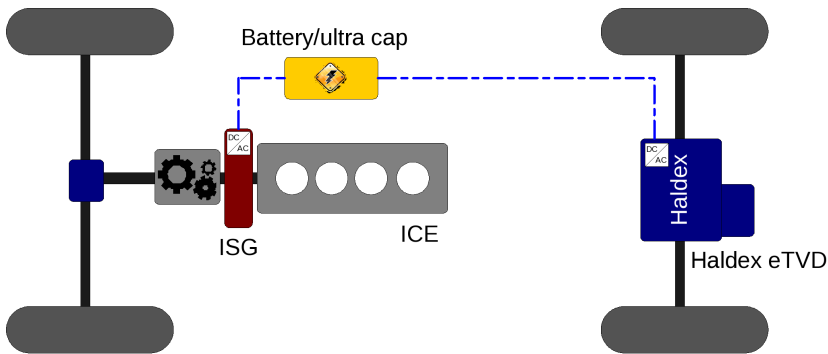


Figure 1: The architecture of the Haldex eTVD concept. The EM is labeled Haldex in the figure. There are two energy paths between the ICE and EM.

## Introduction

A hybrid powertrain utilizes at least two separate energy converters. This has the potential to significantly increase the efficiency of the powertrain. The key to utilizing the full potential of the powertrain lies in the design of the control algorithm. The goal in hybrid powertrain control is normally to minimize the fuel consumption while maintaining the battery State of Charge (SOC) within prescribed limits, sometimes with addition of constraints regarding emissions.

This paper develops an adaptive Equivalent Consumption Minimization Strategy (ECMS), based on [4], and applies it to the Haldex electric Torque Vectoring Drive (eTVD). The optimal torque distribution is calculated offline and stored in tables and the effects of discretization on the fuel consumption is studied. Then two ways of adapting the control to maintain the SOC within the desired limits are investigated.

## The Haldex eTVD and the test vehicle

The system used for modeling, simulation, and experimental evaluation is a SAAB 9-3 XWD with a 2.0L turbo charged spark ignited combustion engine and a six-speed manual gear-box (GB), fitted with the eTVD.

The eTVD is a system designed to combine all-wheel drive (AWD) with hybrid functionality. It also has the ability to control the torque distribution on the rear wheels individually, which is useful to prevent under- and over-steering. In the eTVD concept the combustion engine (ICE) and main electric motor (EM) are connected electrically to each other via the generator (ISG) and mechanically via the wheels, see Fig. 1. The architecture of the system thus resembles that of a split hybrid but since the components in the test vehicle are dimensioned for AWD the series hybrid functionality of the vehicle is reduced. A more fitting description would be advanced parallel hybrid since the powertrain can be viewed as a parallel hybrid with an extra degree of freedom in choosing which energy converter to use during load shifting since the ISG is added to the powertrain.

# 1 Vehicle Model

For the purpose of investigating different control strategies and their fuel consumptions, a quasistatic model approach is used. This is partly due to simplicity but also because it is well suited for both DDP and ECMS. In a backward facing quasistatic approach the speed is known from the driving cycle. When the speed is known the torque required at the wheels to follow the driving cycle is calculated through a longitudinal vehicle model:

$$T_{req} = r_w \left( \underbrace{\frac{\rho_a}{2} C_D A_f V(t)^2}_{F_{air}} + \underbrace{mgf_r}_{F_{roll}} + \underbrace{m\dot{V}(t)}_{F_{acc}} + \underbrace{\dot{V}(t) \frac{J_w}{r_w^2}}_{F_{wi}} \right) \quad (1)$$

where  $F_{air}$  is the aerodynamic drag,  $F_{roll}$  the rolling resistance,  $F_{wi}$  the inertia of the wheels, and  $F_{acc}$  is the acceleration force. Force from road grade is neglected.

## 1.1 Components

The control signals of the system are the energy converter torques  $T_{ICE}$ ,  $T_{ISG}$ ,  $T_{EM}$ , and gear  $\gamma_{GB}$ . The components (ICE, EM, ISG and GB) are all modeled with a power balance and efficiency,  $P_{out} = P_{in}\eta$ , where the efficiencies,  $\eta$ , are assumed to be known and account for all losses in the component. The efficiency  $\eta_{GB}$  is assumed constant while the efficiencies of the energy converters are shown in Fig. 2. The battery is modeled as a Thevenin equivalent circuit with open circuit voltage  $U_{oc}(SOC)$ , coulombic charge efficiency  $\eta_c(SOC)$ , and constant internal resistance  $R_i$ . The battery in the test vehicle outputs its SOC, thus the SOC is assumed to be known. The power required by the auxiliary units,  $P_{aux}$ , is assumed constant. For more details about the modeling see [9].

## 2 Reference Consumptions

As a reference for the implemented optimization, deterministic dynamic programming (DDP) as described in [3] is used. Time and SOC are discretized with a step length of 1s and 0.02% respectively. The SOC discretization is chosen so that one step roughly equals the change in SOC from the auxiliary units during 1s. The operating points from the DDP solution to NEDC are shown in Fig. 2. Interesting to note is the efficient use of the ISG in load shift and that almost all the EMs operating points during braking are on, or close, to the torque limit. This is a result of the EM and ISG primarily being designed for torque vectoring and AWD and not fuel economy.

To evaluate the performance of the real-time control, the consumption as a strictly AWD vehicle is used. For that purpose a control is used where the gear that results in the lowest consumption at each time is engaged. The EM is assumed to be unused both in traction and braking, thus this mode corresponds to pure ICE propulsion.

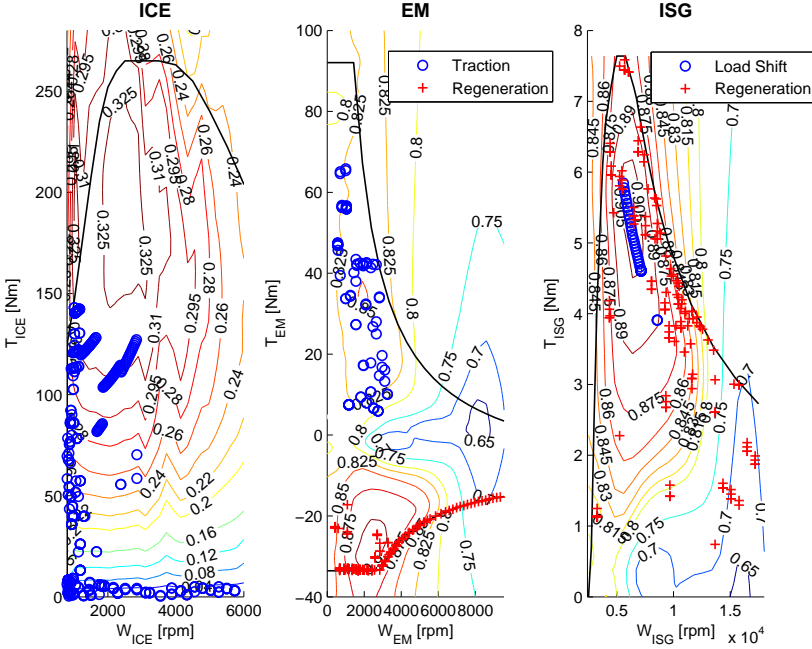


Figure 2: Efficiencies of the ICE, EM, and ISG, as well as the operating points of the three energy converters on the NEDC from the DDP solution

### 3 The ECMS

In ECMS, proposed in [5] and [6], the sum of fuel and fuel equivalent of the electrical power is minimized. Since fuel and battery power are not directly comparable an equivalence factor,  $\lambda$ , is used. The function to be minimized can be written as:

$$H = P_f(T_{ICE}, \gamma_{GB}) + \lambda(t)P_{batt}(T_{EM}, T_{ISG}, \gamma_{GB}) \quad (2)$$

Under the assumption that the battery efficiency is independent of SOC, the equivalence factor  $\lambda$  remains approximately constant along the optimal trajectory. Therefore the optimization problem is reduced to finding the constant  $\lambda$  that approximates the optimal trajectory of a given driving cycle. Since the characteristics of the battery depends on if the battery is charging or discharging,  $\lambda$  is sometimes replaced by two constants. It is however shown in [4] that one constant suffices to get a good approximation on a given driving cycle, which is the approach selected here. For more details on ECMS see [3, 7, 8].

As a consequence of the discussion above the strategy for selecting the control inputs becomes:

$$[T_{ICE}, T_{ISG}, T_{EM}, \gamma_{GB}] = argmin(H) \quad (3)$$

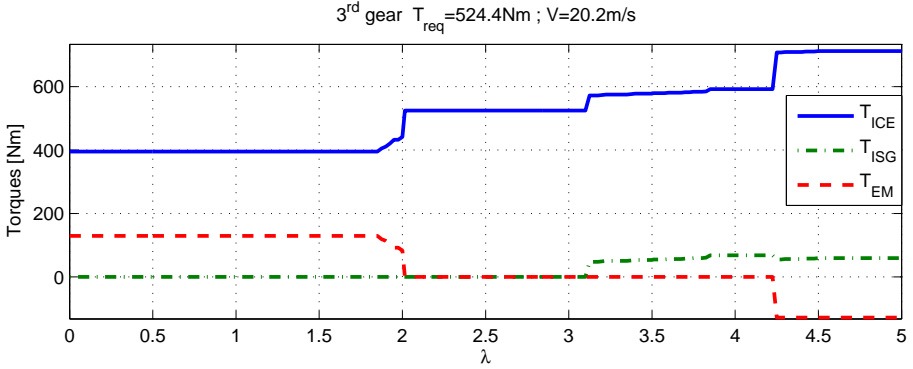


Figure 3: The optimal torques on the energy converters as a function of  $\lambda$  for a specific vehicle speed and required torque. All torques are calculated at the wheels.

Subject to:

$$T_{req} = \eta_{GB}\gamma_{GB} (T_{ICE} - \gamma_{ISG}T_{ISG}) + \gamma_{EM}T_{EM} \quad (4a)$$

$$T_{EM,min}(\omega_{EM}) \leq T_{EM} \leq T_{EM,max}(\omega_{EM}) \quad (4b)$$

$$0 \leq T_{ICE} \leq T_{ICE,max}(\omega_{ICE}) \quad (4c)$$

$$0 \leq T_{ISG} \leq T_{ISG,max}(\omega_{ISG}) \quad (4d)$$

$$P_{batt,min}(SOC) \leq P_{batt} \leq P_{batt,max}(SOC) \quad (4e)$$

### 3.1 Offline Optimization

Instead of solving the computationally demanding three degree of freedom problem in (3)-(4) for all possible controls in real-time, the optimization is performed offline and the result is tabulated. In the real-time implementation the control system interpolates in the stored data to find the optimal torque distribution.

In the offline calculations the three parameters that the ECMS algorithm takes as input, i.e. vehicle speed, required torque, and equivalence factor, are discretized and the optimal torque distribution on the three energy converters, as well as the optimal gear, are calculated as a function of  $(V, T_{req}, \lambda)$  for each point. Since, for each gear, it is a two degree of freedom problem, see (4a), it requires two tables for each gear, one for the ISG and one for the ICE. From these two tables the torque required from the EM can be calculated using (4a). With six gears, not including reverse, a total of 13 tables are calculated: six ICE, six ISG and one for the gear selection. So the system not only optimizes the torque distribution for the current gear, it also assists the driver by recommending the gear that would give the lowest fuel consumption.

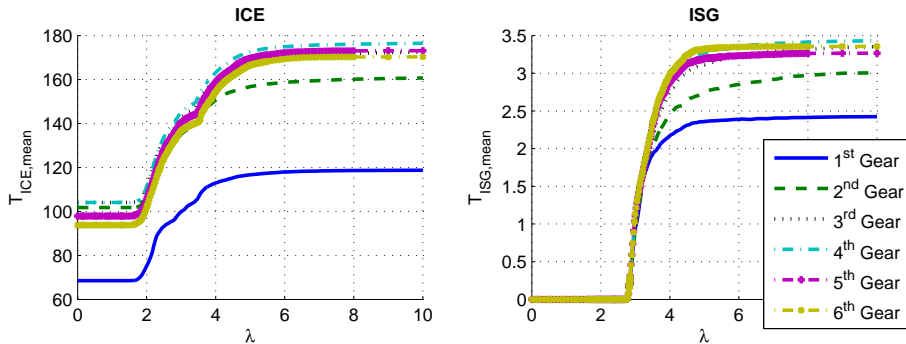


Figure 4: The mean torque in each table changes as a function of  $\lambda$ .

### 3.2 Table Discretization

The real-time algorithm uses linear interpolation in the stored data and the assumption is thus that the solution is linear between two optima. As seen in Fig. 3 the solution is only piecewise linear between two  $\lambda$  so the discretization has to be chosen with care. Fig. 4 shows how the mean torque in each table changes as a function of  $\lambda$ . Since it is desirable to reduce the memory requirements the idea is to make the  $\lambda$  discretization sparser in the segments that could be considered linear and denser where it is clearly non-linear. From Fig. 4 it is clear that the ISG and ICE tables should have separate  $\lambda$  discretizations since the ISG tables remain constant up until  $\lambda \approx 3$  while the ICE tables only remain constant until  $\lambda \approx 2$ . To test how the loss of accuracy, introduced by reducing the size of the tables, affects the consumption, simulations are carried out on two sets of tables: one large set,  $\mathcal{T}_L$ , and one small set,  $\mathcal{T}_S$ . The  $\mathcal{T}_L$  has the same V- and  $T_{req}$ -discretization as the offline optimization itself, but the  $\lambda$ -discretization is made sparser according to the strategy mentioned above. The  $\mathcal{T}_S$ -discretization is made sparser than  $\mathcal{T}_L$  in all three directions. The memory requirement of  $\mathcal{T}_S$  is roughly one eighth of that of  $\mathcal{T}_L$ .

## 4 Real-time Implementation Details

In the implementation the ECMS is only used in traction. During braking the main parameter that affects the ability to recuperate energy is the gear. However the time spent in braking is deemed too short to motivate a gear shift. Instead a heuristic brake control is used. Provided that the SOC is within limits the EM supplies the requested brake torque and if the EM is insufficient, the ISG, providing that a gear is engaged, also provides a regenerative torque and the rest is handled by the friction brakes.

Since the test vehicle has a manual gearbox the gear selector recommends gears to the driver. In simulation the system follows the gear selector and shifts instantaneously without the use of a clutch. To avoid too frequent gear shifts (recommendation changes) a hysteresis is applied to the interpolated optimal

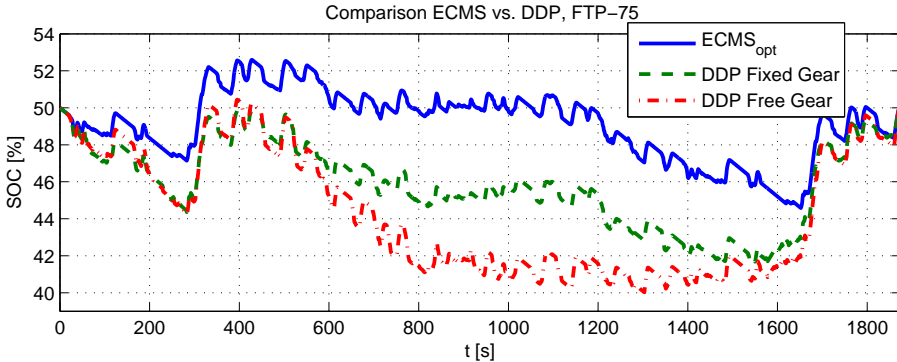


Figure 5: The optimal SOC trajectory on the FTP-75 cycle with ECMS and DDP. The offline optimization results in a different SOC trajectory than DDP, mainly due to the nominal battery parameters used.

gear.

## 5 Equivalence Factor Considerations

An equivalence factor  $\lambda$  is considered optimal if the resulting  $\Delta SOC = SOC(t_{end}) - SOC(t_{start}) = 0$  within a specified tolerance. Since the speed in the driving cycles is discretized, the situation can arise where there exists no  $\lambda$  that results in  $\Delta SOC = 0$ . In those situations the method suggested in [2] is used, where the control switches between two  $\lambda$ ,  $\lambda_1$  leading to  $\Delta SOC > 0$  and  $\lambda_2$  leading to  $\Delta SOC < 0$ , at time  $t$  to achieve  $\Delta SOC = 0$ .

To evaluate the offline optimization a set of tables,  $ECMS_{opt}$ , consisting of  $\lambda_{opt}$  for the NEDC and FTP-75 cycles is created. That is, no interpolation between two optima in the  $\lambda$ -direction is necessary. In Fig. 5 the SOC trajectories of  $ECMS_{opt}$  as well as DDP on the FTP-75 cycle is shown. Since the gear shifting of the DDP solution is highly unrealistic, a DDP Fixed Gear solution using the gear trajectory of  $ECMS_{opt}$  is also shown. The  $ECMS_{opt}$  SOC trajectory still differs from the two DDP solutions. This is due to the offline optimization using only stationary operating points and average battery parameters. However, introducing SOC-dependency in the offline optimization would mean adding an extra dimension in each table and the decrease in consumption using DDP compared to  $ECMS_{opt}$  is small, especially if a more realistic gear shifting strategy is used, as shown in Table 1. Results from simulations on the NEDC and FTP-75 driving cycles are shown in Table 2. The increase in consumption for  $\mathcal{T}_S$  and  $\mathcal{T}_L$  compared to  $ECMS_{opt}$ , as well as the difference in  $\lambda_{opt}$  values, confirm that the solution is not a linear function of  $\lambda$ . However, the increase in consumption is small, only 0.1% from making the  $\lambda$ -dimension sparser and 0.2 – 0.4% when the tables are made sparser in all three dimensions.

Even if the simulations show that the implemented ECMS produce a good result on a given driving cycle, close to that of DDP, it is also seen that the

Table 1: The decrease in fuel consumption with DDP compared to  $ECMS_{opt}$ .

	DDP: Free Gear	DDP: Fixed Gear
<b>NEDC</b>	4.0%	0.2%
<b>FTP-75</b>	10.1%	2.3%

Table 2:  $\lambda_{opt}$  and associated consumption of the different tables. Consumptions are in L/100km and Reduction is compared to AWD.

Cycle	Performance	$EMCS_{opt}$	$\mathcal{T}_L$	$\mathcal{T}_S$
<b>NEDC</b>	$\lambda_{opt}$	2.8384	2.8238	2.8426
	<b>Consumption</b>	5.728	5.733	5.738
	<b>Reduction</b>	17.23 %	17.15 %	17.08 %
<b>FTP-75</b>	$\lambda_{opt}$	2.6353	2.6615	2.7146
	<b>Consumption</b>	5.505	5.512	5.534
	<b>Reduction</b>	24.33 %	24.23 %	23.93 %

optimal values of  $\lambda$  are specific and the system seems to be quite sensitive. A  $\lambda_{opt}$  from one driving cycle is not necessarily charge sustaining on another, see Fig. 6. The controller has to adapt to the driving scenario.

## 5.1 Static Prediction Based on SOC

In [1] it is suggested that  $\lambda_{opt}$  is approximated by an affine function in SOC. Since the eTVD mainly is an AWD concept, the charge sustenance of the controller is crucial. Therefore another adaptation function is suggested. Under the assumption that there exists one  $\lambda$  that approximates a given driving cycle, the controller should ideally find that  $\lambda$  for the future driving mission and use that value for the entire mission. To allow the system to use as much of the battery capacity as possible the idea is to create a function that is relatively flat around the center of the desired SOC window. However, when the SOC approaches the limits of the SOC window it needs to adapt to ensure charge sustenance. The chosen function that fulfills these requirements is a tangens function, see Fig. 7-left. The adaptation of  $\lambda$  is of the form:

$$\lambda = f_{SP}(\lambda_c, k_c, SOC) \quad (5)$$

where  $f_{SP}$  has the shape of a tangens function centered at  $\lambda_c$ , with the slope  $k_c$ . As seen in Fig. 7-right the fuel consumption increases with the slope but it is also apparent that the ability of the system to keep the SOC within the desired SOC window, increases with the slope, since a change in SOC results in a larger change in  $\lambda$ . However, since there is no way of knowing the optimal  $\lambda$  for the current driving mission there is no slope that guarantees charge sustenance. The choice is a trade-off between charge sustenance and fuel consumption. Here  $k_c = -1.9$  is chosen. In Fig. 6 the same test as in Section 5 is shown, now with the use of the Static Prediction based on SOC (SP) in (5). With the use of the new adaptation the system is not as sensitive to the initial  $\lambda$ . The system is

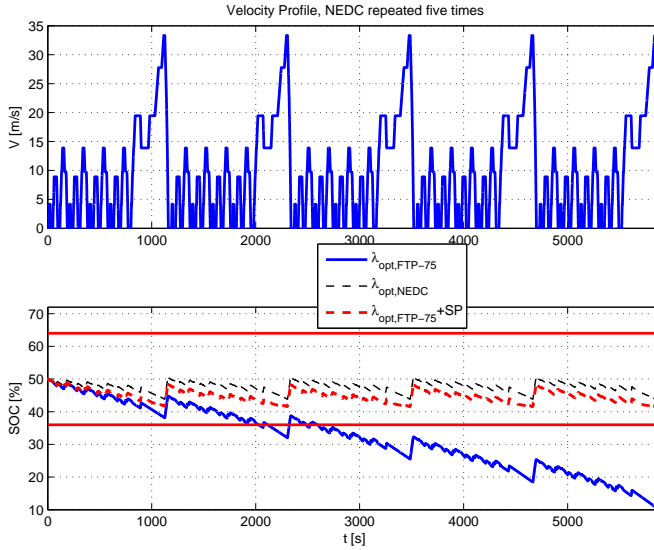


Figure 6: The NEDC cycle repeated five times with  $\lambda_{opt,NEDC}$ ,  $\lambda_{opt,FTP-75}$  and  $\lambda_{opt,FTP-75}$  with the use of Static Prediction based on SOC. The system is sensitive to the equivalence factors. The  $\lambda_{opt}$  for one driving cycle leads to poor performance on another, but with the adaptive control the system is charge sustaining.

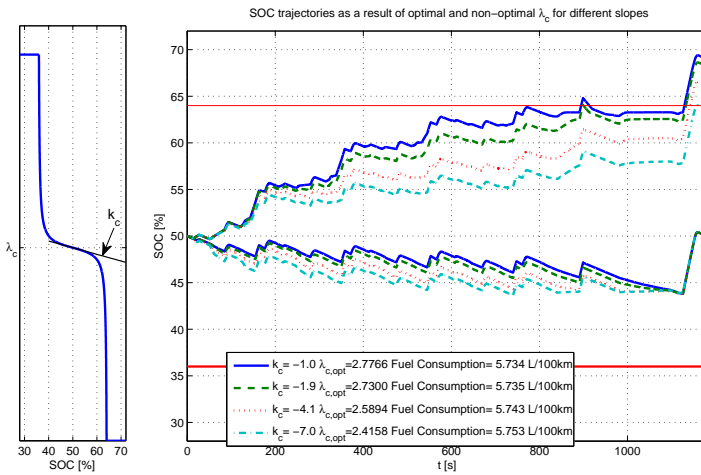


Figure 7: Left: The shape of the function used for adaptive control. Right: SOC trajectories for different slopes on the NEDC cycle with  $\lambda_{c,opt}$  as well as with  $\lambda_c = 4$ . The plot indicates that a steeper slope is more able to keep the SOC within the limits but it also shows that a steep slope alone does not guarantee that the SOC stays within the desired SOC window. A steep slope also increases the consumption.

Table 3:  $\lambda_{c,opt}$  and associated consumptions. Consumptions are in L/100km and reduction is compared to AWD.

Cycle	Performance	$\mathcal{T}_L$	$\mathcal{T}_S$
NEDC	$\lambda_{c,opt}$	2.73	2.7374
	Consumption	5.735	5.739
	Reduction	17.12 %	17.07 %
FTP-75	$\lambda_{c,opt}$	2.6365	2.6823
	Consumption	5.515	5.533
	Reduction	24.19 %	23.95 %

now charge sustaining with  $\lambda_c = \lambda_{opt,FTP-75}$ . However the fuel consumption increases slightly, see Table 3 compared to Table 2. Also interesting to note is that  $\lambda_{c,opt}$ , the  $\lambda_c$  that gives  $\Delta SOC = 0$ , is not the same as the  $\lambda_{opt}$  that approximates the driving cycle.

## 5.2 Adaptive Prediction Based on SOC

The proposed strategy has introduced some adaptivity to the system, but since there is no way of knowing the  $\lambda_c$  that approximates the future driving mission, it is not necessarily enough. The value of  $\lambda_c$  is still important. As seen in Fig. 8 the SOC does not stay within the SOC window when the  $\lambda_c$  value differs too much from  $\lambda_{c,opt}$ . The system instead varies around a SOC value that is not necessarily within the SOC window. The corresponding  $\lambda$  value seems to vary around a value close to the  $\lambda_{c,opt}$  found in Section 5.1. The idea is thus to let the center of the function proposed in Section 5.1 change according to the trend of the  $\lambda$  values. To find the trend a low-pass filter is used according to:

$$\lambda_c^{p+1} = (1 - \alpha)\lambda_c^p + \alpha\lambda^p \quad (6)$$

$$\lambda^{p+1} = f_{SP}(\lambda_c^{p+1}, k_c, SOC) \quad (7)$$

The trade-off is between response time and fuel consumption. If the time constant is small, the system will find the optimal  $\lambda$  region fast, but a fast filter also means that  $\lambda_c$  becomes sensitive to the current  $\lambda$  which increases the fuel consumption. Here  $\alpha$  is chosen so the time constant of the filter is around 200s. To avoid build-up in the low-pass filter, similar to integral wind-up,  $\lambda_c$  is only allowed to move in what can be considered a feasible region, chosen to be between 2 and 6. With the use of the Adaptive Prediction based on SOC (AP) in (6)-(7) the control manages to maintain the SOC within the desired SOC window despite the use of a too high initial  $\lambda_c$ , as seen in Fig. 8.

## 6 Tests

So far the systems have been designed and evaluated using known driving cycles. To investigate how well the systems perform in a more realistic situation the system is tested both on unknown driving cycles as well as in a real vehicle.

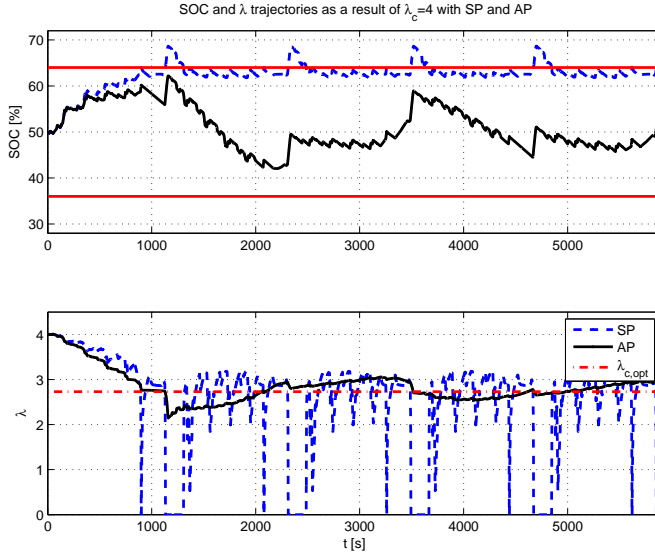


Figure 8: SOC and  $\lambda$  trajectories as a result of  $\lambda_c = 4$ , NEDC repeated 5 times. With static prediction based on SOC the system finds a point on the tangens function, around which it varies, that is not necessarily within the desired SOC window. With adaptive prediction based on SOC the control maintains the SOC within the desired SOC window.

## 6.1 Randomized Driving Cycle

To simulate real driving a driving cycle is constructed out of a random set of driving cycles. The 30 selected driving cycles represent roughly 8 hours of driving and a distance of 350km. On this driving mission the ECMS with both adaptive and static prediction based on SOC is tested with both  $\mathcal{T}_L$  and  $\mathcal{T}_S$  and the result is shown in Fig. 9 and Table 4. Because of the length of the driving mission the fuel equivalent of the deviation in end SOC is deemed negligible. Both the functions proposed for adaptive control are charge sustaining and imply a fuel consumption reduction of 19-20% compared to AWD. AP results in a slightly higher consumption than SP, as well as  $\mathcal{T}_S$  results in a slightly higher consumption than  $\mathcal{T}_L$ .

## 6.2 Vehicle Tests

The system that is chosen to be implemented in the test vehicle is the one with  $\mathcal{T}_S$  and adaptive prediction based on SOC. The set  $\mathcal{T}_S$  is used because of the substantial decrease in memory usage and only slight increase in fuel consumption. Even though it is implied in Section 6.1 that static prediction is charge sustaining under normal driving circumstances the extra robustness of the adaptive prediction is considered desirable. The test drive, see Fig. 10, represents urban driving with many transients and low speed, and is done to

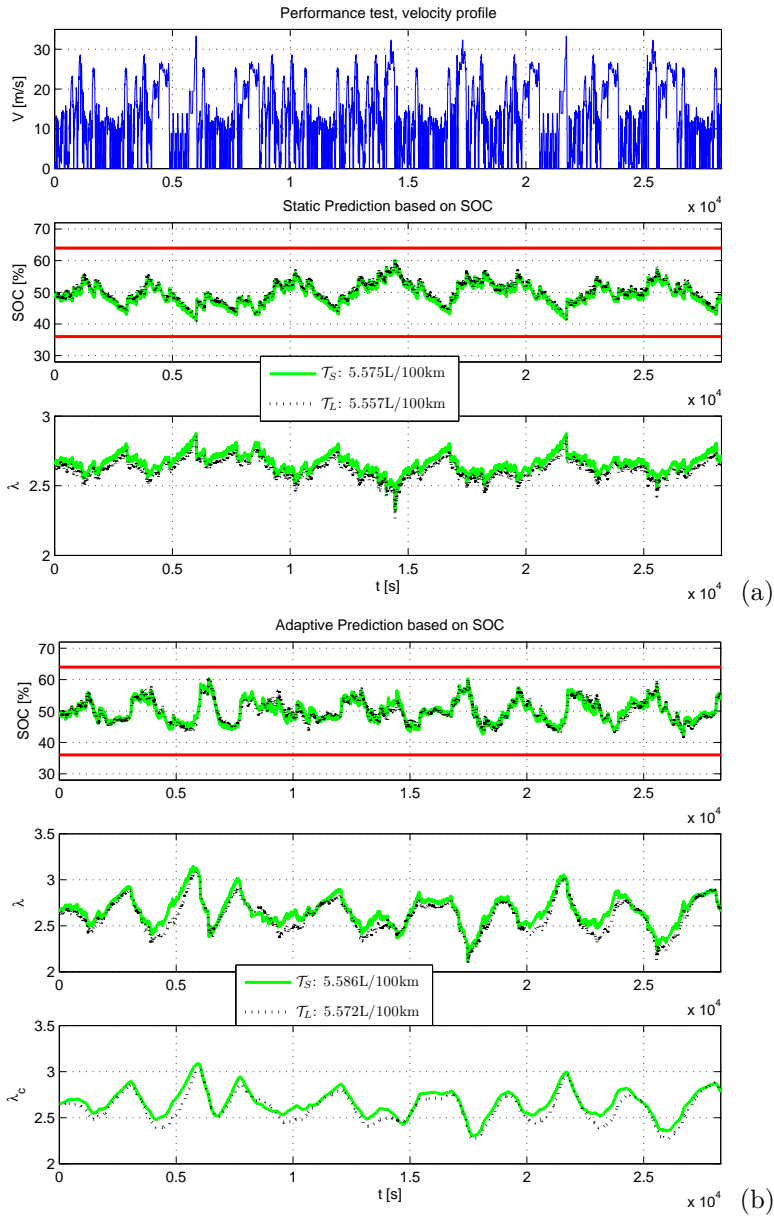


Figure 9: Performance test with (a) SP and (b) AP. Both systems are charge sustaining over the randomized driving mission and the  $\mathcal{T}_S$  result in a slightly higher consumption than the  $\mathcal{T}_L$ .

Table 4: The consumptions for  $\mathcal{T}_L$  and  $\mathcal{T}_S$  with the two different adaptive controllers during a set of randomized driving cycles. Red. is the reduction compared to AWD

Config.	Tables	Consumption	Red.
AWD	-	6.963 L/100km	-
ECMS w. SP	$\mathcal{T}_S$	5.575 L/100km	19.19%
	$\mathcal{T}_L$	5.557 L/100km	20.19%
ECMS w. AP	$\mathcal{T}_S$	5.586 L/100km	19.78%
	$\mathcal{T}_L$	5.572 L/100km	19.98%

test the driveability and the charge sustenance of the control system. The test drive is done with an initial SOC at reference level but a high  $\lambda_c$ . As seen in the figure the control is charge sustaining despite the initially high  $\lambda_c$ . The AP adapts  $\lambda$  and maintains the SOC within the desired SOC window. It is also seen that the gear recommendation often is too high for comfort. For more test data see [9].

## 7 Conclusion

A map-based implementation of ECMS is developed and the effects of the discretization are studied. Performing the optimization offline with stationary operating points and average battery parameters increases the consumption by only a few percent compared to DDP if the same gear trajectory is used. DDP implies a potential to decrease the consumption further by a couple of percent if no restrictions on gear selection is enforced, but the resulting gear trajectory is highly unrealistic, making the solution infeasible.

The effect on the consumption by reducing the size of the tables is small. Making the discretization sparser in the  $\lambda$ -dimension according to the strategy proposed in Section 3.2 only increases the consumption by 0.1% and making all three dimensions sparser only results in an increase of less than 1%.

Both methods suggested for adaptive control are charge sustaining and only result in a slight increase in consumption compared to when  $\lambda_{opt}$  is used. The static prediction based on SOC increases the consumption less than the adaptive prediction based on SOC, but the latter is more robust. The use of static prediction based on SOC reduces the importance of knowing the optimal equivalence factor for the future driving mission, as the control manages to maintain the SOC within the desired window as long as the used  $\lambda_c$  doesn't differ too much from the  $\lambda_{c,opt}$  of the driving mission. With the use of adaptive prediction based on SOC the need for information about the future mission is eliminated. Instead the control adapts so that  $\lambda$  varies around  $\lambda_{opt}$  of the driving mission, ensuring charge sustenance.

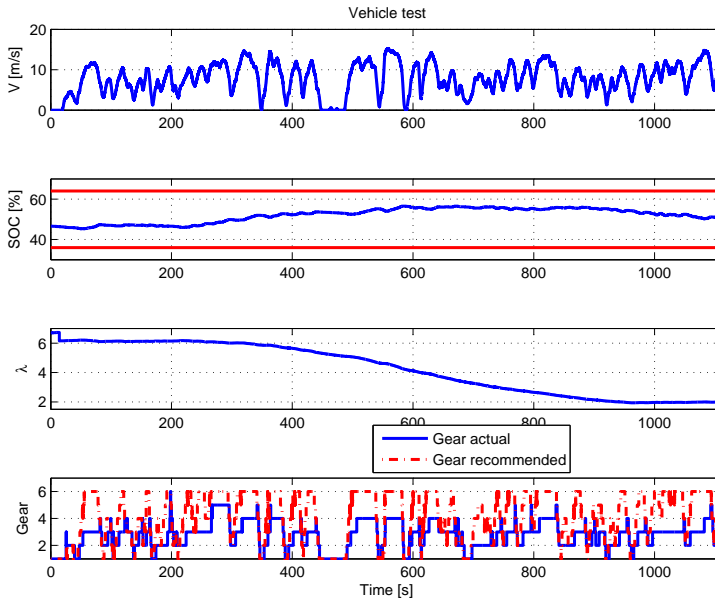


Figure 10: The SOC and control trajectories during the vehicle test. The system is charge sustaining despite a high  $\lambda_c$  but the gear recommendation is often too high for comfort.

## Acknowledgements

The help and support from Haldex Traction AB is gratefully acknowledged.

## References

- [1] D. Ambühl, A. Sciarretta, C. Onder, L. Guzzella, S. Sterzing, K. Mann, D. Kraft, and M. Küsell. A causal operation strategy for hybrid electric vehicles based on optimal control theory. In *IFAC Workshop on Engine and Powertrain Control, Simulation and Modeling*, pages 109–117, 2009.
- [2] A. Chasse, Gh. Hafidi, Ph. Pognant-Gros, and A. Sciarretta. Supervisory control of hybrid powertrains: an experimental benchmark of offline optimization and online energy management. In *IFAC Workshop on Engine and Powertrain Control, Simulation and Modeling*, pages 109–117, 2009.
- [3] L. Guzzella and A. Sciarretta. *Vehicle Propulsion Systems - Introduction to Modeling and Optimization*. Springer-Verlag, 2nd edition, 2007.
- [4] C. Musardo and G. Rizzoni. A-ECMS: An adaptive algorithm for hybrid electric vehicle energy management. In *IEEE Conference on Decision and Control and the European Control Conference*, pages 1816–1823, 2005.

- [5] G. Paganelli, M. Tateno, A. Brahma, G. Rizzoni, and Y. Guezennec. Control development for a hybrid-electric sport-utility vehicle: Strategy, implementation and field test results. In *Proceedings of the American Control Conference*, pages 5064–5069, 2001.
- [6] G. Paganelli, S. Delprat, T.M. Guerra, J. Rimaux, and J.J. Santin. Equivalent consumption minimization strategy for parallel hybrid powertrains. In *IEEE Conference on Vehicular Technology*, pages 2076–2081, 2002.
- [7] P. Pisu and G. Rizzoni. A comparative study of supervisory control strategies for hybrid electric vehicles. *IEEE Transactions on Control Systems Technology*, 15(3):506–518, 2007.
- [8] A. Sciarretta, M. Back, and L. Guzzella. Optimal control of parallel hybrid electric vehicles. *IEEE Transactions on Control Systems Technology*, 12(3): 352–363, 2004.
- [9] M. Sivertsson. Optimization of fuel consumption in a hybrid powertrain. Master's thesis, Linköpings Universitet, SE-581 83 Linköping, 2010.

# A control benchmark on the energy management of a plug-in hybrid electric vehicle<sup>†</sup>

A. Sciarretta<sup>a</sup>, L. Serrao<sup>c</sup>, Dewangan, P. C.<sup>a, e</sup>, P. Tona<sup>a</sup>,  
Bergshoeff, E. N. D.<sup>h</sup>, C. Bordons<sup>i</sup>, L. Charmpa<sup>e</sup>, Ph. Elbert<sup>d</sup>, L.  
Eriksson<sup>f</sup>, T. Hofman<sup>h</sup>, M. Hubacher<sup>h</sup>, P. Isenegger<sup>h</sup>, F. Lacandia<sup>g</sup>,  
A. Laveau<sup>e</sup>, H. Li<sup>e</sup>, D. Marcos<sup>i</sup>, T. Nüesch<sup>d</sup>, S. Onori<sup>g</sup>, P. Pisu<sup>b</sup>, J.  
Rios<sup>b</sup>, E. Silvas<sup>h</sup>, M. Sivertsson<sup>f</sup>, L. Tribioli<sup>g</sup>, A.-J. van der  
Hoeven<sup>h</sup>, and M. Wu<sup>e</sup>

<sup>a</sup>*IFP Energies nouvelles, France*

<sup>b</sup>*Clemson University, United States*

<sup>c</sup>*Dana Corp., Italy*

<sup>d</sup>*ETH Zurich, Switzerland*

<sup>e</sup>*IFP School, France*

<sup>f</sup>*Linköping University, Sweden*

<sup>g</sup>*Ohio State University, United States*

<sup>h</sup>*TU Eindhoven, The Netherland*

<sup>i</sup>*University of Sevilla, Spain*

---

<sup>†</sup>This is a formatted version of “A control benchmark on the energy management of a plug-in hybrid electric vehicle” by A. Sciarretta and L. Serrao and Dewangan, P. C. and P. Tona and Bergshoeff, E. N. D. and C. Bordons and L. Charmpa and Ph. Elbert and L. Eriksson and T. Hofman and M. Hubacher and P. Isenegger and F. Lacandia and A. Laveau and H. Li and D. Marcos and T. Nüesch and S. Onori and P. Pisu and J. Rios and E. Silvas and M. Sivertsson and L. Tribioli and A.-J. van der Hoeven and M. Wu, *Control Engineering Practice*, Volume 29, pages 287-298, ©Elsevier 2014. Reproduced with the permission of Elsevier. The original paper can be found at [sciencedirect.com](http://www.sciencedirect.com) <http://www.sciencedirect.com/>, and can be found using the Digital Object Identifier (DOI):10.1016/j.conengprac.2013.11.020. The formatting is restricted to changing the article into a single-column format, adjusting sizes of figures and tables, and adjusting the referencing style. Corrections are made to Fig. 13-14.

## **Abstract**

A benchmark control problem was developed for a special session of the IFAC Workshop on Engine and Powertrain Control, Simulation and Modeling (E-COSM'12), held in Rueil-Malmaison, France, in October 2012. The online energy management of a plug-in hybrid-electric vehicle was to be developed by the benchmark participants. The simulator, provided by the benchmark organizers, implements a model of the GM Voltec powertrain. Each solution was evaluated according to several metrics, comprising of energy and fuel economy on two driving profiles unknown to the participants, acceleration and braking performance, computational performance. The nine solutions received are analyzed in terms of the control technique adopted (heuristic rule-based energy management vs. equivalent consumption minimization strategies, ECMS), battery discharge strategy (charge depleting–charge sustaining vs. blended mode), ECMS implementation (vector-based vs. map-based), ways to improve the implementation and improve the computational performance. The solution having achieved the best combined score is compared with a global optimal solution calculated off line using the Pontryagin's minimum principle-derived optimization tool HOT.

## Introduction

Energy management of Hybrid Electric Vehicles (HEV) is nowadays a more-than-ten-years-old field of research in control engineering [1, 2, 3, 4, 5, 6, 7, 8, 9, 10]. Indeed, energy management is a control task since it consists in determining the setpoints (mostly, torque) to the various power converters (internal combustion engine, electric machines with their power electronics, mechanical transmission devices, electrical power converters, etc.) that constitute the HEV powertrain. These setpoints are chosen by the energy management strategy (EMS) in order to fulfil the driver's request and at the same time exploit the remaining degrees of freedom to obtain the most suitable powertrain behaviour. "Optimal" EMS that have been disclosed in these years are aimed at minimizing an objective function that typically represents the overall fuel consumption, but might include pollutant emissions, battery life degradation, under several constraints concerning battery charge, drivability, etc. In particular, charge-sustaining or autonomous HEV imply that the battery State Of Charge (SOC) at the end of a vehicle mission is required to be as close as possible to its initial value. A mathematical formulation of such a control problem has been posed in terms of optimal control [11, 12, 13, 14, 15] and numerous practical implementations for various architectures such as parallel [4, 5, 7, 16, 17, 18], series [19, 20], and combined HEV [11, 21, 22, 23] have been presented.

The class of plug-in HEV (PHEV), where the battery can be recharged from an external source (grid) also, has attracted less research than charge-sustaining HEV, although pioneering papers have already treated this topic in terms of optimal control and presented simulation or experimental results [24, 25, 26, 27, 28]. The specific difficulty in this class of EMS is to generate an optimal discharge of the battery. Indeed it is known that a simple CD-CS strategy, i.e., a fully-electrical operation (charge depleting, CD) followed by a Charge-Sustaining (CS) operation from when the battery is discharged onwards, although attractive as it allows presenting the HEV as an "electric vehicle", is far from being optimal from a fuel economy standpoint. Therefore, progressive battery discharge ("blended-mode") operation is expected to be the output of an optimal EMS.

While several EMS have been generally presented in the scientific literature, a way to compare them is obviously not generally available, since studied systems and driving conditions vary from case to case. Clearly, the ability to make direct comparisons between systems, employing these algorithms, would be highly beneficial for the scientific community to verify common claims concerning both performance (optimality) and implementability (flexibility or reusability, easiness of calibration and implementation, etc.) of EMS and focus future efforts in the most promising directions. Such comparison tools have been deployed for other control applications [29] and consist of benchmark control problems that are typically solved using simulation models replacing real systems. As a second step, functional solutions might be benchmarked on physical systems as well. Recently, the Japanese automotive societies JSAE and SICE have jointly proposed a benchmark HEV control problem [30] based on a simulator of a combined hybrid (Prius-like) vehicle and driver and aimed at challenging

academic researchers.

This paper presents a benchmark PHEV control problem and analyzes a set of solutions. The benchmark was developed for a special session of the IFAC Workshop on Engine and Powertrain Control, Simulation and Modeling (E-COSM '12), held in Rueil-Malmaison, France, in October 2012. The participation of nine teams presenting their own solution demonstrated the interest in such initiative. All teams were provided with a fully functional simulator of a PHEV, and were to implement an EMS to optimize a set of criteria. The simulator (see Sect. 1) is of the quasi-static type and accounts for longitudinal vehicle dynamics and battery SOC dynamics, while the engine and electric machines are modeled using stationary maps. Solutions were to be submitted in the form of a Simulink block with a specific format (inputs/outputs/solver). The evaluation of the strategies was done on the basis of the fuel and energy consumption for two realistic driving cycles that were unknown to the participants, as well as acceleration performance and controller runtime performance (details in Sect. 2). In the cycle tests, the battery is completely charged at the beginning of the cycle and can be depleted at the end of the cycle. The participants were able to make use of some approximated information about the cycle, namely the total distance and average speed, which could be easily retrieved from a GPS device. Given the focus of the benchmark problem, this information was included in the simulator as perfectly known, albeit in practice it is affected by measurement uncertainties. A special jury, presided by the holder of the IFP School – Fondation Tuck Chair on Hybrid vehicle and energy management, defined the two test cycles and guaranteed the correct evaluation of the solutions to be benchmarked. The nine solutions evaluated are presented in Sect. 3, while Sect. 4 discusses the results obtained. The software developed for this benchmark will be made available on the web site [www.ecosm12.org](http://www.ecosm12.org).

## 1 Simulator

Although a detailed description of vehicle propulsion systems would require the modeling of several dynamic phenomena, it has long been recognized [31] that for the purpose of fuel economy estimation, quasi-static models, i.e., based on efficiency maps measured under stationary operation of the various components, suffice to a large extent. For such a reason, quasi-static models are largely used to design and pre-assess energy management strategies of HEV, as per the literature cited within the paper. Of course, the mutual relationship between the EMS and typical transient maneuvers would not be represented by such models, but if the main focus is on the fuel economy, they can still reasonably serve to compare the global performance of different EMS. These are also the reasons why the present benchmark PHEV control problem is based on a quasi-static simulator.

The simulator provided implements a model of Chevrolet Volt, validated with published GM data, which are well reflected in the simulation results [32, 33, 35, 34]. The simulator implements three main blocks (Fig. 1): (1) Driving cycle, which computes the torque demand based on the specified driving

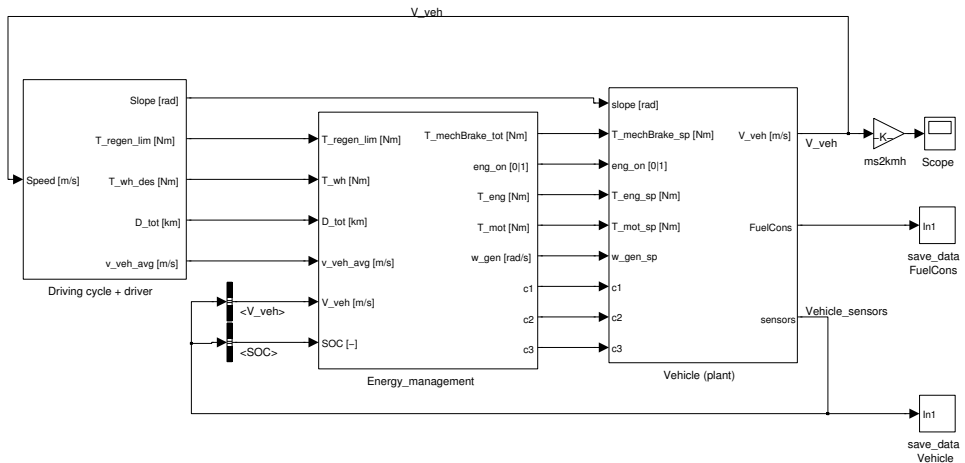


Figure 1: Benchmark simulator layout.

cycle, and also outputs the preview information (nominal distance and average speed); (2) Control strategy (EMS), which was to be filled with the benchmark solutions respecting given input and output ports; (3) Vehicle and powertrain model, which contains the quasi-static model of the powertrain and vehicle dynamics.

The participants had access to the content of the driving cycle and the vehicle model block, but they were not to be modified. Only their respective outputs could be used for developing the EMS, and only the controller block was to be submitted at the end.

## 1.1 Powertrain model: GM Voltec

The powertrain architecture powering the Chevrolet Volt consists of a power-split, planetary-based system, named Voltec and shown in Fig. 2. Three clutches (C1, C2, C3) allow connecting or disconnecting the internal combustion engine (ICE), the generator (GEN) and the main traction machine (MOT). Both electric machines can actually work in both motoring and generating mode, and for both of them the sign convention is that positive torque and positive electric power indicate motoring operation.

The powertrain can operate in the following modes [32, 33, 35]:

1. One-motor EV (C1 locked, C2 open, C3 open, engine off). MOT alone propels the vehicle, powered by the battery. The planetary gear set introduces a fixed reduction between the machine MOT and rest of the driveline (final ratio and differential).
2. Two-motor EV (C1 open, C2 locked, C3 open, engine off). In this case, the machine GEN acts on the planetary ring through C2 and thus it changes the gear ratio between MOT and the powertrain output. This mode is

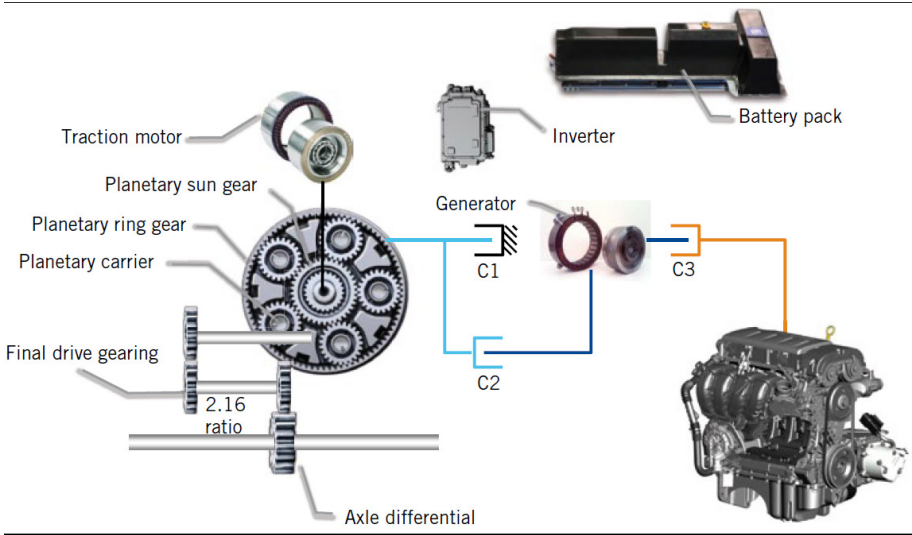


Figure 2: Kinematic architecture of GM's Volt ec [33].

useful to reduce MOT speed at high vehicle speed, thus increasing overall powertrain efficiency by combining the use of both electric machines.

3. Range-extender mode (C1 locked, C2 open, C3 locked, engine on). This is a traditional series-HEV mode: the engine and generator are connected and produce electric power; MOT alone propels the wheels.
4. Power-split mode (C1 open, C2 locked, C3 locked, engine on). In this mode, the three machines are all connected together with a variable speed ratio that depends on the generator speed. The mode allows transmitting mechanical power directly from the engine to the wheels, thus resulting in overall higher efficiency than a pure series mode.

As a whole, the vehicle and powertrain model takes as inputs the outputs of the EMS, i.e., engine torque setpoint  $T_e$  ( $T\_eng\_sp$  in Fig. 1), motor torque setpoint  $T_m$  ( $T\_mot\_sp$ ), generator speed setpoint  $\omega_g$  ( $w\_gen\_sp$ ), brake torque  $T_{br}$  ( $T\_mechBrake\_sp$ ), engine on/off signal ( $eng\_on$ ), and clutch commands C1 to C3 ( $c1, c2, c3$ ). The outputs are vehicle speed  $v$  ( $V\_veh$ ), fuel consumption  $\dot{m}_f$  ( $FuelCons$ ), and the battery SOC  $\xi$  ( $SOC$ ), to be used within the EMS.

## Vehicle Model

The vehicle submodel takes the wheel torque  $T_{wh}$  from the powertrain and the brake torque  $T_{br}$  command as inputs and yields the vehicle speed  $v$  and the wheel speed  $\omega_{wh}$  as output. The submodel implements vehicle's longitudinal dynamics

$$\dot{v} = \frac{r_{wh}}{J_v} [T_{wh} + T_{br} - m_v r_{wh} g \sin \alpha - r_{wh} (c_0 + c_1 v + c_2 v^2)] \quad (1)$$

Table 1: Vehicle parameters

Curb weight $m_v$	1812 kg
Road law coefficient $c_0$	105.95 N
Road law coefficient $c_1$	0.01 N·s·m <sup>-1</sup>
Road law coefficient $c_2$	0.4340 N·s <sup>2</sup> ·m <sup>-2</sup>
Wheel radius $r_{wh}$	33 cm
Vehicle inertia $J_v$	207 kg·m <sup>2</sup>
Wheelbase	2685 mm
Center of gravity height	550 mm
Front/rear static weight distribution	49%/51%

where  $\alpha$  is the road slope and  $J_v$  the vehicle moment of inertia.

The relevant vehicle parameters have been extracted from [33] or estimated from similar vehicles and are listed in Table 1. All simulations are carried out by considering 97 kg in addition to the vehicle mass (75 kg driver and 35 ℓ, i.e., 22 kg full tank of fuel).

### Transmission Model

The transmission consists of a differential gear ( $R_d = 2.16$ ), a planetary gear set (PGS), and a node (unit ratio). The generator is connected to the ring (r), the motor is connected to the sun (s) and the transmission output is the satellite carrier (c) of the PGS. The node connects the engine and the generator.

The forward transmission submodel takes the generator and wheel speeds,  $\omega_g$  and  $\omega_{wh}$ , as well as the engine and motor torques,  $T_e$  and  $T_m$  as inputs, and yields the engine and motor speeds,  $\omega_e$  and  $\omega_m$ , as well as the generator and wheel torques,  $T_g$  and  $T_{wh}$ , as outputs.

The kinematic relation between the speeds of three elements of the planetary gear set is

$$\rho \cdot \omega_r + \omega_s = \omega_c \cdot (\rho + 1), \quad (2)$$

where  $\rho$  is the ratio between the number of teeth of the ring and the sun gear:  $\rho = N_r/N_s = 83/37 = 2.24$ . The torque relations imposed by the planetary gear set are

$$\frac{T_r}{\rho} = \frac{T_c}{\rho + 1} = T_s \quad (3)$$

The connection between PGS elements and power converters depends on the mode in which the powertrain is operated. See Table 2 for mode-dependent correspondances.

The simulator is implemented using these relations, including the gear efficiencies but neglecting the dynamics of the machines and the inertia of the gears.

### Engine Model

The engine submodel takes  $\omega_e$  and  $T_e$  as inputs and yields the fuel consumption  $m_f^*$ . Since a quasi-static modelling approach is used, the engine is represented

Table 2

Mode 1	$\omega_r = 0 \quad \omega_e = 0$ $T_g = 0$
Mode 2	$\omega_r = \omega_g \quad \omega_e = 0$ $T_g = \rho \cdot T_m$
Mode 3	$\omega_r = 0, \quad \omega_e = \omega_g$ $T_g = -T_e$
Mode 4	$\omega_r = \omega_g \quad \omega_e = \omega_g$ $T_g = \rho \cdot T_m - T_e$
All Modes	$\omega_m = \omega_s, \quad \omega_c = R_d \cdot \omega_{wh}$ $T_m = T_s, \quad T_{wh} = R_d \cdot T_c$

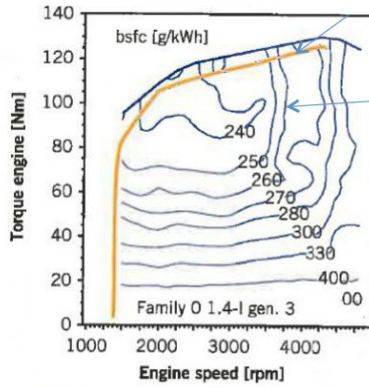


Figure 3: Engine fuel map [33].

by its fuel maps, shown in Fig. 3. Torque and speed limits are enforced. Special treatments are used to represent cranking and idle phases. When the engine is switched on, the model generates a predefined negative torque (-25 Nm) for a short period (1 s), after which the torque generated matches the setpoint.

### Motor and Generator Model

The motor submodel takes the motor torque  $T_m$  and speed  $\omega_m$  as inputs and yields the electric power  $P_m$  as output. Similarly for the generator submodel  $T_g$  and  $\omega_g$  are the inputs and  $P_g$  is the output. The electric machines are represented by their efficiency maps, which are shown in Fig. 4. Torque and power limits are enforced. The generator model also enforces a maximum rate of change of  $\omega_g$  (200 rad/s<sup>2</sup>) to represent machine inertia.

### Battery Model

The battery submodel takes the overall electrical power  $P_b = P_g + P_m$  and the current SOC as input and yields the SOC at next time step as well as the

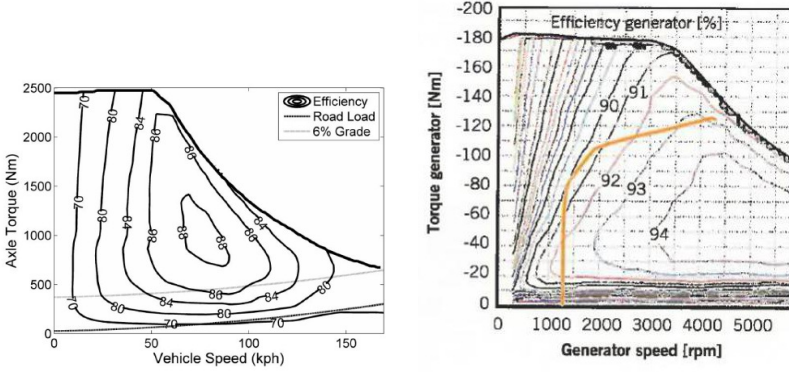


Figure 4: Combined motor-transmission efficiency map (left) [34] and generator efficiency map (right) [33].

Table 3: Battery parameters

parameter	value	source
Total energy capacity	16 kWh	[33]
Total nominal voltage	360 V	[33]
SOC range	65%	[33]
Number of cells in series	96	[35]
Number of strings in parallel	3	[35]
Peak current	400 A	[35]
Peak power (charge)	110 kW	
Peak power (discharge)	-60 kW	

inner or electrochemical battery power  $P_{ech}$ . The model is based on a simple equivalent circuit composed of a voltage source  $V_{oc}$  and a resistance  $R_b$  in series, both functions of the SOC ( $I_b$  is the battery current),

$$P_{ech} = V_{oc}I_b, \quad I_b = \frac{V_{oc}}{2R_b} - \sqrt{\frac{V_{oc}^2 - 4R_bP_b}{4R_b^2}} \quad (4)$$

$$\dot{\xi} = -\frac{I_b}{Q_b} \quad (5)$$

where  $Q_b$  is the charge capacity. Power, current, and voltage limits are enforced. Moreover, SOC operation within a prescribed window is enforced.

In the case of the Volt, only the basic battery parameters, collected in Table 3, are published. For the lack of specific data, the internal resistance and the open circuit voltage characteristic of a single Li-ion cell are assumed to be the same as the experimental data in [36].

## 1.2 Driver model

The driver model is responsible for yielding the powertrain torque request  $T_d$  ( $T_{wh\_des}$  in Fig. 1) to the EMS as a function of the vehicle speed  $v$  ( $V_{veh}$ ) measured from the vehicle model output. For the two cycle tests, the model is a cascade of (i) a feedforward calculation of the torque request as a function of the desired speed  $v$ , and (ii) a PI regulator as a function of the difference between cycle speed and  $v$ . The term (i) is calculated as

$$T_d = \begin{cases} T_{d,tot}, & T_{d,tot} \geq 0, \\ (1 - \sigma)T_{d,tot} - \frac{T_{d,tot}H_{CG}}{m_v g r_{wh} B_w}, & T_{d,tot} < 0 \end{cases} \quad (6)$$

$$T_{d,tot} = \frac{\dot{v}J_v}{r_{wh}} + r_{wh} (c_0 + c_1 v + c_2 v^2 + m_v g \sin \alpha) \quad (7)$$

where the wheel torque request  $T_{d,tot}$  is obtained from the inversion of (1),  $H_{CG}$  is the height of the center of gravity,  $B_w$  the wheelbase, and  $\sigma$  the static weight distribution (see Table 1). The proportional and integral gains of the term (ii) are tuned as  $K_P = 500$  N·s,  $K_I = 1$  N.

For acceleration tests, only the PI regulator is used, with a reference speed set to a very high value in order to enforce full torque demand. The test end is detected as a function of the speed or the distance covered, according to the particular test. Conversely, the braking test is split into two parts, with a first part to reach 100 km/h through a PI regulator, then a second part with constant negative torque request.

## 1.3 EMS

The EMS block to be filled by benchmark participants takes as inputs the driver torque demand  $T_d$  output by the driver's model ( $T_{wh}$  in Fig. 1) and the vehicle speed  $v$  ( $V_{veh}$ ) and the SOC  $\xi$  ( $SOC$ ) yielded by the vehicle and powertrain model. The expected outputs of the EMS model are the engine and motor torque setpoints, the generator speed setpoint, the clutch commands, the engine on/off state, and the mechanical brake torque, all sent to the vehicle and powertrain model.

# 2 Benchmarking

## 2.1 Scoring metrics

Each solution has been evaluated according to several metrics, listed in Table 4. The overall score is obtained by weighting each metric by the factor shown in the table. The weights are intended to be a compromise between energy efficiency (50%) and expectations of manufacturers (20%) and end users (30%). Since they intervene only in the final evaluation stage of the benchmark, they can be easily modified in future versions of the benchmark to reflect a different focus. Although a correlation is expected between energy efficiency sub-metrics, they are accounted for separately in order to emphasize the effects of residual battery

Table 4: Scoring metrics

	Metric	Weight
Performance (30%)	Acceleration 0–100 km/h [s]	7.5%
	Acceleration 70–120 km/h [s]	7.5%
	Acceleration 0–1000 m on 4% slope [s]	7.5%
	Braking distance from 1000 km/h [m]	7.5%
Energy and economy (50%)	Total energy use (fuel+electricity) [MJ]	15%
	Fuel consumption [MJ]	20%
	Tailpipe emissions (not modeled)	0%
	Well-to-wheel CO <sub>2</sub> emissions [kg]	15%
Computational performance (20%)	Processor use [s]	10%
	Memory use [kB]	10%

Table 5: Data for CO<sub>2</sub> emissions

Gasoline well-to-tank emissions [37]	12.5 gCO <sub>2</sub> /MJ of fuel
Gasoline combustion [37]	73.4 gCO <sub>2</sub> /MJ of fuel
Electricity production (emissions for electricity and heat production [38], average 2007–2009)	Europe average: 94.7 gCO <sub>2</sub> /MJ
	France: 24.7 gCO <sub>2</sub> /MJ
	US: 147.5 gCO <sub>2</sub> /MJ
	China: 207.8 gCO <sub>2</sub> /MJ
	World average: 140 gCO <sub>2</sub> /MJ

energy and the CO<sub>2</sub> factor. The actual scoring is obtained by normalizing the result obtained in each metric with respect to the average value for that metric calculated over all valid solutions. Note that all scores are best when minimized.

## Performance

Four performance tests are enforced in the driver’s model, see Sect. 1.2. Elapsed simulation time or distance covered until the simulation stop are monitored and used as metrics.

## Energy and economy

These metrics are the sum of the results in two different driving cycles, based on real-world data, whose length (see Sect. 2.2) exceeds the all-electric range of the vehicle. In each cycle, the initial SOC must match the value given in the data file provided with the simulator, while the final SOC must be at least equal to a target final value. CO<sub>2</sub> emissions were calculated from energy use results as the total emissions from fuel combustion, fuel production (well-to-tank), and electricity production. For electricity, Europe average emissions were to be taken into account (data for France, US, and China were also provided for information). The coefficients in Table 5 were used to compute the CO<sub>2</sub> emissions. Tailpipe emissions were not considered for simplicity (unavailable reliable modeling) and due to their weak dependency on the EMS for warm engine conditions.

Table 6: Cycle statistics. Notes: a) the actual test cycle consists of three repetitions of Aachen urban cascaded by Aachen mixed.

	Aachen urban <sup>a</sup>	Aachen mixed <sup>a</sup>	Arco–Merano
Length [km]	16.2	28.4	157.7
Max speed [km/h]	71.6	132.6	115.4
Average speed [km/h]	30.3	53.8	49.2
Duration [s]	1926	1871	11549
Max acceleration [m/s <sup>2</sup> ]	3.9	4.7	5.7
Max deceleration [m/s <sup>2</sup> ]	3.0	4.6	7.4
No. of vehicle stops	14	11	15
Total stop time [s]	430	185.5	671.5
Total stop time [%]	22	10	6
Altitude variation [m]	0	0	1579

## Computational Performance

Processor use and memory use were monitored on the computer running the simulation. The former was evaluated using MATLAB functions `tic` and `toc` before and after each test, the latter using MATLAB function `sldiagnostics`. Only for fuel economy tests, the actual results are averaged over four runs, in order to reduce the effects of other possible instances running on the test computer. Counting of floating point operations could be used to make these metrics less dependent on the particular machine. However, albeit an option for future versions of the benchmark, this solution has not implemented due to the lack of a simple flop counting function in the most recent versions of MATLAB.

## Solution validity

At all times, all component limitations detailed in the data file (max/min power, torque, state of charge, speed etc.) were to be respected in all components; failure to do so during any simulation invalidated the corresponding results.

## 2.2 Driving cycles

Driving cycles were defined by the benchmark jury as “surprise” cycles, not communicated in advance to the participants. The two real-life cycles selected are shown in Figs. 5–6. The first cycle is actually the combination of two trips recorded in the German city of Aachen, namely, an urban trip spanning 16.2 km and a mixed-drive trip spanning 28.4 km. Elevation has been set to zero for the whole cycle. In order to allow full battery depletion if the HEV would be operated in EV modes, the combined Aachen cycle is repeated three times.

The second cycle is a trip recorded between Arco and Merano, Italy (in the Alps), spanning 157.7 km and including severe altitude variations that are visible in Fig. 6.

A summary of cycle statistics is listed in Table 6.

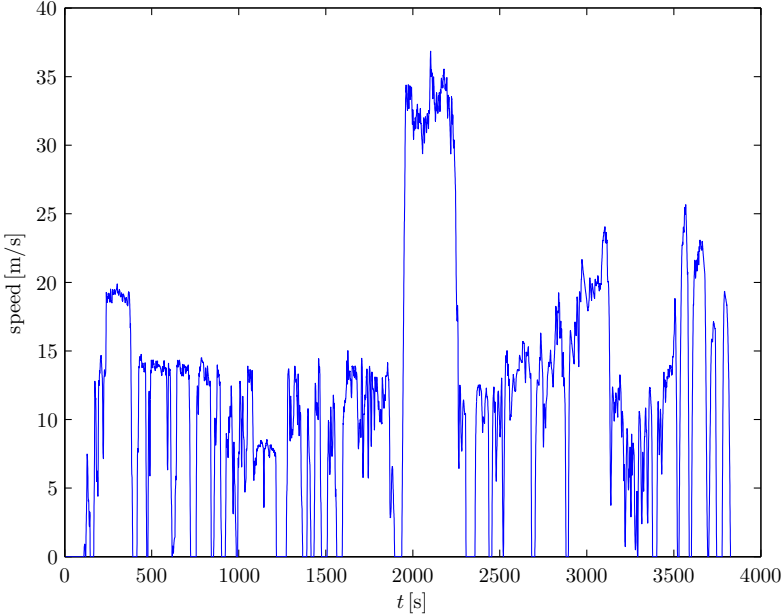


Figure 5: Aachen cycle.

## 3 Proposed Solutions

### 3.1 Introduction

The benchmark control problem can be summarized as to find a control policy  $u(t)$  for  $t = 0, \dots, T$  where  $T$  is any test duration, in such a way to minimize the score defined in Sect. 2. For each single metrics, this is equivalent to minimize a cost function  $J(u)$ , where the control vector  $u \triangleq \{T_e, T_m, \omega_g, C_1, C_2, C_3, B_e, T_{br}\}$  defines the powertrain mode and the operating point of each component. In the example of the total energy use metrics,

$$J = LHV \cdot \int_0^T \dot{m}_f^*(u, w) dt + \int_0^T P_{ech}(u, w) dt \quad (8)$$

where the disturbance vector  $w(t) \triangleq \{v(t), T_d(t)\}$  comprises the exogenous inputs (not known in advance) and  $LHV$  is the lower heating value of the fuel. The minimization (8) is subject to the SOC constraint,  $\xi(T) \geq \xi_{min}$ , and other constraints. Formulated as such, the benchmark control problem is formally equivalent to a constrained optimal control problem.

Data published by GM [33] show that, in the Volt embodied strategy, mode selection depends primarily on SOC status. For charge-depleting (CD) operation (high SOC), modes 1 or 2 are selected according to vehicle speed and required torque, see Fig. 7. When the SOC becomes low, charge-sustaining operation (CS) is activated, which consists of three modes 1, 3, and 4, again selected as a function of vehicles speed and desired torque. This SOC-regulating policy

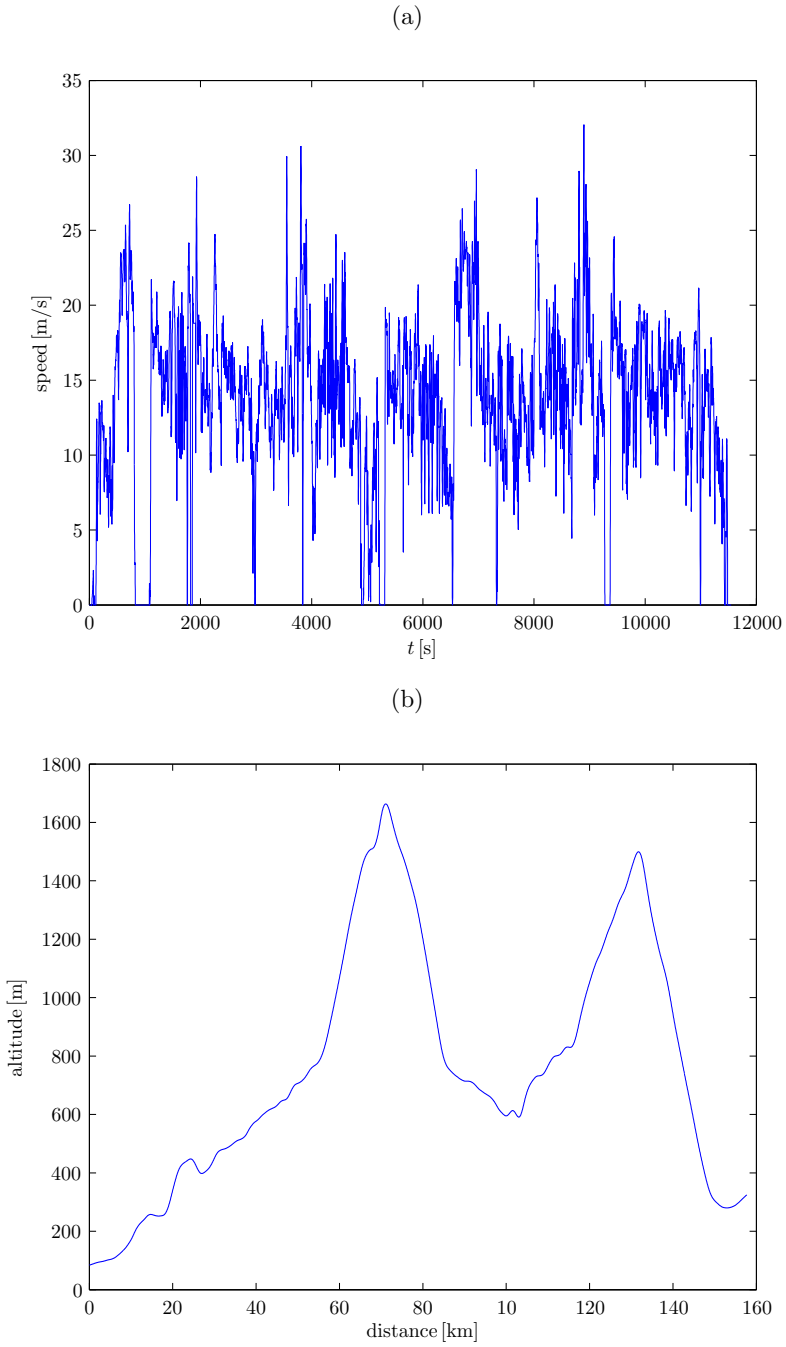


Figure 6: Arco to Merano cycle, (a) speed profile, (b) altitude profile.

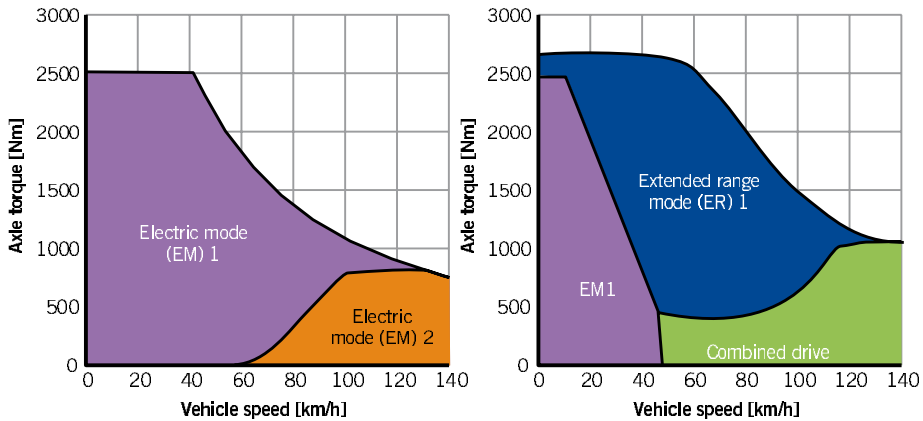


Figure 7: Operating modes of GM's Volt as a function of vehicle speed and desired torque [33].

depends on the fact that the Volt is classified as a range-extended electric vehicle. In the benchmark control problem, participants were allowed to activate a "blended-mode" (BM) strategy to regulate the SOC, i.e., to start the engine before the SOC reaches a lower-end value. Of course, battery-recharge (BR) operation aimed at restoring the battery charge to a certain value was possible as well.

Nine control solutions were submitted to the benchmark problem. Table 7 summarizes the approaches implemented in the proposed solutions. The column "EMS technique" classifies the entries according to the type of control design. Two approaches are represented, namely, based on rules (heuristic) or based on optimal control theory and particularly on the Pontryagin Minimum Principle (PMP). Additionally, the table classifies the nine solution according to the discharge strategy, the mode selection strategy, and the operating point selection strategy.

All the used techniques are further illustrated below. More details on two solutions are provided in the ECOSM'12 papers [39, 40].

### 3.2 Heuristic controllers

Heuristic EMS are based on intuitive rules and correlations involving various vehicular variables. One guiding principle is to use the engine when its efficiency can be relatively high, while in less favorable conditions the electric modes should be given preference and the engine should be turned off. Moreover, when the engine is on, it should be operated in the highest possible efficiency regions (i.e., at high loads). Two common approaches to implement these intuitive principles are the map-based and the rule-based approach. In the map-based approach, the output setpoints are stored in multi-dimensional maps whose entries are measured quantities describing the state of the powertrain. In the rule-based approach, the EMS is either coded as a set of logic rules or implemented as a finite state machine (FSM).

Table 7: List of solutions to the PHEV control benchmark. Notes: a) with 10% driving distance underestimation; b) enhanced with exception rules; c) adaptive ECMS with varying SOC reference

Solution	EMS technique	Discharge strategy	Mode selection	Operating point selection
S1	ECMS	BM <sup>a,c</sup>	Map based	Map based
S2	Heuristic	CD-CS	Map based <sup>b</sup>	Map based
S3	ECMS	BM <sup>c</sup>	Vector based	Vector based
S4	Heuristic	BM	Rule based	Rule based
S5	Heuristic	BM	Rule based	Rule based
S6	Heuristic	BM	Rule based	Map based
S7	ECMS	BM <sup>c</sup>	Vector based	Vector based
S8	ECMS	BM <sup>c</sup>	Vector based	Vector based
S9	Mixed	?	Rule based	Rule based

In most solutions (S2, S4, S6, and S9), a two-level architecture is implemented. A high-level supervisor (see Fig. 8a) first selects the powertrain mode and the engine power setpoint  $P_e$ . The former output is either mapped (S2) as a function of  $v$ ,  $T_t$ , and  $\xi$  and enhanced with exception rules, or calculated by a finite-state machine (S4, S9) with transition rules as a function of the same vehicular quantities. Engine power is calculated from rules as a function of the same variables and of the distance  $D_t$ , either in order to implement a CD-CS SOC-regulation strategy (S2) or a blended-mode strategy (S4) by minimizing a performance criterion.

The cascaded low-level controller evaluates the engine, motor, and generator setpoints, as well as the clutch commands, according to the mode selected and the engine power. While for mode 1 there is no degree of freedom, other modes require additional choices. Optimal operating point map of the engine is used to calculate  $T_e$  and  $\omega_e$  as a function of  $P_e$ , while the other setpoints are such to fulfill transmission kinematics/dynamics. In S9 (a mixed-approach strategy) this task is performed using ECMS (see Sect. 3.3) for mode 4.

An alternative control architecture (used in S6, Fig. 8b) is such that the high-level supervisor selects CD operation or BR operation as a function of  $\xi$ ,  $T_t$ ,  $v$  and the information on the distance-to-go. In the case of CD operation, the low-level controller selects mode 1 or mode 2 by minimizing the electric consumption and determines electric setpoints. In the case of BR operation, the low-level controller operates the engine either to maximize the recharge efficiency or the recharge power and selects accordingly the setpoints using predefined maps.

A simpler approach (used in S5) switches between electric modes and engine modes as a function of the difference between  $\xi$  and a reference SOC profile based on the distance-to-go. If on, the engine is operated at its best-efficiency point and mode 4 is actuated, with exceptions possibly shifting the engine operating point or enforcing mode 3.

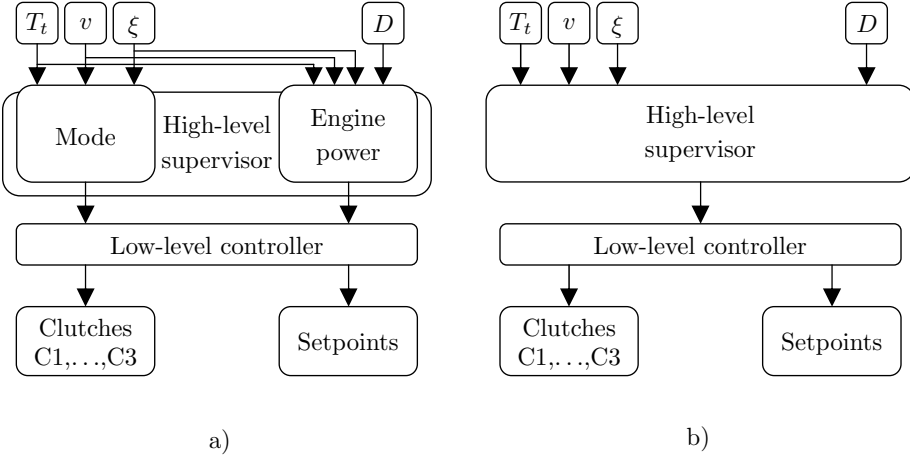


Figure 8: General heuristic strategy flowchart (a) and variant (b).

### 3.3 ECMS

The second approach used in the proposed solution is that based on optimal control. Since early 2000's it has been shown that the control problem of minimizing the fuel consumption of a HEV over a driving mission, while letting its SOC tend to a target value  $\xi_{ref}$  can be formulated as an optimal control problem similar to (8). Offline solutions to such a problem, that is, solutions that make use of the prior knowledge of the driving profile can be calculated using dynamic programming or directly solving the Euler-Lagrange formulation of optimal control. In the latter case, the optimal control policy is found as

$$u^o(t) = \arg \min_u H(u, w(t), \xi(t)) = \arg \min_u LHV \cdot \overset{*}{m}_f(u, w(t)) + \lambda(t) \frac{d\xi(t)}{dt} \quad (9)$$

under the state and costate dynamics

$$\frac{d\xi(t)}{dt} = -\frac{I_b(u, w, \xi)}{Q_b}, \quad \frac{d\lambda(t)}{dt} = -\frac{\partial H(u, w, \xi)}{\partial \xi}. \quad (10)$$

Under the approximation  $\partial V_{oc}/\partial \xi \approx 0$ ,  $\partial R_b/\partial \xi \approx 0$ ,  $\lambda$  is a constant and the strategy (9) reduces to offline technique commonly known as Equivalent Consumption Minimization Strategy (ECMS)

$$u^o(t) = \arg \min_u LHV \cdot \overset{*}{m}_f(u, w(t)) + s^o P_{ech}(u, w(t)) \quad (11)$$

with the equivalence factor defined as  $s^o = -\lambda/(V_{oc}Q_b)$ . The value  $s^o$  fulfills the global constraint on SOC, i.e.,  $\xi(T) = \xi_{ref}$ .

#### Costate adaptation

While in offline ECMS  $s^o$  can be calculated using iterative root-finding algorithms, in online application it has to be continuously adapted and thus a variable  $s(t)$

replaces  $s^o$  in (11). The most common approach for such adaptation, which proves to be directly related to Hamilton-Jacobi-Bellman optimal feedback control [12], is a feedback on current SOC:

$$s(t) = s_0 - k_p(\xi(t) - \xi_{ref}) - \dots, \quad (12)$$

where the ellipsis indicates possible integral or nonlinear terms.

All solutions (S1, S3, S7, S8, and S9 when ECMS is used) include in the right-hand side of (12) a term proportional to the integral of the error  $\xi(t) - \xi_{ref}$ . However, S8 uses a modified coding where  $s$  is initialized to a value  $s_0$ , updated according to a space-depending version of (12) when a prefixed sampling distance is covered, and reset to  $s_0$  at each time the reference SOC is tracked back [41]. A nonlinear term in the form of a tangent-like function of the error is added to the proportional-integral terms in S1 [40]. The feedforward term  $s_0$  is variously calculated as a function of the average speed and the distance (S1, S8), the average speed only (S3), or it is constant (S7).

While  $\xi_{ref}$  clearly equals the initial value of SOC,  $\xi(0)$ , for CS operation, plug-in hybrids allow for discharging the battery and thus a different definition for  $\xi_{ref}$  must be used. Recent literature has addressed this problem and the most common strategy is to use a varying, i.e., decreasing  $\xi_{ref}(t)$  aimed at implementing a BM operation. The decrease of  $\xi_{ref}$  should represent the advance in the mission and toward its end,  $\xi_{ref}(T)$  should tend to  $\xi_{min}$ . All five solutions (S1, S3, S7, S8, and S9) adopt a linear variation of  $\xi_{ref}$  with the distance covered  $D(t)$ , namely,

$$\xi_{ref}(t) = \xi(0) - k_\xi \frac{D(t)}{D_{tot}}, \quad k_\xi = \xi(0) - \xi_{min}. \quad (13)$$

This approach clearly require the prior estimation of the distance to be covered  $D_{tot}$ .

### ECMS Implementation

The vectorial implementation of strategy (11), used in S3, S6, and S8, requires discretizing the field of admissible values  $u(t) \in \{u_q(t)\}$ ,  $q = 1, \dots, N$  at any time step. Thus,

$$\begin{aligned} u^o(t) &= u_{q^o(t)}(t), \quad \text{where} \\ q^o(t) &= \arg \min_q H_q(t), \quad \text{and} \end{aligned} \quad (14)$$

$$H_q(t) = LHV \cdot \overset{*}{m}_f(u_q(t), w(t)) + s(t) \cdot P_{ech}(u_q(t), w(t)).$$

The vector size  $N$  and the nature of  $u$  varies from solution to solution. For each  $q$ ,  $u_q$  is obtained by imposing a set of predefined values to independent components of  $u$  (degrees of freedom, DoF) and calculating the dependent components through kinematic and other physical constraints. The powertrain mode is clearly a DoF itself, thus  $N = \sum_{i=1}^4 N_i$ . In mode 1 there is no additional degree of freedom and thus  $N_1 = 1$ . In mode 2 there is one speed DoF (either  $\omega_m$  or  $\omega_g$ ). In mode 3 the DoF is engine power  $P_e$  since engine speed and torque

are obtained by maximizing the engine–generator efficiency for a given power. In mode 4 there are one speed and one torque independent DoFs. As an example, S8 uses  $N_{\{2,3,4\}} = 21$ .

From (14), it is clear that  $q^o(t)$  and thus  $u^o(t)$  depend only on  $w(t)$  and  $s(t)$ . Since  $w(t)$  is a two-dimensional vector (speed and torque at the wheels), the energy management output is completely determined by three variables. While the dependency of the Hamiltonians  $H_q(t)$  on SOC is neglected in the ECMS,  $s(t)$  does depend on  $\xi(t)$ , as well as on the distance  $D(t)$ . This fact suggests decoupling the evaluation of the energy management output in a two-step process, where first  $s(t)$  is evaluated using (12) and subsequently  $u^o(t)$  is evaluated as

$$u^o(t) = F_U(w(t), s(t)) \quad (15)$$

where  $F_U(w, s)$  is a look-up table where the offline-calculated results of (14) are stored. The advantage of this map-based implementation, used in S1, in terms of computing time with respect to the vectorial implementation, i.e., the online solution of (14) is evident. Moreover, the map-based implementation can be generated off line using a much finer discretization (i.e., a much higher  $N$ ) than its vectorial counterpart. S1 uses a total of 7 maps [40].

### 3.4 Implementation issues

Since CPU use and memory use are among the scoring metrics, all solutions pay a particular attention in trying to reduce them.

Concerning the heuristic solutions, implementation of rules reduces memory use, while use of maps reduces CPU time consumption. Other techniques adopted include:

- simplification of look-up tables (S2),
- disabling of inactive Simulink subsystems, triggered subfunctions (S1, S2, S6),
- only native Simulink blocks without maps (S5),
- reduction of complexity for modes 2 and 3 (S9).

Concerning ECMS-based solutions, vector-based implementation reduces memory use while map-based implementation reduces CPU time consumption. Other techniques adopted include:

- iterative sparsification of maps (S1),
- use of Matlab S–functions (S3),
- setpoint candidate reduction (S3),
- use of vector merging instead of multi-dimensional matrices for setpoint candidates (S7).

Table 8: Benchmark results. Fuel A: cycle Arco–Merano; Fuel B: cycle Aachen; Notes: a) test disqualified due to constraints not met, result set to maximum valid if lower; b) test invalid, cycle not entirely driven; c) entry or test not considered for average calculation.

Solution	Fuel A L/hkm	Fuel B L/hkm	Memory kB	Proc. time 100 = Avg.	Score
S1	2.86	1.83	153	16	0.836
S2	3.18	2.27	81	14	0.850
S3	3.56	1.86	24	84	0.877
S4	3.39	2.57	159	18	0.934
S5	3.66 <sup>a,c</sup>	4.60 <sup>a,c</sup>	36	13	0.993
S6	3.66	4.60	186	18	1.086
S7	3.05	1.88	298	197	1.119
S8	6.06 <sup>a,c</sup>	4.99 <sup>a,c</sup>	353	442	1.873
S9 <sup>c</sup>	NA <sup>b</sup>	8.93	95	361	NA

Enforcing component limits is a delicate issue that has a strong impact on the solution validity (see Sect. 2.1). Two main approaches have been followed in the proposed solutions:

1. A priori limitation (S3, S6, S7), where map inputs or ECMS degrees of freedom are preliminarily saturated to corresponding limits: in this approach actual limits might take into account also limits induced by the concurrent operation of other components; for example, the engine torque could be constrained by the generator limits at the corresponding speed and such a method often introduces iterations, algebraic loops that deserve a special treatment (S7).
2. A posteriori limitation (S2, S5), where map outputs or ECMS candidates are checked and possibly saturated to their respective limits.

A combined approach, with a priori and a posteriori check, is used in S1, S8, and S9.

## 4 Results

### 4.1 Proposed Solutions

Table 8 summarizes the main scores obtained by running the proposed solutions.

A comparison between all valid solutions in terms of SOC trajectory for cycle “Arco–Merano” is shown in Fig. 9. The figure clearly shows that best performing strategies, i.e., S1 and S7 (see respective scores in Table 8), are able to drive the SOC toward the minimum value before the last downhill in a smooth fashion. In contrast, solutions S3 and S5 suffer from SOC oscillations around the best-performing trajectory, solutions S2 and S4 tend to discharge the battery too fast, while S6 and S8 are characterized by heavy SOC deviations with respect

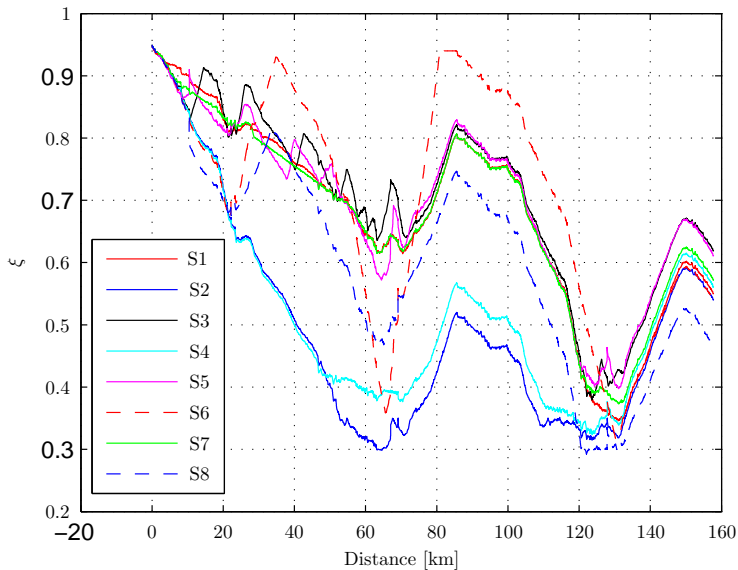


Figure 9: Cycle Arco–Merano, SOC for all valid strategies.

to the best-performing trajectory. In the following section, the best-performing strategy S1 is detailed and compared with the optimal solution of Problem 8 calculated using an offline PMP algorithm.

Two among the three best performing solutions (S1 and S3) have adopted ECMS, alongside with two other solutions (S7, which is among the best performing strategies in the fuel economy tests, and S8). It is apparent that the performance of ECMS strongly depends on the implementation of (12). All four solutions have adopted (13) with possible SOC margins. As a consequence, the  $\xi_{ref}(t)$  signal is decreasing almost linearly with the increase of time and distance covered, as shown in Fig. 10.

Table 8 shows a weak correlation between fuel economy results and memory use, resp., processing time results. Discrepancies are particularly visible for solutions S7 and S5. The latter is the simplest solution, so it performs rather well both in terms of CPU time and memory use. On the other hand, S7 has the second-best aggregate score in the fuel economy tests but it is penalized in terms of CPU time by the use of long ECMS-candidate vectors and in memory use by the use of large maps. Generally speaking, ECMS-based strategies require Hamiltonian minimization and thus need a larger CPU time than heuristic strategies; however S1 that is map-based rather than vector-based performs better than S3, S7, and S8 in terms of CPU time. As for memory use, there is no clear trend among ECMS and heuristic strategies, since both require maps and look-up tables either to represent the various components' efficiency, or to store the pre-calculated setpoints or rules.

The final scores shown in Table 8 were calculated using the European CO<sub>2</sub> emission factor, as explained in Sect. 2.1. If other CO<sub>2</sub> factors were used, the scores would change only slightly and the ranking of the proposed solutions

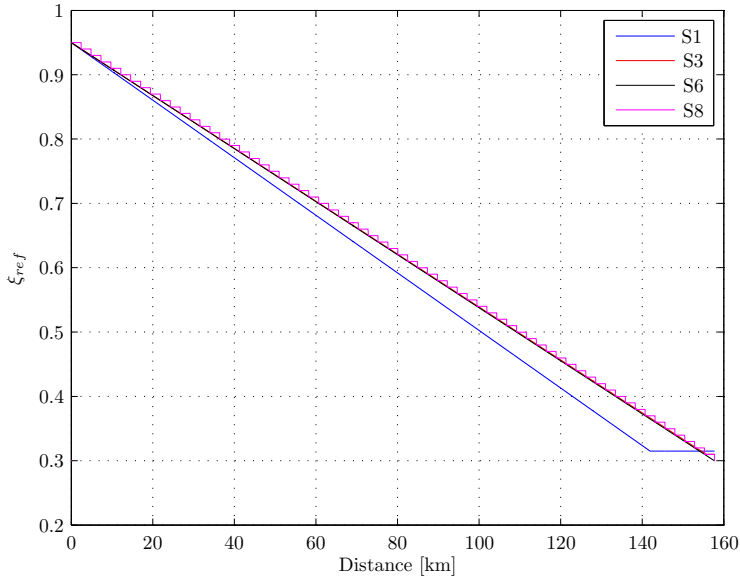


Figure 10: Cycle Arco–Merano, reference SOC for all four ECMS strategies.

would remain the same. A different focus in weighting the scoring metrics would obviously lead to a different ranking. For instance, an enhanced focus on computational performance (raised from 20% to 40%) would let S2 have a better overall score than S1. On the other hand, an enhanced focus on energy efficiency (raised from 50% to 75%) would confirm S1 as the best solution. Since performance metrics are similar for all solutions, enhancing their weight (e.g., raising it from 30% to 65%) would not change the ranking at all. However, setting different weights would have probably led to differently focused solutions, so that the previous discussion must be taken very cautiously.

## 4.2 Globally Optimal Solution

To assess the optimality of the best-performing strategy S1, it has been compared with the outcome of an offline optimization tool (HOT, [42]) that has prior knowledge of the driving cycle. HOT is based on PMP and finds iteratively the initial values of the costates. Model parameters are the same as in the Voltec simulator. The optimization criterion set is fuel consumption. Although having the capability of running cold-start cycles and performing two- or three-state optimization with engine and aftertreatment temperatures as additional state variables ([43]), for this test the standard functionality with SOC as the single state has been used. The constant value of the equivalence factor  $s_0$  is found with a root-finding algorithm based on the SOC at the end of the test cycle,  $\xi(T)$ . The target value for the SOC is set to  $\xi_t = 30\%$ : positive deviations  $\xi(T) - \xi_t$  make  $s_0$  decrease in the next iteration, while negative deviations make  $s_0$  increase.

Figure 11 compares the optimal profiles of SOC and fuel consumption calcu-

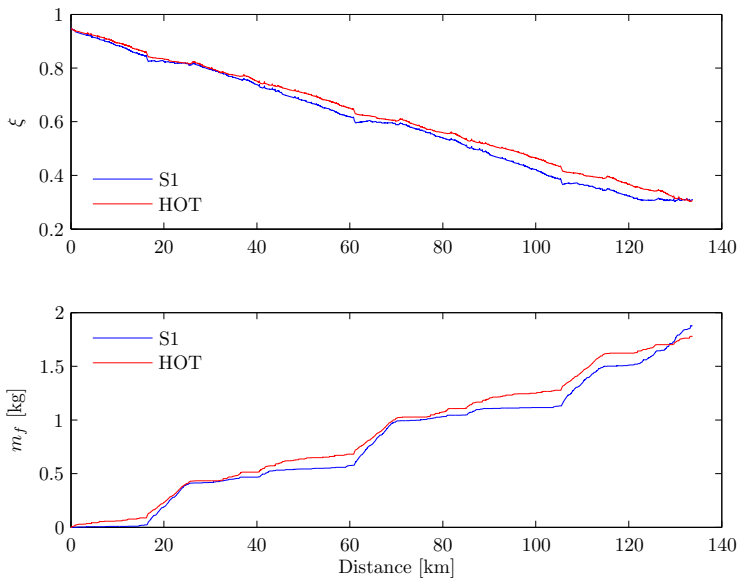


Figure 11: Aachen cycle, SOC and fuel consumption.

lated by HOT for test cycle “Aachen” with the outcome of S1. The two profiles are very close to each other. Wider differences are visible in Fig. 12 that refers to the test cycle “Arco–Merano”. However, in this case too, S1 is able to make the SOC approach the minimum value (30%) before the final downhill, at the end of which both S1 and HOT predict a SOC of about 50%. Consequently, the fuel consumption predicted by S1 is very close to the minimum value calculated by HOT (2.76 l/hkm for test cycle “Arco–Merano”, 1.77l/hkm for test cycle “Aachen”), see Table 8. Figures 13–14 show the distribution of engine operating points during the two test cycles. Both S1 and HOT tend to operate the engine around the best efficiency region, although S1, being an online strategy, is characterized by many more distinct operating points (transient maneuvers, SOC regulation, etc.) than HOT. Figures 15–16 compare the two distributions of powertrain modes as a function of vehicle speed and torque. In both strategies, mode 1 is selected at low speeds, mode 2 for medium speeds and low torques, mode 3 at high torques, and mode 4 for medium to high speeds. The S1 use of the mode 3 is wider than in HOT, certainly in the attempt of perform a blended-mode strategy as a function of SOC. The behavior in the two cycles is similar for both strategies, except for the different speed and torque range.

## 5 Conclusions

The development of benchmark control problems is an engineering practice that can help assessing different methods and techniques under the same circumstances (same system, same operating conditions, same exogenous inputs, etc.). The benchmark control problem illustrated in the paper, concerning the energy

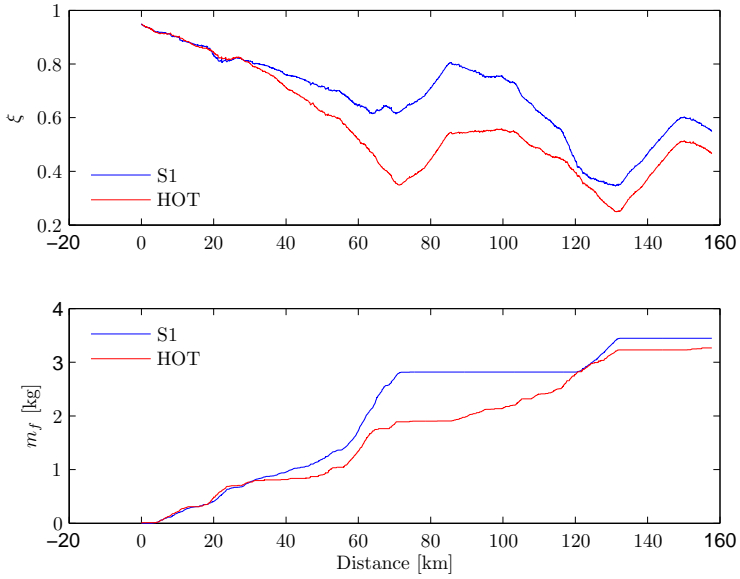


Figure 12: Arco-Merano cycle, SOC and fuel consumption.

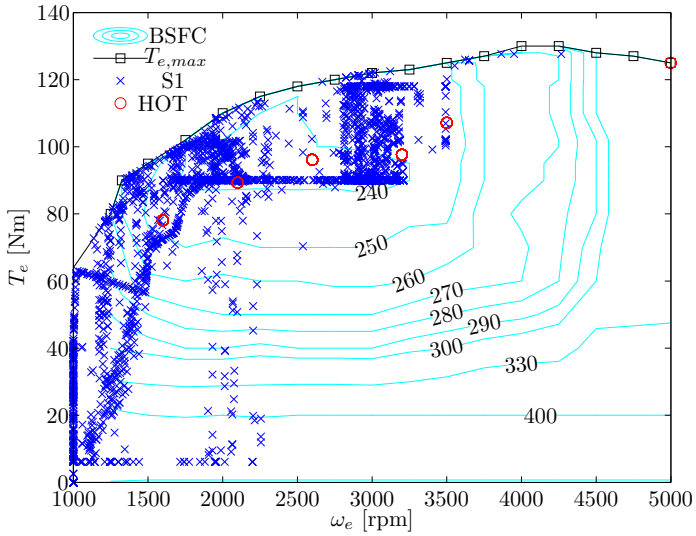


Figure 13: Aachen cycle, engine operating points.

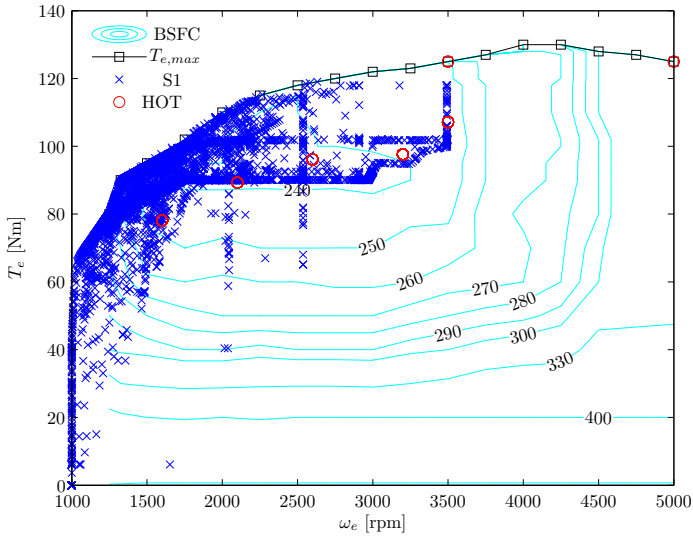


Figure 14: Arco-Merano cycle, engine operating points.

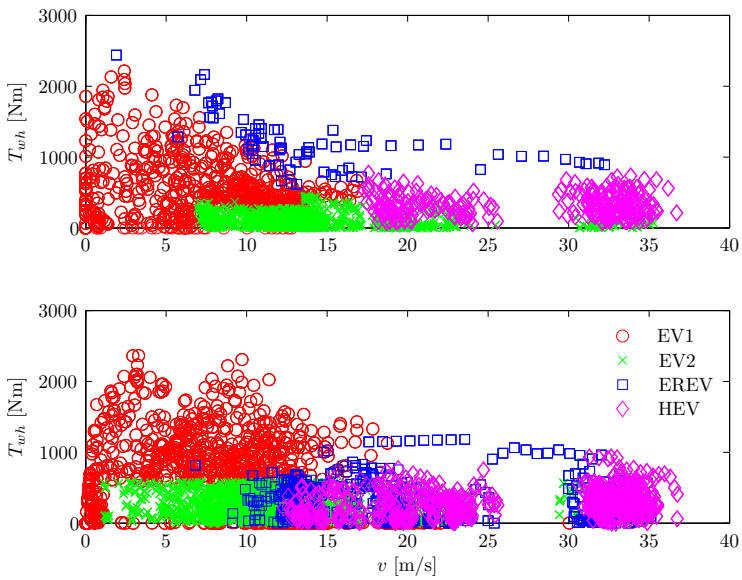


Figure 15: Aachen cycle, powertrain modes, HOT (top) and S1.

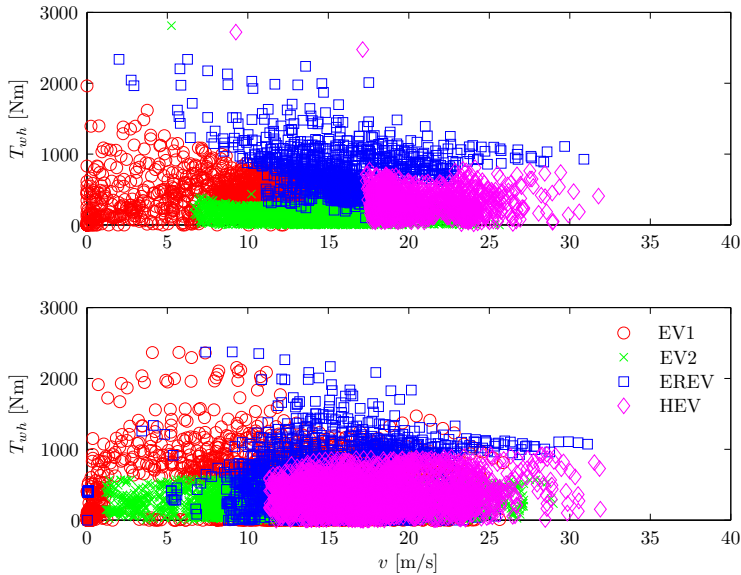


Figure 16: Arco-Merano cycle, powertrain modes, HOTA (top) and S1.

management of a plug-in hybrid-electric car, has fulfilled this goal since it has allowed:

1. a comparison in terms of various performance criteria: while the dispersion among different solutions in terms of vehicle performance is rather low, fuel economy is more sensitive to the energy management strategy adopted, particularly for real-life driving profiles with severe altitude variations; even larger differences can arise in terms CPU time and memory use
2. a comparison between heuristic and optimal control-based techniques: generally speaking the latter outperform the rule-based approach under the same unprevisible circumstances, particularly in terms of fuel economy; however, heuristic algorithms can also achieve good performance, yet they require a higher amount of tuning and they are less robust to system variations
3. a comparison between different implementations of optimal-control-based techniques (ECMS): map-based ECMS induce lower computing efforts but higher memory use, while the opposite is true for vector-based ECMS
4. a comparison between online solutions and a globally optimal solution calculated off line with a prior knowledge of the driving profile: if properly designed, online energy managers can be very close to global optimum in terms of fuel economy.

The software developed for this benchmark will be made available on the web site [www.ecosm12.org](http://www.ecosm12.org) for further use by control engineering students and professionals that desire to test their own energy management solutions. A

parametric PMP algorithm, HOT, will be also accessible to calculate a global optimum reference. Such platform could be enriched in the future with generators of random but realistic driving profiles and the possibility of modifying the structure and the components of the powertrain in the online-running model representing the actual system.

## Acknowledgements

The prize awarded to the winning team was made available by IFP School with the support of the Tuck Foundation. The correct conduct of the benchmark has been guaranteed by the jury members, whose support has been thorough and valuable: Chris Manzie (Univ. of Melbourne), Urs Christen (Ford Aachen), and Andreas Ehinger (IFP Energies nouvelles and Tuck Foundation), besides A. Sciarretta and P. Tona.

## References

- [1] Baumann, B., Rizzoni, G., & Washington, G. (1998) Intelligent Control of Hybrid Vehicles Using Neural Networks and Fuzzy Logic, SAE Paper 981061.
- [2] Brahma, A., Guezennec, Y., & Rizzoni, G. (2000) Optimal Energy Management in Series Hybrid Electric Vehicles, in Proc. of the American Control Conference, 60–64.
- [3] Paganelli, G., Guerra, T.M., Delprat, S., Santin, J.J., Combes, E., & Delhom, M. (2000) Simulation and Assessment of Power Control Strategies for a Parallel Hybrid Car, Journal of Automobile Engineering 214, 705–718.
- [4] Salman, M., Schouten, N.J., & Kheir, N.A. (2000) Control Strategies for Parallel Hybrid Vehicles, in Proc. of the American Control Conference, 524–528.
- [5] Lin, C.C., Kang, J.M., Grizzle, J.W., & Peng, H. (2001) Energy Management Strategy for a Parallel Hybrid Electric Truck, in Proc. of the American Control Conference, 2878–2883.
- [6] Kleimaier, A. & Schroder, D. (2002) An Approach for the Online Optimized Control of a Hybrid Powertrain, in Proc. of the 7th International Workshop on Advanced Motion Control.
- [7] Sciarretta, A., Back, M., & Guzzella, L. (2004) Optimal Control of Parallel Hybrid Electric Vehicles, IEEE Transactions on Control Systems Technology, 12(3), 352–363.
- [8] Koot, M., Kessels, J., de Jager, B., Heemels, W., van den Bosch, P., & Steinbuch, M. (2005) Energy Management Strategies for Vehicular Electric Power Systems, IEEE Transactions on Vehicle Technology, 54(3), 1504–1509.

- [9] Sciarretta, A. & Guzzella, L. (2007) Control of Hybrid Electric Vehicles, *IEEE Control Systems Magazine*, 27(2), 60–70.
- [10] Hofman, T., Ebbesen, S., & Guzzella, L. (2012) Topology Optimization for Hybrid Electric Vehicles with Automated Transmissions, *IEEE Transactions on Vehicular Technology*, 61(6), 2442–2451.
- [11] Hofman, T., Steinbuch, M., Serrarens, A., van Druten, R. (2008) Rule-Based Equivalent Consumption Minimization Strategies for Hybrid Vehicles, in *Proc. of the 17th IFAC World Congress*.
- [12] Ambühl, D., Sciarretta, A., Onder, C., Guzzella, L., Sterzing, S., Mann, K., Kraft, D., & Küsell, M. (2007). A Causal Operation Strategy for Hybrid Electric Vehicles Based on Optimal Control Theory, in *Proc. of the 4th Braunschweig Symposium on Hybrid Vehicles and Energy Management*.
- [13] Serrao, L., Onori, S., & Rizzoni, G. (2009) ECMS as a Realization of Pontryagin’s Minimum Principle for HEV Control, in *Proc. of the American Control Conference*, 3964–3969.
- [14] Kim, N.W., Cha, S.K., & Peng, H. (2011) Optimal Control of Hybrid Electric Vehicles Based on Pontryagin’s Minimum Principle, *IEEE Transactions On Control Systems Technology*, 19(5) 1279–1287.
- [15] van Berkel, K., Hofman, T., Vroemen, B., & Steinbuch, M. (2012) Optimal Control of a Mechanical-Hybrid Powertrain, *IEEE Transactions on Vehicular Technology*, 61(2), 485–497.
- [16] Musardo, C. & Rizzoni, G. (2005) A-ECMS: An Adaptive Algorithm for Hybrid Electric Vehicle Energy Management, *Proc. of the IEEE Conference on Decision and Control and the European Control Conference*, 1816–1823.
- [17] Pisu, P. & Rizzoni, G. (2007) A Comparative Study of Supervisory Control Strategies for Hybrid Electric Vehicles, *IEEE Transactions On Control Systems Technology*, 15(3), 506–518.
- [18] Sivertsson, M., Sundström, C., & Eriksson, L. (2011) Adaptive Control of a Hybrid Powertrain with Map-based ECMS, *Proc. of the IFAC World Congress*.
- [19] Anatone, M., Cipollone, R., Donati, A., & Sciarretta, A. (2005) Control-Oriented Modeling and Fuel Optimal Control of a Series Hybrid Bus, *SAE Paper 2005-01-1163*.
- [20] Pisu, P. & Rizzoni, G. (2005) A Supervisory Control Strategy for Series Hybrid Electric Vehicles With two Energy Storage Systems, in *Proc. of the IEEE Conference on Vehicle Power and Propulsion*.
- [21] Cipollone, R. & Sciarretta, A. (2006) Analysis of the Potential Performance of a Combined Hybrid Vehicle with Optimal Supervisory Control, in *Proc. of the IEEE Int. Conference on Control Applications*.

- [22] Liu, J.M. & Peng, H. (2006) Control Optimization for a Power-Split Hybrid Vehicle, Proc. of the American Control Conference.
- [23] Borhan, H.A. & Vahidi, A. (2010) Model Predictive Control of a Power-Split Hybrid Electric Vehicle with Combined Battery and Ultracapacitor Energy Storage, proc. of the American Control Conference, 5031–5036.
- [24] O’Kneefe, M. & Markel, T. (2006) Dynamic Programming Applied to Investigate Energy Management Strategies for a Plug-in HEV, in Proc. of the 22nd International Battery, Hybrid and Fuel Cell Electric Vehicle Symposium and Exposition.
- [25] Tulpule, P., Marano, V., & Rizzoni, G. (2009) Effects of Different PHEV Control Strategies on Vehicle Performance, Proc. of the American Control Conference.
- [26] Larsson V., Johannesson, L., & Egardt, B. (2010) Impact of Trip Length Uncertainty on Optimal Discharging Strategies for PHEVs, in Proc. of the IFAC Symposium on Advances in Automotive Control, 2010.
- [27] Stockar, S., Marano, V., & Canova, M. (2011) Energy-Optimal Control of Plug-in Hybrid Electric Vehicles for Real-World Driving Cycles, IEEE Transactions On Vehicular Technology, 60(7) 2949-2962.
- [28] Serrao, L., Sciarretta, A., Grondin, O., Chasse, A., Creff, Y., di Domenico, D., Pognant-Gros, P., Querel, C., & Thibault, L. (2013) Open Issues in Supervisory Control of Hybrid Electric Vehicles: A Unified Approach Using Optimal Control Methods, Oil & Gas Science and Technology, ahead of print.
- [29] Spencer, B.F., Dyke, S.J., & Deoskar, H.S. (1998), Benchmark problems in structural Control: Part I – Active Mass Driver System, Earthquake Engineering and Structural Dynamics, 27(11), 1127–1139.
- [30] Yasui, Y. (2012), JSAE-SICE Benchmark Problem 2: Fuel Consumption Optimization of Commuter Vehicle using Hybrid Powertrain, in Proc. of World Congress on Intelligent Control and Automation, 606–611.
- [31] Guzzella, L. & Sciarretta, A. (2013), Vehicle Propulsion Systems, Introduction to Modeling and Optimization, Springer, Chapter 2, p. 13–45.
- [32] Falières, Q., Grasset, O., Roblet, K., Xu, Y., Noiret, C., Serrao, L., & Sciarretta, A. (2011) A Contradictory Analysis of GM Voltec Powertrain, in Proc. of the European Electric Vehicle Congress.
- [33] Grebe, U.D. & Nite, L.T. (2011), VOLTEC – The Propulsion System for Chevrolet Volt and Opel Ampera, ATZ Autotechnology, 5(2011), 4.
- [34] Miller, M.A., Holmes, A.G., Conlon, B.M., & Savagian, P.J. (2011) The GM Voltec 4ET50 Multi-Mode Electric Transaxle, SAE Paper 2011-01-0887.

- [35] Parrish, R., Elankumaran, K., Gandhi, M., Nance, B. et al., (2011), Voltec Battery Design and Manufacturing, SAE Paper 2011-01-1360.
- [36] Do, D.V. (2010), Diagnostic de batteries lithium-ion dans des applications embarquées, PhD Thesis, Université de Technologie de Compiègne.
- [37] TNO Report (2006), Review and Analysis of the Reduction Potential and Costs of Technological and Other Measures to Reduce CO<sub>2</sub> Emissions from Passenger Cars.
- [38] International Energy Agency report (2011), CO<sub>2</sub> Emissions from Fuel Combustion: Highlists.
- [39] Marcos, D. & Bordons, C. (2012), Power Management of a Plug-in Hybrid Electric Vehicle Based on Cycle Energy Estimation, in Proc. of the 2012 IFAC Workshop on Engine and Powertrain Control, Simulation, and Modeling.
- [40] Sivertsson, M. (2012) Adaptive Control Using Map-Based ECMS for a PHEV, in Proc. of the 2012 IFAC Workshop on Engine and Powertrain Control, Simulation, and Modeling.
- [41] Onori, S., Serrao, L., & Rizzoni, G. (2010) Adaptive Equivalent Consumption Minimization Strategy for HEVs, in Proc. of the ASME Dynamic Systems and Control Conference.
- [42] Chasse, A. & Sciarretta, A. (2011), Supervisory Control of Hybrid Powertrains: an Experimental Benchmark of Offline Optimization and Online Energy Management, Control Engineering Practice, 19(11), 1253–1265.
- [43] Merz, F., Sciarretta, A., Dabadie, J.-C., & Serrao, L. (2012) On the Optimal Thermal Management of Hybrid-Electric Vehicles with Heat Recovery Systems, Oil & Gas Science and Technology, 67(4), 610–612.

# Design and evaluation of energy management using map-based ECMS for the PHEV benchmark<sup>†</sup>

Martin Sivertsson and Lars Eriksson

*Vehicular Systems, Department of Electrical Engineering,  
Linköping University, SE-581 83 Linköping, Sweden.*

---

<sup>†</sup>This is a formatted version of “Design and evaluation of energy management using map-based ECMS for the PHEV benchmark” by Martin Sivertsson and Lars Eriksson, *Oil & Gas Science and Technology - Rev. IFP Energies nouvelles*, Volume 70, Number 1, pages 195-211. ©IFP Energies nouvelles 2014. Reproduced with the permission of IFP Energies nouvelles. The original paper can be found at [ogst.ifpenergiesnouvelles.fr](http://ogst.ifpenergiesnouvelles.fr), <http://ogst.ifpenergiesnouvelles.fr>, and can be found using the Digital Object Identifier (DOI): 10.2516/ogst/2014018. The formatting is restricted to changing the article into a single-column format, adjusting sizes of figures and tables, and adjusting the referencing style.

## Abstract

Plug-in hybrid electric vehicles (PHEV) provide a promising way of achieving the benefits of the electric vehicle without being limited by the electric range, but they increase the importance of the supervisory control to fully utilize the potential of the powertrain. The winning contribution in the PHEV Benchmark organized by IFP Energies nouvelles is described and evaluated. The control is an adaptive strategy based on a map-based Equivalent Consumption Minimization Strategy (ECMS) approach, developed and implemented in the simulator provided for the PHEV Benchmark. The implemented control strives to be as blended as possible, whilst still ensuring that all electric energy is used in the driving mission. The controller is adaptive to reduce the importance of correct initial values, but since the initial values affect the consumption, a method is developed to estimate the optimal initial value for the controller based on driving cycle information. This works well for most driving cycles with promising consumption results. The controller performs well in the benchmark; however, the driving cycles used show potential for improvement. A robustness built into the controller affects the consumption more than necessary, and in the case of altitude variations the control does not make use of all the energy available. The control is therefore extended to also make use of topography information that could be provided by a GPS which shows a potential further decrease in fuel consumption.

## Introduction

A hybrid electric vehicle (HEV) utilizes both electric energy and energy from fuel to meet the demands set by the driver. This may lead to a reduction in the environmental impact and fuel consumption of the vehicle. A Plug-In HEV (PHEV) is a HEV with the possibility of recharging the battery from the grid. This adds the potential of using the vehicle as an electric vehicle, without the range limitations in a pure electric vehicle. The supervisory control algorithm for these more complex powertrains plays an important role in achieving the full potential of the powertrain. In order to evaluate different strategies, IFP Energies nouvelles (IFPEN) organized a benchmark for the energy management of a PHEV (see [5], [7]) held at the E-COSM'12 - IFAC Workshop on Engine and Powertrain Control, Simulation and Modeling in Paris, France.

This paper describes the design, and evaluates the performance of the best-performing controller in the PHEV benchmark problem. As such, the paper describes and also contributes with discussions about several engineering trade-offs that were necessary to make, in order to provide a complete and efficient solution for the benchmark problem. This paper is an extension of [8] where the control strategy was outlined. The control is an extension of the adaptive map-based Equivalent Consumption Minimization Strategy (ECMS) developed in [9] for the PHEV problem and it is implemented for the simulator made available in the PHEV Benchmark.

The PHEV problem poses additional problems compared with HEV control since the control should no longer try to maintain the battery State of Charge (*SOC*) around a constant reference value. This is since it is desirable to make use of all the stored energy in the battery, the engine should only be started if the driving mission exceeds the electric range of the vehicle. Therefore the control strategy in [9] is extended to also handle a time-varying *SOC* reference as well as estimation of initial control values from driving cycle data provided in the simulator.

To achieve optimal results using ECMS the optimal value of an equivalence factor needs to be found; see [1]. However, this optimal value is driving cycle-specific and has to be approximated online. Two promising approaches are found in the literature. Both approaches use a cycle independent-equivalence factor and a correction based on the deviation of *SOC* from its reference value, denoted *SOC* error. In [1] the correction is a linear function in *SOC* error. In [10] the equivalence factor is corrected with a product of two terms, a cubic function of the *SOC* error and tanh of the low-pass filtered *SOC* error.

The contribution of the method proposed here is an efficient way of solving and implementing the ECMS control strategy for a PHEV that is also self-contained, using driving distance and average speed to estimate the initial equivalence factor and then adapting it continuously throughout the driving mission to ensure that it is robust to unknown driving missions and that the desired discharge profile is followed.

The main contributions of the paper are the evaluation of the performance in the benchmark, a discussion on the influence of some of the design choices, and finally, the extension of the control to incorporate topology information from

GPS to improve the performance in the presence of altitude variations in the driving missions.

## Outline

In Section 1 the benchmark is presented and the models in the simulator are briefly described. In Section 2 the problem to be solved is formulated and in Section 3 the offline optimization is described. Section 4 describes the architecture of the controller, and the energy management is described in Section 5. Section 6 evaluates the controller's performance in the benchmark and the influence of some of the design choices is discussed in Section 7. Section 8 then suggests some improvements for the controller before the concluding remarks in Section 9. The scoring metrics as well as a nomenclature describing the symbols used in the paper are found in the Appendix.

## 1 IFPEN PHEV Benchmark

In the IFPEN PHEV Benchmark a simulator is provided for which a supervisory control algorithm is to be designed. This simulator is a quasi-static model of the Chevrolet Volt with vehicle and battery dynamics and all energy converters modeled using stationary maps. The architecture of the vehicle and connections between components are shown in Fig. 1. The Chevrolet Volt has three energy converters, an internal combustion engine (ENG), an electric motor (EM) and a generator (GEN), connected through a planetary gear set (GB). Both electric machines can work in both motoring and generating mode. The powertrain also incorporates three clutches that allow the vehicle to be driven in the following four modes:

- Mode 1: One-motor pure electric vehicle. Only the EM is connected to the GB.
- Mode 2: Two-motor pure electric vehicle. Both the EM and GEN are connected to the GB.
- Mode 3: Series HEV. Only the EM is connected to the GB. The ENG and GEN work as an auxiliary power unit, producing electric power.
- Mode 4: Power-split HEV. All energy converters are connected to the GB.

In the benchmark the controller should output desired torque from the ENG, EM and mechanic brakes, the speed of the GEN, the position of the three clutches, and if the engine should be on or off. The inputs to the controller are the requested torque from the driver model,  $T_{req}$ , minimum allowed regenerative torque,  $SOC$ , vehicle speed, average speed in the driving cycle,  $v_{avg}$ , and approximate driving cycle length,  $D_{tot}$ . The aim of the control is to minimize the criteria described in Table 8 with a battery that is fully charged at the beginning of the driving cycle and may be depleted at the end of the driving cycle. There are also rules on how closely the controller has to follow the desired velocity profile; see [5].

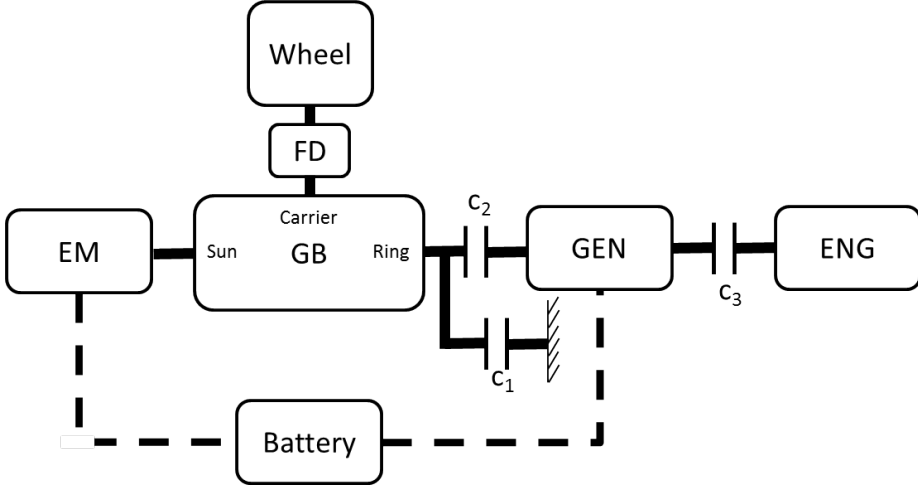


Figure 1: Architecture of the modeled vehicle and the connections between the components.

### 1.1 Models

The model is provided as a Matlab/Simulink file. The key model equations in the simulator are briefly described below, while the interested reader is referred to [5] for more details. A nomenclature describing the symbols used in the paper is shown in the Appendix.

#### Vehicle Model

The vehicle motion equation is implemented as (1) where  $T_{wh}$  is the torque from the powertrain at the wheels,  $T_b$  is the torque applied by the brakes, and  $v$  is the vehicle speed.

$$\frac{dv}{dt} = \frac{r_{wh}}{J_{veh}} (T_{wh} - T_b - r_{wh}(m_{veh} g \sin \theta + c_{v,0} + c_{v,1}v + c_{v,2}v^2)) \quad (1)$$

#### Battery Model

The battery model is of equivalent circuit type with a voltage source and internal resistance and implemented as:

$$I_b = \frac{U_{oc}(SOC)}{2R_c} - \sqrt{\frac{U_{oc}(SOC)^2 - 4R_c P_b}{4R_c^2}} \quad (2)$$

$$P_{ech} = I_b U_{oc}(SOC) \quad (3)$$

$$\Delta SOC = -dt \frac{I_b}{Q_0} \quad (4)$$

## Transmission

The transmission is a planetary gear set with three clutches,  $c_1$ ,  $c_2$  and  $c_3$ . The kinematic relations between the energy converters and the wheels given by the simulator are:

$$\omega_{ENG} = \omega_{GEN} c_3 \quad (5)$$

$$\omega_{EM} = \omega_{wh} \gamma_{fd} (1 + \gamma_{rs}) - \omega_{GEN} c_2 (1 - c_1) \gamma_{rs} \quad (6)$$

$$T_s = T_{EM} \eta_{gb}^{\text{sgn}(T_{EM})} \quad (7)$$

$$T_r = T_s \gamma_{rs} c_2 \eta_{gb}^{\text{sgn}(T_s)} \quad (8)$$

$$T_{GEN} = T_r - c_3 T_{ENG} \quad (9)$$

$$T_c = (1 + \gamma_{rs}) \left( (1 - c_2) T_s + \frac{c_2}{\gamma_{rs}} (T_{GEN} + c_3 T_{ENG}) \right) \quad (10)$$

$$T_{wh} = T_c \eta_{gb}^{\text{sgn}(T_c)} \gamma_{fd} \quad (11)$$

## Consumption

There are two consumptions provided in the simulator and used in this paper; fuel consumption and a fuel equivalent of the electricity consumption. They are defined as:

$$D_{real} = \int \frac{v}{1000} \quad (12)$$

$$m_f = \frac{\int \dot{m}_f}{\rho_f D_{real}} 10^5 \quad (13)$$

$$m_{f,equiv} = \frac{\int P_{ech}}{\eta_{f \rightarrow ech} q_{LHV} \rho_f D_{real}} 10^5 \quad (14)$$

where  $\dot{m}_f$  is the fuel flow,  $\rho_f$  is the density of the fuel,  $D_{real}$  is the distance traveled,  $P_{ech}$  is the electrochemical power,  $\eta_{f \rightarrow ech}$  is the average efficiency from fuel to electricity, and  $q_{LHV}$  is the lower heating value of the fuel.

## 2 Problem Formulation

Looking at the scoring metrics and  $CO_2$  data in Tables 8-9 the problem can be reformulated as delivering the torque requested by the driver,  $T_{req}$ , or as close as possible if the requested torque is infeasible. This should be done in a fuel and computationally efficient way. The performance criteria are actually different measures on torque-tracking ability, therefore they need no further attention than that the controller should follow  $T_{req}$  as closely as possible. Even though the specific  $CO_2$  emissions are higher for electricity production, the higher efficiencies of the electric energy converters compared with the efficiency of the combustion engine result in the fact that the minimization of the well-to-wheel  $CO_2$  emissions can be interpreted as fuel consumption minimization. So, the aim is to minimize the energy use, with emphasis on the fuel consumption, while

fulfilling the driver's requests. This problem is well accommodated by the ECMS, where the sum of fuel and battery power is minimized. However, battery and fuel power are not directly comparable and therefore an equivalence factor  $\lambda$  relating the two is needed; for more information on ECMS, see [4, 6, 3]. The problem is formulated as:

$$H = P_f + \lambda P_{ech} \quad (15)$$

$$[T_{EM}, T_{ENG}, \omega_{GEN}, Mode] = \operatorname{argmin}(H) \quad (16)$$

Subject to:

$$\begin{aligned} T_{wh} &= T_{req} \\ T_{i,min}(\omega_i) &\leq T_i \leq T_{i,max}(\omega_i) \\ 0 &\leq \omega_i \leq \omega_{i,max} \\ i &\in [ENG, GEN, EM] \\ P_{b,min}(SOC) &\leq P_b \leq P_{b,max}(SOC) \end{aligned} \quad (17)$$

where  $\omega$  is the rotational speed of the energy converter, and  $P_b$  is the power at the terminal of the battery. The torque and speed limits are applied to each individual energy converter.

### 3 Offline Optimization

Since the kinematic relations change with the actuation of the clutches, the optimization problem to be solved differs between the modes. Due to the complex nature of the problem the optimal solution is not calculated online. For a given combination of required torque, wheel speed and equivalence factor ( $T_{req}$ ,  $\omega_{wh}$ , and  $\lambda$ ), the cost for each mode can be computed. Therefore, in order to find which mode to use when, the minimum cost for each mode is calculated offline, through discretizing the problem and selecting the combination with the lowest cost. The resulting controls are then stored in tables for a given set of ( $T_{req}$ ,  $\omega_{wh}$ , and  $\lambda$ ). Since the efficiency of the battery does not change much as a function of  $SOC$  in the desired operating region of the battery, the  $SOC$  is found to only have minor effects on the optimal solution, therefore that effect is ignored.

To ensure that (17) are all fulfilled, or in the case of  $T_{req}$  being infeasible, the produced torque is as close to that requested as possible for that mode, the cost function in (15) is augmented so that the closest point, that fulfills all the inequalities is selected.

In order to find which mode is optimal for each combination of  $T_{req}$ ,  $\omega_{wh}$  and  $\lambda$ , the optimal torque and speed setpoints also have to be found. However, instead of just storing all the control variables in tables a few insights can be gained from the kinematic relations in (5)-(11) to reduce the amount of memory used:

- Mode 1:  $T_{EM}$  can be calculated from  $T_{req}$  in all modes. Therefore, Mode 1 requires no tables.
- Mode 2: Only  $\omega_{GEN}$  has to be stored and since  $P_f = 0$  it is independent of  $\lambda$ .

- Mode 3:  $T_{EM}$ ,  $\omega_{EM}$ , and therefore  $P_{EM}$  are given by  $T_{req}$  and  $\omega_{wh}$ . The optimal output power from the generator should be on the optimal operating line of the engine-generator combination (GENSET). Therefore, only the optimal output power for each  $P_{EM}$ ,  $\lambda$  combination has to be stored together with the optimal operating line of the GENSET.
- Mode 4: Both  $\omega_{GEN}$  and  $T_{GEN}$  or  $T_{ENG}$  need to be stored as functions of  $T_{req}$ ,  $\omega_{wh}$  and  $\lambda$ .

### 3.1 Stored data and complexity

With the insight from above the following seven tables are stored for the different modes. An example of the resulting tables is also shown in Fig. 2. This results in 7 tables to be stored, shown in Fig. 2. That is:

- Mode selection (3-D)
- Mode 2:  $\omega_{GEN}$  (2-D)
- Mode 3:  $P_{GENSET}$  (2-D),  $\omega_{opt-line}$  (1-D) and  $T_{opt-line}$  (1-D)
- Mode 4:  $\omega_{GEN}$  (3-D) and  $T_{GEN}$  (3-D)

The optimization is performed for a dense grid in  $T_{req}$ ,  $\omega_{wh}$  and  $\lambda$ . In order to minimize the amount of memory used the calculated tables are sparsened in an iterative manner. This means that the  $T_{req}$ ,  $\omega_{wh}$  or  $\lambda$  resulting in the smallest error in the interpolation scheme used in the online implementation if removed, is removed in an iterative manner. This is performed for all tables, so each table has its own discretization. To simplify the implementation and to reduce the memory consumption Mode 4 is only used when  $T_{req} > 0$ .

## 4 Controller

The basic structure of the controller is shown in a block diagram in Fig. 3. The controller consists of three main subsystems. The first subsystem calculates the value of the equivalence factor,  $\lambda$ , using the *SOC* and driving cycle data, discussed in Section 5.

The second subsystem controls which mode to engage and the third calculates the torque and speed setpoints for the energy converters, both briefly described below.

The mode block consists of five subsystems, one for each mode and one for engine start. The mode controller outputs which mode to activate and if the engine should be started or not. In order to avoid too frequent engine starts/stops two thresholds are used,  $t_{on}$  and  $t_{off}$ . The controller has to request engine on/off for a duration longer than  $t_{on}/t_{off} = 1/4$  s before it is turned on/off. These values are found heuristically, iterating through several values and driving cycles and selecting the values giving the best performance qualitatively. In the simulator the transition between modes is instantaneous, except for engine

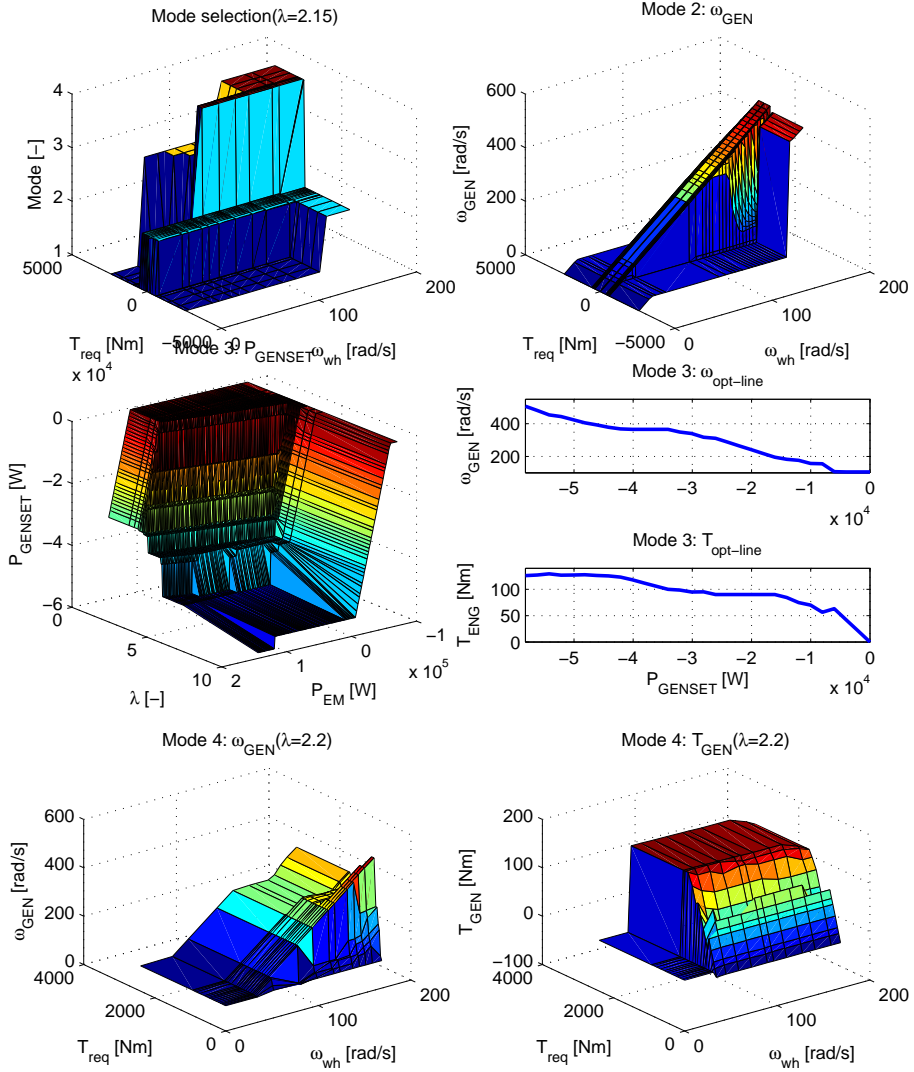


Figure 2: Structure of the stored data, illustrating the complexity of each mode.

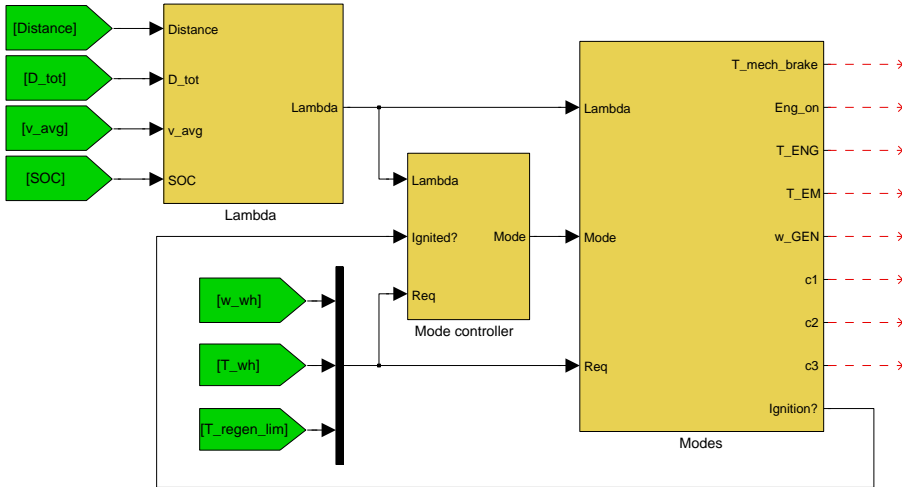


Figure 3: Structure of the controller. The controller consists of three main subsystems, one where the equivalence factor is calculated, one where the mode is selected, and one where the torque and speed setpoints are calculated.

start, which is why no extra penalty or delay on mode switching is implemented. The torques and speed are then calculated using the tables calculated offline and the kinematic relations for that mode defined in (5)-(11). Care is also taken not to exceed any of the constraints in (17).

## 5 Energy Management

Since the optimal solution is calculated offline and  $T_{req}$  and  $\omega_{wh}$  are outputs from the driver model only  $\lambda$  needs to be decided;  $\lambda$  thus controls the energy management. The energy management of a PHEV is often divided into two categories. The first is to make use of all the stored energy in the battery, that is run as an electric vehicle until the *SOC* is under a certain limit, and then operates as a hybrid in charge-sustaining mode. This strategy is commonly denoted charge deplete-charge sustain strategy (CDCS). The main advantage of this strategy is that it is guaranteed to make use of the stored electric energy and does not need information about the future driving mission. The second strategy is to mix usage of fuel and electricity throughout the driving cycle, a strategy known as blended strategy. It is well established in the literature that a blended strategy may result in lower fuel consumption than CDCS; see, for instance [2]. However, in order for a blended strategy to make use of all the energy in the battery the length of the driving cycle has to be known. In the driving cycles provided by the PHEV Benchmark organizers only the approximate distance as well as the mean speed is known. In the provided driving cycles this approximate distance can deviate from the actual distance of the driving cycle by up to almost 10%.

## 5.1 Reference $SOC$

In order to make use of all the stored energy in the battery, a mix between the blended and CDCS strategies is implemented. The strategy is to underestimate the approximate distance by 10%, and use that as a horizon for the blended strategy, then switch to charge-sustaining mode. This is achieved by setting a  $SOC$  reference,  $SOC_c$ , that is linear in the ratio of traveled distance vs. expected distance according to (18), a method also used in [10]. The minimum  $SOC_c$ ,  $SOC_f$ , is set to 0.315 in order to ensure that  $SOC(end) \geq 0.3$ . The shape of  $SOC_c$  is shown in Fig. 4.

$$\begin{aligned} D_x &= \frac{D_{real}}{0.9D_{tot}} \\ SOC_c &= (SOC_f - SOC_0)D_x + SOC_0 \\ SOC_f &\leq SOC_c \leq SOC_{max} \end{aligned} \quad (18)$$

## 5.2 Equivalence factor adaptation

A common strategy when using ECMS is to adapt the equivalence factor according to an affine function of the  $SOC$  error; see [1, 7]. Here, for robustness reasons, another approach is used. The strategy used in [9] is extended to fit the PHEV problem. The strategy is to adapt the equivalence factor according to a tangent function in  $SOC$ . The idea is that as long as the  $SOC$  is near the desired  $SOC$  the control should remain rather constant; but when the  $SOC$  approaches the limits the control needs to adapt. In [9] this is used in a HEV where the aim is to maintain the  $SOC$  around a constant level. Here, since it is a PHEV, it is desirable to use the energy stored in the battery, therefore the center of the tan-function is  $SOC_c$ . The  $SOC$  window used is also decreased linearly with distance traveled. This is to allow larger deviations early in the driving mission, and then make the control follow the  $SOC_c$  on a narrower band towards the end of the driving cycle. The  $\lambda$ -adaptation is given by (19), where  $l_1$  and  $l_s$  are constants that control the slope and range of the tangent function, and  $dSOC$  is the allowed deviation from  $SOC_c$ .

$$\begin{aligned} dSOC &= (dSOC_{max} - dSOC_{min})D_x + dSOC_{max} \\ dSOC &\geq dSOC_{min} \\ \lambda &= \lambda_c - l_1 \tan\left(\frac{l_s \pi}{2dSOC}(SOC - SOC_c)\right) \end{aligned} \quad (19)$$

A benefit with this formulation is that the smaller the  $dSOC$ , the steeper the slope around  $SOC_c$  becomes and the faster the control reacts to deviations. In Fig. 4 the shape of the control is shown for the case when the approximate distance is correct. That is, the  $SOC_c$  undershoots the distance traveled, and thus results in the control going over to charge-sustaining mode. Also shown is that the allowed  $SOC$  deviation gets smaller with distance.

The variable  $\lambda_c$  still has to be decided. In Table 1 the change in consumptions compared with the consumptions with optimal  $\lambda_c$  and end  $SOC$  are shown for different values of  $\lambda_c$  and different driving cycles. A  $\lambda_c$  is considered optimal

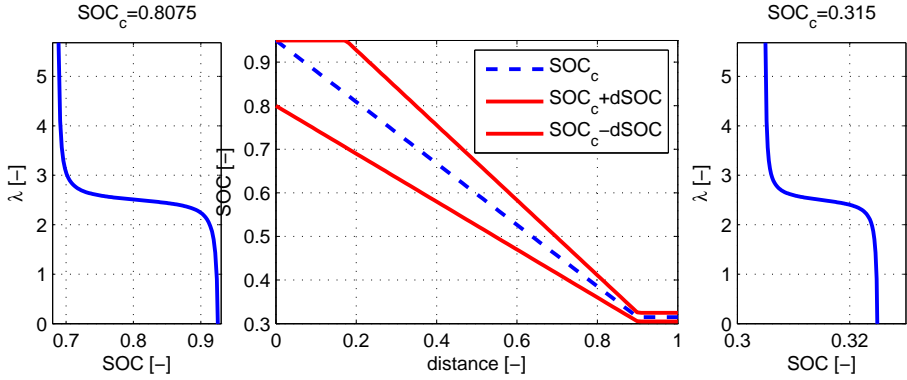


Figure 4: The outline of the basic control shape,  $\lambda$ -function for  $D_x \approx 0.2$  (left),  $SOC_c$  and  $dSOC$  (center) and  $\lambda$ -function for  $D_x \geq 0.9$  (right).

if the  $\lambda$  trajectory follows the desired discharge profile,  $SOC_c$ . However, since  $SOC_c$  is based on undershooting the approximate driving cycle length, there are  $\lambda_c$  values that result in lower consumptions; this is, however, hard to predict. Instead, the optimality of  $\lambda_c$  is qualitatively assessed and the parameter is found in an iterative manner. It is seen that the optimal value changes with the driving cycle. The control ensures  $SOC(end) \geq 0.3$  for all  $\lambda_c$  but it might come with a substantial increase in consumption if the  $\lambda_c$  value is wrong.

In Fig. 5 the  $\lambda$  and  $SOC$  trajectories for the different values of  $\lambda_c$  on 10xUS06 driving cycle is shown, as well as the mode selection for the final repetition of the cycle. Due to the driving mission length provided only being approximate, the control undershoots the length in order to make sure all electric energy is used. The US06 cycle is, however, 7% longer than the length provided, resulting in an undershoot of roughly 16% for the controller. It is seen that the control for  $\lambda_c \neq \lambda_{c,opt}$  does not follow the  $SOC_c$ ; instead it follows  $SOC_c \pm dSOC$ . For  $\lambda_c = 2$  this results in a control that switches rapidly between  $\lambda \approx 2.5$  and  $\lambda \approx 5$ , something that comes with a large consumption penalty. It also affects the number of engine starts, seen in Table 1.

### 5.3 Adaptive control of $\lambda_c$

In order to avoid the switching nature of the  $\lambda$ -control seen in Fig. 5 the idea is to adapt  $\lambda_c$  if the  $SOC$  deviates too much from  $SOC_c$ . This is done with a PI controller according to:

$$\lambda_c = \lambda_{c,init} + K_p(SOC_c - SOC) + K_i \int (SOC_c - SOC) dt \quad (20)$$

where  $K_p$  and  $K_i$  control how fast the controller adapts, but a faster controller comes with a slight consumption penalty. In Table 2 the consumption change compared with  $\lambda_{c,opt}$  for adaptive  $\lambda_c$  is shown for different driving cycles and  $\lambda_{c,init}$ . The number of engine starts is also shown. A  $\lambda_{c,init}$  is considered optimal if it roughly produces a  $SOC$  trajectory that follows the desired trajectory without

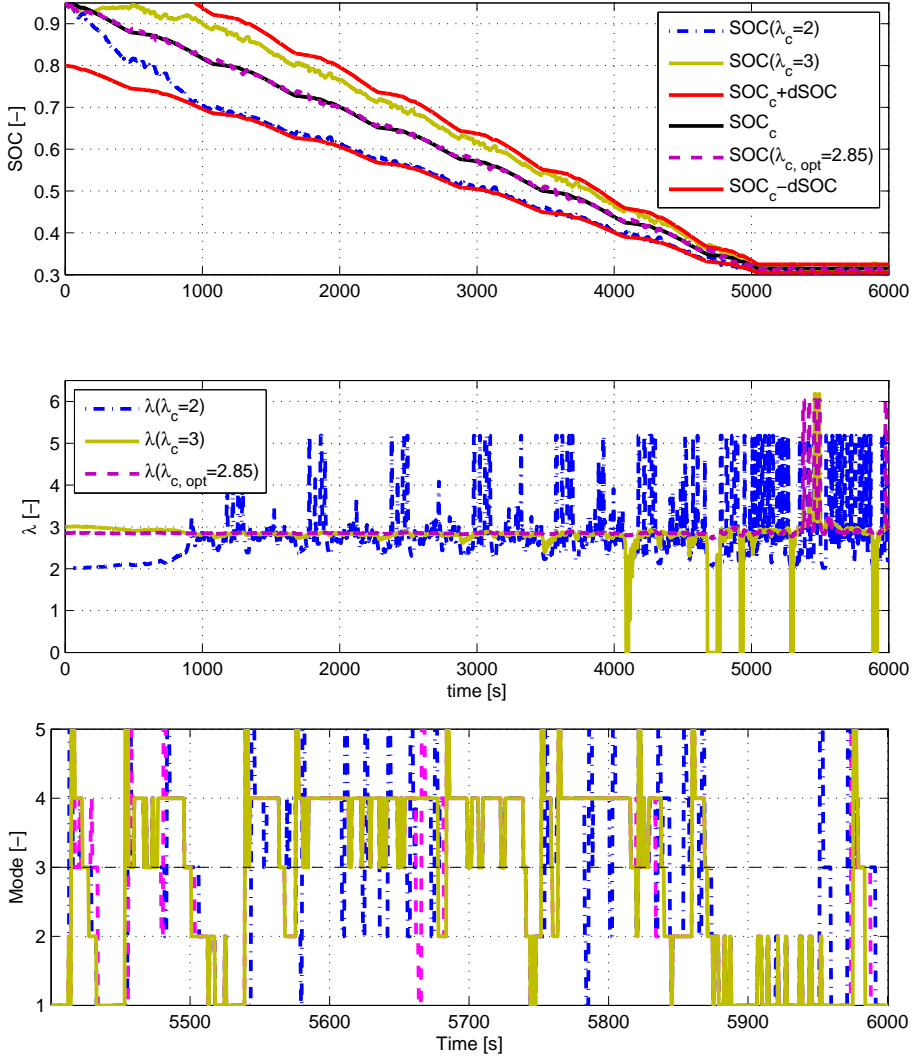


Figure 5: The  $SOC$  and  $\lambda$ -trajectories for different  $\lambda_c$  values on 10xUS06 driving cycle as well as the modes used for the last repetition of US06. Mode=5 represents engine start. A poor  $\lambda_c$  may lead to a switching characteristic of the control, which is also visible in the number of engine starts.

Table 1: The change in consumptions compared with  $\lambda_{c,opt}$  for different values of  $\lambda_c$ . All controls ensure  $SOC(end) \geq 0.3$ .  $n_{on}$  is the number of engine starts.

Cycle-info	$\lambda_c$	$\Delta m_f$ [%]	$\Delta m_{f,equiv}$ [%]	$SOC(end)$	$n_{on}$
10xFUDS	3	-0.65	-0.19	0.3099	66
$D_{tot} = 119.9km$	$\lambda_{c,opt}=2.65$	-	-	0.3076	62
$D_{real} = 119.9km$	2	10.35	2.32	0.3066	73
10xNEDC	3	27.02	15.87	0.3420	25
$D_{tot} = 119.9km$	$\lambda_{c,opt}=2.63$	-	-	0.3197	10
$D_{real} = 110.1km$	2	0.80	0.56	0.3162	15
10xUS06	3	-0.03	-0.71	0.3147	110
$D_{tot} = 119.9km$	$\lambda_{c,opt}=2.85$	-	-	0.3103	125
$D_{real} = 128.9km$	2	5.30	2.20	0.3078	130

Table 2: The change in consumption with adaptive  $\lambda_c$  for different  $\lambda_{c,init}$ , compared with  $\lambda_{c,opt}$ .  $n_{on}$  is the number of engine starts.

Cycle-info	$\lambda_{c,init}$	$\Delta m_f$ [%]	$\Delta m_{f,equiv}$ [%]	$SOC(end)$	$n_{on}$
10xFUDS	3	0.10	-0.29	0.3110	68
$D_{tot} = 119.9km$	$\lambda_{c,init,opt}=2.65$	-0.57	-0.05	0.3075	61
$D_{real} = 119.9km$	2	-0.87	-0.16	0.3081	57
10xNEDC	3	15.61	0.45	0.3306	22
$D_{tot} = 119.9km$	$\lambda_{c,init,opt}=2.55$	-0.16	0.08	0.3188	10
$D_{real} = 110.1km$	2	1.69	0.45	0.3184	16
10xUS06	3	0.07	-0.41	0.3143	125
$D_{tot} = 119.9km$	$\lambda_{c,init,opt}=2.85$	0.03	-0.18	0.3109	125
$D_{real} = 128.9km$	2	0.39	-0.05	0.3101	119

$\lambda_c$  deviating too far from  $\lambda_{c,init}$ , i.e. producing a roughly constant  $\lambda$  trajectory. This value is, as with  $\lambda_{c,opt}$ , qualitatively assessed and found in an iterative manner. It is seen that the adaptive  $\lambda_c$  performs as well as  $\lambda_{c,opt}$ , better in some cases, worse in some cases, but most of all it reduces the effect of poor initial values. This is also confirmed in Fig. 6, where the  $SOC$  and  $\lambda$  trajectories are shown for 10xUS06 driving cycle, as well as the mode selection for the final repetition of the cycle. The switching nature is almost completely removed, resulting in a nearly constant  $\lambda$  value during the entire blended phase.

## 5.4 Estimating $\lambda_{c,init}$

Although the developed control has been seen to perform well for all reasonable initial  $\lambda_c$ , the consumption is still affected by it. Therefore, it is desirable to achieve an estimate as close as possible to the optimal  $\lambda_c$ . In Fig. 7, the optimal  $\lambda_{c,init}$  is plotted against approximate distance for the driving cycles used. It is seen that the shape of the profiles is similar for all driving cycles. The all-electric range, seen in Fig. 7 as  $\lambda_{c,init} \geq 2$ , differs up to almost 100% for the different driving cycles. In Fig. 8 the approximate distance required to exceed the all-electric range is plotted against mean speed. Even if the mean speed is not

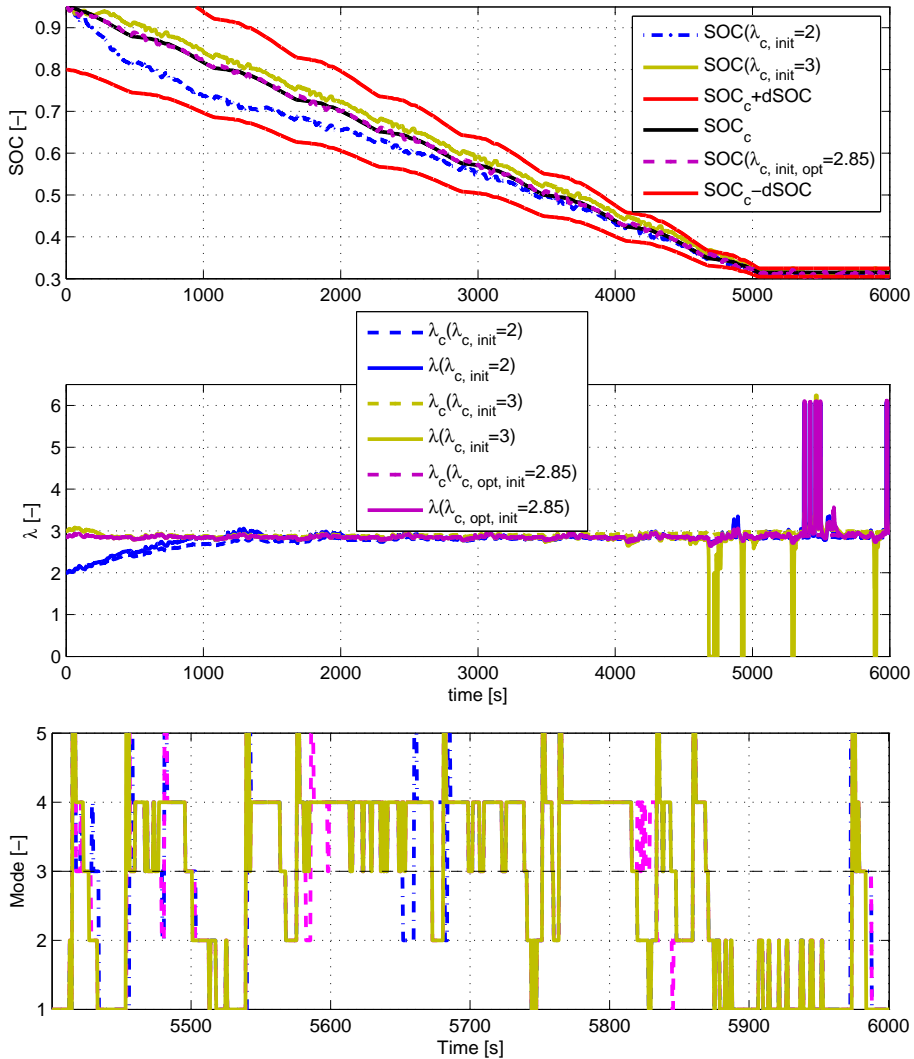


Figure 6: The  $SOC$  and  $\lambda$  trajectories with adaptive  $\lambda_c$  for different values on  $\lambda_{c,init}$  on 10xUS06 driving cycle as well as the modes used for the last repetition of US06. Mode=5 represents engine start. The adaptive  $\lambda_c$  reduces the effect of poor initial values.

Table 3: The change in consumption with  $\lambda_{c,init,mod}$ , compared with  $\lambda_{c,init,opt}$ .  $n_{on}$  is the number of engine starts.

Cycle-info	$\lambda_{c,init,mod}$	$\Delta m_f$ [%]	$\Delta m_{f,equiv}$ [%]	SOC(end)	$n_{on}$
10xFUDS( $\lambda_{c,init,opt}=2.65$ )	2.518	13.62	2.32	0.3066	65
10xNEDC( $\lambda_{c,init,opt}=2.55$ )	2.533	0.80	0.56	0.3162	12
10xUS06( $\lambda_{c,init,opt}=2.85$ )	2.741	5.30	2.20	0.3078	124
20xArtemis Urban( $\lambda_{c,init,opt}=2.84$ )	2	-6.69	-1.41	0.3104	105

enough to describe the driving cycle, since neither the slope nor how transient it is are captured by the mean speed, the all-electric range is approximated by a linear function, shown in Fig. 8. Artemis Urban is plotted in magenta to mark that it is considered an outlier and is not included when the line is fitted. Since the losses in the vehicle motion equation (1) are quadratic in speed, a straightforward assumption would be that the all-electric range decreases with mean speed, an assumption that is also used here. The approximate distance is then corrected with the proposed linear correction, in order to compensate for the different all-electric ranges. The result is shown in Fig. 9. It is seen that the correction shifts the points to the same region, a trend that is well captured by an exponential function. The final scheme to estimate  $\lambda_{c,init}$  is of the form:

$$D_{corr} = D_{tot} - (k_1 v_{avg} + k_2) \quad (21)$$

$$\lambda_{c,init,mod} = k_3(1 - \exp(-k_4 D_{corr} + k_5)) \quad (22)$$

In Table 3 the results for the full controller with  $\lambda_{c,init,mod}$  are compared with the results for  $\lambda_{c,init,opt}$ . Even if the estimated  $\lambda_{c,init}$  is not too far from the optimal, the consumption can differ substantially. Interesting to note is that the driving cycle with the largest  $\lambda_{c,init}$  error shows the best result. Looking at Fig. 10 this appears to be due to the  $\lambda_{c,init,mod}$ -control that has a higher  $\lambda$  value when entering charge-sustaining mode which results in less switching behavior and lower consumption.

Another important property of the  $\lambda_{c,init}$  estimation is that it should be such that it avoids unnecessary engine starts if the driving mission is within the all-electric range. This is achieved for all tested driving cycles except FHDS (1 unnecessary start) and Artemis Extra-Urban (2 unnecessary starts), which is deemed acceptable.

## 6 Benchmark evaluation

In the PHEV Benchmark the controller is tested on two unknown driving cycles, hence not used in the design of the controller; see Fig. 11. Both cycles are rather transient and the first cycle, Arco-Merano, has substantial altitude variations, whereas the second, Aachen, is on flat road. The results for the benchmark tests are shown in Table 4. For both tested cycles the controller performs relatively well and is close to the solution predicted by HOT, described in [1]. The results are within 3.6 % in fuel consumption. This is despite the fact that the controller is implemented without knowledge of the future driving profile and road slope

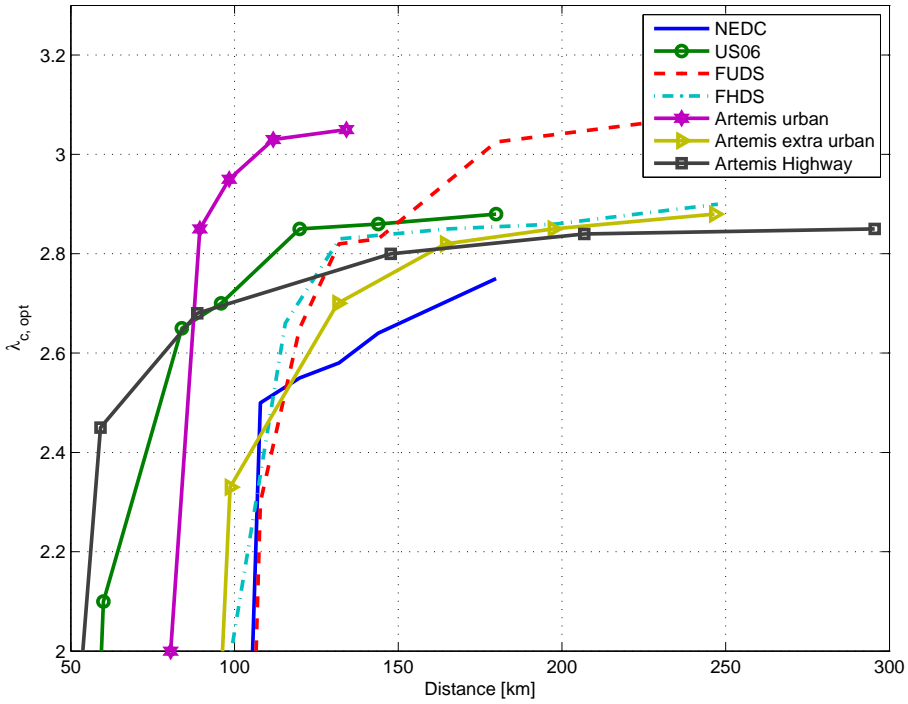


Figure 7: The optimal  $\lambda_{c,init}$  as a function of approximate distance for different driving cycles. The general shape of the curves are similar; however, the all-electric range differs among the cycles.

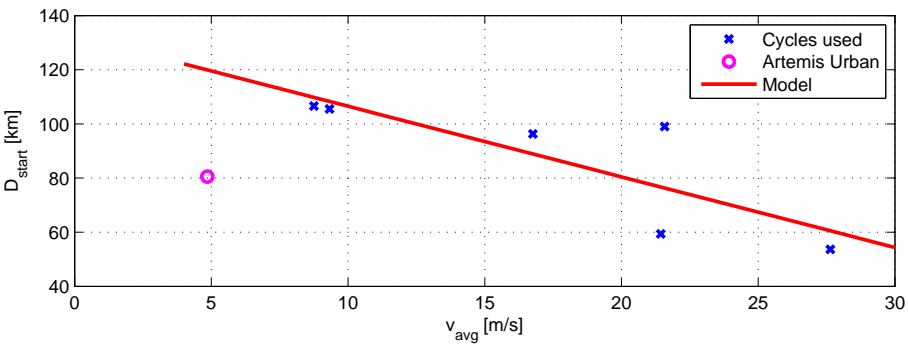


Figure 8: The approximate distance required to exceed the all-electric range for different driving cycles and a linear model to capture the behavior. Artemis Urban is considered an outlier and is not included when the line is fitted.

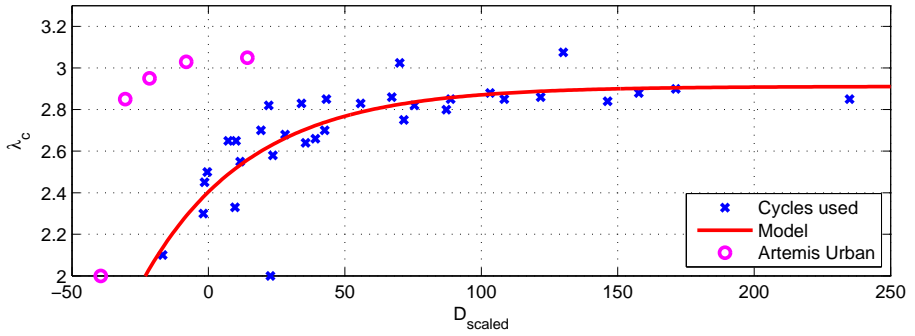


Figure 9:  $\lambda_{c,init,opt}$  vs. corrected approximate distance and how it is modeled. Artemis Urban is considered an outlier and is not included when the curve is fitted.

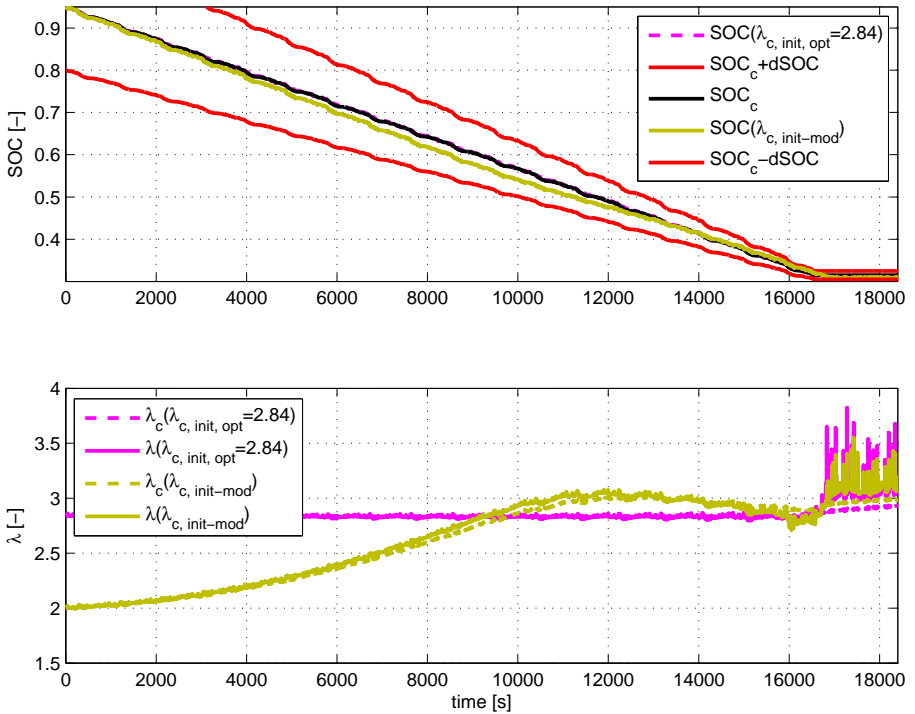


Figure 10:  $SOC$  and  $\lambda$  trajectories for the full controller, with  $\lambda_{c,init,mod}$ , compared with  $\lambda_{c,init,opt}$ . The modeled  $\lambda_{c,init}$  is quite far from the optimal but still  $SOC(end) \geq 0.3$ .

Table 4: Benchmark results for the developed controller

Metric	Arco-Merano	Aachen
Total energy use (fuel+electricity) [MJ/km]	1.0809	0.8664
Fuel consumption [MJ/km]	0.9259	0.5913
Well-to-wheel $CO_2$ emissions [kg/km]	0.0942	0.0768
Processor use [s]	2.9874	2.9631
Memory use [MB]	0.1535	
Acceleration 70-120km/h [s]	9.1	
Acceleration 0-100km/h [s]	7.3	
Acceleration 0-1000m on 4% slope [s]	32.6	
Braking Distance from 100km/h [m]	37.7614	

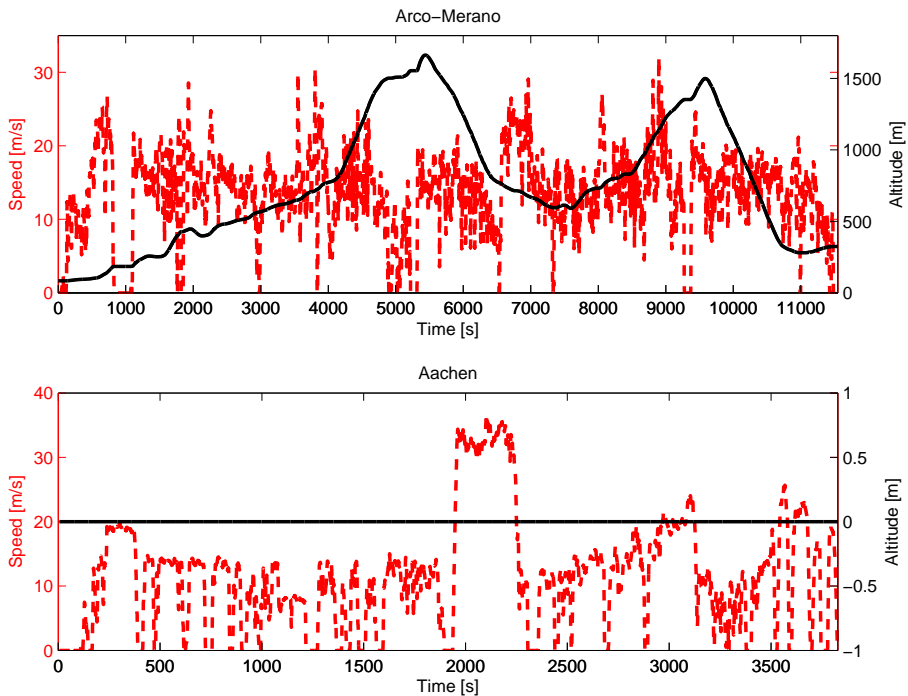


Figure 11: The two driving cycles used in the benchmark.

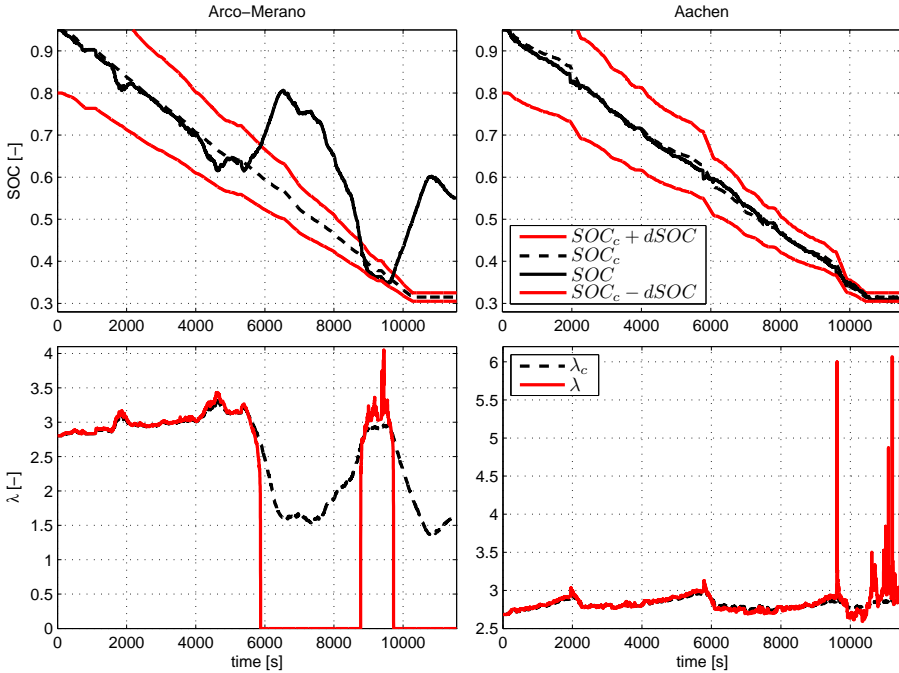


Figure 12: The  $SOC$  and  $\lambda$  trajectories for the two cycles used in the benchmark.

and with a memory usage of just 154 kB. For a closer comparison between the resulting controls and the solution predicted by HOT, see [7].

The resulting  $SOC$  and  $\lambda$  trajectories for the tested cycles are shown in Fig. 12. For both cycles  $D_{tot}$  is accurate and therefore the  $SOC_c$  reference has both a blended and a charge sustaining phase. For Aachen it is seen that the controller performs well, the  $\lambda_{c,init}$  is fairly close to the desired  $\lambda$ -region and the control manages to maintain  $SOC$  near  $SOC_c$  during the entire blended phase without large variations in  $\lambda$ . During the charge-sustaining phase the control becomes a bit switching to maintain  $SOC$  within the desired window.

For Arco-Merano it is apparent that a linear discharge profile is not optimal. This is since the altitude variations, or more accurately the road slope, acts as a disturbance and is unknown to the controller. During the first uphill the control works as expected, maintaining the  $SOC$  near  $SOC_c$ , but during the subsequent downhill phase the recuperation moves  $SOC$  outside the desired  $SOC$  window. In the second uphill phase the control then brings the  $SOC$  back into the  $SOC$  window, but the final downhill yet again brings the  $SOC$  outside of the  $SOC$  window.

## 7 Discussion

The main objective of the controller is to minimize fuel, and one of the basic ideas to accomplish this is to make sure that all the energy in the battery is used.

However, since one of the requirements is that  $SOC(end) \geq 0.3$  for the entry not to be disqualified, this needs to be taken into account. This is accomplished by underestimating the total distance, setting a  $SOC$  target higher than  $SOC_{min}$ , and decreasing the allowed deviation from the desired  $SOC$  the closer to the end of the cycle the vehicle gets. Using a tan-function can also be considered a safety measure since it is seen in Fig. 5 that the tan-function does not make the control follow the desired discharge profile; instead it makes sure that the control stays within the desired  $SOC$  window. All these safety measures affect the consumption, but how much and in what way depends on the driving cycle.

For instance, for Arco-Merano, setting  $\lambda = \lambda_c$ , that is, removing the tan part, improves the fuel economy by 2.9 %, but instead for Aachen  $SOC(end) < 0.3$ . In a real vehicle the lower  $SOC$  limit would be more of a soft constraint and this might not be critical. Without perfect look-ahead the control will potentially end up in charge-sustaining operation and this is something that needs to be handled. One way could be with gain scheduling of the gains in (20), or as here with a tan-function. This is also true for  $SOC_f$ . For some cycles, especially with downhill phases, it would be beneficial to set  $SOC_f < 0.3$ , forcing the controller to follow a steeper discharge profile but then for other cycles  $SOC(end) < 0.3$ .

Removing the underestimation of driving cycle length is not as trivial since the design of  $\lambda_{c,init,mod}$  depends on it. However, since the aim is to minimize fuel consumption, a reasonable assumption is that the fuel penalty of ending with energy left in the battery is larger than the fuel penalty of the strategy not being completely blended, which supports the under-estimation as long as the driving cycle length is not exactly known.

## 8 Controller Extensions

Up until now the focus has been on the controller implementation and design trade-offs that were made for the benchmark. This section describes some extensions that were implemented after the benchmark was completed. Both cycles used in the benchmark evaluation highlight different aspects of potential improvement for the controller. Two suggested improvements for the controller are increasing the allowed  $SOC$  window and incorporating topology information, both described in the following subsections.

### 8.1 Increasing the allowed $SOC$ window

For Aachen the control during the charge-sustaining phase switches between  $\lambda \approx 3$  and  $\lambda \approx 6$ , something that is also visible to a lesser extent in Arco-Merano around 9000 s, which increases the consumption. This is almost completely removed if  $dSOC_{min}$  is increased from 1% to 2.5%, with a corresponding fuel consumption decrease of 2.7 % (Aachen) and 0.9 % (Arco-Merano). Even with this larger  $SOC$  window  $SOC(end) > 0.3$  for both cycles, something that also holds for all other tested cycles except 10xFUDS, where  $SOC(end) = 0.298$ , but in a real application such small deviations might be acceptable.

## 8.2 Including topography information

In Arco-Merano during the downhill segments braking is needed and energy can be recuperated, energy that could be used in the uphill phases. However, to be able to make use of this potential energy some look-ahead is necessary. If the topography is known beforehand and provided to the controller from map and GPS data this could be used in the controller. Vehicle potential energy recuperated in the downhill phases is not taken into account when setting the  $SOC$  reference; if estimates of this can be used this could offer potential for improvement. A suggested extension to the control strategy, given that this information is available, is to relate the potential energy to  $SOC$  and decrease the target  $SOC$ ,  $SOC_f$ , with the amount of energy that can be expected to be recuperated. The requirement is still that  $SOC(end) \geq 0.3$  and therefore  $SOC_f$  is increased as a function of the traveled distance. The new  $SOC_f$  strategy used together with (18) thus becomes:

$$\begin{aligned} SOC_f &= SOC_{f,o} - (1 - D_x) \frac{h_{neg} m_{veh} \eta_{avg} g}{Q_{tot}} \\ SOC_f &\leq SOC_{f,o} \end{aligned} \quad (23)$$

In (23)  $SOC_{f,o} = 0.315$ ,  $h_{neg}$  is the sum of altitude difference in the downhill phases in the driving cycle,  $\eta_{avg}$  is an estimate of the average efficiency from the wheels to the battery, set to 0.8, and  $Q_{tot}$  is the energy capacity of the battery. In the presence of altitude variations this evaluates to a quadratic expression in distance traveled, but on flat road it is equivalent to (18). The results for Arco-Merano with this strategy, as well as the results when just increasing  $dSOC_{min}$ , are shown in Fig. 13.

The resulting trajectories are similar, but as expected the control with varying  $SOC_f$  increases the battery usage during the first uphill and therefore ends at a lower  $SOC$ ,  $SOC(end) = 0.5036$  vs  $SOC(end) = 0.5454$ . When  $dSOC_{min}$  is increased the switching nature of  $\lambda$  disappears but with the addition of varying  $SOC_f$  the switching returns. This is, however, deemed acceptable since the controller still needs to be robust to the other driving cycles. The extra depletion of the battery results in an additional fuel consumption reduction of 4.9 %, results that also hold for the other driving cycle with altitude variations provided by the organizers (VAIL2NREL, 12.4 % decrease).

## 9 Conclusions

The design and development of the winning control strategy in the IFPEN PHEV Benchmark is described. The strategy is an adaptive map-based implementation of ECMS striving to be as blended as possible, but still ensuring that all electric energy is used. The controller tries to follow a  $SOC$  reference that is linear in traveled distance, but to ensure that all electric energy is used this distance is underestimated. The equivalence factor is adapted according to a function in  $SOC$ , a function whose center adapts according to how well the  $SOC$  reference is followed. Finally, a method for estimating the initial value for the controller from driving cycle data is developed.

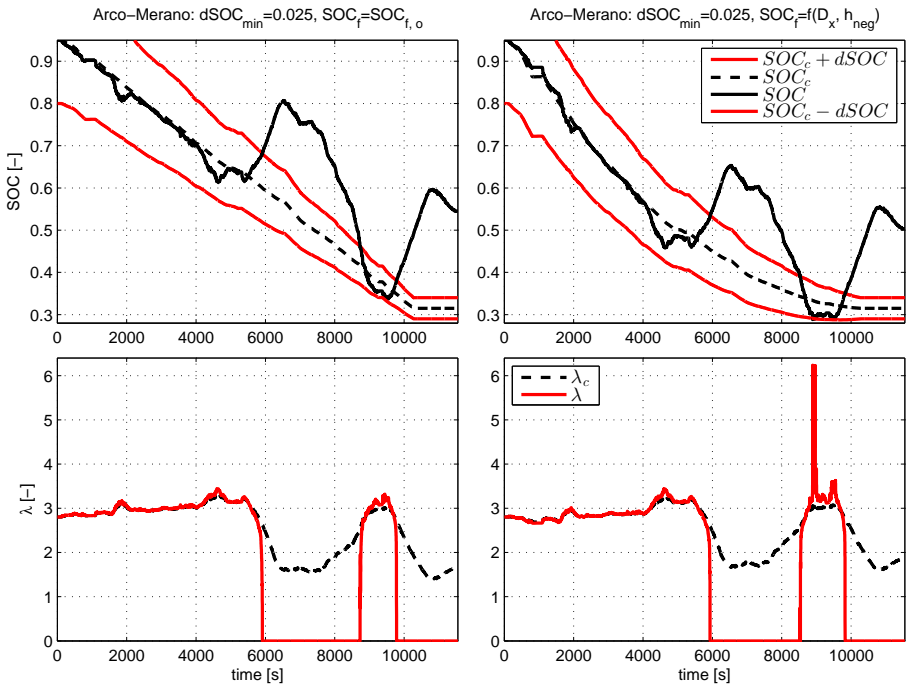


Figure 13: The  $SOC$  and  $\lambda$  trajectories for the case with increased  $dSOC_{min}$  (left) and with topology taken into account (right), Arco-Merano.

In the benchmark the controller is seen to perform well, close to the results predicted by HOT. This is despite being implemented just using the approximate driving distance and average velocity. In the case of altitude variations the assumed linear discharge profile is not followed, due to the fact that the slope of the road is unknown to the controller. Also, the allowed *SOC* window, kept narrow to ensure complete use of the battery energy whilst still ensuring that the final *SOC* is within the limits prescribed in the benchmark, affects the consumption more than necessary.

The controller is therefore extended, first to be allowed to make use of more of the battery, and finally to incorporate topology if available, a strategy that is seen to perform well with promising consumption results.

## References

- [1] A. Chasse, Gh. Hafidi, Ph. Pognant-Gros, and A. Sciarretta. Supervisory control of hybrid powertrains: an experimental benchmark of offline optimization and online energy management. In *E-COSM'09 – IFAC Workshop on Engine and Powertrain Control, Simulation and Modeling*, pages 109–117, 2009.
- [2] Viktor Larsson, Lars Johannesson, and Bo Egardt. Impact of trip length uncertainty on optimal discharging strategies for phev. In *AAC'10 – IFAC Symposium on Advances in Automotive Control*, Munich, Germany, 2010.
- [3] C. Musardo and G. Rizzoni. A-ECMS: An adaptive algorithm for hybrid electric vehicle energy management. In *IEEE Conference on Decision and Control and the European Control Conference*, pages 1816–1823, 2005.
- [4] G. Paganelli, S. Delprat, T.M. Guerra, J. Rimaux, and J.J. Santin. Equivalent consumption minimization strategy for parallel hybrid powertrains. In *IEEE Conference on Vehicular Technology*, pages 2076–2081, 2002.
- [5] PHEV Benchmark Rules. "<http://www.ecosm12.org/sites/ecosm12.org/files/PHEVbenchmarkrules.pdf>", 2012. Downloaded 2012-07-18.
- [6] A. Sciarretta, M. Back, and L. Guzzella. Optimal control of parallel hybrid electric vehicles. *IEEE Transactions on Control Systems Technology*, 12(3): 352–363, 2004.
- [7] A. Sciarretta, L. Serrao, P.C. Dewangan, P. Tona, E.N.D. Bergshoeff, C. Bordons, L. Charmpa, Ph. Elbert, L. Eriksson, T. Hofman, M. Hubacher, P. Isenegger, F. Lacandia, A. Laveau, H. Li, D. Marcos, T. Nüesch, S. Onori, P. Pisu, J. Rios, E. Silvas, M. Sivertsson, L. Tribioli, A.-J van der Hoeven, and M. Wu. A controller benchmark on the supervisory control of a plug-in hybrid electric vehicle. *Accepted for Publication in Control Engineering Practice*, 2013.
- [8] Martin Sivertsson. Adaptive control using map-based ecms for a phev. In *E-COSM'12 – IFAC Workshop on Engine and Powertrain Control, Simulation and Modeling*, Paris, France, October 2012.

- [9] Martin Sivertsson, Christofer Sundström, and Lars Eriksson. Adaptive control of a hybrid powertrain with map-based ECMS. In *IFAC World Congress*, Milano, Italy, 2011.
- [10] Pinak Tulpule, V Marano, and G Rizzoni. Effects of different PHEV control strategies on vehicle performance. In *American Control Conference*, St. Louis, USA, 2009.

## A Notation used

Table 5: Symbols used and their meaning.

Symbol	Meaning	Unit
$r_{wh}$	Wheel radius	$m$
$J_{veh}$	Driveline moment of inertia at the wheels	$kg\ m^2$
$m_{veh}$	Vehicle mass	$kg$
$g$	Gravitational acceleration	$m/s^2$
$\theta$	Road slope	$rad$
$v$	Vehicle speed	$m/s$
$c_{v,0-2}$	Longitudinal vehicle model parameters	$[N, Ns/m, Ns^2/m^2]$
$U_{oc}$	Open-circuit voltage	$[V]$
$R_c$	Internal resistance	$[\Omega]$
$Q_0$	Battery capacity	$[As]$
$Q_{tot}$	Energy capacity of the battery	$[J]$
$SOC$	State of Charge	$[-]$
$\rho_f$	Fuel density	$[kg/m^3]$
$q_{LHV}$	Lower heating value of the fuel	$[J/kg]$
$\dot{m}_f$	Fuel massflow	$[kg/s]$
$m_f$	Fuel consumption	$[L/100km]$
$m_{ech}$	Fuel equivalent of consumed electricity	$[L/100km]$
$h_{neg}$	Height meters downhill in the driving cycle	$[m]$
$c_{1-3}$	Position of clutch 1-3	$[-]$
$T$	Torque	$[Nm]$
$\omega$	Angular velocity	$[rad/s]$
$P$	Power	$[W]$
$\eta$	Efficiency	$[-]$
$I$	Current	$[A]$
$\gamma$	Gear ratio	$[-]$
$D_{tot}$	Estimated driving cycle distance	$[km]$
$D_{real}$	Actual distance traveled	$[km]$
$n_{on}$	Number of engine starts	$[-]$

Table 6: Subscripts used

Subscript	Meaning
<i>ENG</i>	Engine
<i>GEN</i>	Generator
<i>EM</i>	Electric Motor
<i>GENSET</i>	Engine-generator combination (Mode 3)
<i>rs</i>	Ring-Sun
<i>fd</i>	Final Drive
<i>wh</i>	Wheel
<i>gb</i>	Planetary gear box
<i>req</i>	Requested
<i>s</i>	Sun wheel of planetary gear box
<i>r</i>	Ring wheel of planetary gear box
<i>c</i>	Carrier wheel of planetary gear box
<i>f</i>	Fuel
<i>b</i>	At the terminal of the battery
<i>ech</i>	Electrochemical, inside the battery
<i>f</i> → <i>ech</i>	Fuel to electrochemical
<i>avg</i>	Average

Table 7: Control parameters

Name	Meaning
<i>SOC<sub>c</sub></i>	<i>SOC</i> reference
<i>dSOC</i>	Allowed deviation from reference
<i>dSOC<sub>max/min</sub></i>	Maximum and minimum allowed <i>dSOC</i>
<i>SOC<sub>f</sub></i>	Final <i>SOC</i> reference
<i>SOC<sub>f,0</sub></i>	Final <i>SOC</i> reference with adaptive <i>SOC<sub>f</sub></i>
<i>SOC<sub>0</sub></i>	Initial <i>SOC</i>
<i>t<sub>on</sub>/t<sub>off</sub></i>	Thresholds for changing the engine state
$\lambda$	Equivalence factor, relating fuel and electricity
$\lambda_c$	Center of the $\lambda$ -control
$\lambda_{c,init}$	Initial $\lambda_c$
$\lambda_{c,init,mod}$	Modeled initial $\lambda_c$
$l_{1,s}$	Shape parameters of the tan-function
$k_{p,i}$	Gains for the $\lambda_c$ control
$k_{1-5}$	Parameters for the $\lambda_{c,init,mod}$ estimation
$D_x$	Corrected actual distance driven

## B Benchmark Data

Table 8: The scoring metrics used in the benchmark

	<b>Metric</b>	<b>Weight</b>
Performance(30%)	Acceleration 0-100km/h [s]	7.5%
	Acceleration 70-120km/h [s]	7.5%
	Acceleration 0-1000m on 4% slope [s]	7.5%
	Braking Distance from 100km/h [m]	7.5%
Energy and Economy(50%)	Total energy use (fuel+electricity) [MJ/km]	15%
	Fuel consumption [MJ/km]	20%
	Well-to-wheel $CO_2$ emissions [kg/km]	15%
Computational performance (20%)	Processor use [simulation time]	10%
	Memory use [MB]	10%

Table 9: Data for  $CO_2$  emissions

Gasoline well-to-tank emissions	12.5g $CO_2$ /MJ of fuel
Gasoline combustion	73.4g $CO_2$ /MJ of fuel
Electricity production(Europe average)	94.7g $CO_2$ /MJ of electric energy

Linköping studies in science and technology. Dissertations.  
Division of Vehicular Systems  
Department of Electrical Engineering  
Linköping University

- No. 1 Magnus Pettersson *Driveline Modeling and Control*, 1997
- No. 2 Lars Eriksson *Spark Advance Modeling and Control*, 1999
- No. 3 Mattias Nyberg *Model Based Fault Diagnosis: Methods, Theory, and Automotive Engine Applications*, 1999
- No. 4 Erik Frisk *Residual Generation for Fault Diagnosis*, 2001
- No. 5 Per Andersson *Air Charge Estimation in Turbocharged Spark Ignition Engines*, 2005
- No. 6 Mattias Krysander *Design and Analysis of Diagnosis Systems Using Structural Methods*, 2006
- No. 7 Jonas Biteus *Fault Isolation in Distributed Embedded Systems*, 2007
- No. 8 Ylva Nilsson *Modelling for Fuel Optimal Control of a Variable Compression Engine*, 2007
- No. 9 Markus Klein *Single-Zone Cylinder Pressure Modeling and Estimation for Heat Release Analysis of SI Engines*, 2007
- No. 10 Anders Fröberg *Efficient Simulation and Optimal Control for Vehicle Propulsion*, 2008
- No. 11 Per Öberg *A DAE Formulation for Multi-Zone Thermodynamic Models and its Application to CVCP Engines*, 2009
- No. 12 Johan Wahlström *Control of EGR and VGT for Emission Control and Pumping Work Minimization in Diesel Engines*, 2009
- No. 13 Anna Pernestål *Probabilistic Fault Diagnosis with Automotive Applications*, 2009
- No. 14 Erik Hellström *Look-ahead Control of Heavy Vehicles*, 2010
- No. 15 Erik Höckerdal *Model Error Compensation in ODE and DAE Estimators with Automotive Engine Applications*, 2011
- No. 16 Carl Svärd, *Methods for Automated Design of Fault Detection and Isolation Systems with Automotive Applications*, 2012.
- No. 17 Oskar Leufvén, *Modeling for control of centrifugal compressors*, 2013.
- No. 18 Christofer Sundström, *Model Based Vehicle Level Diagnosis for Hybrid Electric Vehicles*, 2014.

- No. 19** Andreas Thomasson, *Modeling and control of actuators and co-surge in turbocharged engines*, 2014.
- No. 20** Emil Larsson, *Model Based Diagnosis and Supervision of Industrial Gas Turbines for Hybrid Electric Vehicles*, 2014.
- No. 21** Andreas Myklebust, *Dry Clutch Modeling, Estimation, and Control*, 2014.
- No. 22** Tomas Nilsson, *Optimal Predictive Control of Wheel Loader Transmissions*, 2015.